Feasibility study of a wood-concrete hybrid super tall building and optimization of its wind-induced behaviour

A case study on a skyscraper in the city-centre of Rotterdam

E.C.Slooten

W350 (Sumitomo, 2018)

TUDelft

zonneveld ingenieurs®

Feasibility study of a wood-concrete hybrid super tall building and optimization of its wind-induced behaviour

by

E.C. Slooten

to obtain the degree of Master of Science
at the Delft University of Technology,
to be defended publicly on September 14, 2018 at 04:00 PM.

An electronic version of this thesis is available at `http://repository.tudelft.nl/`.

Cover image: Copyright by Sumitomo Forestry Co. Ltd.

TUDelft   **zonneveld** ingenieurs®

Abstract

The demand for sustainable high-rise buildings is growing. Such sustainable high-rise could be realized by the use of mass timber for the structural design instead of more conventional building materials such as steel and concrete. Timber is a renewable resource which can be CO_2 neutral if reforestation takes place to close its carbon cycle. In addition, the light-weight of timber reduces the loads on the foundation, and the timber could be used as an architectural feature as well. The height boundaries for tall timber buildings are currently extending, as illustrated by the ongoing realization of a 70 metres tall timber building in Amsterdam. However, the light-weight of timber make tall timber buildings prone to dynamic wind loading. In addition, the current trend to design slender high-rise further increases the wind-induced dynamic response of the building.

In this thesis, the technical feasibility of a super tall hybrid wood-concrete building was evaluated and its wind-induced dynamic behaviour was optimized. To this end a 300m tall building of timber and concrete was designed for construction in the city-centre of Rotterdam, The Netherlands. Due to the absence of seismic activity in the area, wind loading was identified as the governing parameter for lateral stability design. The structural design was therefore optimized to satisfy serviceability criteria for lateral drift and occupant comfort. Based on these requirements, the structure was designed as a reinforce concrete core surrounded by a glued-laminated timber (GLT) frame and floor slabs consisting of a cross-laminated timber (CLT) panel with a thin concrete top layer. Lateral stability was ensured by an outrigger/belt-truss system at three levels, resulting in a significant increase of the global stiffness in the structure, and in a reduction of the maximum lateral inter-storey drift by a factor two.

In order to fully design a 300m tall wood-concrete hybrid building, design aspects such as the floor plan, core layout, lateral stability system and timber frame were designed first. The floor plan layout and storey height were based on a typical office building. The length from the perimeter to the core of the building was set to 9 metres and a storey height 3.75 metres was applied. These dimensions ensured that enough sunlight would fall into the office spaces. The entrance level with double storey height was performed in reinforced concrete to create a more open layout and to achieve a higher safety in the case of accidental blast loading.

Stiffness optimization of the structure was carried out in order to satisfy the serviceability criteria for lateral inter-storey drift and displacement. Consequently, a parametric study of the cross-sectional dimension of the columns, of the thickness of the reinforced concrete core wall, and of the outrigger/belt-truss layout was performed. The cross-sectional dimension of the columns and the thickness of the core wall were tapered down over the height of the structure. A diagonally- and orthogonally-oriented layout of the outrigger trusses were compared. For the final design the orthogonally-oriented layout was applied, because it resulted in more lateral stiffness of the structure. Each outrigger level consists of 8 outrigger trusses which are orthogonally oriented with respect to the reinforced concrete core, and a belt-truss surrounds the perimeter of the structure. The outrigger levels were also designed to accommodate the mechanical, electrical and public health system (MEP) facilities.

Due to the large tension forces caused by lateral wind loading the connection design of the GLT frame is paramount for the feasibility of a hybrid wood-concrete tall building. The outrigger trusses transfer large tension and compression forces to the perimeter columns, making the outrigger connections critical for the overall stiffness of the structure. Therefore, the connections in the outrigger truss, as well as the belt truss, were designed with two slotted-in steel plates and dowels. Beam-to-columns and beam-to-wall connections were designed with only one slotted-in steel plate and dowels. Column splices were carried out with glued-in rods and bolts. In-between the column splices adjustment devices were installed to compensate for the vertical differential shortening of the reinforced concrete core and mass timber frame. Consequently, an additional steel plate with the required adjustment thickness could

be placed between the bolted steel plates of the connection. Continuous columns were applied over a height of 4-storey levels in order to reduce the number of expensive steel-timber connections. Due to transportation constraints, the length of the columns was limited to 15 metres.

Vortex shedding and end-effects of the wind due to lateral wind loading cause peak response accelerations mainly in the across-wind direction. For a return period of 50 years of wind loading to satisfy the serviceability criterion for the occupant comfort, the peak response acceleration should be lower than 0.390 m/s^2. This criterion is dependent on the natural frequency of the structure which is equal to 0.130 Hz. To improve the structure's dynamic behaviour, a passive tuned mass damper (TMD) and a chamfered corner modification were applied, resulting in a decrease of the peak acceleration to a level satisfying the occupant comfort criterion.

The tall building was considered as consequence class 3 (CC3), meaning that a fire-resistance time of at least 120 minutes should be guaranteed. To this end, the mass timber structural elements were covered with protective cladding and a sprinkler system was applied in the building. The reinforcement bars in the concrete core wall were placed at a 35 mm cover to satisfy the required fire resistance time. The fasteners in the dowel-type connection were sealed with wooden plugs and the slotted-in steel plates are hidden and covered by the timber beam element. Dowels, bolts and steel plates in the column splice connection were protected by a double layer of gypsum plasterboard. During a fire, the protective cladding would eventually fall off and charring of the mass timber element would start. The developing char-layer would protect the rest of the cross-section against the fire load. In the GLT beams, a charring depth of 34 mm developed after 120 minutes of fire loading, and as a consequence all steel plates, connectors, and dowels were placed at a minimum distance of about 40 mm from the outer surface.

The designed tall and slender hybrid wood-concrete structure satisfied the serviceability criteria for lateral displacements and accelerations, and the critical connections in the timber frame are able to resist the large forces in the structure. However, a hybrid wood-concrete super tall building required shape optimization and a tuned mass damper to avoid peak acceleration levels exceeding the occupant comfort criterion. Furthermore, the design process established in this case study could serve as a roadmap for the design of future hybrid wood-concrete super tall buildings.

Keywords: *wind-induced dynamic behaviour, tall timber building, occupant comfort, tuned mass damper, shape optimization, high-rise*

Acknowledgements

Contents

List of Figures

List of Tables

Introduction

This chapter describes the problem statement and the aim of the research. The research questions are presented and the methodological approach is elaborated.

1.1. Problem statement and aim

Recent years showed a trend in high-rise demand towards more slender design and towards increased sustainability of building materials. Indeed, architectural proposals emerged for high-rise of up to 300 metres tall designed in mass timber, including the River Beech tower, the Oakwood tower and the W350 (CTBUH, 2018). However, the wind-induced dynamic behaviour of such projects has not yet been researched. As timber is a relatively light-weight material, mass timber high-rise is prone to dynamic wind loading. The resulting large wind-induced response acceleration could cause discomfort and even nausea for the occupants.

This thesis consisted of a design case study in consultation with Zonneveld ingenieurs for a 300 metre wood-concrete hybrid high-rise aimed at a tender for a sustainable tall building next to Rotterdam Central Station. The usage of mass timber reduces the CO_2 footprint compared to traditional reinforced concrete high-rise buildings. To ensure sustainability via a closed carbon cycle, only FSC certified timber should be used combined with reforestation. Due to the light-weight of wood, craning times can be significantly reduced resulting in less construction time (Pilon et al., 2016).

The high slenderness ratio of 1:10 of such a tall building would result in high structural flexibility due to the relatively light-weight of timber. The wind-induced dynamic response can become governing for the structural design of tall and slender buildings. In particular, the low weight and a high flexibility of timber cause problems with peak response accelerations in tall timber structures (Smith and Frangi, 2008). Such dynamic effects can cause large deflections or even collapse depending on the natural frequency of the building. In addition, the acceleration response should be minimal for the occupant comfort. This type of high-rise must satisfy two main serviceability criteria: acceptable peak response accelerations and acceptable maximum lateral storey displacements and drifts. As a result, optimal design of the wind-induced dynamic behaviour is required. Analysis of the dynamic response at an early design stage can reduce the costs of the structural design. An extensive literature review and a parametric study were performed to obtain adequate lateral stability, including an investigation of the possibility to improve the dynamic behaviour by application of a damping system.

The aim of this thesis was to determine the technical feasibility of such a hybrid wood-concrete super tall building and to optimize its wind-induced dynamic behaviour. To this end, a complete design of the hybrid structure including the connection detailing was made. In addition to the wind-dynamic behaviour, other important design aspects such as fire safety design, alternative load path design, and manufacturability were also addressed. At the end of this thesis, recommendations are given on the design improvements needed to fulfil these requirements.

1.2. Research questions

The aim of the research was to answer the following main research question:

- To what extent is a hybrid wood-concrete super tall building technically feasible and how can its wind-induced dynamic behaviour be improved?

To answer this question, a specific super tall hybrid wood-concrete structure will be designed. In the process, the following sub-questions were addressed in the context of the designed structure.

- What are the important/critical design aspects of a hybrid wood-concrete structure?

- What are the relevant serviceability design criteria?

- Which lateral stability system for the design is most adequate?

- Which global damping ratio should be applied for the designed structure, and what influence does this damping have on the peak response acceleration?

- What is the natural frequency of the designed structure?

- How large are the lateral drift and displacement due to wind loading in the structure?

- How large are the peak response accelerations in the structure?

- Are additional damping systems necessary to reduce the wind-induced response, and how effective are these additional damper systems?

- What kind of shape optimizations of the structure are possible, and how effective are these aerodynamic treatments?

1.3. Methodological approach

In order to identify critical factors for the design of a hybrid wood-concrete structure, a literature study was carried out. The focus was primarily on the following topics: super tall building design, timber design, timber connection design, occupant comfort criteria, structural damping, and wind engineering. In addition, the state-of-the-art of tall timber buildings was reviewed. However, since super tall hybrid wood-concrete buildings have not been built up to now, a new design approach was needed for this type of structure. Such a design strategy was developed based on an overview of the program of requirements and applied for the design of a specific 300-metres tall hybrid wood-concrete structure in the city-centre of Rotterdam. This strategy was developed to optimize the wind-induced dynamic behaviour of the design and minimize occupant discomfort due to its acceleration response. Important design aspects such as the fire safety design, alternative load path design, and manufacturability were also included. The structural design of the hybrid structure included the connection detailing.

First a preliminary design of the main structure was made, and design aspects such as a floor plan, core layout, floor slab layout and timber frame were designed. The required strength properties for the mass timber frame and reinforced core walls were determined, and based on this the material strength class was chosen. The outrigger/belt-truss system was applied for the lateral stability and this system was designed and engineered in mass timber. Optimization of the stiffness in the structure was performed in order to satisfy the serviceability criteria for lateral inter-storey drift and displacement. The stiffness optimization was carried out with a parametric study of the cross-sectional dimensions of the columns, the reinforced core wall thickness, and the outrigger/belt-truss. The influence of mega-bracing at the perimeter of the structure on the lateral stiffness was also researched. The stiffness

optimization resulted in a design that satisfied the lateral drift and displacement criteria. Subsequently, this design was further extended with the connection detailing, fire safety design, and alternative load path design.

The critical connection in the timber frame were designed, and also connection detailing of the outrigger and belt-truss was performed. Literature study on mass timber connections was used as a basis for the connection design, and subsequently the connections were designed and checked according to the Eurocode. The connection details were designed to be repeatable over the height of the structure.

Furthermore, the static and dynamic behaviour of the structure were studied. The wind-induced response accelerations due to the along-wind buffeting and vortex shedding were assessed by the serviceability criterion for occupant comfort found in the building code. While across-wind is disregarded for most structures, the across-wind response can become governing for slender tall buildings (Hallebrand and Jakobsson, 2016). Therefore, both the along- and acrosswind response of the structure were studied. Viscous damping was used for the structural dynamic model, and the global damping was estimated based on experimental measurements. The global damping is normally based on measurements from previous projects with a similar structure. However, few hybrid wood-concrete tall buildings have been built and measured so far. Estimation of the damping of the structure is complicated by uncertain factors influencing the global damping behaviour, including: the soil type, the foundation type, the structural materials, joint types, the structural frame system, exterior- and interior walls, cladding, and other non-structural members. The damping properties and stiffness of a structure govern its dynamic response. Therefore, various damping ratios were analysed to study the effect on the dynamic behaviour of the structure.

The wind-induced behaviour was studied by a three-dimensional numerical model performing a quasi-static analysis and a dynamic analysis. The lateral wind load was determined using the Eurocode NEN-EN1991-1-4. The lateral displacement resulting from this wind load was determined using the finite element model in CSi ETABS. The dynamic wind loading was determined using the wind response spectrum method by Davenport (Tamura and Kareem, 2013). A wind force spectrum was acquired and the response of the structure was taken into account with a dynamic amplification factor. The dynamic analysis in the finite element model was done using time history analysis (THA), and the results were compared by response spectrum analysis (RSA). For THA, the time evolution of the wind-induced response can be computed, while this is not possible for RSA. The model was also analysed as a single degree of freedom (SDOF) system to check and globally compare the results with the output of the multi degree of freedom numerical model.

Subsequently, the structure was optimized by modifying its stiffness, mass and damping properties during the design process. First, the stiffness capacity was optimized with a parametric study to satisfy the serviceability criteria for lateral inter-storey drift and lateral displacement. Secondly, the shape and damping properties of the structure were modified to improve the wind-induced dynamic behaviour. The tall building design was optimized to satisfy the occupant comfort criterion for tall office buildings.

A more conventional all-concrete tall building with a similar program of requirements was designed in order to compare the results to the hybrid wood-concrete tall building. The concrete design was designed with the same grid and floor plan layout, and the outrigger/belt-truss system for the lateral stability was applied as well.

It should be noted that this design study was carried out under three main assumptions: the structure was assumed to behave linearly under dynamic wind loading, the wind load combination was assumed to be governing for the lateral stability design, and only main structural components were considered.

2

Literature study

In this chapter, background information is given on the design with mass timber and previous tall timber building are discussed. Furthermore, a literature review is given on lateral stability systems for high-rise buildings and wind engineering.

2.1. Structural mass timber

General

The most common mass timber products on the market are cross-laminated timber, nail-laminated timber, dowel-laminated timber and glued-laminated timber. Structural mass timber makes it possible to build higher in wood. This is due to its higher strength and stiffness properties and larger mass compared to traditional timber. Timber has a low modulus of elasticity compared to the structural materials such as steel and concrete. Figure 2.1 shows the linear stress strain relations for steel, concrete and glued-laminated timber.
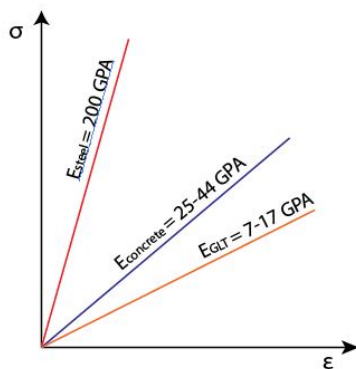
Figure 2.1: Stress strain relations for steel, concrete and glued-laminated timber

The main advantages of using timber structural elements are:
- Light-weight structure and therefore reduced loads on foundations
- Less construction time
- CO2 footprint reduction
- Architectural feature

Disadvantages of using timber structural elements:
- Increase in accelerations during wind-induced vibrations
- Increase in uplift forces resulting from overturning moments
- More material volume compared to concrete or steel

Sustainability

Figure 2.2 shows the life cycle of timber. Timber is a renewable resource and this one of the main advantages over the building materials such as steel and concrete. One of the main requirements for sustainable timber is that reforestation takes place, and due to this the carbon cycle will continue. Figure 2.3 shows the impact on the environment of wood, concrete and steel building designs. Especially, the water pollution is much less for wood design compared to steel and concrete designs.
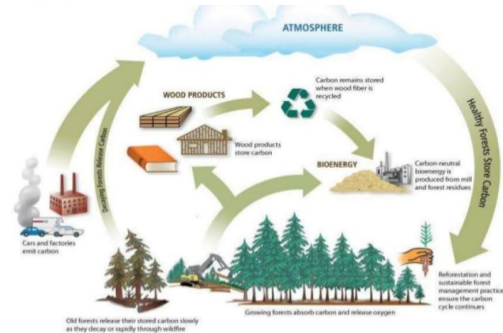
Figure 2.2: Sustainable forestry carbon cycle (Rethink-Wood, 2018)
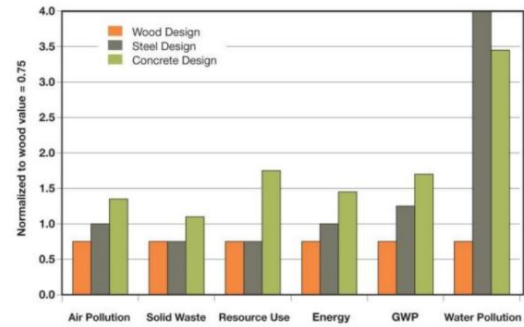
Figure 2.3: Embodied effects relative to wood design across all measures (Rethink-Wood, 2018)

Cross-laminated timber

Cross-laminated timber (CLT) is a timber panel which consists of several layers of lumber oriented at right angle to one and another. Therefore the grain direction of the individual members are orthogonal to one and another. C16-C24 classified timber planks are commonly used and these timber planks are glued together. The CLT panels have a high strength and dimensional stability. The timber planks are kiln dried and have a moisture content of about 12% at the end of the process. One of the disadvantages of timber is its sensitivity to moisture content changes, but fortunately CLT is not very sensitive to moisture changes. The CLT panels can be used as floor panels or as shear walls. To get the desired length the panels are finger-jointed. For the CLT floor panels there is the possibility of two-way span behaviour. The mechanical properties of CLT made of spruce C24-lumber are presented in Table 2.1.

The number of layers are an odd number with a minimum of three layers. The grain direction of the outer layers is parallel to the main loading direction. Figure 2.4 shows the layout of a CLT panel with 5 layers.

Table 2.1: Mechanical properties of CLT with C24 board, NEN-EN1194

Strength and stiffness properties CLT		
Bending strength	$f_{m,k}$ [N/mm^2]	24.0
Rolling shear	$f_{r,k}$ [N/mm^2]	1.5
In plane compression	$f_{c,k}$ [N/mm^2]	30.0
Compression perp. to the plane	$f_{c,90,k}$ [N/mm^2]	2.7
In plane tension	$f_{t,k}$ [N/mm^2]	16.5
Shear strength	$f_{v,k}$ [N/mm^2]	2.7
Modulus of elasticity par. to grain	$E_{0,mean}$ [N/mm^2]	12000
Modulus of elasticity perp. to grain	$E_{90,mean}$ [N/mm^2]	370
Rolling shear modulus	$G_{R,mean}$ [N/mm^2]	50
Poisson ratio	ν [-]	0.3
Characteristic density	ρ_k [kg/m^3]	350
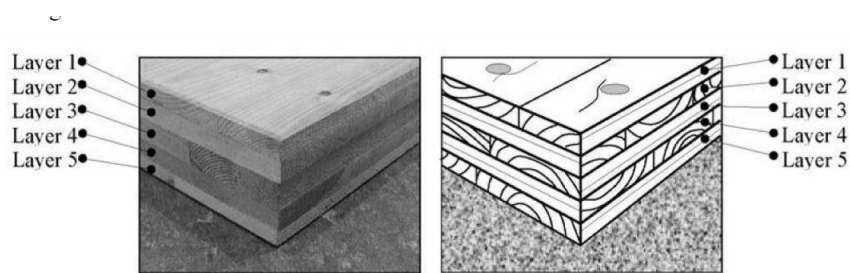
Figure 2.4: A five-layered cross-laminated timber panel (Vessby, 2010)

Mechanically Jointed Beams Theory
The effective bending stiffness can be calculated using the mechanically jointed beams theory which is included in the Eurocode 5 Annex B. The method is developed for mechanically jointed beams but can also be used for CLT. In this theory the effective bending stiffness depends on the connection efficiency factor, γ, and the section properties. The γ-factor is dependent on the the slip characteristics of the fasteners and is equal to one for glued connections. When applying this theory to CLT it is assumed that only the boards oriented in the longitudinal direction are carrying the load (Gagnon and Pirvu, 2011). In this case the rolling shear stiffness of the cross layers can be seen as the stiffness of the imaginary fasteners between the longitudinal layers. This method is only valid for high span-to-depth ratios ($l/d > 30$) since it ignores the contribution of the shear deformation (Gagnon and Pirvu, 2011).

Glued-laminated timber

Glued-laminated timber (GLT) consist of several layers of dimensioned lumber glued together with adhesives. The glued-laminated timber can be used for beams and columns and can also be used for curved elements. The glued-laminated timber has many advantages over traditional solid timber. The beam sizes can have unlimited width and length due to the continuous laminations. However, due to transport limitation the beam length has a maximum of 16 metres. The GLT has higher strength and stiffness properties because the knots are spread more evenly and this leads to a more homogeneous material. Higher quality lamination can be used at the position in which higher levels of stress occur. The planks are kiln dried and have a moisture content of 12 percent. This excludes the danger of damage cause by deformation during the drying process in the construction. Another advantage is that the dimensions are very accurate. This is due the drying of the laminations and the controlled production process. Table 2.2 shows the mechanical properties of glued-laminated timber for the strength classes GL28, GL32 and GL36.

Table 2.2: Mechanical properties of glued-laminated timber (NEN-EN14080, 2013)

Strength and stiffness properties GLT		GL28h	GL32h	GL36h
Bending strength	$f_{m,g,k}$ $[N/mm^2]$	28	32	36
Tension parallel to the grain	$f_{t,0,g,k}$ $[N/mm^2]$	21	24	27
Tension perpendicular to the grain	$f_{t,90,g,k}$ $[N/mm^2]$	0.45	0.45	0.45
Compression parallel to the grain	$f_{c,0,g,k}$ $[N/mm^2]$	27	29	31
Compression perpendicular to the grain	$f_{c,90,g,k}$ $[N/mm^2]$	6.0	6.0	6.3
Shear strength	$f_{v,g,k}$ $[N/mm^2]$	3.0	3.5	3.5
Mean modulus of elasticity parallel	$E_{0,mean,g}$ $[N/mm^2]$	12600	13700	14700
Mean modulus of elasticity perpendicular	$E_{90,mean,g}$ $[N/mm^2]$	420	460	490
5 % modulus of elasticity	$E_{0,05,g}$ $[N/mm^2]$	10200	11100	11000
Mean shear modulus	$G_{0,mean}$ $[N/mm^2]$	780	850	910
Poisson ratio	ν [-]	0.3	0.3	0.3
Characteristic density	$\rho_{g,k}$ $[kg/m^3]$	410	440	480

Laminated veneer lumber

Laminated veneer lumber (LVL) is a mass timber product that consist of multiple layers of thin wood are assembled with adhesives. This product can reach higher strength than glued-laminated timber. Laminated veneer lumber is a product that is quite similar to plywood except that most veneers are parallel and also larger dimensions are available (Blass et al., 1995). In the United States of America laminated veneer lumber has the trade mark Micro-Lam, and in Finland it is also called Kerto-LVL. The thin veneer layers typically have a thickness of 3 to 4mm. Laminated veneer lumber is very suitable for large spans, and is competing with steel large span structures. The LVL also has higher strength properties than glued-laminated wood and can be used in for example trusses. The modification factors k_{mod} and deformation factors k_{def} given in the Eurocode 5 for plywood can also be used for LVL (Blass et al., 1995). A partial safety factor γ_M of 1.3 should be used. Table 2.3 shows the strength and stiffness properties of laminated-veneer timber.

Table 2.3: Mechanical properties of Kerto-S-Laminated-Veneer Timber (Blass et al., 1995)

Strength and stiffness properties Kerto-S-LVL		
Bending strength edgewise	$f_{m,k} \ [N/mm^2]$	51
Bending strength flatwise	$f_{m,k} \ [N/mm^2]$	48
Tension parallel to the grain	$f_{t,0,k} \ [N/mm^2]$	42
Tension perpendicular to the grain	$f_{t,90,k} \ [N/mm^2]$	0.6
Compression parallel to the grain	$f_{c,0,k} \ [N/mm^2]$	42
Compression perpendicular to the grain	$f_{c,90,k} \ [N/mm^2]$	9
Shear edgewise	$f_{v,0,k} \ [N/mm^2]$	5.1
Rolling shear	$f_{r,k} \ [N/mm^2]$	1.5
Mean modulus of elasticity parallel	$E_{0,mean} \ [N/mm^2]$	14000
Mean modulus of elasticity perpendicular, edgewise	$E_{90,edge,mean} \ [N/mm^2]$	430
Mean modulus of elasticity perpendicular, flatwise	$E_{90,flat,mean} \ [N/mm^2]$	130
5 % modulus of elasticity	$E_{0,05} \ [N/mm^2]$	12400
Mean shear modulus	$G_{0,mean} \ [N/mm^2]$	960
5 % shear modulus	$G_{0,05} \ [N/mm^2]$	820
Poisson ratio	$\nu \ [-]$	0.3
Characteristic density	$\rho_k \ [kg/m^3]$	480

2.2. History timber high-rise

In this section an overview is given of the history of tall timber buildings. Some innovative projects that stand out are discussed in more detail further on. Table 2.4 shows a short overview of the history of tall timber buildings. Also some case studies are included to give an idea what visions there are on super tall building in timber.

Tall Wood Building, UBC Common Brocks, Canada

Tall Wood Building is a hybrid wood-concrete tall building located in Vancouver, Canada. The building provides student housing and is part of the campus of the University of British Columbia. The building is 53-metres tall and has 18 stories, and is one of the tallest mass-timber buildings in the world. Figure 2.5 shows the building during the construction in 2016.

The main structure consists of two concrete cores and cross-laminated timber panels supported on parallel strand lumber and glued-laminated timber columns with steel connections (Pilon et al., 2016). The façade is made of prefabricated steel-stud frame panels with wood-fibre laminated cladding. At the ground floor level concrete columns are used instead of timber columns, and a concrete transfer slab is applied at the second floor. The concrete podium at ground level is chosen to get a more open layout at the entrance level due to the fact that larger spans can be created. The parallel strand lumber columns have higher strength properties than the glued-laminated columns and are used at the positions where

Table 2.4: Overview of history timber high-rise (CTBUH, 2018).

Building	City	Stories	Construction System	Status	Completion date
Baobab	Paris	35	Timber/Steel	Proposed	-
Hoho	Vienna	24	Timber/Concrete	Under construction	2017
HAUT	Amsterdam	22	Timber/Concrete	Under construction	2019
TallWood Building	Vancouver	18	Timber/Concrete	Completed	2017
The Treet	Bergen	14	All Timber	Completed	2015
Forte Tower	Melbourne	10	All Timber	Completed	2013
Life Cycle Tower One	Dornbirn	8	Timber/Concrete	Completed	2012
Stadthaus	London	9	All Timber	Completed	2009
SOM Timber Tower	Chicago	42	All Timber	Case study	-
W350	Tokyo	82	Timber/Steel	Case study	-
Oakwood Tower	London	80	All Timber	Case study	-
River Beech Tower	Chicago	80	All Timber	Case study	-

the floor loading is high. A steel perimeter beam is applied at each floor level to stiffen the edge of the perimeter CLT panels and support the building envelope (Pilon et al., 2016). The cross-laminated timber panels are joined together by a 25mm thick plywood spine screwed to each panel. The floor panels have a 40mm thick concrete topping. This concrete layer increase the acoustic properties and also provides additional fire protection. In tall wood building this additional concrete mass also has a positive influence on the wind-induced behaviour of the structure. The CLT panels are 169mm thick and the typical glued-laminated timber columns have a dimension of 265mm x 265mm. The roof structure is made of metal decking on steel beams, and this is done to avoid any water-damage issues. The erection speed of the building was high due to the high prefabrication and the light weight of the timber structural elements.

Figure 2.5: Tall wood building, UBC Brock Commons Vancouver (Pilon et al., 2016)
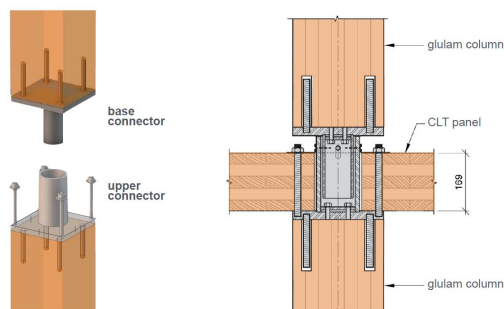
Figure 2.6: Connection detail, Tall wood building, UBC Brock Commons Vancouver (Pilon et al., 2016)

Case study SOM

The Skidmore, Owings, and Merril LLP (SOM) design group has done a research project for a conceptual timber structural system for tall buildings in 2014. A consisting tall concrete building located in Chicago was used as a reference project. This made it also possible to compare the material quantities an the carbon footprint. Figure 2.7 shows the three dimensional view of the case study (SOM, 2014). The building has 42-stories and the goal was to use as most timber elements as possible. This resulted in a design of cross-laminated timber shear wall panels, glued-laminated timber columns and cross-laminated timber floor panels. For the floor slabs cross-laminated panels are used with on top a precast composite topping. The floor panels are moment connected to the CLT shear walls and to the timber columns with a reinforced concrete beam and joint. Along the length of the wall runs a reinforced concrete joint. This type of timber-concrete connection has not been applied before and SOM has done a study for this connection type. A connection detail of this concrete

joint is shown in figure 2.8. In the link beams large stresses will occur and therefore those are designed with reinforced concrete. The case study also considers composite structural systems because this can lead to more economical buildings (SOM, 2014).
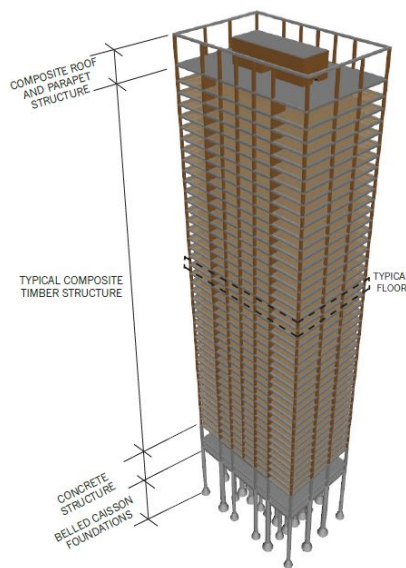
Figure 2.7: 3D view of SOM case study (SOM, 2014).
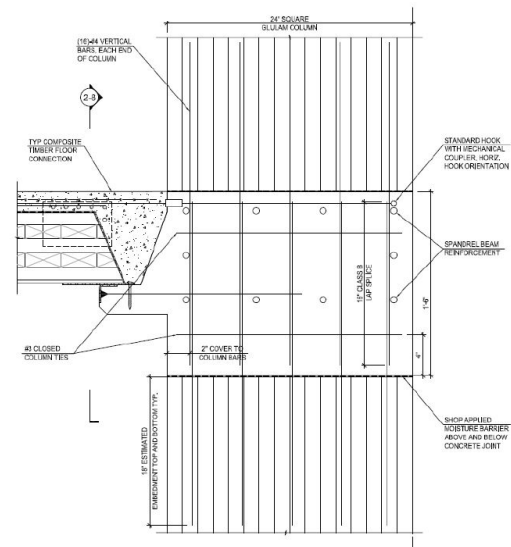
Figure 2.8: Typical column connection detail (SOM, 2014).

Case study Oakwood tower

The Oakwood tower is a proposal by PLP architects for an all-timber skyscraper located in London. The tower has a height of 300-metres and the used timber elements have a volume of around 65.000 cubic metres. The largest timber columns have a dimension of 2.5 x 2.5 metres, and the timber walls at the base have a thickness of 1.75 metres. The structure makes use of mega bracing at the perimeter for the stability. The mega bracing consist of large glued-laminated timber elements. According to Smith and Wallwork (2017) structural engineers, who worked on the structural design, the structure would be four times lighter than an equivalent concrete frame tower. Figure 2.9 shows the 3-D view of the Oakwood tower and the occurring forces and deflections due to gravitational loading.
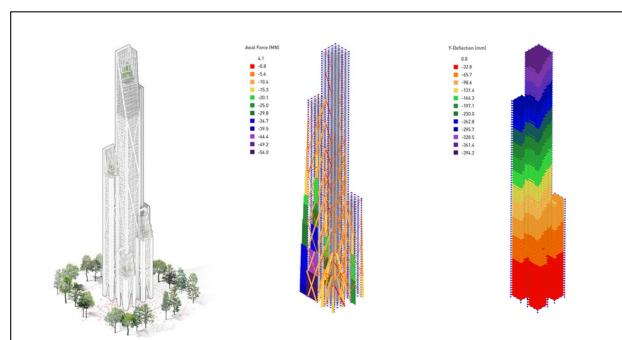
Figure 2.9: Oakwood tower London (PLP-architecture, 2017).

W350 Tokyo

The W350 building is a proposal for the tallest timber building in the world with a height of 350 metres. The Japanese construction company Sumitomo Forestry wants to deliver

this building in 2041. The building will contain 180 000 m^3 timber, which is 90% of the total structural building material (Sumitomo, 2018). The building will also contain steel, and because of this it should be classified as a hybrid wood-steel super tall building. The timber frame will consist of glued laminated timber beams and columns. Diagonal steel braces are placed in the framework to resist the wind and earthquake loading, and creates a braced tube structure. How the structure will behave during extreme wind and earthquake loading is not known yet. The timber elements can be reused for other building projects after the life cycle of the building, and can be used as biomass in the end (Sumitomo, 2018). Figure 2.10 and 2.11 show the three-dimensional view and an impression of the interior of the W350 building, respectively.

Figure 2.10: 3D-view of W350 (Sumitomo, 2018).

Figure 2.11: Impression of interior (Sumitomo, 2018).

Treet, Norway

The 'Treet' is a 14-storey timber residential building located in Bergen, Norway. The structural design consist of glulam trusses and two intermediate strengthened storey levels. Prefabricated building modules are used for the 62 apartments and are stacked on top of the concrete parking level at the base. CLT panels are used for the balconies, elevator shaft and internal walls. The CLT panels are not part of the main load-bearing system. Figure 2.12 shows the 3D view of the building which is located next to a large road bridge. The main structure that gives the building the required stiffness are the glulam beams, columns and braces. The CLT walls do not contribute to the main lateral stability system. The prefabricated modules are stacked up every four storey levels. The first four storey levels are stacked on top of the concrete garage, and the other modules are supported by the strengthened storey levels. The two strengthened storey levels consist of a glulam truss and a concrete top layer connects the trusses. An other advantage of the addition of the concrete slab is the addition of mass to the structure which helps to improve the dynamic behaviour.

The building has a footprint of 23 by 21 metres and has a height of 45 metres. The clearance between the modules and the glulam trusses is 34mm to allow for horizontal movements. The timber connections of the glulam members are done with slotted steel plates, which is a common connection type in timber bridges. The façade consist of glass and metal sheeting, and protects the timber from the rain. The fire safety resistance is 90 minutes for the main structure. The reduced cross-section method according to the Eurocode is applied for the fire safety design. This method leads to a charring depth of 63mm, and based on this all the steel plates and dowels are placed at a minimum distance of 70mm from the surface. The gaps in the timber connections are covered by a fire resistant gap filler. The building was completed in the autumn of 2015.

Figure 2.12: Treet building in Norway (Abrahamsen and Malo, 2014).

2.3. Design issues for tall timber structures

Tall timber structures have several important design aspect which should be given enough attention to, such as fire safety and vibrations. The design issues are discussed in this section.

Fire safety

The fire safety is still one of the first things that come to mind when building with timber. This is also due to historical accidents such as the Great Fire of London in 1666 and the Boston fire in 1872. The main reason why buildings have burnt down in the past is due to the absence of fire compartments, fire-fighting technologies, and fire detection and suppression (Smith and Frangi, 2008). Still a lot of building codes have restrictions for the height of timber buildings to about four stories. Nowadays, the timber buildings are much better protected against fire and do not burn down before the fire fighters arrive. This is due to the usage of mass timber elements and/or non-combustible surface protection. The large mass of the mass timber elements develops a coal layer on the outside during a fire which protects the rest of the timber. This in combination with sprinkler installations should suggest that there is no continuing reason to limit the permissible height of timber buildings (Smith and Frangi, 2008).

Floor slab vibrations

Timber floor panels are light-weight and therefore will be more sensitive to vibrations due to foot-fall. The eigenfrequency of the floor panel should be estimated and should be above a certain limit according to the building code. Acoustic measurements could be necessary for the floor design. A additional concrete top layer could be applied to give the floor design more mass, and this will improve the dynamic behaviour of the floor slab.

Differential Vertical Shortening

Figure 2.13 shows the differential shortening effect of the concrete core walls and the timber columns. The concrete core walls will shorten due to creep, elastic shortening and shrinkage. The timber columns will shorten due to shrinkage, elastic shortening, creep and joint settlement. The shortening of the concrete core walls will differ from the timber columns and can also be seen in figure 2.13. In the case a tall hybrid wood-concrete structure is designed the differential shortening should be accounted for. This could be done by adjustment of the height in the joints which is the solution applied in the Tall Wood Building in Vancouver. Another solution could be to already adjust the length of the timber columns in the factory. The effect of differential shortening is not only a problem for hybrid structures but will also occur in tall concrete buildings between the core walls and the concrete frame. However, for concrete buildings it is easier to solve due to the fact that adjustments to account for the

settlement are easily made with in-situ concrete.
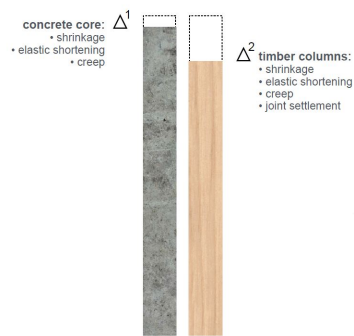
Figure 2.13: Differential shortening between concrete core and timber columns (Pilon et al., 2016).

Peak accelerations

Timber buildings are light-weight structures and therefore sensitive to wind-induced vibrations. The wind fluctuations will make the building sway and this could cause discomfort and nausea for the occupants. The peak accelerations are often the governing criterion for the structural design. Especially, for tall buildings the acceleration in the across-wind can be expected to be large. The large across-wind accelerations are due to the vortex shedding of the wind.

Uplifting forces

The light-weight of the structure reduces the weight on the foundation. Tension forces could occur in the foundation piles due to the wind loading. These tension forces are also called the uplifting forces. The uplifting force in the foundation should be checked and adequate reinforcement should be added.

2.4. Structural timber connections

The connections should provide sufficient structural strength to transfer the loads. In the case the connections are well designed they also mitigate the moisture ingress. Another important design aspect is to avoid excessive tension perpendicular to the grain. The structural frame of the design consists of glued-laminated timber and therefore first a general overview on the different types of glued-laminated timber connections are given. Figure 2.14 shows the load-slip graphs for different types of joints from a research done by Dallas in 2005. It can be seen that the glued-in rod connection has the highest strength and stiffness. On the other hand, the dowel type connection has a much smaller strength and stiffness, but a much higher plastic deformation capacity (Dias, 2005). A high plastic deformation capacity could be useful for seismic design in particular.

Glued connection

The glued connection is a moment-resistant connection between glued-laminated members. Due to the the high stiffness of the connection it should not be applied in seismic design due to its lack of ductility (Buchanan and Fairweather, 1993). In the case the design has an elastic response the glued connection can be applied. The connection failure will be brittle. The connections have a good fire resistance and should be glued in the factory. However, the gluing in the factory can cause transportation problems. Figure 2.15 shows two examples of a glued connection applied in a portal frame.

Nailed connection

Figure 2.16 shows an example of a nailed beam-column connection for a multi-storey building. The thin steel side plates are nailed onto the GLT structural members. It is also possible
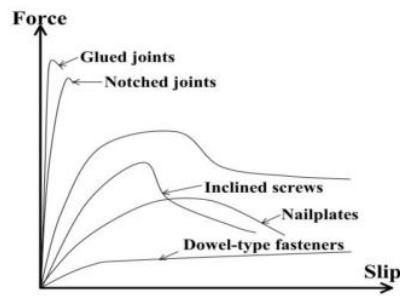
Figure 2.14: Typical load-slip behaviour for different types of joints, (Dias, 2005)
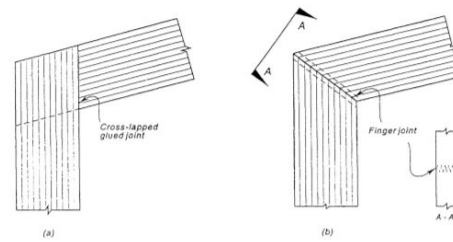
Figure 2.15: Glued portal frame knee joint connections, (Buchanan and Fairweather, 1993)

to use plywood side plates or a composite plywood-steel side plate. This connection has an average strength and stiffness as can be seen in figure 2.14. The nailed connection type is functional but expensive due to the large number of holes that need drilled, and also it has a poor fire resistance (Buchanan and Fairweather, 1993).

Dowel connection

Figure 2.17 shows a dowel type connection for a multi-storey building. The steel rods are driven into pre-drilled holes in the glued-laminated timber. The connections are easily assembled, however it is difficult to develop full strength of the GLT members (Buchanan and Fairweather, 1993). In the case slender dowels and large spacing are applied the connection has good energy dissipating characteristics. On the other hand when thick dowels and small spacing are applied the connections tend to brittle failure. The connections should be designed in such a way that ductile failure will occur instead of brittle failure. This assumption is also implemented in the design rules of Eurocode 5.
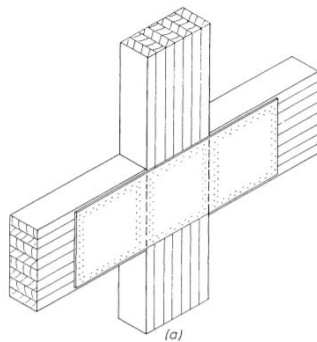
Figure 2.16: Nailed beam-column connection for multi-storey building (Buchanan and Fairweather, 1993).
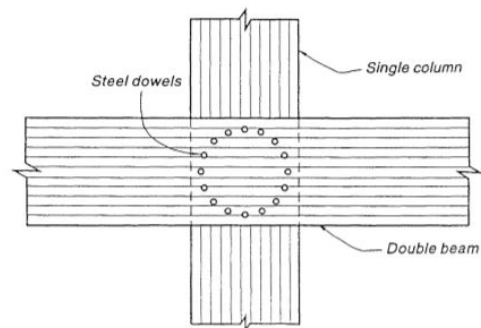
Figure 2.17: Dowel beam-column connection for multi-storey building (Buchanan and Fairweather, 1993).

Figure 2.19 shows the glulam Kjilster bridge in Norway. The bridge has a span of 158 metres, and is designed by the structural engineer Rune Abrahamsen. The timber bridge connects two military training areas, and is therefore designed for heavy military transport. Figure 2.18 shows a detail of the connection in the timber truss. The glulam members are connected with slotted steel plates and dowels.

Epoxied connection

Figure 2.20 shows an epoxied connection with steel rods for a multi-storey building. There are many variants of a epoxied connection with steel rods, and it is also possible to use the connection without a steel box profile in between the column and beam. A glued-in rod timber connection has a high strength and a low ductility. This is similar to the strength stiffness characteristics of glued joints without steel rods. In figure 2.14 the typical load-slip
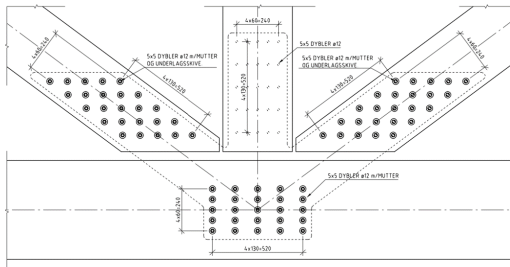
Figure 2.18: Detail of Kjilster Bridge in Norway designed by SWECO.

Figure 2.19: Kjilster timber bridge in Norway (photo by: SWECO Norge AS).

behaviour of glued joints can be seen. Design formulas for this connection are not included in the Eurocode but can be found in the German DIN1052.

Failure mechanisms for a glued-in rod:

- Yield failure of the rod
- Shear failure along the rod
- Tensile failure of timber cross-section
- Splitting failure of timber
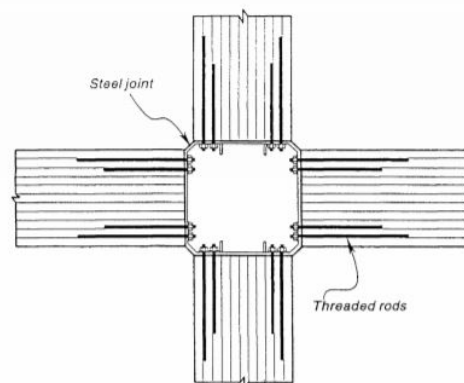
Figure 2.20: Epoxied connection beam-column connection for multi-storey building (Buchanan and Fairweather, 1993).

Screws connection

The screw connection is also a good option for timber connections. The thread of the screws reduces the slip in the connection and the pull-out strength is increased. For example, the screw connection could be used for connecting the CLT floor panels to the adjacent supporting beams. The screw connection can also be applied for connections in which large forces occur. Figure 2.21 shows a reference project of a large timber screw connection used in a truss. From tests at the university of Stuttgart this connection has an ultimate load per shear plane of about 6.5 MN (Blass, 2010).

Continuous tie-down systems

Continuous steel rods can be placed inside the timber to tie-down the structure to the foundation. This is typically done to withstand the uplift forces due to lateral wind loading. Also timber elements can be post-tensioned with steel rods. This way the timber element can withstand larger tension forces. The post-tensioned elements are especially used in earthquake design. Figure 2.22 shows the interconnecting detail of steel tension rods which post-tension the CLT-panels in the H8 building, which is located in Bad Aibling, Germany.

Figure 2.21: Large timber screw connection in truss (Blass, 2010).
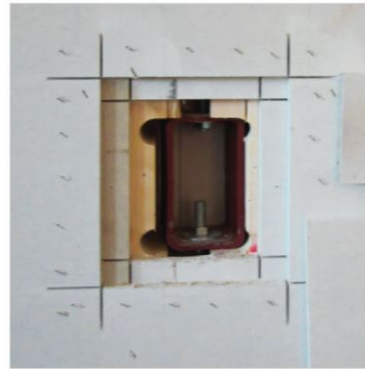
Figure 2.22: Steel tension rods interconnecting in H8 building (Mayo, 2015).

Connections under lateral wind loading

In multi-storey timber buildings the connections are an important design aspect. The connections are the governing for the strength of the building, and the steel connectors will start yielding before the brittle failure in the timber can occur. For the wind load design the structure's response can be modelled as linear elastic, and therefore the design does not rely on the ductility in the connections which would be the case for a seismic design. In the case frame action is used the connection should be designed as moment resisting connections. An alternative is to design a pin-jointed gravity frame and the lateral loads are resisted by shear walls (Buchanan and Fairweather, 1993). In practice it is difficult and expensive to design fully moment resisting connections in the timber frame and therefore the connections are designed as semi-rigid.

Stiffness characteristics connections

The stiffness of the fasteners is represented by K_{ser} which is the stiffness modulus. The stiffness modulus is dependent on the material properties of the timber, the diameter of the fastener and the type of the connection. In the case a dowel type connection is used most of the slip in the connection is caused by the tolerance of the pre-drilled holes for the fasteners. Also yielding of the dowels or the timber which gets compressed could cause additional slip in the connection. In the Eurocode 5 the stiffness modulus for a connection is given as follows:

$$K_{ser} = \sum_{i=1}^{s} \sum_{j=1}^{n} \rho_m^{1.5} \cdot \frac{d}{23} \tag{2.1}$$

Where:

n is the number of fasteners in the connection

s is the number of section in the connection
ρ_m is the mean density of the timber
d is the diameter of the fastener

The rotational stiffness in the connections is dependent on the placing of the fasteners and the stiffness of the fasteners. The rotational stiffness can be calculated as follows:

$$K_{rot;connection} = K_{ser;fastener} \cdot I_p \qquad (2.2)$$

Where:

$K_{ser;fastener}$ is the stiffness in one fastener
I_p is the polar moment of area

Figure 2.24 shows the typical hysteretic behaviour of a structural timber connection. The hysteretic behaviour is the load deformation response of timber connections under cyclic loads, and the strength of the connection degrades under cyclic loading. In the first loading cycle the load-deformation curve follows the virgin curve. The cyclic loading may cause cavities in the timber around the fasteners. The crushing of the timber around the fasteners is called 'pinching' (Boellaard, 2012). The fasteners loose contact with the timber and should should regain contact which creates a new load path shown in figure 2.24. The connection are assumed linear elastic for the lateral wind load design. Therefore the timber connections will probably not reach the point where the 'pinching' effect occurs. In the case the model stays in the elastic range, the hysteresis damping is in principle zero. Figure 2.23 shows the typical load-deformation loops for a dowel-type joint in the elastic range. For structures with a low amplitude due to dynamic vibrations, a viscous damping less than 1 percent can be measured (Blass et al., 1995). However, the total damping ratio in elastic range is usually assumed as 5 percent. This is due to the fact that the damping ratio due to friction between the different elements, and the damping due to compression perpendicular to the grain can reach 4 percent or more (Blass et al., 1995).
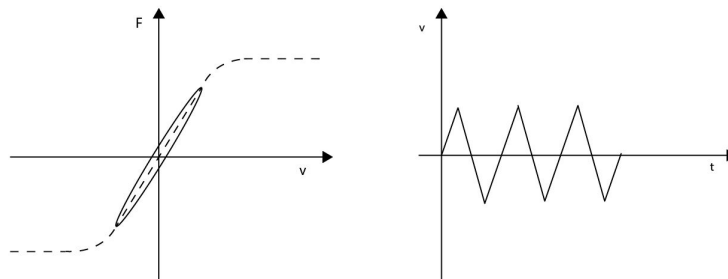
Figure 2.23: Typical load-deformation loop for dowel-type joint under cyclic loading in elastic range (Blass et al., 1995).

The timber elements exhibit a generally linear elastic behaviour under cyclic loading (Blass et al., 1995). The timber will experience brittle failure and there is little dissipation of energy. In the case glued joints are applied the connection can be seen as a rigid and will behave linear elastically. On the other hand, in the case a dowel-type connection is applied the connection can be seen as semi-rigid, and plastic deformation will occur in the fasteners. Energy dissipation can be achieved in the connections.
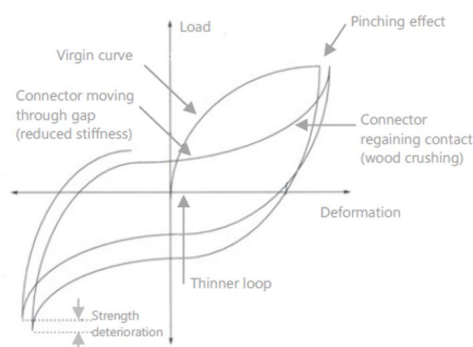
Figure 2.24: Hysteretic behaviour of structural timber connection (Thelandersson and Larsen, 2003).

2.5. Lateral stability systems

Tall buildings can be designed with several different types of lateral stability systems. Over the last decades a lot of new lateral stability systems are implemented which make it possible to build higher each time. Figure 2.25 gives an overview of the several option of the lateral stability systems and their practical height. A division is made between steel, concrete and composite systems.

Table 2.5 shows the maximum storey height for each system, and based on this a choice can be made for the preferred lateral stability system. In this case the construction material composite means that the used structural materials are a combination of steel and concrete. However, in most cases this could also be applied for a combination of timber and concrete.

Table 2.5: Overview limit no. of storey levels for several lateral stability systems (Sarkisian, 2016)

System	Limit no. of stories	Limit height [m]	Construction material
Concrete Frame	20	67	Reinforced Concrete
Concrete Shear Wall	35	115	Reinforced Concrete
Concrete Frame – Shear Wall	50	163	Reinforced Concrete
Concrete Framed Tube	55	179	Reinforced Concrete
Concrete Tube-in-Tube	65	214	Reinforced Concrete
Concrete Modular Tube	75	246	Reinforced Concrete
Concrete Diagonal Braced Frame	90	294	Reinforced Concrete
Concrete Belt Shear Wall-Stayed Mast	110	358	Reinforced Concrete
Concrete Diagonal Mesh Tube Frame	120	390	Reinforced Concrete
Composite Frame	30	122	Composite
Concrete Shear Wall – Steel Gravity Columns	45	182	Composite
Concrete Shear Wall – Composite Frame	60	246	Composite
Composite Tubular Frame	65	266	Composite
Composite Tube-in-Tube	75	306	Composite
Composite Modular Tube	75	306	Composite
Composite Diagonal Braced Tube	90	366	Composite
Composite Belt Outrigger-Stayed Mast	110	446	Composite
Composite Diagonal Mesh Tube Frame	120	486	Composite

Outrigger/belt-truss system

The outriggers have the function to provide additional stability to the core. The outrigger system provides a lever arm for the global bending moments. The outrigger system can have several lay-outs. A common layout is to make steel trusses from the stability core to the perimeter of the building. The façade at the outrigger level is made stiff with a belt-truss, and this belt-truss activates the all the perimeter columns. Another option for an outrigger
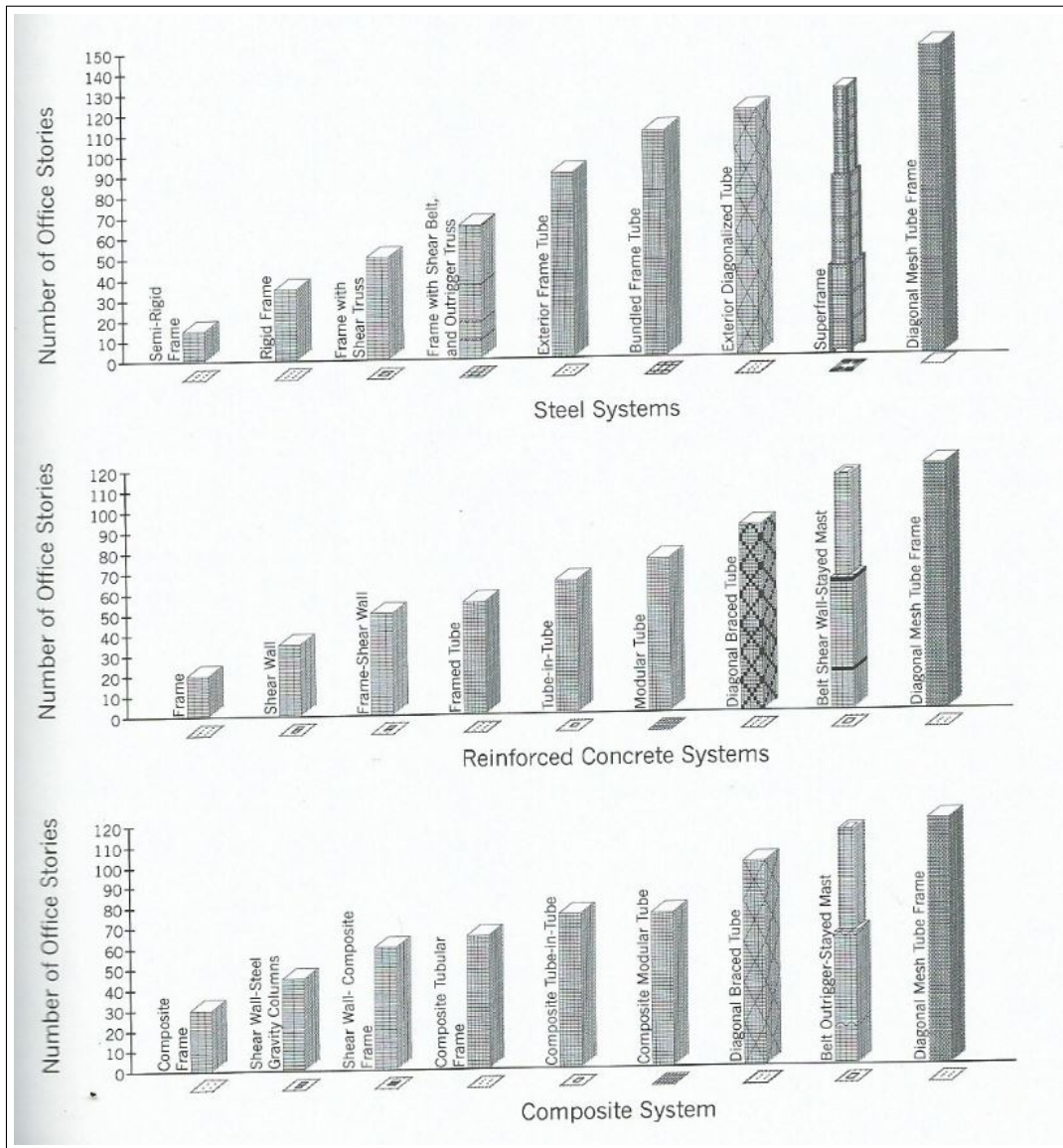
Figure 2.25: Overview lateral stability systems and their practical height (Sarkisian, 2016).

system is to make a very stiff concrete level. In this case the stiff concrete slab acts as a lever arm to withstand the lateral wind load.

The outrigger system makes the floor space less functional for residential function and therefore it is often decided to place the mechanical, electricity and plumbing (MEP) facilities at this location. The outrigger levels can also provide a division between the timber section for fire safety reasons. For a tall building with uniform characteristics the optimum height of for one outrigger system is at 0.455 times the height (Taranath, 2010). Therefore, the optimal position is not at the top of the building which is perhaps unexpected. In the case the outrigger is placed at the top only a maximum reduction of the storey drift of fifty percent can be achieved compared to seventy-five percent reduction for an outrigger positioned at mid-height (Taranath, 2010). However, for architectural reasons it can be preferred to place the outrigger system at the top of the building. The rule-of-thumb for two outriggers is at one-third and two-thirds heights, and for three outriggers is at one-quarter, two-quarters and three-quarters height (Taranath, 2010). Figure 2.26 shows the method of analysis for two outriggers system.
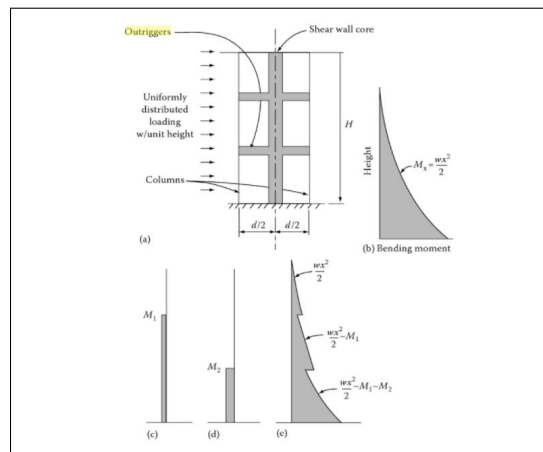
Figure 2.26: Method of analysis for two outriggers system: a) two-outrigger structure, b) external moment diagram, c) M1 diagram, d) M2 diagram and e) core resultant moment diagram (Taranath, 2010).

Diagonal braced tube-in-tube system

A tube-in-tube system consists of two rigid tubes along the height of the tall building. A reinforced concrete core is common for these type of structures. The outer tube is the perimeter of the building. The perimeter of the of the building can be made stiff with diagonal bracing and is also called a mega braced frame system. A mega braced frame system consists of large diagonal elements that span over multiple floor levels. These diagonal element stiffen up the structure's perimeter and therefore the global stiffness of the building. If this system is applied in combination with a stiff core the system it is classified as a tube-in-tube system.

2.6. Wind engineering

Introduction

Wind is an important design aspect for tall buildings and is in most cases governing for the design of the main structure. The effect of the wind loading on the building should be checked on the following three aspects: the structure should have sufficient strength to resist the wind-induced forces, the structure should have adequate stiffness to satisfy the occupant comfort and serviceability criteria, and the wind may produce a dynamic response of the structure (Boggs and Dragovich, 2006). The dynamic response can amplify the first two aspects and therefore has particular importance. For the design of tall buildings the ultimate limit state design is nowadays well known. However, there is less known about the serviceability limit state design for tall buildings which is of great importance for tall buildings. The tall buildings are getting more slender and light-weight which make them more sensitive to dynamic loads (Oosterhout, 1996). The wind-induced vibrations may cause discomfort for the occupants in the building. At an early design process attention should be devoted to the control of the vibrations (Oosterhout, 1996). In the case the dynamic behaviour is only checked at the end of the design process this can lead to a lot of additional costs. At that point the design can not easily be changed any more and expensive auxiliary damping systems could be required. The most commonly used method for wind design of buildings is the equivalent static wind load. The wind load calculation in the Eurocode is also based on this method.

Irwin identifies the following wind issues for the structural design of tall buildings: structural integrity under ultimate loads, deflections under service loads, building motions and occupant comfort, uncertainties in building structural properties, uncertainties in wind loading and the uncertainties in wind climate. The damping and stiffness are the building structural properties which can have large uncertainties in the case there is not adequate experimental data available. There is not many experimental data available for timber buildings, and

therefore it is difficult to set a realistic damping ratio of the structure without experimental verification.

The horizontal wind load can be split up into the along-wind and the across-wind load. In this chapter the wind response spectrum method and the occupant comfort serviceability criteria will be discussed.

Along-wind response

The along-wind response displacement is in most cases governing for tall buildings. For the determination of the along-wind load a wind response spectrum can be used. Figure 2.28 shows an overview of the components included into the wind response spectrum. It can be seen that the important parameters from the oncoming wind are the mean wind velocity and the turbulence. The building shape will also have a large influence on the wind-induced behaviour. The effect of the wind can be split up in two parts: the mean wind velocity and the fluctuating wind velocity. Figure 2.27 shows the random vibration of the wind and the statically defined average wind pressure, w_s, and the pulsation wind pressure, w_p.
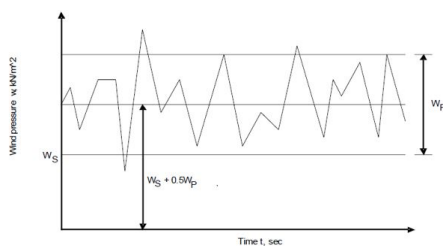
Figure 2.27: Wind effect due to pulsation (Auta et al., 2006).
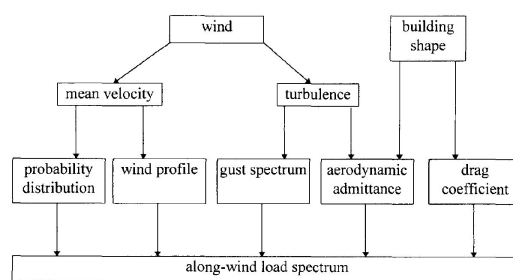
Figure 2.28: Dynamic along-wind load assessment scheme (Oosterhout, 1996).

Across-wind response

Especially for cylindrical-shaped building the across-wind can become an major concern. For tall slender buildings with a rectangular shape the wake excitation can also become governing. The most effective counter measure is to reduce the vortex-shedding. For example, this can be done by adjusting the façade elements or to make openings in the façade. Figure 2.30 shows the influence of several shapes on the vortex shedding. It can be seen that cylindrical shaped buildings have the poorest vortex-shedding behaviour and that openings in the facade give a much better vortex-shedding behaviour. It is recommended to check the across-wind response for flexible tall buildings. The National Building Code of Canada (NBCC:2005) and the Dubai wind code give several conditions and if one of those requirements is fulfilled the code recommends that also the across-wind vibrations should be checked.

The NBCC advices the designer to check the vibrations in serviceability limit state according to the ISO standard. This international building code gives several conditions, and if one of those is fulfilled the across-wind response should also be checked. The conditions are stated below (Kryh and Nilsson, 2012):

- the building height is greater than four times its minimum effective width;
- the building height is greater than 120 m;
- the building is light-weight;
- the building has low frequencies;
- the building has low damping properties;

The main cause of the across-wind load is the vortex shedding of the wind. It can be seen that also for rectangular shaped tall buildings a large vortex shedding effect occurs. The vortex

shedding is dependent on the Strouhal number and is especially very large for cylindrical shapes. The shedding frequency N is given by:

$$N = S \cdot \frac{U}{b} \tag{2.3}$$

Where:

S is the Strouhal number
U is the wind velocity
b is the building width

Figure 2.29 shows the wind vortex shedding for a tall building in a wind tunnel test. The vortex shedding can be reduced with optimizing the shape of the building. Shape strategies are: softening of the corners, tapering and setbacks, varying cross-section shape, spoilers and porosity or openings (Irwin, 2010).
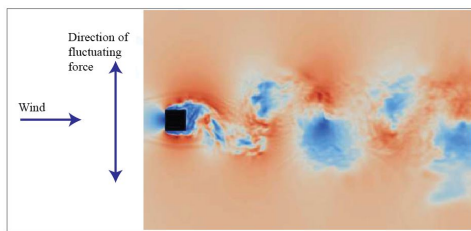
Figure 2.29: Vortex shedding effect for a tall building in a wind tunnel test (Irwin, 2010).
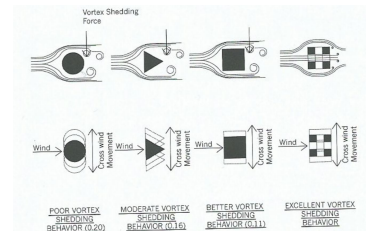
Figure 2.30: Vortex shedding for several shapes (Sarkisian, 2016).

Figure 2.31 shows the aerodynamic load spectra for the along-wind and across-wind components. As can be seen the along-wind component decreases with the natural frequency of the building. However, the across-wind component has an intermediate peak and this is caused by vortex shedding. This peak could greatly affect the resonant response (Boggs and Dragovich, 2006).
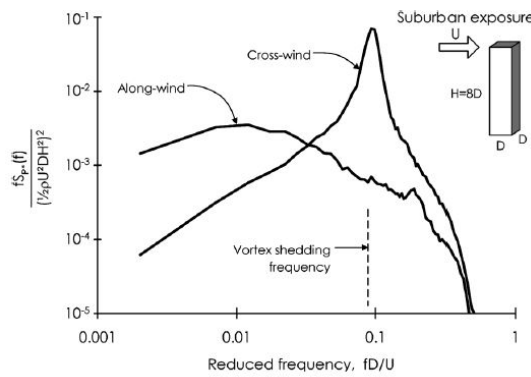
Figure 2.31: Aerodynamic load spectra measured on a wind-tunnel model (Boggs and Dragovich, 2006).

Dynamic wind load

The dynamic wind load is varying over time and the wind direction will also vary over time. The dominant frequency for the wind load is low compared to the dominant frequency for earthquakes. Therefore, structures with a low natural frequency are more vulnerable for wind loading. Tall buildings have a lower natural frequencies than short buildings, and this means the wind load is often decisive for the tall building design. Figure 2.32 shows the
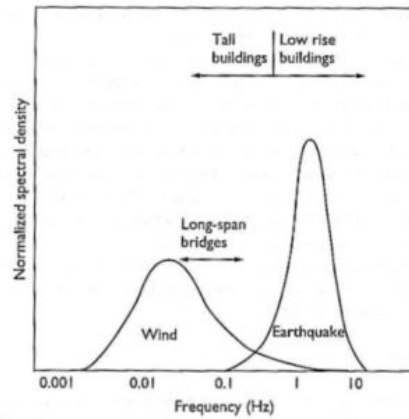
Figure 2.32: Dominant frequency of wind and earthquake load (Holmes, 2007).

dominant frequencies for wind and earthquake loading.

The dynamic wind load can be classified into three categories according to Davenport:
- Wind-induced loading caused by buffeting of oncoming wind in along-wind direction;
- Wind-induced loading from unstable flow phenomena, such as vortex shedding, separation and reattachment effects;
- Wind-induced loading which is caused by the wind-induced excitations of the structure.

The dynamic wind load can cause the following design issues:
- Exceeding the serviceability requirements for the displacements and accelerations;
- Fatigue due to cyclic-loading;
- Mechanical damage due to high dynamic loading;

A high dynamic load can occur in the case the wind vibrations induce a large dynamic response of the structure. This happens when the frequency of the dynamic wind load is close to the natural frequency of the building. The structure's natural frequency is dependent on the stiffness, geometry, mass distribution and the damping properties. Therefore, these properties are important for improving the dynamic behaviour and to satisfy the functional requirements.

Equivalent static wind response spectrum

The response to the wind load can be calculated with the equivalent wind response spectrum method. The along-wind load can be determined with the help of a spectrum of the turbulent along-wind velocity fluctuations. The wind spectrum method from Davenport is the most well-known and is based on a stochastic approach (Oosterhout, 1996). The along-wind load calculation according to the Eurocode is also based on the principles of Davenport. The main difference in the Eurocode is that the wind spectrum by Solari is used instead of the wind spectrum by Davenport. Figure 2.33 shows the wind spectra by Davenport and Solari. It can be seen that especially for the low frequencies the Solari spectrum is more accurate than the spectrum by Davenport. This is probably one of the reasons that the Eurocode recommends to use the wind spectrum by Solari. The wind spectrum method is also called the gust factor approach and will be discussed in more detail further on.

Figure 2.34 shows the procedure of the equivalent wind response spectrum method by Davenport. The method is based on the premise that the along-wind motion of a tall slender building is driven primarily by the onset turbulence (Tamura and Kareem, 2013). The turbulence excites the structure as a single degree of freedom system with low damping. The response is divided in three parts: the static response, the background response and the res-
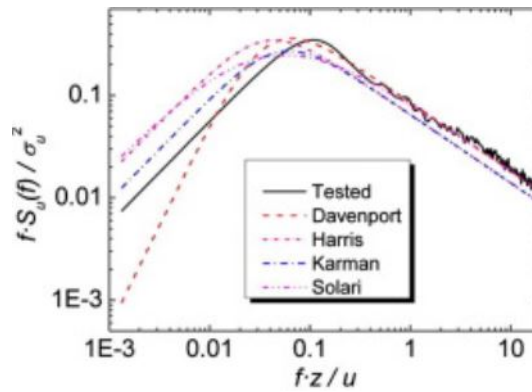
Figure 2.33: Comparison of wind spectra by Harris, Solari, Davenport, Karman, and the spectrum from wind tunnel tests on the Kilometer skyscraper (Sun et al., 2017).
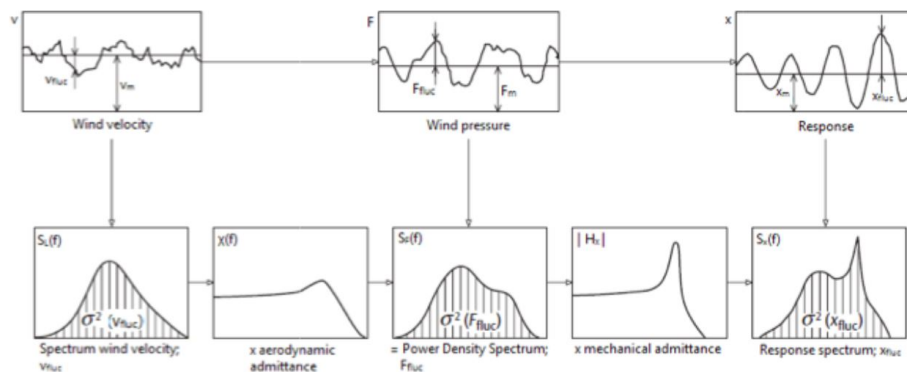
Figure 2.34: Wind spectrum method by Davenport (Holmes, 2007).

onant response. The static response is due to the mean wind load, and the background and resonant response are due to the fluctuating wind load. In the case the natural frequency of the wind is close the structure's natural frequency it is classified as the resonant response. The background response is dominant for structures with a low natural frequency and for structures with a higher natural frequency the resonant response becomes more significant (Holmes, 2007). The building should be designed such that the natural frequency is as far as possible from the resonant response. The stiffness, mass, and damping properties can be varied to change the natural frequency of the building. The spectral analysis can be used to determine the dynamic response.

Occupant comfort

The occupant comfort is an important aspect for tall buildings. The occupants can experience discomfort due to swaying in the top floor levels. For the serviceability criteria limits are set on the acceleration at the top floor. The acceleration can be presented in two ways: with the peak acceleration or normalized root-mean-square (RMS) values. The peak accelerations are a good indicator for the human motion threshold and are also used in the Eurocode. However, when evaluating the continuous nature of vibration it is better to use the RMS values (Boggs, 1995). Therefore, the peak accelerations are good for studying the vibrations induced by gust winds which have a short duration and high magnitude, and the RMS are studied in the case the vibrations have a lower magnitude with a longer duration (Kryh and Nilsson, 2012). Table 2.6 shows the different ranges of the human perception levels on wind-induced acceleration. It can be seen that the perception levels vary per person and sensitive people can already perceive motions below $0.10 \; m/s^2$.
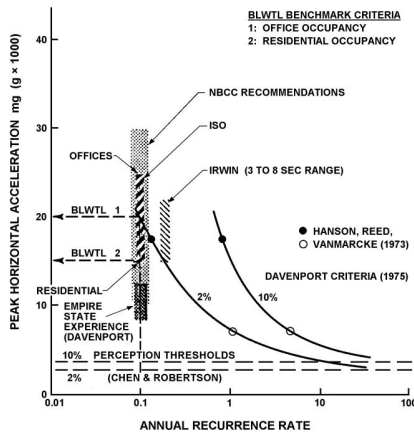
Figure 2.35: Peak acceleration limits versus return period (Boggs, 1995).
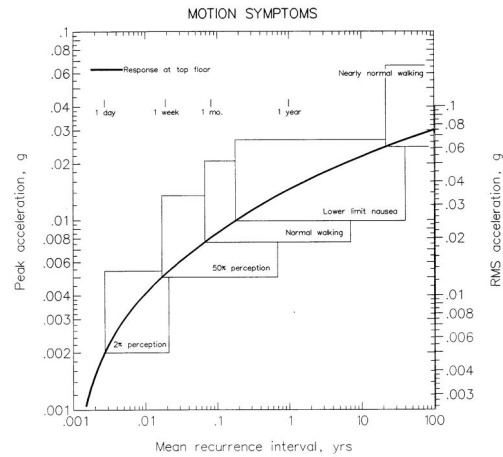
Figure 2.36: Motion symptoms for a typical tall building (Boggs, 1995).

Table 2.6: Human perception levels of response acceleration (Smith and Coull, 1991).

Range	Acceleration [m/s^2]	Effect
1	< 0.05	Humans cannot perceive motion.
2	$0.05 - 0.10$	Sensitive people can perceive motion; hanging object may move slightly.
3	$0.10 - 0.25$	Majority of people will perceive motion; level of motion may affect desk work; long-term exposure may produce motion sickness.
4	$0.25 - 0.40$	Desk work becomes difficult; ambulation still possible.
5	$0.40 - 0.50$	People strongly perceive motion.
6	$0.50 - 0.60$	Most people cannot tolerate motion and are unable to walk naturally.
7	$0.60 - 0.70$	People cannot walk or tolerate motion.
8	> 0.85	Objects begin to fall and people may be injured.

Figure 2.35 shows the peak acceleration limits for different codes and researches. As can be seen the building codes only give requirements for a certain return period. Figure 2.36 shows the peak accelerations plotted against the return period and indicated the motion perception for the occupants in the building. It can be seen that there is also a difference in perception level for the occupants, and not every occupant will experience the same motion symptoms. Therefore, a separation is made between 2% and 50% of the occupants experiences motion symptoms. The serviceability criteria are based on the motion symptoms and the recurrence of the event. The limit for the peak response accelerations is dependent on the structure's eigenfrequency. The criterion is also based on the function of the building, and is divided in two categories: the office building and the residential buildings.

Eurocode

The peak response acceleration at the top floor can be calculated using the Annex B in the EC1-4. The peak accelerations are calculated for a return period of 50 years. The Dutch Na-
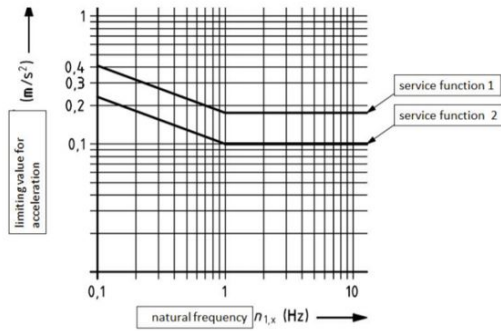
Figure 2.37: Acceleration criteria according to Dutch National Annex on NEN-EN1991-1-4
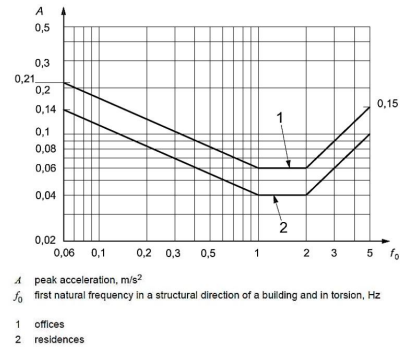
Figure 2.38: Occupant comfort criteria for wind-induced vibrations for a one-year return period according to ISO 10137 (ISO, 2007).

tional Annex on the NEN-EN1990 gives recommendations for the peak accelerations. A distinction is made between buildings with the functions residential and offices. The buildings with a residential function have stricter rules for the occupant comfort than office buildings. Figure 2.37 shows the limits for the peak accelerations at the top floor level.

ISO 10137

The ISO10137 standard building code includes different levels of acceptable vibrations in tall structures depending on the occupancy and function of the building (Hallebrand and Jakobsson, 2016). The criteria that are included in the ISO10137 standard are for a return period of one year. To check the vibrations for other return periods an amplification factor should be applied (Kryh and Nilsson, 2012). Figure 2.38 shows the occupant comfort criteria according to the ISO10137 standard. It can be seen that also a distinction is made between the office and residential function, which is similar to the criteria presented in the Eurocode.

The occupant comfort criteria mentioned above are for different return periods. To be able to compare the serviceability criteria the peak accelerations should be scaled to the same return period. This could be done with the formula suggested by Melbourne and Palmer (1992):

$$\frac{response\ for\ R\ years}{response\ for\ R = 5} = 0.68 + \frac{\ln(R)}{5} \tag{2.4}$$

Wind Tunnel Test

Wind tunnel test can give more accurate results of the wind load than calculated with the code. In a wind tunnel test also the different wind angles can be analysed. The most commonly used wind tunnel methods are the Data-base-Assisted Design Approach (DAD) and the High-Frequency Force Balance Method (HFFB). The DAD-method is done with a rigid model of the building and the wind pressures are measured on all four sides of the buildings. The HFFB-method also uses a rigid model and this model is supported by a high-frequency force balance. This way the base shear and overturning moments can be measured. The wind force can be calculated from the support reactions.

2.7. Damping

Damping is a measure of the energy dissipation in a system when it vibrates. For a damped system the amplitude of the free vibrations will decay with time. In the case a structure is in resonance than the logarithmic decrement of the damping is equal to the dissipated energy in the system. The energy dissipated in the individual components of the structure are proportional to the work done on that component. The combination of the damping in the components can be used to get the contribution of the damping of all the components. However, this is only allowed in a classical modal analysis for as the equation of motion for

each mode are uncoupled (Stathopoulos, 2007).

The damping can be categorized as follows:
- Viscous damping
- Hysteresis damping
- Coulomb damping
- Radiation damping

The viscous damping is due to the vibrating of the system in a fluid or gas. The viscous friction absorbs the energy in the system. The hysteresis damping is the material damping, and the Coulomb damping is due to surface friction. The radiation damping is the energy loss to a surrounding medium. It is impossible to identify all damping contributions precisely for an actual structure. Therefore in structural dynamics the damping is represented by the viscous damping. The viscous damping can be in the form of the Rayleigh damping or modal damping. In the Eurocode the viscous damping is subdivided as follows:

$$\zeta = \zeta_N + \zeta_M + \zeta_{SD} + \zeta_{AE} + \zeta_{SDS} \qquad (2.5)$$

Where:

ζ_N is the non-structural component damping (1-1.5%)
ζ_M is the material damping (concrete uncracked members=0.75%)
ζ_{SD} is the structural damping (concrete cracked members= 0.5-1.5%)
ζ_{AE} is the aero-elastic damping (0-0.75%)
ζ_{SDS} is the supplemental damping systems (viscoelastic= 5-30%)

This division in five parts is a common representation of the damping in buildings. To determine the damping ratio of a building, a vibration experiment should be done on actual structures in the field. The Eurocode gives damping ratios for several kind of buildings based on these experiments.

Structural damping
The structural damping includes all the energy dissipated by the structure. The Eurocode does not give any values for the structural damping of timber buildings, however, the structural damping for timber bridges is given. Table 2.7 shows the structural damping for several structures according to the Eurocode.

Table 2.7: Structural damping coefficients according to Eurocode, Table F2

Structure	ξ_s	δ_s
Reinforced concrete buildings	1.59%	0.10
Steel buildings	0.80 %	0.05
Composite buildings	1.28%	0.08
Timber bridges	0.96-1.91 %	0.06-0.12

2.8. Dynamic parameters timber buildings
To estimate the structural damping in timber buildings experimental data on similar projects are required. However, the current codes and research give only few indications for the dynamic properties of timber structures under wind loading (Feldmann et al., 2016). Feldmann has done a research on the dynamic properties of tall timber structures under wind-induced vibration in 2016. During this research several on-site ambient vibration measurements are done on tall timber structures. Figure 2.39 shows the timber buildings on which are on-site measurements are executed. From these measurements the dynamic parameters including the natural frequencies, damping ratios, and mode shapes are derived. The vibration measurements on existing structures is a powerful method to extract the dynamic parameters,

and it has been applied to establish a data base of damping reference values for concrete and steel structures (Feldmann et al., 2016). For example, the Eurocode gives guidelines for the structural damping ratio for concrete and steel buildings but not for timber buildings. Figure 2.41 shows the damping ratios according to the code and the measurements on tall timber structures. The given damping ratios are all for the fundamental mode of the structure. The damping ratio for concrete and steel buildings is in the range of 0.5-1.6 %. For timber bridges the damping ratio is 1.5 % and for timber floors 1 %. Therefore it can be concluded that timber structures have a better capacity to dissipate wind-induced vibrations compared to conventional tall buildings. The damping ratios found from the experimental data gives damping ratios in the range of 0.5-3.0 %, and the average of the measurements is around the 2 %. The damping ratios found from the tests is only for buildings in the range from 20m to 45m and one of 100 metres height, and therefore no conclusions can be made for buildings above the 100 metres tall.

The overall damping is a summation of damping values given for material, type of construction, and foundation (Feldmann et al., 2016). The results from the experimental data of Feldmann's research are shown in figure 2.40. It can be seen that the slender and tall structures have the lowest eigenfrequency. Also the stiffer the structure is the lower the damping ratio is. The Eurocode NEN-EN1991-1-4 also gives a formula ($n_{1,x} = 46/H$) to estimate the structure's eigenfrequency which is quite accurate for tall structures.
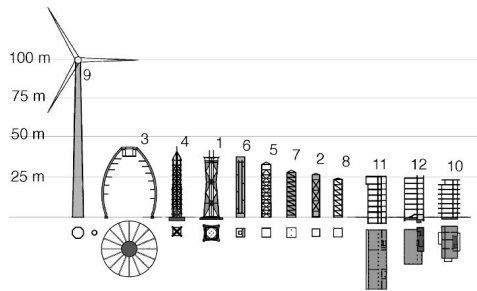
Figure 2.39: Tested tall timber structures, (Feldmann et al., 2016)
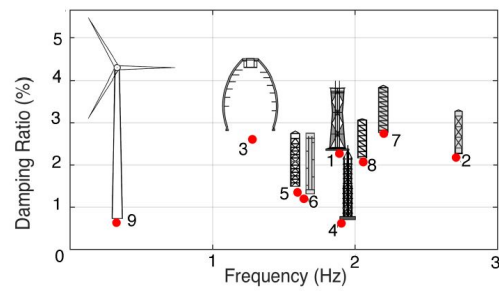
Figure 2.40: Results vibration measurements, (Feldmann et al., 2016)

The timber connections have a large influence on the total damping of the structure. A hysteric fastener model can be used to describe the dynamic behaviour of the connections. Timber frame towers have higher damping ratios than solid timber towers, and this is due to the fact that there is more movement between the elements and friction in the dowel-type connections (Stathopoulos, 2007).
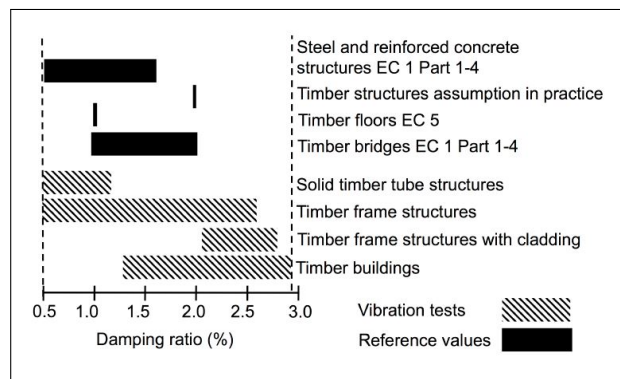
Figure 2.41: Damping ratios from codes compared to results from vibration measurements (Feldmann et al., 2016).

The global damping value is a summation of the values given for the material, the type of construction and the foundation (Feldmann et al., 2016). In the book of Petersen (2000), the damping values are discussed in more detail. The material damping of timber is in the range 0.4-0.8 %, and is similar as the material damping for concrete, which is in the range 0.5-0.9 %. Dowel-type connections contribute an additional 0.6-0.8 % and glued connections contribute an additional 0.2-0.4 %. The type of foundation support contributes an additional 0.1-0.3 %. This will give a total of 1.1-1.9 % for timber buildings with dowel-type connections, and a range of 0.7-1.5 % for timber buildings with glued connections. In this case the aerodynamic damping is neglected, which should not be neglected for tall buildings. Also, the secondary structure affects the damping capacity. For steel and concrete structures an additional damping value in the range of 0.1-0.4 % is added (Petersen, 2000). From the research of Feldmann et al. (2016) it is found that timber buildings which have slotted steel plate connections, the damping is higher than for the similar timber buildings with dowel-type or steel box profile connections. The wood-concrete hybrid buildings with a concrete core have a slightly higher damping value than the all-timber buildings.

2.9. Dynamic analysis

Single Degree of Freedom system

The tall building can be represented as a single degree of freedom (SDOF) system. This way the behaviour of the structure due to the wind load can be estimated. Figure 6.3 shows the schematization of the structure as a SDOF system. A common example of a SDOF freedom system is a mass connected to a spring and/or a dashpot. The equation of motion of the SDOF system is defined as follows:

$$m\ddot{x} + c\dot{x} + kx = F(t)$$
$$\ddot{x} + 2nx + \omega_n^2 x = F(t)$$

(2.6)

Where, m is the mass, k the stiffness, and c the damping in the structure. F(t) is the external loading on the system, and n is equal to $c/2m$. The dynamic properties of the structure can be described with the circular eigenfrequency, ω, mode shapes, ϕ, and the damping ratio, ζ.

$$\omega_n = \sqrt{\frac{k}{m}}$$

(2.7)

$$[k - \omega_n^2 m]\phi_n = 0$$

(2.8)

$$\zeta = \frac{c}{2m\omega_n}$$

(2.9)

For a forced vibration mechanism can be solved with a particular solution. For a harmonic force a particular solution can be described as follows:

$$x_{part} = X_c \cos(\omega t) + X_s \sin(\omega t)$$

(2.10)

The particular solution can also be found with $x_{part} = Re(Xe^{i\omega t})$ for a cosinusoidal load or for a sinusoidal load with $x_{part} = Im(Xe^{i\omega t})$. The total response of the system is found by the sum of the free vibration and forced vibration response. The steady-state response for a damped system can be found with Eq (2.11), and the static response with Eq (2.12).

$$x_{steady} = |X| \cos(\omega t - \phi)$$

(2.11)

$$x_{static} = \frac{F_0}{k}$$

(2.12)

The dynamic amplification factor indicates the dynamic response of the system. By multiplying this amplification factor with the static response the dynamic response of a system

can be found. If the damping in the system is equal to zero than the natural frequency is equal to the frequency of the load ($\omega/\omega_n = 1$). This means that the response will go to infinity, and this phenomenon is also known as resonance. Eq.(7.3) gives the dynamic amplification factor.

$$|X| = \frac{F_0}{k} \frac{1}{\sqrt{(1 - \frac{\omega^2}{\omega_n^2})^2 + (\frac{2n}{\omega_n})^2 \frac{\omega^2}{\omega_n^2}}} \tag{2.13}$$

$$\frac{|X|}{x_{static}} = \frac{1}{\sqrt{(1 - \frac{\omega^2}{\omega_n^2})^2 + (\frac{2n}{\omega_n})^2 \frac{\omega^2}{\omega_n^2}}} \tag{2.14}$$

Resonance

Resonance occurs when the natural frequency of the structure is near the frequency of the dynamic load applied on the structure. In the case the structure is in resonance the amplitude of the vibrations increases significantly, and could cause damage to the structure.

In the case the natural frequency is equal to the exciting frequency the displacement will go to infinity. In reality there will also be damping in the structure which will reduce the displacements of the structure due to dynamic loading. The damping can be included for the SDOF system with the following formula:

$$\omega_d = \omega_n \cdot \sqrt{1 - \zeta^2} \tag{2.15}$$

ω_d is the angular frequency of damped system
ω_n is the natural angular frequency
ζ is the damping coefficient of the system

The damping coefficient, ζ, is a fraction of the critical damping. In the case $\zeta = 1$ this will result in a periodic and critically damped motion, and if $\zeta > 1$ this will result in an overdamped aperiodic motion. For $\zeta < 1$, the system is underdamped and this will result in a decaying periodic motion. The global structural damping coefficient will be less than one for tall buildings. Figure 2.42 shows the free vibrations of three cases described above.
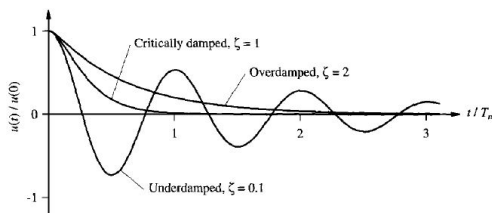
Figure 2.42: Free vibrations of underdamped, critically damped, and overdamped systems (Chopra, 1995).
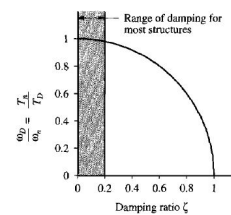
Figure 2.43: Effect of damping on the natural vibration frequency (Chopra, 1995).

The effect of the damping on the natural angular frequency is negligible for damping coefficients below 2 percent (Chopra, 1995). This can be seen in figure 2.43 in which the ratio of the damped and natural frequency is plotted against the damping ratio. For most structures the damping coefficient is below 2 percent, and therefore the natural frequency of the structure will not change. However, an increase of the structure's damping will reduce the required time of the vibration to return to its equilibrium.

2.10. Structural analysis software CSi ETABS

The features of the CSi ETABS software package are briefly described in this section. This is done to give the reader an expression of the possibilities of the software and research on what aspects of the structural design the software can be used. In the software description published by CSi software developers the following specifications is given: "The latest CSi ETABS offers 3D object based modelling and visualization tools, linear and non-linear analytical power, sophisticated and comprehensive design capabilities for a wide-range of materials, and insightful graphic displays, reports, and schematic drawings that allow users to quickly and easily decipher and understand analysis and design result (CSi-ETABS, 2013)."

The geometry can be constructed by first setting up the grid system of the building. The plans and elevation views are automatically generated at every grid line and there is a possibility to create a custom view by making use of cutting planes. The feature of 'apply on all stories' helps to quickly copy similar floor plans over the height of the building. Especially for tall buildings this can save a lot of time. Also, the stories setup is efficient because similar stories can save space in the database. Similar stories have the same beam at each level and a specific beam is only an 'instance' of that general beam object. This is one of the main advantages of CSi ETABS over other similar structural analysis software packages. Another way to build up the geometry quickly is to import AutoCAD drawings into the ETABS model. The AutoCAD drawings can help by building up the model and layers can be used to turn off the visibility of the CAD lines.

CSi ETABS includes the design of steel and concrete frames, concrete and masonry shear walls and composite columns and beams. The section properties can be user determined for the concrete, steel and timber sections. The steel sections can also be picked from the available steel section libraries. The libraries include the most common steel section from several steel profile producers such as ArcelorMittal. Section modifiers can be applied to the elements to reduce the stiffness and in the case of modeling cracked concrete elements the section modifiers are used.

To define the loading in CSi ETABS first the load types need to be specified. These include the Dead, Superimposed Dead, Live, Reducible Live, Seismic and Wind loading. After setting up the load types the load cases are specified. Most commonly used is the linear static analysis but also nonlinear load cases are possible. For the load combination there can be made use of linear addition, envelopes or the square root sum of squares method. The live loads on the floors can be set in the 'shell uniform load sets' and are applied on the floor slabs. The façade can be modeled with cladding elements. However, in practice the façade loads are modeled as a uniform frame load on the perimeter beams of the building. For the seismic loading the Response Spectrum Analysis or the Time History Analysis can be used. The wind loading can put in according to the chosen building code. The analysis of the ETABS model is done with the SAPFire 64-bit solver and the solver can also run nonlinear modeling, such as the time history analysis or static push-over method. A commonly used linear analysis method is the response spectrum analysis.

The software CSi ETABS has a variety of formats to import or export to another software package. As already mentioned earlier, the AutoCAD drawings can be imported into the CSi ETABS model. Another possibility is to import the geometry from the software Rhinoceros. For example, the meshing can be done in Rhinoceros in combination with the Grasshopper plugin. The meshing can also be done in CSi ETABS directly. Exporting from CSi ETABS to CSi SAP2000 is also an option which can be useful because CSi SAP2000 has a bit more freedom for the analysis input. It should be carefully checked if there is no information lost after the exporting process. Several import formats can be useful dependent on how you receive the initial geometry.

<div style="text-align: right;">

3

</div>

Design and verification

This chapter describes the hybrid wood-concrete tall building design, and elaborates the choices and assumptions that are made to get to this design.

3.1. Program of requirements

In this section the program of requirements for the design are presented. Table 3.1 shows the general requirements of the building. The building will have a height of 300 metres and has a slenderness ratio of about 1:10. The storey height is set to 3.75m for the office space and the building will have a total of 76 storey levels. The program of requirements is split into two categories: the spatial and functional requirements. Table 3.2 shows the required surface area per function. It can be seen that the main function of the building is for offices, and most of the net floor area is used for the office spacing. The vertical transportation will take up also a lot of surface area and will be located in the central core of the building. The entrance level and the outrigger/belt-truss levels will have a double storey-height.

Table 3.1: General requirements

General requirements	
Function	Offices, restaurant, hotel
Location	City-centre Rotterdam, The Netherlands
Height	300 m
Footprint	31.5m x 31.5m
Structural materials	Timber and Reinforced Concrete

Table 3.2: Surface area per function

Function	Surface area $[m^2]$	Number of storey levels
Offices	54270	67
Restaurant	810	1
Hotel	3240	4
MEP	2430	3
Vertical Transportation	13851	-
Entrance	810	1
Total	75411	76

<div style="text-align: center;">

33

</div>

Table 3.3: Spatial requirements

Spatial Requirements	Dimensions
Footprint	31.5m x 31.5m
Height of building	300m
Grid of the columns	4.5m
Vertical Transportation (Core)	13.5m x 13.5m
Storey height (Offices)	3.75m
Storey height (Entrance level, MEP and Restaurant)	7.0m

3.2. Design aspects

The design aspects are divided in two parts: the design aspects which can be determined at an early design stage, and secondly the design aspects that are still changing during the preliminary design process. Especially, the latter aspects are important aspects that need to be researched, and these design components have a lot of influence on the dynamic response of the structure. The design aspects that will be researched until the end of the concept design stage are:

- Column dimensions
- Beam dimensions
- Core wall thickness
- Structural connection details
- Outrigger/belt-truss system
- Mega bracing at perimeter
- Aerodynamic treatments (i.e. rounded corners)
- Auxiliary damping system
- Fire Safety Design

The design aspects that can be determined at an early stage are:

- Floor slabs
- Façade elements
- Core lay-out/Vertical Transportation
- Roof structure
- Construction phasing
- Second load path
- Entrance level layout

The design strategies presented below describe the procedure that is undertaken in the case the structure does not fulfil the serviceability criteria. The strategies have effect on the stiffness, mass and damping capacity of the main structure, which are all parameters that will influence the dynamic behaviour.

- Increase the core wall thickness
- Increase the number of outrigger/ belt-truss systems
- Increase the column dimensions
- Increase the outrigger/belt-truss dimensions
- Additional auxiliary damping devices
- Optimize the shape of the building

Or other alternatives would be:

- Mega bracing at perimeter
- Steel rods inside timber
- Lower part done with a concrete frame

3.3. Design strategy

First the structure has been designed for the ultimate limit state (ULS) load combinations. This concept design will be used as the basis of the design. Thereafter, the design will be checked for the SLS criteria and based on these checks improvements on the design will be made. Optimization of the dynamic behaviour can be done by modifying the structure's parameters such as stiffness, mass and damping capacity. Also, a conventional tall building design has been made which consist of all concrete structural elements. The conventional tall building has the same program of requirements as the hybrid wood-concrete tall building, and the conventional tall building will give a comparison to the hybrid wood-concrete option.
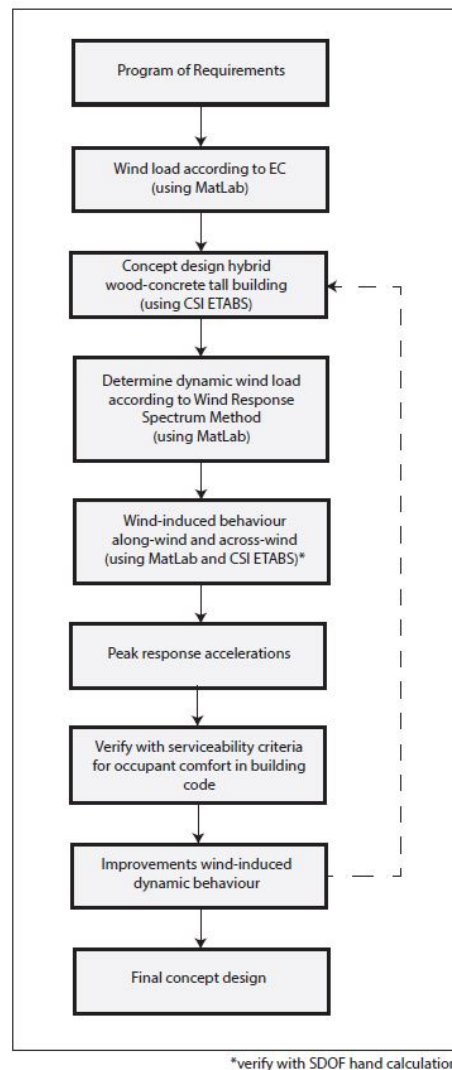
Figure 3.1: Design strategy

Figure 3.1 shows the scheme of the design strategy. From the program of requirements a concept design of the main structure will be designed. First, the structural components are going to be designed for the wind load according to the Eurocode. Then the wind response spectrum according to the method by Davenport will be obtained. By using the wind response spectrum method the dynamic behaviour of the structure can be analysed. The wind response will be analysed in the structural analysis software CSi ETABS in the time domain. The Eurocode only gives a wind load for the along-wind direction. Due to the vortex shedding

of the wind the across-wind should also be checked for a tall and slender building. Therefore, an across-wind spectrum will be set up in MatLab using the equivalent across-wind spectrum model developed by Liang et al. (2002). From the response spectrum of acceleration the peak response acceleration will be acquired, and the acceleration will be checked with the service-ability criteria for occupant comfort. In the case the requirements are not met improvements should be made to the design of the tall building. These improvements could be adjustments to the mass, stiffness, and damping properties of the structure. The shape of the building could also be modified to optimize the wind-induced dynamic behaviour. After these modifications have been applied to the structure the dynamic analysis starts over again, and the peak response accelerations should be determined for the optimized structure. The whole design process will give a better understanding of the wind-induced dynamic behaviour, and it will give insight in the feasibility of a 300m tall hybrid wood-concrete building.

3.4. Load combinations

The tall building has been designed for the load combinations given in the EC0 and the Dutch National Annex. The building is taller than 70 metres, and therefore the building should be designed for consequence class 3 (CC3). This means that for this building there is a high consequence for loss of human life, or economic loss, or environmental loss. The reliability class is three with a reliability index β of 4.3 for a return period of 50 years. For CC3 the load combinations in ultimate limit state should be multiplied by a factor K_{FL} and are formulated as follows:

$$1.1\left(1.35G" + " \sum_{i \geq 1} 1.5\psi_{0,1}Q_{k,i}\right) = 1.49G" + " \sum_{i \geq 1} 1.65\psi_{0,1}Q_{k,i} \tag{3.1}$$

$$1.1\left(1.2G" + "1.5Q_{k,1}" + " \sum_{i \geq 1} 1.5\psi_{0,1}Q_{k,i}\right) = 1.32G" + "1.65Q_{k,1}" + " \sum_{i \geq 1} 1.65\psi_{0,1}Q_{k,i} \tag{3.2}$$

The magnitudes of the imposed loading can be found in EC1. Table 3.4 presents the characteristic loading for the self-weight, permanent and variable load. For the imposed vertical floor loading in multi-storey buildings a reduction factor, α_n, should be used. For the ultimate limit state design the structural elements should be checked according to the following requirement:

$$E_d \leq R_d \tag{3.3}$$

Where:

$$R_d = k_{mod} \cdot \frac{R_k}{\gamma_M} \quad and \quad E_d = \frac{E_{mean}}{\gamma_M} \tag{3.4}$$

The k_{mod} is a modification factor which takes into account the service class and the duration of the load. This factor should only be taken into account for timber design. Table 3.5 presents the different values for the modification factor in service class 1 for glued-laminated timber.

Table 3.4: Characteristic loading according to EC1

Category	Type	Characteristic load, q_k
Self-weight, G	Structural elements	Based on ETABS model
Permanent load, G	Interior walls	$0.5 \; kN/m^2$
	Ceiling construction	$0.3 \; kN/m^2$
	Facade load	$0.5 \; kN/m^2$
Variable load, Q	Imposed floor load offices	$2.5 \; kN/m^2$
	Imposed floor load communal area offices	$3.0 \; kN/m^2$
	Lateral wind load	Based on EC1-1-4
	Snow load	$0.56 \; kN/m^2$

Table 3.5: Modification factors for GLT SC1

Load action	Load duration	k_{mod}
Self-weight	Permanent	0.6
Permanent load	Permanent	0.6
Imposed floor load	Medium	0.8
Wind load	Short	0.9
Snow load	Short	0.9

3.5. Serviceability criteria

The serviceability criteria are an important aspect in the design of tall buildings. These criteria can become governing for the required dimensions of the structural elements. Table 3.6 shows the serviceability criteria for which the structure will be checked and those criteria can be found in the Eurocode. The criteria for the lateral peak response accelerations are dependent on natural frequency. A more detailed description of these occupant comfort criteria can be found in Chapter 2, section 2.7.

Table 3.6: Overview serviceability criteria

Structural element	Serviceability aspect	Requirements
Global structure	Lateral displacement	$u_{max} \leq H/500$
Global structure	Lateral storey drift	$\Delta_{max} \leq h/300$
Global structure	Horizontal accelerations	$a_{max} \leq 0.390 \ m/s^2$*
Floor/beam	Total vertical displacement	$w_{max} \leq 0.004 \cdot L_{rep}$
Floor	Vibrations	$n_1 \geq 9$ Hz

*dependent on natural frequency of the structure

3.6. Floor plan lay-out

The floor layout is based on a typical office building. The length from the perimeter to the core of the building is equal to 9 metres, and the height of the stories is equal to 3.75 metres. These dimensions should ensure that enough sunlight will fall into the office spaces (Van der Windt, 2006). The partitioning walls for the office space are not yet included in the model and will be excluded from the main structural design. The partitioning walls are light-weight and a flexible placement is preferred for office buildings. A double storey height is preferred at the entrance level. Concrete columns are used to create a more open layout at the entrance level. This is because the dimensions of the concrete columns can be smaller compared to the GLT-columns. The concrete columns also have other advantages, namely the higher safety in case of explosions at the ground level, and the introduction of the forces to the foundation slab is better to do in concrete than in timber due to the high stress concentrations.

3.7. Outrigger/Belt-truss system

For the lateral stability an outrigger/belt-truss system has been chosen. This due to the fact the system is well suited for a tall building with a height of 300 metres. Also, it is often applied for conventional tall hybrid structures with a reinforced concrete core and a steel frame. For designed tall building the frame will be done in timber instead of steel. Fortunately, the outrigger/belt-truss system also seems promising for a hybrid wood-concrete tall building. At first, the outrigger and belt-trusses were designed in glued-laminated timber, but this gave too large dimensions due to large tensile stresses. An alternative would be to use laminated veneer timber (LVL) or post-tensioned timber. Several options for the outrigger/belt-truss system have been studied, and important design choices that had to be made were the number of outrigger levels, the positioning of the outrigger over the height of the building, and the

layout of the outrigger trusses. These design choices are made based on a literature study and a parametric study, which can be found in chapter 2 and 7, respectively. The parametric study for the outrigger/belt-truss design can be found in Chapter 7, section 7.2.1.

In the book of Taranath (2010), the optimum heights for an outrigger system are discussed. A rule-of-thumb for the positioning of three outrigger levels is at one-quarter, two-quarters and three quarters height. The optimum height is dependent on the distribution of the mass and stiffness of the structure. The optimum height of the outrigger levels for a specific structure could be found by varying the heights in an iterative process to reduce the lateral displacements. However, in this study it is chosen to apply the rule-of-thumb for the concept design. Applying the rule-of-thumb results in outrigger levels located at storey level 20, 38 and 57. The outrigger levels have a height of 7.5 metres, which equals the height of two office storey levels. Two outrigger levels will be used for the mechanical, electricity and public health facilities (MEP), and the outrigger level at storey level 57 will be used for the restaurant. This way the timber outrig-

Figure 3.2: Schematic view of structure with 3 outrigger levels

ger trusses will be kept in sight for the guests of the restaurant. The belt-truss consist of a timber truss which surrounds the perimeter of the building and has braces in between the perimeter columns. The belt-truss transfers the forces of the outrigger trusses to all the perimeter columns, and therefore all the perimeter columns will be activated in the outrigger system.

The effect of the outrigger system on the lateral storey displacement at the top can also be estimated by a hand calculation. The structure is schematised by a stiff core and a hinged frame. The outrigger storey levels have a much larger stiffness compared to the other storey levels. Figure 3.2 show a schematic 2D view of the structure used for the hand calculation. The deflection of the structure due to the lateral wind loading can be estimated with the following expression:

$$\delta_{bending} = \frac{q_w \cdot H^4}{8 \cdot (EI)_{eff}} \quad and \quad \delta_{shear} = \frac{q_w \cdot H^2}{2 \cdot (GA)_{eff}} \tag{3.5}$$

Where:

q_w is the uniformly distributed wind load
H is the height of the building
$(EI)_{eff}$ is the bending stiffness of the building
$(GA)_{eff}$ is the shear stiffness of the building

3.8. Diagonal braced tube-in-tube system

Another option for the lateral stability could have been a diagonal braced tube-in-tube system, and is also suitable for a hybrid timber and concrete structure. The diagonal mega-bracing has also been used for the concept design of the Oakwood tower in London by PLP architects which has been discussed in Chapter 2, Literature study. The mega-bracing is put at the perimeter of the building. The bracing consist of large timber diagonals which span over the whole width of the building façade, and cross multiple storey levels.

It is decided to only apply the mega-bracing if the tall building design does not have a large enough stiffness capacity to satisfy the serviceability criteria for the lateral inter-storey drifts and displacements. The diagonal braced tube-in-tube lateral stability system will be further analysed in the Chapter 7, Parametric Study and Optimization.

3.9. Reinforced concrete core

The reinforced concrete core is the most important part for the lateral stability design. The larger the width of the core the better this would be for the lateral stability. However, the design should be practical and a large central core also reduces the usable office floor area. The usable floor area is also called the net floor area (NFA). A net floor area of 75 percent or higher is recommended for an office building (Sev and Özgen, 2009). The structure has a stability core with a footprint of 13.5 by 13.5 metres. These dimensions are based on the vertical transportation design and reference projects in which almost 20 percent of the gross building floor area is reserved for the vertical transportation. One of these reference projects is for example the Emirates office Tower in Dubai with a height of 300-metres. Inside the core the technical facilities, lavatories and vertical transportation will be located. The interior walls in the core can also add stiffness to the building, and for this reason the interior walls will be included in the ETABS model as well.

In most designs the stability core has been based on the required space for the vertical transportation. The needs of the vertical transportation will be dependent on a number of parameters, such as the population in the building, the number of floor levels, and the maximum transportation time. For this concept design the required space for the vertical transportation will be based on reference projects and on a rule-of-thumb. A rule-of-thumb is to serve a maximum of 15-16 floors with a lift (Barney, 2003). For the 76 stories this rule-of-thumb would give a total of five elevators. Therefore, a minimum of five elevators plus one service elevator should be adequate. The layout of the core is based on similar projects and the main focus of the design is that the proportions are realistic. A minimum of two stairs is required in the core. Also shafts and space for the mechanical, electricity and public health (MEP) facilities should be included, and the sanitary is located at the floor area inside the core. The net floor area will be about 80 percent for the designed tall building.

3.10. Foundation design

The foundation for the tall building consists of a large concrete foundation slab placed on foundation piles. The concrete foundation slab helps to introduce the forces of the columns and the core walls. The slab should be able to withstand the large base shear and overturning moments due to the lateral wind loading. Special attention should be given to the uplift forces in the foundation piles. These tension forces can occur for light-weight structures, which is a typical characteristic for timber buildings.

The axial stiffness of the foundation piles should be included in the 3D-finite element model, because this will affect the natural frequency and lateral displacement of the structure. The axial stiffness is dependent on the soil type, and normally the characteristics of the soil will be provided by the geotechnical engineer. For cast in-situ piles the full skin resistance is mobilized at a settlement of 0.5 to 1.0 percent of the pile diameter (Sitharam, 2013). In the preliminary design phase, it has been assumed that the pile will have a settlement of 1 percent of the pile diameter. This is a common approach in the case the geotechnical soil tests are not available or have not been executed yet. The vertical stiffness of the pile can be approximated by the following equation:

$$K_{pile} = SWL/(0.01 \cdot d) \qquad [kN/m] \qquad (3.6)$$

In which, SWL, is the working load on the pile, and d is the diameter of the pile. The calculated vertical pile stiffness can be used as the characteristic translational spring stiffness in the model. The pile stiffness has been modelled with translational springs in the vertical and

horizontal direction. The horizontal stiffness will be taken the same as the vertical stiffness. Figure 3.3 shows the translational springs of the foundation in the finite element model. The contribution of the rotational stiffness of the foundation is about one third of the total wind-induced lateral displacements. This is similar to the other high-rise projects located in the city-centre of Rotterdam, such as the 'Zalmhaven' tower with an height of 218 metres.

The foundation design is an important part of the design of the tall building and its stiffness has a significant influence on the structure's wind-induced behaviour Poulos. (2016) discusses several characteristics of tall buildings which have influence on the foundation design and these characteristics will now be briefly discussed. The total weight of the structure, and this means the vertical load should be supported by the foundation. The high-rise buildings are often surrounded by low-rise structures. These low-rise buildings are subjected to much smaller loadings, and therefore the differential settlements between the high-rise and low-rise should be checked. The lateral wind loading will give overturning moments and base shear in the foundation. The moment can impose additional vertical loading on the foundation piles, especially on the perimeter foundation piles. The wind-induced loads are cyclic, and therefore this cyclic loading can also cause fatigue to the piles and decrease the foundation capacity (Poulos, 2016). The wind load can cause dynamic resonance, and the dynamic behaviour of the structure needs to be assessed.
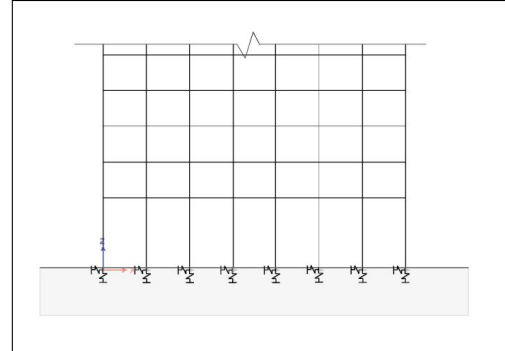
Figure 3.3: Foundation modelling with horizontal and vertical translational springs in CSi ETABS

3.11. Façade design

The façade will consist of prefab elements which have large glazing panels. These large glazing panels are often preferred in an office building so that sufficient daylight will enter the office space. The large glazing panel façade is also known as a glass curtain wall. The façade loading is estimated based on the volumetric weight of the glass panels. The glass panels consist of toughened double glass of each 10mm thick. The calculation is presented in the Appendix B.3, and resulted in a characteristic façade load of 0.5 kN/m^2. The façade has not been modelled in the finite element model, but the weight of the façade will be applied as a line load on the perimeter beams of the building. The façade design could also be adjusted to improve the structure's dynamic behaviour. Especially, the vortex shedding behaviour can be improved by adding fins or openings to the façade.

3.12. Construction sequencing

The construction sequencing is important for the vertical differential shortening in particular. Adjustment devices between the timber columns will be installed to compensate for the differential shortenings of the timber and the concrete walls. Between the bolted steel plates of the column splice connection an additional steel plate with the required adjustment thickness can be placed. Also, a thin layer of resin between the head plates will be applied to straighten out inequalities in the steel plates. Continuous columns can be used over the height of four storey levels, and this will reduce the number of expensive steel connection profiles. Due to the transportation limits the maximum length of the columns is set to four storey level heights, which is equal to 15 metres. The timber structural elements are light-weight compared to conventional concrete and steel structural elements. Therefore, the craning time can be reduced, and the overall construction time of the tall building could be reduced.

3.13. Manufacturability

The glued-laminated timber (GLT) and laminated veneer lumber (LVL) structural components in the designed tall building have large dimensions, and the columns at the lower levels have a dimension of 1200mm x 1200mm. These dimension sizes are not common for GLT and for that reason close attention should be given to the manufacturability. The GLT consists of multiple layers of dimensioned lumber glued together with adhesives. The beam sizes can have unlimited width and length due to the continuous laminations, and the column length will have a maximum of 16 metres because of transport limitations.
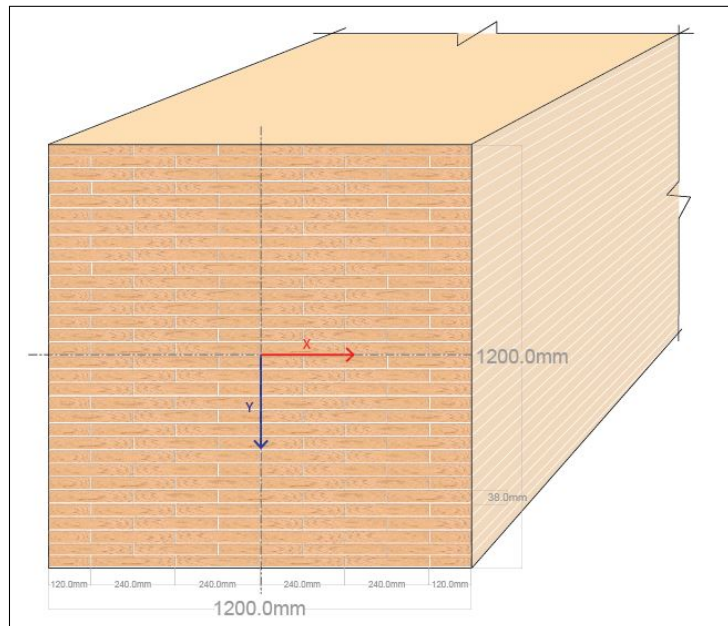
Figure 3.4: GLT column layout with dimensions 1200mm x1200mm, lamination thickness = 38mm

The standard depths for GLT range from 114mm to 2128mm, and the laminations have a thickness of 38mm (CWC, 2018). A single lumber plank will be used for GLT members with a width up to 275mm, and for larger dimension multiple lumber boards will be laid side by side. The standard width size of the GLT ranges from 80mm to 365mm according to the Canadian Wood Council (2018). The width of the GLT can be increased, but the non-standard dimensions will be more expensive due to the fact that additional trimming of the lumber boards is required. The standard dimensions will vary for most mass timber manufacturers. Figure 3.4 shows the layout of the columns at the lower levels of the designed structure. The laminations have a thickness of 38mm and a total of 32 laminations will be used to reach the required depth. The width of the lumber boards is 240mm and this means 5 boards will be laid side by side. Each layer of boards will be reversed so that there will be an overlap of the lumber boards. This way no straight-through vertical joints will occur.

The pre-drilling of the holes for the dowel-type connections will already be done in the factory, and also the openings in the beams for the slotted-in steel plates will be sawn during the manufacturing process. For the column splice connection the end-plates will be connected to the column with glued-in bolts. The glued-in bolts will be glued with epoxy to the columns in the factory under controlled climate conditions. It is important that the glueing process occurs under controlled condition so that connection strength can be guaranteed. The connection of the column end-plates with the bolts can be done on site. For the belt-truss connection horizontal holes in the columns will be pre-drilled. The bolts will be placed through these holes on site, and the bolts will connect the belt-truss brace to the column. For the beam-to-wall connection openings for the slotted-in steel plates and dowels will be prefabricated.

The steel anchor plate will be connected to the concrete wall with headed studs.

3.14. Floor slab design

The floor slabs are made of cross-laminated timber panels with a thin top layer of concrete. The span of the CLT floor panels is 4.5 metres and has a width of 2.25 metres. The panel has five layers of C24 solid wood boards, and has a total thickness of 153 mm. The CLT floor slab spans in one direction and is supported by GLT beams. The floor panels are placed perpendicular to each other on each grid-line of 4.5 metres. The floor slab is connected to the beams with long self-drilling screws. The floor slabs are also connected to each other using screws and a small LVL strip to interlock the CLT floor panels. The maximum dimensions for most CLT manufacturers are a span up to 16 metres and a width up to 3.5 metres. This is also based on the limits of the transportation vehicles. Therefore, it has been decided to use CLT floor panels with a width of 2.25 metres will be used instead of a panel with a width of 4.5 metres, which corresponds with the applied grid. Figure 3.5 shows the CLT floor slab design.
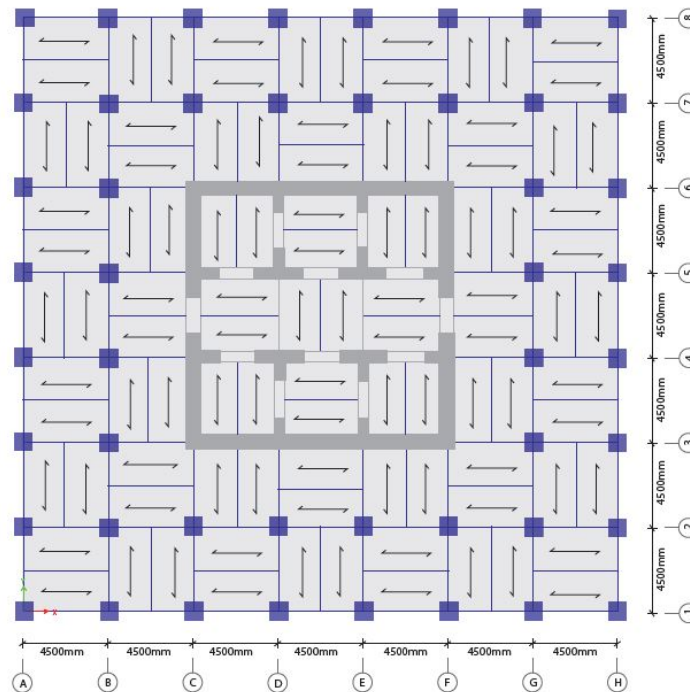
Figure 3.5: CLT floor spans in principal dir. (panels with dimensions of 4.5m x 2.25m)

The floor slabs have been designed in both ultimate limit state and serviceability limit state. The mechanically jointed beam theory has been used for calculating the effective bending stiffness, which is described in Chapter 2, Literature study. For the serviceability limit state the deflections and vibrations are checked. In the calculation of the deflections also the deformation factor, k_{def}, should be included. This deformation factor takes into account the increased deflection and the effect of the moisture content. The final deflection can be calculated with the following formulas:

$$\delta_{fin,G} = \delta_{inst,G}(1 + k_{def}) \tag{3.7}$$

$$\delta_{fin,Q1} = \delta_{inst,Q1}(1 + \psi_2 \cdot k_{def}) \tag{3.8}$$

The CLT handbook by Gagnon and Pirvu (2011) recommends to keep the fundamental frequency of the floor for simply supported panels above 9 Hz. The fundamental frequency of the floor is determined with:

$$n_{1x} = \frac{\pi}{2 \cdot l^2} \sqrt{\frac{(EI)_{eff}}{\rho A}}$$ (3.9)

l is the floor span $[m]$
ρ is the characteristic density $[kg/m^2]$
$(EI)_{eff}$ is the effective bending stiffness $[Nm^2/m]$

The fundamental frequency of the floor panel that has been found using Eq.(3.9) is equal to 11.4 Hz, and this means the serviceability criterion has been been satisfied. The concrete top layer of 25 mm adds significant mass to the floors and has a positive influence on limiting the vibrations in the floor slab. A thicker top layer of concrete could have been included if the serviceability criterion would not have been satisfied. The floor slab layout and design calculation can be found in the appendix B.2.

3.15. Fire safety design

The structural calculation for fire should be based on the design fire cases according to Eurocode NEN-EN1995-1-2. The fire safety of the structure should be checked as a whole, or the structural elements can be assessed separately. It is also possible to guarantee the fire safety based on experimental tests. For high-rise structures, which are considered consequence class 3, the building should be fire resistant for at least 120 minutes according to Dutch building regulations.

The fire safety design will be checked on structural element level, and the structural members are checked for the fire safety design criteria. For the concrete structural members the concrete cover of the reinforcements should be sufficient. The timber structural elements can be covered with fire protective cladding. Another option is to use the effective cross-section of the timber. This means the char layer which develops during the fire is subtracted from the total thickness of the cross-section. This will result in a residual cross-section of the structural members, and their resistance should be checked.

The fire protection of the structural members is called a passive method. Also, an active method could be used for the fire safety design. An example of an active method of fire protection is the use of a sprinkler system in the building. a sprinkler installation is required for a office building with height above 70 metres. The application of a sprinkler installation could reduce the fire resistant time. Due to the fact a timber structure of these heights is not done before, it is decided to use a bit conservative approach and design the structure for a fire resistance of 120 minutes.

The fire safety design should limit the spread of fire, and this should be guaranteed by the load-carrying capacity of the structure and the separating function of the walls and floors. For a fire resistance of 120 minutes it is recommended to use a concrete cover of 35mm for the reinforcement bars in the core wall according to Eurocode NEN-EN1992-1-2. In the steel-to-timber connections the steel plates and fasteners should be protected to direct fire. For the dowel-type connection the fasteners are sealed and hidden with wooden plugs. All timber elements are protected by gypsum plasterboard, and fire resistant/intumescent strips can be applied at the critical locations in the connection. For the beam-to-column connections the steel plates are hidden and covered by the timber, and will have a higher fire resistance. The gaps between the timber beams and slotted-in steel plates will be filled with fire resistant strips which will swell in the case of fire. In the column-to-column connection the dowels, bolts and steel plates will be protected by a double layer of gypsum plasterboards. Figure 3.7 shows the additional gypsum plasterboard around the column-to-column connection. The
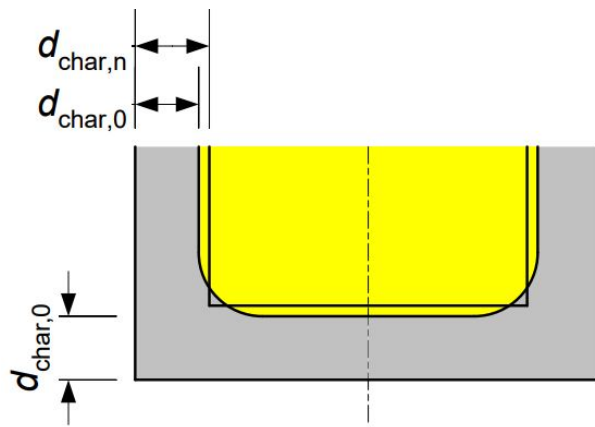
Figure 3.6: Equivalent residual cross-section, (Frangi, 2012)
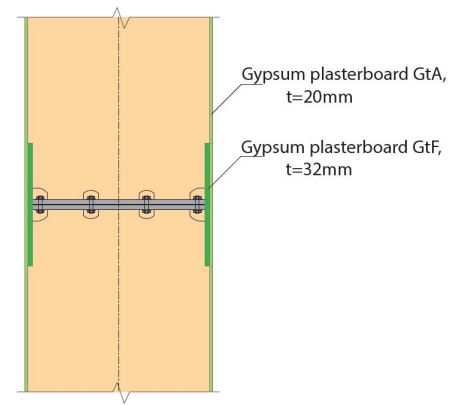
Figure 3.7: Fire protection of column splice connection

additional plasterboard will give a fire resistance time of 120 minutes, and as a consequence the steel bolts and plates will be protected during a fire.

The GLT corner columns will be kept in sight from the outside of the building. This is done from an aesthetic point of view, and this way not all the timber elements will be covered by a non-translucent cladding. The corner columns will be protected by glass panels which are attached at the two columns faces at the outside. The building material glass is classified as non-combustible and is given class A.1 according to EN13501. The translucent external cladding will protect the timber columns against the fire load.

The structural timber members have gypsum plasterboard cladding. This will increase the fire resistance of the member and protects the timber from high temperatures. However, the gypsum plasterboard will fall off after a period of intense fire. From this point on the timber mass element will get a char-layer at the perimeter of the cross-section. The char-layer will also protect the residual cross-section from high temperatures. For a tall office building of consequence class 3 a fire resistance of 120 minutes is required, and it should be checked if the mechanical resistance (R) is still sufficient after a period of 120 minutes of fire.

The charring rate, β, is the ratio between the charring depth, d_{char}, and the fire time, t, and can be calculated with Eq.(3.10).

$$\beta = \frac{d_{char}}{t} \tag{3.10}$$

The charring rate is dependent on the wood species. For example, the charring rate for spruce is 0.7 mm/min. For the fire safety design calculation the notional charring rate, β_n, is used, and this parameter is needed to find the equivalent residual cross-section. Figure 3.6 shows the difference between the charring rate, β_0, and the notional charring rate, β_n. The char-ring rate for glued-laminated timber (GLT) and laminated veneer lumber (LVL) is about 0.65 mm/min, and the notional charring rate is 0.7 mm/min. To get the reduced cross-section also a zero strength layer should be subtracted from the depth of the beam. This zero strength layer is about $7mm$ for glued laminated timber.

Figure 3.8 shows the charring model for initially protected surfaces. The charring process of the timber can be divided in different phases: the time that the charring starts, t_{ch}, the failure time of the cladding, t_f, and the time at which the original charring rate of the timber is reached again, t_a. After the fall-off of the cladding the charring of the timber element will start, and this part is indicated in blue in figure 3.8. There will be an increased charring rate after the failing of the cladding. This is due to the high temperature the timber will be exposed to at the time of the fall off of the cladding, and the timber has not produced a protective char layer yet. The increased charring rate will continue till time, t_a. At the time,
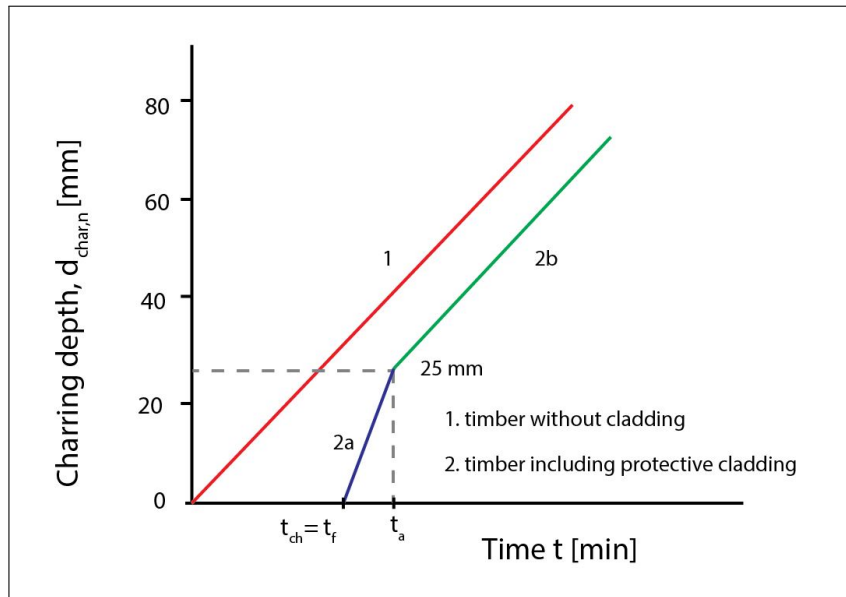
Figure 3.8: Charring model for timber and gypsum plasterboard

t_a, the charring rate will return to the original charring rate of the glued laminated timber. The maximum charring depth at time t_a is 25 mm, and for the protected GLT columns this means it already endured a fire load for 60 minutes.

There are several classifications of gypsum plasterboard which have different fire resistance properties. The most common gypsum plasterboards are types, A, H and F (GtA, GtH, and GtF). The gypsum boards type A and H have a porous gypsum core and no reinforcement (Just et al., 2010). The paper laminated surface provides stiffness to the gypsum board of type A and H. The gypsum board type F has an improved core cohesion at high temperatures, and will have an higher fire resistance than the regular gypsum boards (Just et al., 2010). For structural timber member protected with a gypsum plasterboard type A or H the time that the charring starts, t_{ch}, can be calculated by Eq.(3.11). For a gypsum plasterboard type F the time that the charring starts can be calculated with Eq.(3.12).

$$t_{ch} = 2.8 \cdot h_p - 14 \qquad \text{(for GtA and GtH)} \tag{3.11}$$

$$t_{ch} = 2.8 \cdot h_p - 23 \qquad \text{(for GtF)} \tag{3.12}$$

Where, h_p, is the plate thickness of the gypsum plasterboard in mm.

When the reduced cross-section has been determined the strength of the members should be checked for the ultimate limit state design. The design strength of the timber elements can be determined as follows:

$$f_{d,fi} = k_{mod,fi} \cdot \frac{f_{20}}{\gamma_{M,fi}} \tag{3.13}$$

Where:

$k_{mod,fi}$	is the modification factor for fire safety design
f_{20}	is the 20 %-fractile strength
$\gamma_{M,fi}$	is the material factor for fire safety design

The load combination of action for accidental design situation according to the EC0 should be used for the verification of the load-bearing of the structure. The charring depth for the

timber structural beams is $34mm$ after 120 minutes of fire. As a consequence, all the steel plates, connectors and dowels are placed at an minimum distance of $40mm$ of the outer surface. The gaps in the connections will be covered by a fire resistant joint filler which will swell in the case of a fire.

The calculations of the fire safety design for the timber columns and beams can be found in Appendix B.7.

3.16. Alternative load path

For a building with a consequence class 3 (CC3) the structure should also be designed for accidental loading. An alternative load path of the forces should be possible in the case of failure of a structural member. For example, a column failure could occur due to an explosion or an vehicle impact. In the case of a fire the alternative load path can also reduce the force on the structural members which are exposed to the fire. It should be checked that the building will not collapse during such occasions.
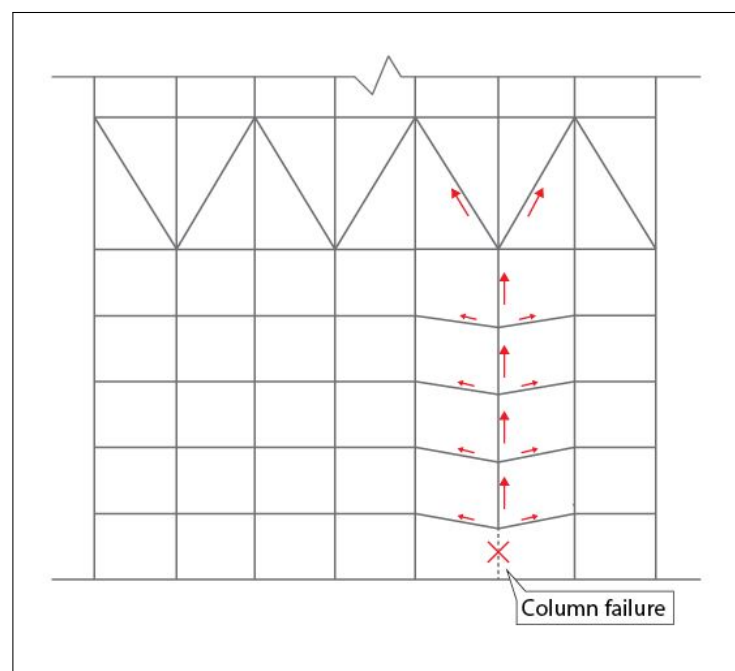
Figure 3.9: Elevation view of alternative load path due to column failure with indication of the tension forces

An alternative load path could be accomplished in several ways. For example, the force on a column which is exposed to fire could be passed on to a neighbouring column. As a consequence, the column will not be part of the main structural design any more. To check the second load path design a column should be able to get taken out of the design. The structural design will then be checked with a load combination for accidental loading. The load combination for accidental loading in the Eurocode NEN-EN1990 is given by Eq.(3.14).

$$\sum_{j\geq1} G_{k,j} \text{''} + \text{''} P \text{''} + \text{''} A_d + \text{''} (\psi_{1,1} \; or \; \psi_{2,1}) Q_{k,1} \text{''} + \text{''} \sum_{i>1} \psi_{2,1} Q_{k,i} \tag{3.14}$$

If a column fails the structure should not progressively collapse and an alternative load path should be possible. The alternative load path will be possible through the beams and columns located above the failed column. The columns start to hang onto the stiff outrigger levels, and the tension force will be transferred through the columns to the perimeter belt-truss. Figure 3.9 shows the alternative load path in elevation view. It can be seen that also a small part of

the tension force will be transferred through the beams. The beams are not continuous over the full height of the structure, and therefore the tensile resistance of the beam-to-column connection should be checked. Also, the tensile capacity of the column splice connection should be checked. If the tensile forces become too large a cable could be applied underneath the beams. The tension cables could be placed underneath the beams over a length of three spans, and the cables would go through the continuous columns. When the column fails the tension cable will be activated. The cable will keep the beams in place, and consequently the floor slab stays supported. The load will be transferred through the alternative load path to the subsequent columns.

The deflections in the beam and floor slab will increase a lot, but for the accidental load design the serviceability criteria for the deflections can be neglected according to NEN-EN1991-1-2. For the accidental load combination the maximum deflection in the beams due to column failure is 27 mm. The maximum tension force that should be resisted by the columns for the accidental load combination is equal to 1180 kN, and the maximum tension force in the beam is 70 kN. The largest tension force in the column occurs just below the truss. The tensile capacity of the timber members and connections turns out to be sufficient, and an alternative load path will be possible. Therefore, the additional steel cables underneath the beams will not be necessary. The alternative load path design calculation can be found in Appendix B.8.

3.17. Summary of design aspects

For the design of a hybrid wood-concrete super tall building important issues such as fire safety, manufacturability, vertical differential shortening, uplift forces, and the accidental loading design should be addressed. Vertical differential shortening can occur between the GLT frame and the reinforced concrete walls. Adjustment devices between the timber columns will be installed to compensate for the differential shortening. An additional steel plate with the required adjustment thickness can be placed between the bolted steel plates of the column splice connection. The mass timber structural components have large dimensions, and these are not common for mass timber. Therefore, close attention should be given to the manufacturability of these structural components. The beam sizes can have large width and lengths due to the continuous lamination. The timber structural components are glued in the factory, and the laminations overlap each other so that no straight through vertical joints occurs in the cross-section. The pre-drilling of the holes for the dowel-type connection will already be done in the factory, and also the openings in the beams for the slotted steel plates will be sawn in during the manufacturing process.

Tension forces can occur in the piles for light-weight structures due to the overturning moment at the base. The maximum uplift force in the foundation pile for the designed structure is equal to 590 kN in ULS. This means additional reinforcement should be placed in the foundation piles in order to resist the uplift forces.

For the design of a hybrid wood-concrete tall building fire safety design is an important issue. The high-rise structure is considered consequence class 3 (CC3), and the Dutch building regulation requires that the building should be fire resistant for at least 120 minutes. If the timber structural elements have enough mass a protective char-layer develops during a fire. It is decided to also protect the timber elements with gypsum plasterboard, and this will increase the fire resistance of the structural members. The gypsum plasterboard will fall off after a period of intense fire, and the charring of the mass timber starts. The timber beams with protective cladding will have a charring depth of 34 mm after 120 minutes of fire loading. As a consequence, all the steel plates, connectors, and dowels should be placed at a minimum distance of about 40 mm from the outer surface. The slotted steel plates are hidden in the timber and the ends of the dowels are covered by wooden plugs. An additional protective layer is placed next to the steel end-plates for the column splice connection so that the connection will also have a fire resistance of 120 minutes.

The structure has been checked for accidental loading and a second load path should be possible in the case of a column failure. When this happens the forces are redistributed through the surrounding columns and beams. The structure will start to hang onto the stiff outrigger/belt-truss level. Most of the tension force will be transferred through the columns to the outrigger level and a smaller part of the force will be redistributed through the beams. Especially, the timber connections will be critical for the accidental load combination and have been checked. It shows that the beam-to-column and column-to-column will be able to resist the occurring tension forces, and therefore it can be concluded that an alternative load path is possible during a column failure in the structure. The deflections in the beam and floor slab will increase a lot and the maximum deflection due to column failure is equal to 27 mm. However, the serviceability criterion for the deflections can be neglected for the accidental loading combination.

4

Connection details

This chapter discusses the connection details in the hybrid wood-concrete tall building.

4.1. Introduction

The connection details are an important design aspect for the stiffness and damping behaviour of the structure. For timber frame connections it is difficult to accomplish fully-rigid connection details, and slip often occurs in dowel-type connections. Therefore, the timber frame has been designed as a hinged frame. It is decided to work out the critical connections in the mass timber frame and also the connections details for the outrigger and belt-truss have been designed. The outrigger trusses transfer large tension and compression forces to the perimeter columns, and the outrigger connections will be critical details for the lateral stiffness of the structure. Figure 4.1 shows the specific connections that are worked out in more detail further on. The connection details are shown in the Appendix A and its design calculations can be found in Appendix B.

Beam-wall detail

Column splice detail

Beam-column detail

Column-podium slab detail
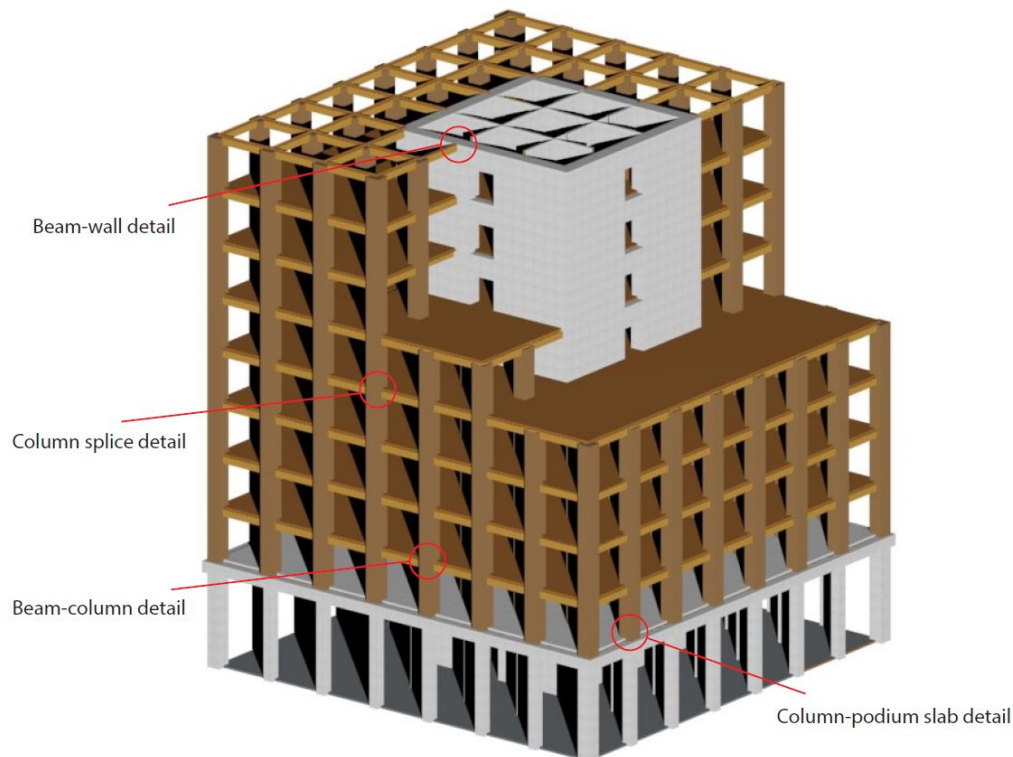
Figure 4.1: Overview of the connection details

4.2. Beam-to-column connection

From the parametric study it has been found that in the case of a rigid frame in which the beam-to-column connection is designed as moment resistant, it will increase the stiffness capacity of the structure by about 20 percent. Therefore, this would be a very effective measure to decrease the wind-induced response. However, it is more expensive and it increases the construction time to make all the connections moment resistant in the timber frame. For the final design, it is chosen to make the beam-to-column connection not moment resistant. The beam-to-column connection will be done with slotted steel plates with dowels. The dowels are loaded in two direction: parallel to the grain and perpendicular to the grain. In both direction the shear capacity of the dowels should be checked. The slotted steel plates are connected to the column with screws. As a reference for the connection is the slotted steel plate connection from the Rothoblaas catalogue used, which is shown in figure 4.2. The beam-to-column connection is a hidden connection, and the slotted-in steel plates lay inside the timber structural element. Advantages of this type of connection is that the steel connection is protected and isolated from fire by the timber element. This will increase the fire resistance time. Another advantage is the aesthetic part of a hidden connection.

Figure 4.2: Slotted steel plate connection Alumidi Rothoblaas

The forces which will occur in the connection are the shear force due to the vertical floor loading and the lateral force due to the wind load. The beam-to-column connection should be repeatable over all the storey levels in order to increase the efficiency of construction. The governing beam-to-column connection, in which the largest forces occur, is chosen for the design. The final connection design will be applied at all storey levels of the building.

The load-carrying capacity of the dowels has been checked. The shear capacity can be calculated with the Johansen's equations. These equations represent the failure modes that can occur in the connection. Figure 4.3 shows the failure modes for a steel-to-timber connection with a central plate. Failure mechanism (f) represents the crushing of the timber only, mechanism (g) represents one plastic hinge in the fastener, and mechanism (h) represents three plastic hinges in the fastener. The load-carrying capacity of a steel-to-timber connection is dependent on the thickness of the steel plate. The steel plate is classified as thin if the thickness is less than $0.5d$, where d is the diameter of the fastener. In the case the steel plate thickness is equal or great than d than the plate is classified as thick. In the case of the slotted steel plate, the formulas for a central plate with double shear planes can be used. Eq.(4.1) shows the equations for determining the characteristic load-carrying capacity for a central steel plate of a double shear connection.

$$F_{v,Rk} = \min \begin{cases} f_{h,1,k}t_1 d & (f) \\ f_{h,1,k}t_1 d \left[\sqrt{2 + \dfrac{4M_{y,Rk}}{f_{h,1,k}dt_1^2}}\right] + \dfrac{F_{ax,Rk}}{4} & (g) \\ 2.3\sqrt{M_{y,Rk}f_{h,1,k}d} + \dfrac{F_{ax,Rk}}{4} & (h) \end{cases} \qquad (4.1)$$

Where:

$f_{h,k}$	is the characteristic embedment strength in the timber member
t_1	is the smaller thickness of the timber side member
d	is the diameter of the fastener
$M_{y,Rk}$	is the characteristic fastener yield moment
$F_{ax,Rk}$	is the characteristic withdrawal capacity of the fastener
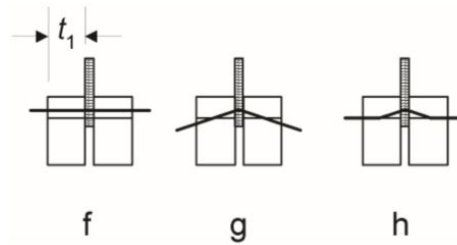
Figure 4.3: Failure mechanisms for a steel-to-timber connection with a central plate (NEN-EN1995, 1995)

The characteristic embedment strength in the timber member for a dowel-type connection can be calculated with Eq.(4.2), and the characteristic fastener yield moment can be calculated with Eq.(4.3). The given formula for the characteristic embedment strength parallel to the grain. For loading under an angle or perpendicular to the grain the embedment strength should be reduced.

$$f_{h,k} = 0.082(1 - 0.01d) \cdot \rho_k \tag{4.2}$$

$$M_{y,k} = 0.3 \cdot f_{u,k} \cdot d^{2.6} \tag{4.3}$$

Where:

d	is the diameter of the fastener
ρ_k	is the characteristic density of the timber
$f_{u,k}$	is the ultimate strength of the fastener

The withdrawal strength, $F_{ax,Rk}$, for dowels is taken equal to zero. On the other hand, for screw connections the withdrawal strength should be taken into account for determining the load-carrying capacity. The lateral force introduces tension and compression forces in the timber beam parallel to the grain. In the case the dowels are loaded parallel to the grain the effective number of fasteners should be used for the load-carrying capacity. The effective number of fasteners indicates how many dowels in a row are effective in carrying the load. For the beam-to-column connection only one dowel per row parallel to the grain is applied. Therefore, the effective number of fasteners is equal to the number of applied fasteners. The vertical shear force due to floor loading introduces a force perpendicular to grain in the timber beam element. A similar design calculation procedure as for the dowels loaded parallel to the grain is followed. It should be noted that the embedment strength of the timber is dependent on the angle of the force to the grain. The effective number of fasteners for loads perpendicular to the grain should be taken the same as the number of fasteners.

The screws connect the head steel plate of the connection to the column. The load carrying capacity of the screws should be checked. The screws are axially loaded and are loaded in shear. The following failure modes for the axially loaded screws should be checked: the withdrawal failure, the pull through of the head, the group effect, and the tensile failure of the screws. The pull through of the head of the screw will be acquired from tests, and is often given by the supplier of the fasteners. The characteristic withdrawal capacity for axially loaded screws can be calculated as follows:

$$F_{ax,Rk} = n_{ef}(\pi d l_{ef})^{0.8} f_{ax,k} \tag{4.4}$$

Where:

n_{ef} is the effective number of screws
l_{ef} is the penetration length of the threaded part
$f_{ax,k}$ is the characteristic withdrawal strength ($= 3.6 \cdot 10^{-3} \rho_k^{1.5}$)

The group effect of the screws in taken into account with the effective number of screws. The effective number of screws which are loaded by a force component parallel to the shank is given by:

$$n_{ef} = n^{0.9} \tag{4.5}$$

The screws are also loaded laterally, and for this the Johansen's equations for determining the load-carrying capacity are used. The connection type is a thick steel plate for a single shear plane. Eq.(4.6) shows the formula for calculating the characteristic load-carrying capacity for a thick steel plate in a single shear connection. The contribution of the rope effect for screw connections to the load-carrying capacity is 100%. This means the right term in Eq.(4.6) should also be included.

$$F_{v,Rk} = \min \begin{cases} f_{h,k}t_1 d\left[\sqrt{2 + \dfrac{4M_{y,Rk}}{f_{h,k}dt_1^2}} - 1 \right] + \dfrac{F_{ax,Rk}}{4} & (c) \\[3mm] 2.3 \sqrt{M_{y,Rk}f_{h,k}d} + \dfrac{F_{ax,Rk}}{4} & (d) \\[3mm] f_{h,k}t_1 d & (e) \end{cases} \tag{4.6}$$

The threaded part of the screw should be taken into account, and for the determining the load-carrying capacity the effective diameter is used. The effective diameter, d_{ef}, can be taken the same as the smooth shank diameter of the screw. The screw connection is subjected to a lateral load ($F_{v,Ed}$) and an axial load ($F_{ax,Ed}$). Therefore, the load-carrying capacity should be checked for a combined lateral and axial unity check. This combined axial and lateral loaded unity check is given by Eq.(4.7).

$$\left(\frac{F_{ax,Ed}}{F_{ax,Rd}} \right)^2 + \left(\frac{F_{v,Ed}}{F_{v,Rd}} \right)^2 \leq 1 \tag{4.7}$$

Where $F_{v,Rd}$ and $F_{ax,Rd}$ are the design load-carrying capacities for the lateral and axial load, respectively.

The minimum spacings and end distances of the fasteners should be determined. Based on the minimum spacings and end distances the layout of the dowels and screws can be designed. The minimum spacing and end distances are dependent on the type of fastener and in which direction the load is applied.

For timber which is subjected to a force perpendicular to the grain, the splitting capacity should be checked. There is a possibility of splitting of the timber caused by the tension force perpendicular to the grain. The design splitting capacity ($F_{90,Rd}$) should be larger than the tension force component (F_{Ed}). The characteristic splitting capacity can be calculated as follows:

$$F_{90,Rk} = 14bw \sqrt{\frac{h_e}{\left(1 - \dfrac{h_e}{h} \right)}} \tag{4.8}$$

Where:

b   is the thickness of the timber element
w   is the modification factor
h   is the height of the timber element
h_e is the loaded edge distance to the centre of the most distant fastener

Figure 4.4 shows the beam-to-column detail, and a larger figure of the detail can be found in the Appendix A.4. The calculation of the connection design can be found in Appendix B.6.1.
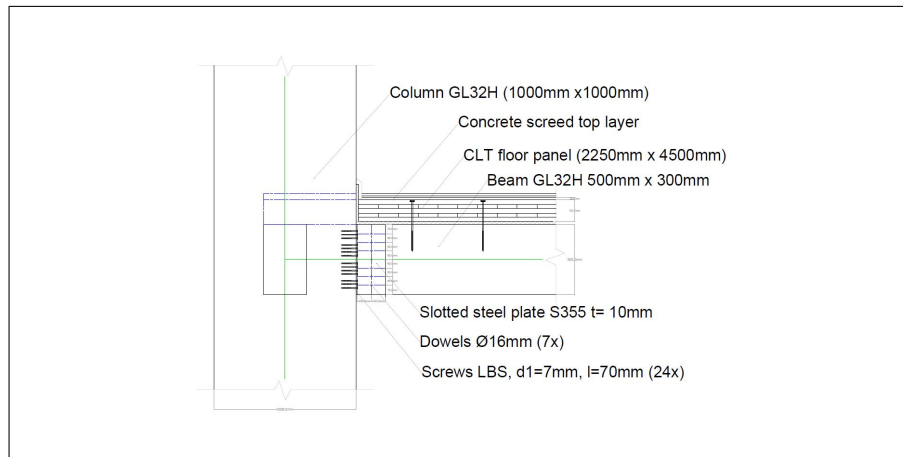
Figure 4.4: Beam-to-column connection detail

4.3. Column-to-column connection

The column splice connection will be carried out with glued-in rods and bolts. The column splice is applied every four storey levels of the structure, and this way the number of steel-timber connections in the structure can be reduced. The columns will have a length of 15 metres which is just within the limit for the transportation to the building site.

An important aspect of the column splice connection is that the columns should be placed in a straight line on top of each other. Imperfection in the steel plate surface could cause a small angle between the two columns. To avoid this a small layer of resin will be put in between the bolted steel plates to straighten out the imperfections. The connection of the columns could already be done in the factory. An additional steel plate could also be added in between the columns to adjust for differential shortening between the reinforced concrete core and the timber frame.

The following elements in the connection should be checked:
- Glued-in rods
- Bolts
- Steel head plate
- Welds

Glued-in rods

The load-carrying capacity of the glued-in rods will be checked in tension, compression and shear. The characteristic tension load-carrying capacity of the glued-in rods can be determined with the Eq.(4.9) found by Riberholt. This formula is used for glued-in rod with an embedment length greater than 200 mm.

$$F_{ax,Rk} = f_{ws} \cdot \rho_k \cdot d \cdot \sqrt{l_g} \qquad (4.9)$$

Where, l_g, is the embedment length of the glued-in rod, d is the diameter of the rod, ρ_k is the density of the timber, and f_{ws} is the strength parameter, and is dependent on the properties of the epoxy. For polyurethane adhesives f_{ws} is equal to 0.650 and for epoxy 0.520(Deng, 1997). The polyurethane adhesive is a non-brittle glue and the epoxy will give a brittle failure. The non-brittle failure is preferred and therefore the polyurethane adhesive will be applied for the glued-in rod connection.

The effective tensile area in the timber should also be checked for the glued-in rods. The effective area can be determined by a square around the centre of the rod with a length equal to the shortest distance from the fastener to the edge of the material (Boellaard, 2012). The effective tensile area can be checked with Eq.(4.10).

$$\sigma_{t,0,d} = \frac{N_{t,d}/4}{A_w} \leq f_{t,0,d} \tag{4.10}$$

Where:

A_w is the effective tensile area per rod
$N_{t,d}$ is the design tensile load
$f_{t,0,d}$ is the design tensile strength of timber

The lateral strength of the glued-in rods is checked. Eq.(4.11) gives the load carrying capacity per rod (Riberholt, 1986). The lateral strength is dependent on the embedment strength of the timber, $f_{h,k}$, and the characteristic yield moment of the fastener, $M_{y,Rk}$. Also, the eccentricity, e, which is the distance to the acting force, should be taken into account.

$$F_{v,Rk} = \left(\sqrt{e^2 + \frac{4M_{y,Rk}}{df_{h,k}}} \right) df_{hk} \tag{4.11}$$

The minimum end distance of the glued-in rod should be checked, and also the minimum required internal length of the rod. Based on the minimum spacings and end distances a design of the column splice connection can be made.

Bolts
The tension, shear and bearing resistance of the bolts in the steel head plate are checked according to NEN-EN1993-1-8. The tension resistance of the bolts can be determined as follows:

$$F_{t,Rd} = k_2 \cdot f_{u,b} \cdot \frac{A_s}{\gamma_{M2}} \tag{4.12}$$

Where the factor k_2 is 0.63 for countersunk bolts, $f_{u,b}$ is the ultimate tensile strength of the bolt, γ_M is the material factor, and A_s is the tensile stress area of the bolt.

The bearing resistance and shear resistance of the bolts can be calculated with Eq.(4.13) and Eq.(4.14), respectively.

$$F_{b,Rd} = k_1 \cdot \alpha_b \cdot \frac{A}{\gamma_{M2}} \tag{4.13}$$

$$F_{v,Rd} = 0.6 \cdot f_{u,b} \cdot \frac{A}{\gamma_{M2}} \tag{4.14}$$

Where, A, is the gross area of the bolt, k_1 is the factor for the edge bolt, and α_b the factor for the end bolt. The punching shear resistance of the steel head plate, $B_{p,Rd}$, is checked as follows:

$$B_{p,Rd} = 0.6 \cdot \pi \cdot d_m \cdot t_p \cdot \frac{f_u}{\gamma_{M2}} \tag{4.15}$$

Where:

d_m is the nominal diameter of the bolt
t_p is the thickness of the plate
f_u is the ultimate tensile strength of the plate
$\gamma_{M,2}$ is the material factor

The combined shear and tension forces in the bolts should be checked with Eq.(4.16).

$$\frac{F_{v,Ed}}{F_{v,Rd}} + \frac{F_{t,Ed}}{1.4F_{t,Rd}} \leq 1.0 \tag{4.16}$$

Steel head plate
The steel head plate will be designed using the T-stub method presented in NEN-EN1993-1-8. The bolted head plate is schematised as a T-stub. First, the effective length, l_{eff}, needs to be determined. The effective length is dependent on the yield pattern, the location of the bolt, and if an individual bolt or a bolt row is considered. The yield pattern around the bolt can be split up in a circular or non-circular pattern. Figure 4.5 shows the circular and non-circular yield pattern in the steel plate. In the calculation of the design tension resistance three modes are considered. The first mode is for complete yielding of the head plate, the second mode is for bolt failure with yielding of the plate, and the third mode is for bolt failure only. For the design resistance it is allowed that prying forces may develop. The design resistance of the T-stub flange is calculated as follows:

$$F_{T,Rd} = \begin{cases} \dfrac{4M_{pl,1,Rd}}{m} & \text{(Mode 1)} \\ \dfrac{2M_{pl,2,Rd} + n\sum F_{t,Rd}}{m + n} & \text{(Mode 2)} \\ \sum F_{t,Rd} & \text{(Mode3)} \end{cases} \tag{4.17}$$

Where, $M_{pl,Rd}$, is the design moment of plasticity, m is the distance from the centre of the bolt to the rod, and n is equal to e_{min} but should be smaller than $1.25m$. The distance from the edge of the plate to the centre of the bolt is defined as e_{min}.

Circular yield pattern   Non-circular yield pattern
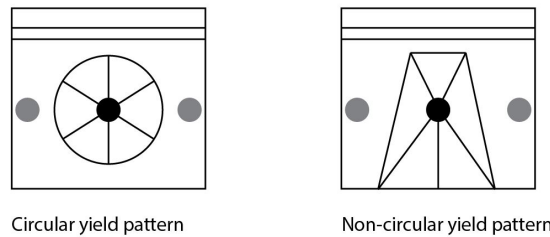
Figure 4.5: Circular and non-circular yield pattern in T-stub model, EC3

Welds
A fillet weld around the rod is applied to connect the rods to the head plate. The directional method for fillet welds is used to determine the strength of the welds. The resistance of the weld should be checked with Eq.(4.18).

$$\sqrt{\sigma_\perp^2 + 3(\tau_\perp^2 + \tau_\parallel^2)} \leq f_u/(\beta_w\gamma_{M2}) \tag{4.18}$$

Where:

$\sigma_\perp$ is the normal stress perpendicular to throat of the weld
$\tau_\perp$ is the shear stress perpendicular to the axis of the weld
$\tau_\parallel$ is the shear stress parallel to the axis of the weld

f_u is the ultimate tensile strength of the steel
β_w is a correlation factor of the weld

Translational stiffness

The translational stiffness of the column-to-column connections is determined. This is done to see the influence of the stiffness of the connection on the lateral wind-induced displacements. To find the total translational stiffness the connection is split up into three components: the glued-in rods, the bolts and the steel plate. For each component the translational stiffness is determined and combined as one spring stiffness according to Eq.(4.19).

$$K_{v,column} = \sum \frac{1}{k_n} \tag{4.19}$$

The determined spring stiffness of the components are modelled in series. Therefore, the total stiffness in the column is equal to the sum of the inverse of the individual stiffness of the components. The total stiffness in the column-to-column connection can be represented as a translational spring in the finite element model. The translational springs are placed every four storey levels, and the effect on the wind-induced lateral displacements will be analysed for the SLS wind load combination. Tension forces will occur in the perimeter columns, however, most columns are loaded in compression due to the self-weight of the structure. The connection has a large stiffness, and the increase in the lateral displacements will be small. An increase of less than one percent of the lateral displacement is found, and this means the translational stiffness of the column-to-column connection is sufficient.

Figure 4.6 shows the detail of the column-to-column connection. It can be seen that there are also small openings in the column so that the surplus of the epoxy around the glued-in rods can flow away. The connection design calculation can be found in Appendix B.6.2.
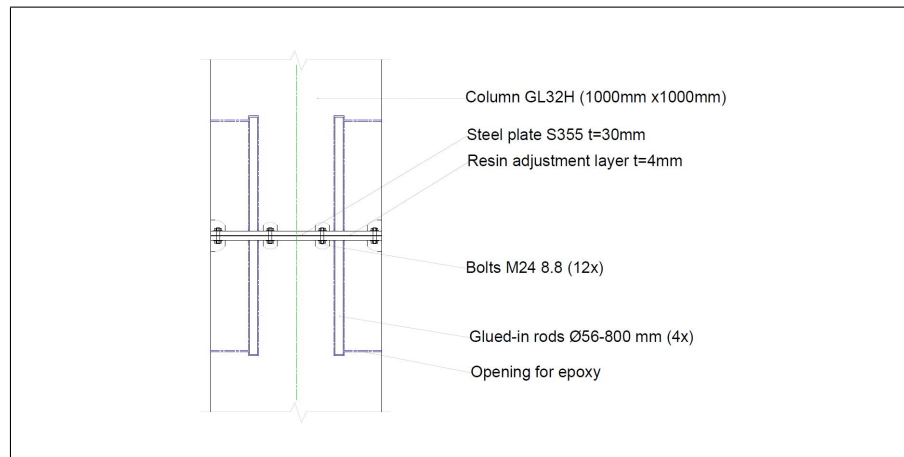
Figure 4.6: Column-to-column connection detail

4.4. Outrigger/belt-truss connections

4.4.1. Outrigger-truss connection

The connections of the outriggers will be done with slotted-in steel plates and dowels. The tension forces in these connections can become very large. The connections should be designed with great care because the outrigger levels are essential for the global stiffness of the structure. Such large timber connection types are not common, but current research shows that even large tensile forces up to 6.5MN can be resisted (Blass, 2010). Especially, in large timber bridges such connection details are more conventional.

Two details that are part of the outrigger truss will be designed, and in these connection details occur the governing forces. The other connections in the outrigger trusses will have a similar design as for detail A and B, and the only difference will be that less dowels are required for these connection details. Figure 4.7 shows the connection details A and B. It can be seen that the largest forces occur in the diagonals of the outrigger truss. Two slotted steel plates with dowels are used for connecting the members in the truss. The outrigger truss consist of LVL timber elements, which have a higher strength than the glued laminated timber.
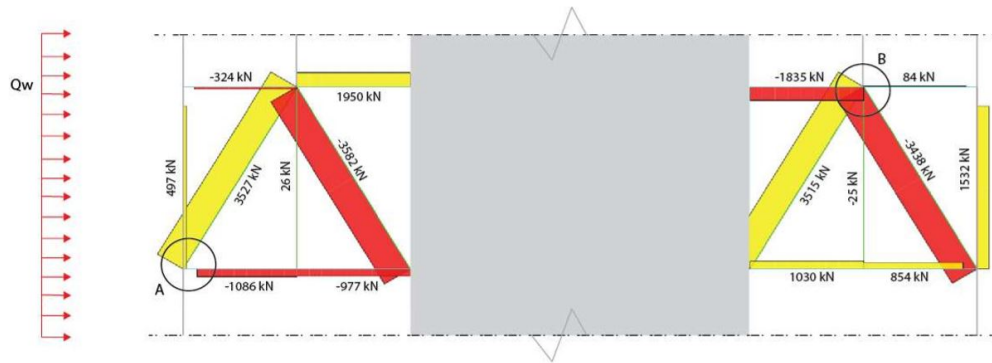
Figure 4.7: Outrigger truss at storey level 21 with axial forces for SLS wind load case.

The lateral stiffness of the dowels will be checked with the Johansen equations for a thick plate in a single shear plane. Eq.(4.6) can be used for determining the load-carrying capacity of the steel-to-timber connection. In each connection two slotted-in steel plates are used, and this will result in a steel-to-timber connection with a total of four shear planes. The load-carrying capacity of the dowels in the beam-to-column part is checked in two direction: parallel and perpendicular to the grain. Due to the diagonal the tension strength at an angle to the grain should be checked. For dowels, the embedment strength in the timber under an angle to the grain can be calculated with the Hankinson formula, which is formulated as follows:

$$f_{h,\alpha,k} = \frac{f_{h,0,k}}{k_{90} \cdot \sin^2 \alpha + \cos^2 \alpha} \tag{4.20}$$

Where:

$f_{h,0,k}$ is the characteristic embedment strength parallel to the grain
α is the load angle to the grain
and: $k_{90} = 1.30 + 0.015d$

For the design of the dowel parallel to the grain the effective number of dowels should be determined. The effective number of fasteners can be calculated as follows:

$$n_{ef} = \min \begin{cases} n \\ n^{0.9} \sqrt[4]{\dfrac{a_1}{13d}} \end{cases} \tag{4.21}$$

Where:

n is the number of fasteners
a_1 is the spacing of the fasteners
d is the diameter of the fasteners

The minimum end distances and spacing of the fasteners should be calculated. Based on these minimum distances a design of the connection can be made. The connection design

calculation will be split up into a column, beam and diagonal part, and for each part the required number of fasteners has been calculated. The splitting capacity of the timber, and the strength of the steel plates are also checked for each connection detail.

Figure 4.8 and 4.9 show the outrigger truss detail A and B, respectively. It can be seen in the details that the truss will be done in laminated veneer timber due to the fact this has higher strength properties than the glued laminated timber. The connection design calculation can be found in Appendix B.6.4.
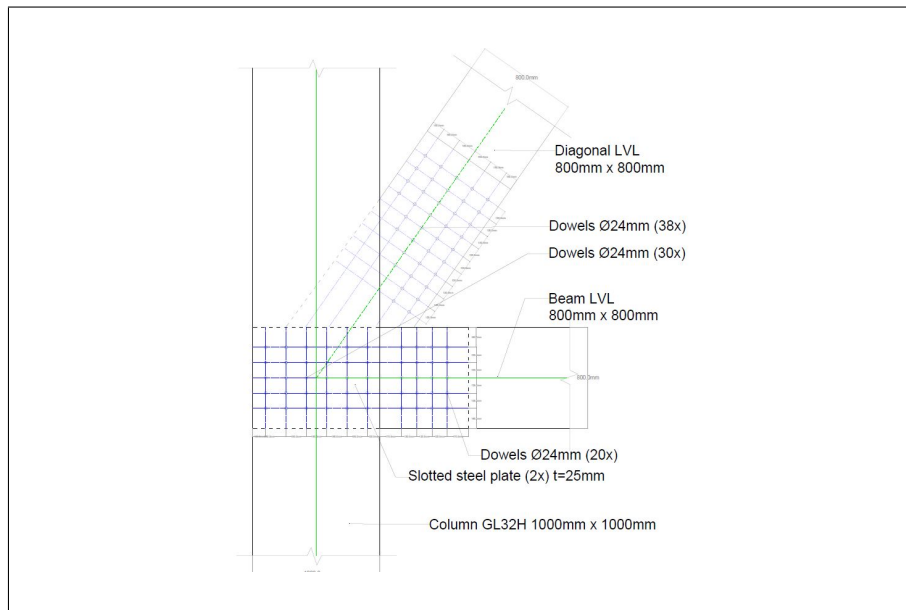
Figure 4.8: Outrigger truss detail A at storey level 21
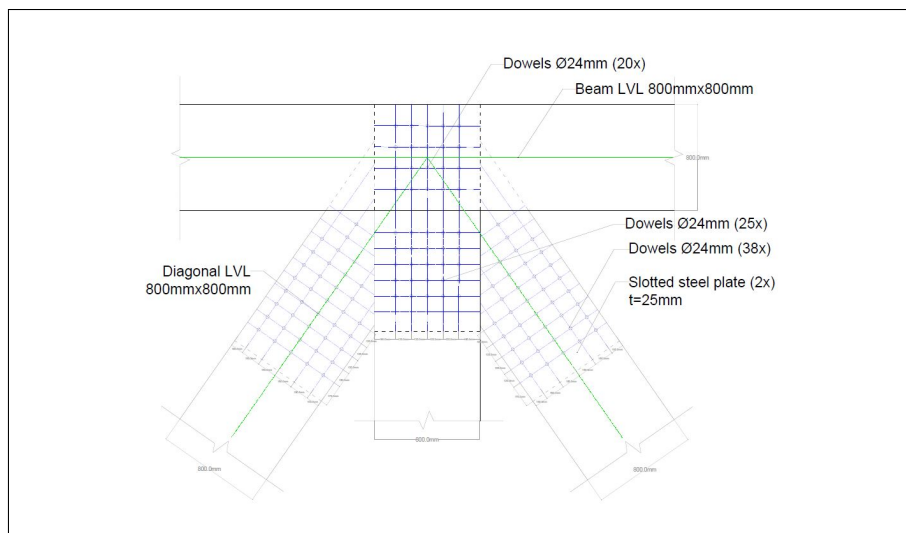
Figure 4.9: Outrigger truss detail B at storey level 21

4.4.2. Belt-truss connection

The belt-truss transfers the force from the outrigger to the perimeter columns. Figure 4.10 shows the forces that occur in the belt-truss for the SLS wind load case. It can be seen that large tension forces occur in the diagonals of the truss. The dowel-type connection should have adequate strength to resist these large tension forces. The connection of the diagonals to the column will be done with two slotted-in steel plates and dowels. The slotted-in steel plates are welded to the head steel plate which in its turn is connected to the column with bolts. These bolts will go through the column and will connect the head plate at the opposite side of the column.
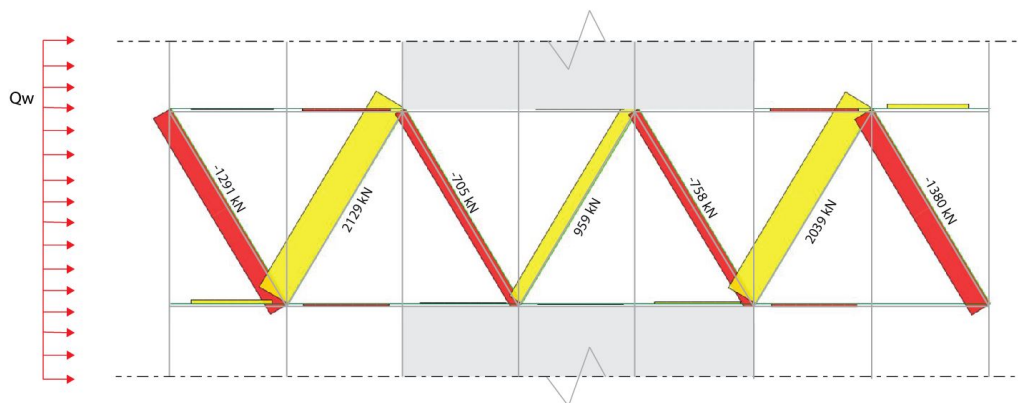
Figure 4.10: Belt-truss at storey level 21 with axial forces for SLS wind load case

Figure 4.11 shows the diagonal-to-column detail of the belt-truss. For the dowel-type connection two slotted-in steel plates are used, which will result in a total of four shear planes. The dowels have been checked for their tension resistance parallel to the grain. A total of 24 dowels with a diameter of 24mm will be used for the connection, and this results in a tension resistance of 3992 kN. For the governing ULS load combination the design tension force in the diagonal is equal to 3602 kN. The bolts in the column will be checked for the tension and lateral resistance. For the bolts in the head plate only one shear plane exists. Therefore, a large number of bolts is required to have sufficient lateral load-carrying capacity. As an alternative solution, to reduce the number of bolts, a block of steel at the ends of the head plate will be added. These additional elements will introduces the lateral force to the timber column. The GLT column will be loaded parallel to the grain, and the compression stress in the timber should be checked. The load-carrying capacity of the head plate has been checked using the equivalent T-stub model according to the NEN-EN1993-1-8.

The calculation of the belt-truss connection design can be found in Appendix B.6.5.
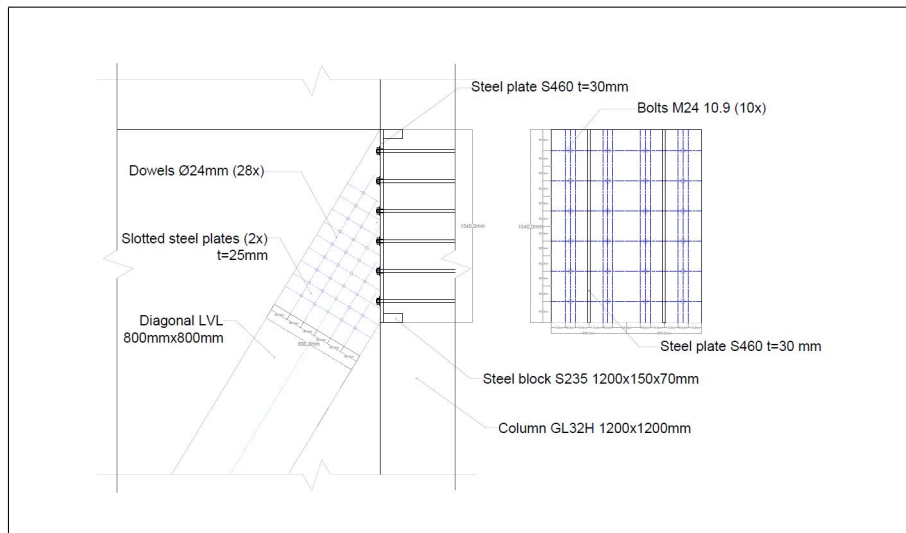
Figure 4.11: Belt-truss detail at storey level 21

4.5. Inter-connection floor slabs

The inter-connections between the CLT floor panels will be done with an internal spline and screws connection. The internal spline consists of a laminated veneer strip with a thickness of 35mm. Figure 4.12 shows the detail of the inter-connection of the floor slabs. The LVL strip is hidden in the CLT floor panels and connected with self-tapping screws. After the two floor slabs are connected a thin concrete layer will be poured on top. The connection provides a double-shear connection, and the connection should be designed to resist in-plane shear and bending out-of-plane. The floor slab connection should also be able to transfer the in-plane diaphragm forces due to the wind-load. Adhesives could be added to the connection if more stiffness is required. The inter-spline connections will be established on site.
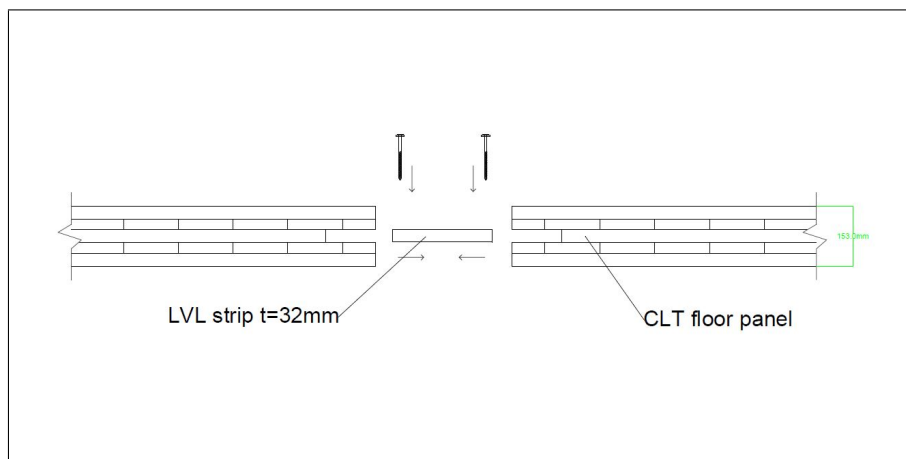
Figure 4.12: Inter-connection of floor panels

4.6. Beam-to-concrete wall connection

The beam-to-wall connection will be done in a similar way as the beam-to-column connection. Figure 4.13 shows the detail of the beam-to-concrete wall detail. The main difference with the calculation for beam-to-column connection is the calculation of the headed studs. The

headed studs are used to connect the steel plate to the wall and the headed studs will be poured into the concrete wall. The headed studs should be checked for their tension and shear resistance, and also the pull out resistance should be checked. The concrete should have sufficient strength and the load bearing area of the headed should be large enough. The pull-out failure of the headed studs can be calculated as follows:

$$N_{Rd,p} = n \cdot \frac{p_{uk}}{\gamma_{Mc}} \cdot A_h \tag{4.22}$$

In which:

n is the number of headed studs
p_{uk} is factor for considering head pressing
γ_{Mc} is partial safety factor for concrete
A_h is the cross-sectional area of effective head

For the connection design 4 headed studs will be used with each a diameter of 22mm and a head diameter of 35mm. These will give sufficient pull-out resistance. The calculation of the beam-to-wall connection can be found in the Appendix B.6.3.
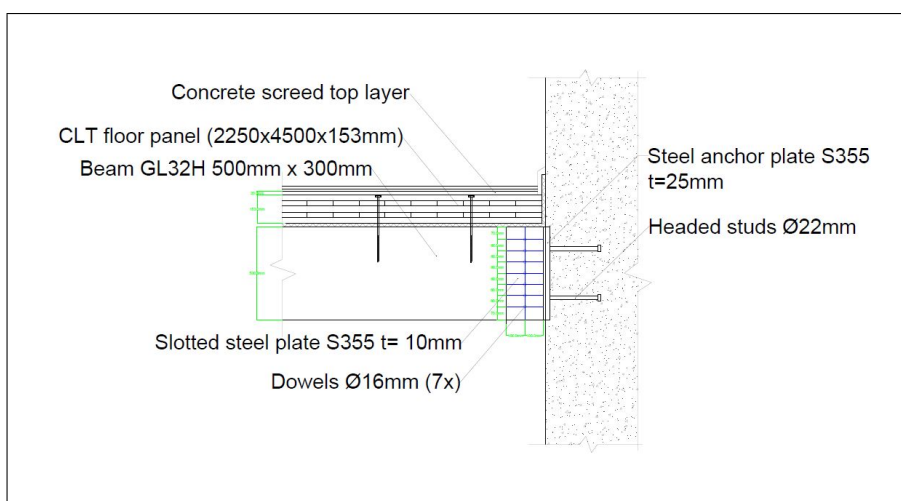
Figure 4.13: Beam-to-wall connection detail

4.7. Summary of connection design

The connection details are an essential design aspect for the stiffness and damping behaviour of the structure. For timber frame connections it is difficult to accomplish fully rigid connection details, and slip often occurs in dowel-type connections. Therefore, the timber frame connections have been designed as hinges. The beam-to-column connection is performed with slotted-in steel plates with dowels. The forces which will occur in the connection are the shear force due to the vertical floor loading and the lateral force due to the wind load. The beam-to-column connections are repeatable over all the storey levels and will make the construction more efficient. The beam-to-concrete wall connection is similar to the beam-to-column connection, and the main difference with the beam-to-column connection is the calculation of the headed studs which are poured into the concrete wall. The headed studs are checked for their tension, shear and pull-out resistance.

The column-to-column connection has been carried out with glued-in rods and bolts. The column splice is applied at every four storey levels of the structure. The resistance of the glued-in rods, bolts, steel head plate, and welds in the connection are checked. The maximum design tensile load that occurs in the column-to-column connection is equal to 1260 kN in ULS.

The outrigger trusses transfer large tension and compression forces to the perimeter columns, and the outrigger connections are critical details for the overall stiffness of the structure. The connections of the outriggers have been carried out with slotted steel plates and dowels. The design of the connection is mostly governed by the large tension force of 4247 kN in the diagonal of the truss, and to resist this forces a total number of 38 dowels with a diameter of 24mm will be required.

The connection of the belt-truss is similar to the outrigger truss connection and consists of two slotted steel plates and dowels. The slotted steel plates are welded to the head steel plate which is connected to the column with bolts. Only one shear plane exists for the bolts in the head plate compared to the four shear planes for the dowels in the slotted steel plates. Therefore, a large number of bolts is required to have sufficient lateral load-carrying capacity. As an alternative solution, to reduce the number of bolts, a block of steel at the end of the head plate will be added, which introduces the lateral force to the timber column.

5

Lateral wind load according to Building Code

Within this chapter, the calculation procedure of the lateral wind load on a structure according to building codes are described.

5.1. Wind loading according to Eurocode

5.1.1. Introduction

The Eurocode describes two procedures to calculate the wind pressures on the building: the force coefficient method and the surface pressure method. For structures with an aspect ratio $H/D > 5$ the force coefficient method should be applied. In this chapter only the force coefficient method is going to be further discussed. The characteristic global wind loading on a building is given by:

$$
\begin{aligned}
F_w &= c_s c_d \cdot \sum_{surfaces} w_e \cdot A_{ref} \\
&= c_s c_d \cdot \sum_{surfaces} q_b \cdot c_e(z_e) \cdot c_f \cdot A_{ref}
\end{aligned}
$$

(5.1)

where:

q_b	is the basic velocity pressure
$c_e(z_e)$	is the exposure factor
c_f	is the force coefficient
$c_s c_d$	is the structural factor
A_{ref}	is the reference area

In the following sections the calculation procedure of the above parameters will be described. The wind calculation in the Eurocode is valid for buildings with a maximum height of 200 metres. For buildings taller than this height an additional wind tunnel study is recommended. The Dubai wind building code is similar to the Eurocode and can be used to determine the wind load for building with a height above 200 metres.

5.1.2. Mean wind velocity

The mean wind velocity $v_m(z)$ is the basic wind velocity which is corrected for the height z with the terrain orography and the terrain roughness. The mean wind velocity can be calculated as follows:

$$v_m(z) = c_r(z) \cdot c_0(z) \cdot v_b$$

(5.2)

Where $c_r(z)$ is the terrain roughness factor, and this factor can be calculated as follows:
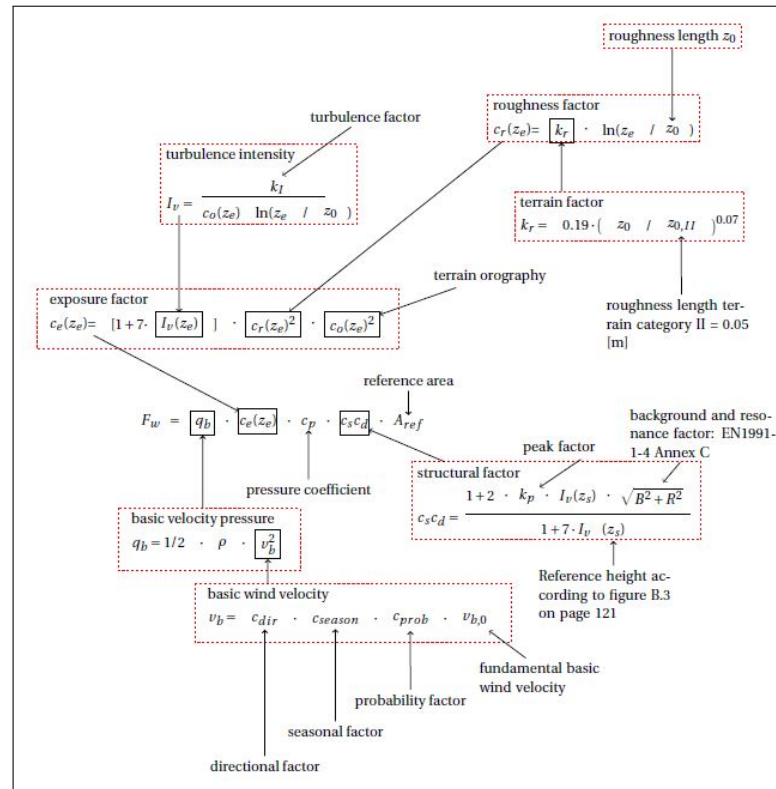
Figure 5.1: Overview wind calculation Eurocode, (La Gasse, 2017)

$$c_r(z) = k_r \cdot \ln(\frac{z}{z_0}) \quad for \ z_{min} \leq z \leq z_{max}$$
$$c_r(z) = c_r(z_{min}) \quad for \ z \leq z_{min} \tag{5.3}$$

In the Eurocode the z_{max} is defined as 200 metres. The Dubai building code has no building height limit for the wind load calculation. The procedure for the wind load calculation in the Dubai building code is similar to the one described in the Eurocode. The main difference is that for the calculation of the terrain roughness factor no height limit is applied, and the formula for heights above 200 metres is defined as follows:

$$c_r(z) = k_r \cdot \ln(\frac{z}{z_0}) \quad for \ z > z_{min} \tag{5.4}$$

The terrain roughness factor accounts for the variability of the mean wind velocity due to the height above the ground level and the ground roughness upstream of the building (La Gasse, 2017).

The terrain factor k_r is given by the following formula:

$$k_r = 0.19(\frac{z_0}{0.05})^{0.07} \tag{5.5}$$

Where z_0 is the roughness length and characterizes the terrain category roughness. The Dutch Annex describes three terrain categories: sea or coastal area, non-urban area and an urban area. For category three urban area the roughness length, z_0, is 0.5 metre and the minimum height, z_{min}, is equal to 7 metres.

The terrain orography factor $c_0(0)$ takes into account the landscape around the building. The Dutch annex advises to use the unit value for this factor.

The basic wind velocity v_b can be calculated as follows:

$$v_b = v_{b,0} \cdot c_{dir} \cdot c_{season} \cdot c_{prob} \tag{5.6}$$

where $v_{b,0}$ is the mean wind velocity with a return period of 50 years at 10 metres above the ground level. The city Rotterdam is located in wind area two and therefore the $v_{b,0}$ is 27.0 m/s^2.

The directional factor c_{dir} accounts for the wind direction. This directional factor is the ratio between the characteristic wind velocity for a certain wind direction and the characteristic wind velocity irrespective of the wind direction (La Gasse, 2017). The Dutch National Annex advices to use a value of 1.0 and this is a conservative value.

The seasonal factor, c_{season}, accounts for the season for which the building will be designed. This is especially important for temporary structures. The Dutch National Annex recommends also to use the unit value for this factor.

The c_{prob} accounts for the probability of exceeding the basic wind velocity. This factor is only taken into account in the case the return period is not 50 years.

When the Dutch National Annex recommendations are followed and the unit value for the directional and seasonal factor are chosen, the v_b will be equal to the $v_{b,0}$.

5.1.3. Peak wind pressure
The peak wind pressure calculated in the Eurocode NEN-EN1991-1-4 has a return period of 50 years and can by calculated with the following formula:

$$q_p(z) = (1 + 7I_v(z)) \cdot \frac{\rho}{2} \cdot v_m{}^2 \tag{5.7}$$

Where:

v_m the mean wind velocity
ρ is the density of the air
$I_v(z)$ is the turbulence intensity

The gust amplification factor is described by the term, $(1 + 7I_v(z))$. The turbulence of the wind is influenced by the surrounding terrain. This turbulence causes short duration peak loads on the structure. To account for this effect the characteristic mean wind velocity is multiplied by an amplification factor. This method is called the gust factor approach and was first described by Davenport. The turbulence intensity $I_v(z)$ is calculated as follows:

$$I_v(z) = \frac{\sigma_v}{v_m(z)} = \frac{k_l}{c_0(z) \cdot \ln(\frac{z}{z_0})} \quad for \ z_{min} \leq z_{max}$$

$$I_v(z) = I_v(z_{min}) \quad for \ z < z_{min} \tag{5.8}$$

Where, v_m, is the mean wind velocity and, σ_v, is the standard deviation of the wind velocity.

In the Eurocode the wind calculation is valid up to a height of 200 metres ($z_{max} = 200m$). The Dubai building code has no height limit for the wind load calculation. The procedure for the wind load calculation in the Dubai building code is similar to the one described in the Eurocode. The main difference is that for the calculation of the turbulence intensity there is no height limit, and the formula for heights above 200 metres is defined as follows:

$$I_v(z) = \frac{1}{c_0(z) \cdot \ln(\frac{z}{z_0})} \tag{5.9}$$

The turbulence factor k_l is given in the Dutch National Annex and it is recommended to take the unit value for this factor. The orography factor c_0 and the roughness length z_0 are already described earlier in this chapter.

5.1.4. Structural dynamic factor

A structural dynamic factor, $c_s c_d$, should be applied for buildings higher than 15 metre, for façades and roof elements with a natural frequency lower than 5 Hz, and for framed buildings with structural walls with a height above 100 meters and a height over width aspect ratio larger than four. For the concept design with a height of 300 metres the slenderness ratio is equal to 10 and a structural dynamic factor should be applied.

The structural factor, c_s, takes into account the reduction effect of the wind loading due to the non-simultaneous action of the peak wind pressures on the building facade. The dynamic factor, c_d, accounts for the increasing effect of the vibrations due to the turbulence in resonance with the structure. The dynamic factor defines the structure's response due to the wind turbulence. The structural dynamic factor can be calculated as follows:

$$c_s c_d = \frac{1 + 2 \cdot k_p \cdot I_v(z_s) \cdot \sqrt{B^2 + R^2}}{1 + 7 \cdot I_v(z_s)} \geq 0.85 \tag{5.10}$$

Where z_s is the reference height for determining the building shape factor. For slender high-rise buildings this is equal to 0.6 times the building height. The peak factor k_p is the determined ratio of the maximum value of the fluctuating part of the response to its standard deviation. The background response factor B^2 allows for the lack of full correlation of the wind surface pressure on the structure's facade. The resonance response factor R^2 takes into account the turbulence in resonance with the vibration mode.

The peak factor k_p can be calculated as follows:

$$k_p = \sqrt{2 \ln(\nu T)} + \frac{0.6}{\sqrt{2 \ln(\nu T)}} \geq 3 \tag{5.11}$$

Where ν is the frequency of a gust:

$$\nu = n_1 \sqrt{\frac{R^2}{B^2 + R^2}} \geq 0.08 Hz \tag{5.12}$$

The natural frequency n_1 can be estimated by:

$$n_1 = \frac{46}{H} \tag{5.13}$$

The background response factor, B^2, allows for the lack of full correlation of the wind surface pressure on the structure and takes into account that the wind pressure always has a local behaviour on the facade. The Dutch Annex states that the background response factor should be determined with the Annex C of the Eurocode NEN-EN1991-1-4, and can be calculated as follows:

$$B^2 = \frac{1}{1 + \frac{3}{2} \sqrt{\left(\frac{b}{L(z_s)}\right)^2 + \left(\frac{h}{L(z_s)}\right)^2 + \left(\frac{b}{L(z_s)} \cdot \frac{h}{L(z_s)}\right)^2}} \tag{5.14}$$

Where:

b   the width of the structure
h   is the height of the structure
$L(z_s)$ is the turbulence length scale

The turbulence length scale is given in Annex B.1 of the NEN-EN1991-1-4:

$$L(z_s) = L_t \left(\frac{z_s}{z_t}\right)^\alpha \quad for \ z \geq z_{min}$$
$$L(z_s) = L(z_{min}) \quad for \ z < z_{min}$$

(5.15)

Where:

L_t the reference length scale
z_t is the reference height
α-factor $= 0.67 + 0.05 \ln z_0$

The resonance response factor, R^2, should be determined with the Annex C according to the Dutch National Annex, and can be calculated as follows:

$$R^2 = \frac{\pi^2}{2\delta} S_L K_S$$

(5.16)

Where:

δ is the logarithmic decrement of the total damping
S_L is the non-dimensional spectral density function
K_S is the size reduction factor

The logarithmic decrement of the total damping can be split up into three parts: the logarithmic decrement of the structural damping δ_s, the logarithmic decrement of the aerodynamic damping δ_a, and the logarithmic decrement of the damping due to auxiliary devices. The Eurocode gives the structural damping for several construction types, however, for timber buildings no value is given. Therefore, it is chosen to use the logarithmic decrement of the structural damping for timber bridges of 0.06-0.12. The logarithmic decrement of the structural damping for reinforced concrete buildings is 0.10.

The logarithmic decrement of the aerodynamic damping for the natural frequency can be estimated as follows:

$$\delta_a = \frac{c_f \rho b v_m(z_s)}{2 n_1 m_e}$$

(5.17)

Where:

c_f the force coefficient
ρ the air density (=1.25 kg/m^3)
$v_m(z_s)$ is the mean wind velocity at height z_s
n_1 is the natural frequency of the building
m_e is the equivalent mass

The force coefficient, c_f, takes into account the building shape and the end effect factor. The force coefficient for structures with a rectangular cross-section can be calculated as follows:

$$c_f = c_{f,0} \cdot \psi_r \cdot \psi_\lambda$$

(5.18)

The $c_{f,0}$ is the force coefficient factor without corrections and could be used for buildings with a rectangular cross-section and sharp corners. The required $c_{f,0}$ can be read from figure 5.2, which can be found in the NEN-EN1991-1-4, Chapter 7. For a squared cross-section the value for $c_{f,0}$ is equal to 2.1. However, the Dutch National Annex recommends to take a value of 2.0 for all structures with a rectangular cross-section and sharp edges.

The ψ_r is the reduction factor to account for rounded corners and is dependent on the Reynolds number. In the case the structure has sharp edges no reduction should be applied and the unit value should be taken as input. The effect of the rounded corners for the concept design will also be analysed and discussed further on of this report in Chapter 7, Parametric Study and Optimization. Figure 5.3 shows the values for ψ_r for a building with a squared cross-section and rounded edges.
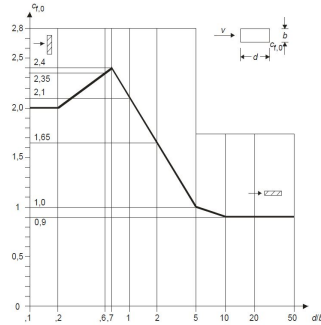
Figure 5.2: Force coefficient, $c_{f,0}$ (NEN-EN1991, 2002)
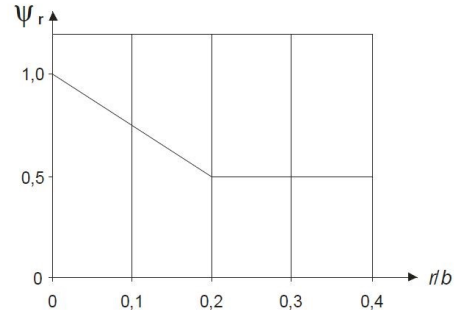
Figure 5.3: Reduction factor ψ_r for a squared cross-section with rounded edges (NEN-EN1991, 2002)

The ψ_λ is the end effect factor, and this factor takes into account the reduced resistance of the building due to the wind flow near the structure's ends. The end effect factor can be determined with the help of figure 5.4 which can be found in the NEN-EN1991-1-4, Chapter 7, figure 7.36. To acquire the value for the end effect factor ψ_λ, first the effective slenderness λ and the degree of fullness ϕ should be determined. The effective slenderness for structures with a rectangular cross-sections can be calculated as follows:

$$\lambda = \min \begin{cases} 1.4 \cdot \dfrac{l}{d} \\ 70 \end{cases} \tag{5.19}$$

The degree of fullness λ is given by:

$$\phi = \frac{A}{A_c} \tag{5.20}$$

Where, A, is the sum of the projected surfaces of all the elements, and A_c is the total enclosed surfaces ($A_c = l \cdot b$). In the case the facade is fully closed the degree of fullness can be taken as 1.0.
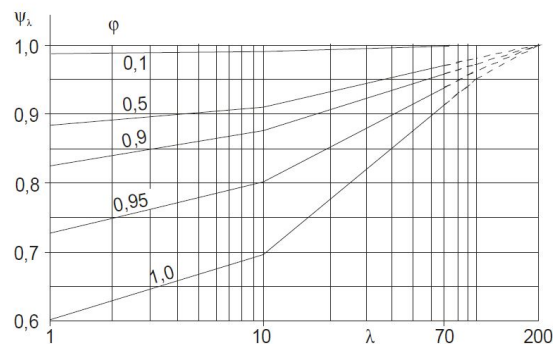
Figure 5.4: Indicative values of the end effect factor ψ_λ as function of the degree of fullness ϕ versus the effective slenderness λ, (NEN-EN1991, 2002)

The non-dimensional spectral density function is also called the wind variance spectrum and is an empirically based formula. In the spectral approach by Davenport a different wind variance spectrum could be used, and for example the Karman, Davenport and Harris variance spectra are common. Figure 5.5 shows the spectral density function S_L used in the Eurocode, and the wind variance spectrum can be calculated as follows:

$$S_L = \frac{6.8 f_L}{\left(1 + 10.2 f_L\right)^{5/3}} \tag{5.21}$$

Where the dimensionless frequency $f_L = \dfrac{n_1 L(z_s)}{v_m(z_s)}$
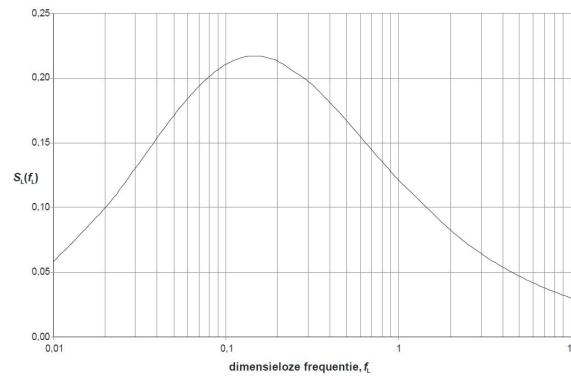
Figure 5.5: Spectral density function $S_L(f_L)$, Figure B.1 EC1-1-4

The size reduction factor K_s is given by:

$$K_s = \frac{1}{1 + \sqrt{\left(G_y \phi_y\right)^2 + \left(G_z \phi_z\right)^2 + \left(\frac{2}{\pi} G_y \phi_y G_z \phi_z\right)^2}} \tag{5.22}$$

$$\phi_y = \frac{c_y b n_1}{v_m(z_s)}; \quad \phi_z = \frac{c_z h n_1}{v_m(z_s)} \tag{5.23}$$

The constants c_y and c_z are both equal to 11.5. The constants G_y and G_z are dependent on the vibration mode. For tall buildings the vibration mode over the height can be assumed parabolic, and in this case $G_z = 5/18$ should be used. The vibration mode over the width of the building can be assumed uniform, and this gives $G_y = 1/2$.

5.1.5. Peak accelerations
In this section the peak accelerations will be calculated according to the EN-NEN1991-1-4 Annex C. The Annex B also gives a calculation procedure to get the peak acceleration, however, the Dutch National Annex recommends to use the Annex C.

The characteristic peak acceleration can be determined as follows:

$$a_{max}(y, z) = \sigma_{a,x}(y, z) \cdot k_p \tag{5.24}$$

Where:

$\sigma_{a,x}(y, z)$ is the standard deviation of the characteristic along-wind acceleration
k_p is the gust peak factor

The standard deviation $\sigma_{a,x}$ of the characteristic along-wind acceleration can be estimated as follows:

$$\sigma_{a,x}(y,z) = c_f \cdot \rho \cdot I_v(z_s) \cdot v_m^2(z_s) \cdot R \cdot \frac{K_y \cdot K_z \cdot \Phi(y,z)}{\mu_{ref} \cdot \Phi_{max}} \tag{5.25}$$

Where:

c_f	the force coefficient
ρ	is the air density
μ_{ref}	is the reference mass per unit surface
$I_v(z_s)$	is the turbulence intensity at height z_s
R	is the square-root of the resonance response factor
K_y, K_z	are non-dimensional coefficients
$\Phi(y,z)$	is the vibration mode

The peak factor k_p is the ratio of the maximum fluctuating response and its standard deviation. The peak factor can be calculated according to the following formula:

$$k_p = \max \begin{cases} \sqrt{2 \cdot \ln(v \cdot T)} + \dfrac{0.6}{\sqrt{2 \cdot \ln(v \cdot T)}} \\ 3 \end{cases} \tag{5.26}$$

T	is the average period of the reference wind velocity, $T = 600$ seconds
v	is the estimation of the gust frequency

The gust frequency can be determined as follows:

$$v = n_{1,x} \sqrt{\frac{R^2}{B^2 + R^2}} \quad ; \quad v \geq 0.08 \ Hz \tag{5.27}$$

The limit of the gust frequency of 0.08 Hz corresponds with a peak factor of 3.0. The $n_{1,x}$ is the natural frequency of the building, R^2 is the resonance response factor, and B^2 is the background response factor.

The μ_{ref} is the reference mass per unit surface and can be determined by Eq.(5.28) according to section F.5 in the Eurocode. A good estimation of the reference mass would be to take the mass per unit surface at the location with the largest amplitude of the vibration mode.

$$\mu_{ref} = \frac{\int_0^h \int_0^b \mu(y,z) \cdot \Phi_1^2(y,z) dy dz}{\int_0^h \int_0^b \Phi_1^2(y,z) dy dz} \tag{5.28}$$

The fundamental vibration mode in the vertical direction is assumed parabolic. Figure 5.6 shows this fundamental vibration shape of the tall building.

5.1.6. Results

The distribution of the peak wind pressure depends on the shape of the building. For buildings in which $h > 2b$ is valid the distribution shown in figure 5.9 should be used. For the designed tall building the middle part of the building will be divided into twenty-four strips and the division of those strips can be seen in Annex A, Table C.4.

Table 5.1 shows the damping values that are used for the calculation. The total global damping ratio is equal to 2.15 %, and this is without an additional damping device or optimization of the building shape. Figure 5.7 shows the global wind pressure over the height of the building on the windward façade. Figure 5.8 shows the results of the peak response accelerations. The calculation is done in MatLab and the script can be found in the Appendix E.
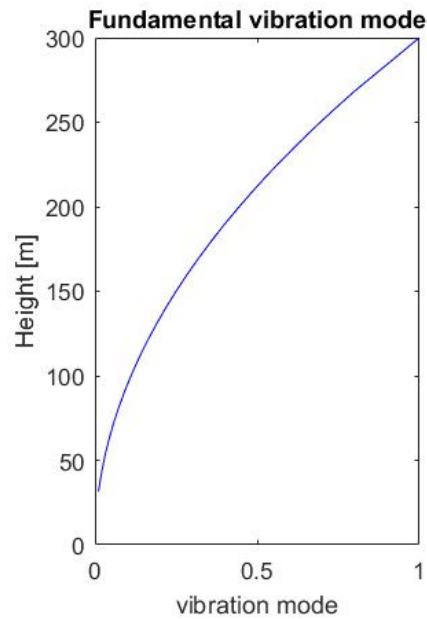
Figure 5.6: Fundamental vibration mode $\Phi_1(y,z)$

As can be seen in figure 5.8 the peak wind acceleration at the top level of the building is equal to $0.402 \ m/s^2$. Figure 5.10 shows the comfort criteria for the peak accelerations according to the NEN6702 with a return period of 50 years. The service function 1 line is for office buildings and the service function 2 is for residential buildings. The peak acceleration criterion for residential buildings is more strict than for offices, and as an explanation can be given that the human perception of motion is higher in the case residents are laying horizontally in their bed. At first, the natural frequency of the structure is estimated with $46/H$, and this results in a natural frequency of $0.153 \ Hz$. For the final calculation the natural frequency of the structure acquired from the finite element model used, which is $0.130 \ Hz$, will be used. The peak acceleration criterion for this natural frequency is $0.390 \ m/s^2$. The occurring peak acceleration in the along-wind direction of $0.402 \ m/s^2$ just exceeds the acceptable limit for the design of the office building. The stiffness, mass and damping properties of the structure should be optimized. It should also kept in mind that the peak response acceleration in across-wind direction are expected to be larger than in along-wind direction.

Table 5.1: Damping

	Logarithmic decrement, δ	Damping ratio , ζ
Structural damping	0.0900	1.43 %
Aerodynamic damping	0.0451	0.72 %
Damping due to auxiliary devices	0.0	0.0 %
Total damping	0.1351	2.15 %
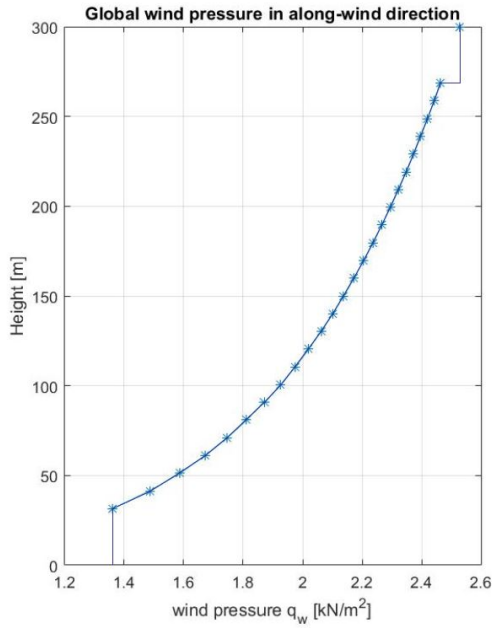
Figure 5.7: Characteristic global wind load, q_w
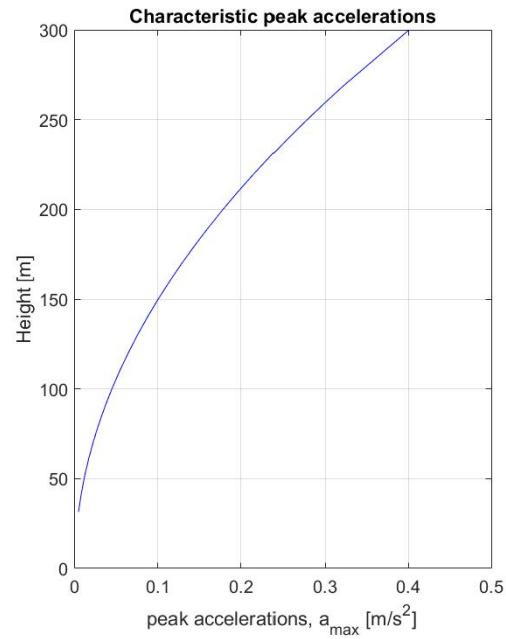
Figure 5.8: Peak response accelerations, $a_{D,max}$
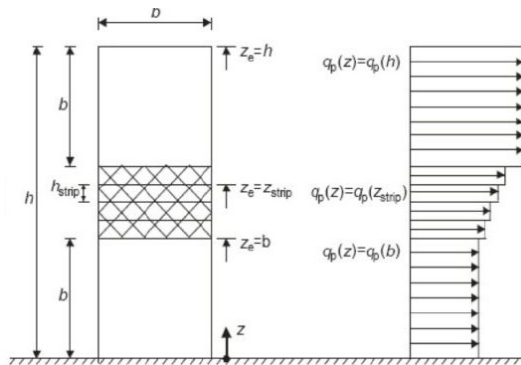
Figure 5.9: Distribution of peak wind pressures according to NEN-EN1994-1-4
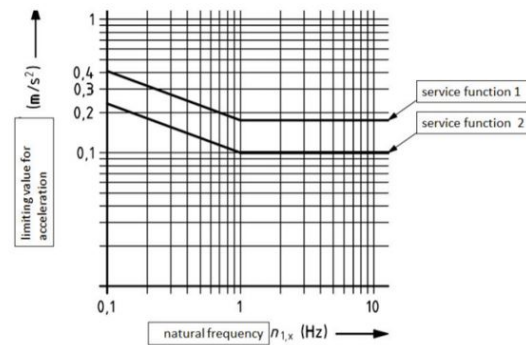
Figure 5.10: Comfort criteria accelerations according to Dutch Annex on the NEN-EN1991-1-4

5.2. Wind-induced response in across-wind direction

The maximum deflection of the tall building generally occurs in the along-wind direction.(Hallebrand and Jakobsson, 2016) However, the largest peak response acceleration could occur in the across-wind direction for slender and tall buildings. The Eurocode does not give regulations on how to calculate the across-wind response for tall buildings. Therefore, it is decided to use the National Building Code of Canada (NBCC:2005) to get an estimation of the peak acceleration in the across-wind direction. That the across-wind response should be checked also follows from requirements which can be found in the Dubai building code for wind. The vortex shedding can be neglected according to the Dubai building code if the following requirements are fulfilled (Dubai, 2013):

$$H/B_{min} < 6 \qquad (1) \tag{5.29}$$

$$v_{crit} > 1.25 \cdot v_m(H) \qquad (2) \tag{5.30}$$

$$v_{crit} = \frac{B f_{n,y}}{S_t} \tag{5.31}$$

Where:

H is the height of the structure;

B is the smallest width of the building in across-wind direction;

$v_m(H)$ is the average wind velocity at the top of the building;

v_{crit} is the critical wind velocity due to vortex shedding;

$f_{n,y}$ is the natural frequency in across-wind direction;

St is the Strouhal number.

The Strouhal number is dimensionless and describes the fluctuating vortex-shedding behaviour. According to the Dubai wind code, for rectangular shaped buildings with a depth to width ratio of 1 the Strouhal number is equal to 0.12. The tall building has a slenderness ratio of about 1:10, and therefore it can already be concluded that the first requirement is not fulfilled. The critical wind velocity due to vortex shedding is equal to 48.8 m/s^2. The second requirement is also not fulfilled, and this means the across-wind response should be checked. The maximum acceleration in the across-wind direction according to the NBCC can be found with Eq.(5.32).

$$a_W = f_{n,W}^2 \cdot g_p \cdot \sqrt{BD} \cdot \left(\frac{a_r}{\rho_B g \sqrt{\beta_W}} \right) \tag{5.32}$$

$$a_r = 78.5 \cdot 10^{-3} [v_H/(f_{n,W} \sqrt{BD})]^{3.3} \ [N/m^3] \tag{5.33}$$

Where:

g_p is the gust peak factor [range 3-4];

$f_{n,W}$ is the natural frequency in across-wind direction;

β_W is the fraction of critical damping;

ρ_B is the density of the building;

v_H is the mean wind velocity at the top;

B is the breath of the building;

D is the depth of the building.

The peak response acceleration in across-wind direction has been calculated, and this resulted in an acceleration of 0.598 m/s^2 for the designed structure. This is much higher than the peak response in along-wind direction, and does not satisfy the serviceability criterion for the peak response acceleration. Therefore, it can be concluded that the across-wind direction will be governing for the wind-induced dynamic response of the structure.

Dynamic analysis of hybrid wood-concrete tall building

In this chapter, the dynamic wind analysis method will be described. First, the natural frequency of the structure has to be determined. Secondly, the wind response spectrum method in along- and across wind direction will be described.

6.1. Natural frequency estimation

6.1.1. Eurocode

The Eurocode formulates a short formula to estimate the fundamental frequency of tall buildings at an early design stage, and is based on experimental data. This formula has been suggested by Ellis in 1980, and the fundamental frequency for tall buildings can be estimated as follows:

$$n_{1,x} = \frac{46}{H} \tag{6.1}$$

The calculated natural frequency using the above equation is equal to 0.153 Hz for a tall building with a height of 300 metres. This formula is based on conventional tall building designs in steel and concrete, so it can be expected that this estimation will probably be less accurate for tall timber structures. Timber structures are lighter and have less stiffness than similar structures constructed from steel or concrete. The natural frequency of the structure is dependent on the stiffness, and the mass capacity. Therefore, it could be expected that the natural frequency of the designed hybrid wood-concrete structure will be lower than for the conventional concrete structure.

6.1.2. Cantilever beam model

To verify the calculated fundamental frequency the structure has been schematised as a cantilever beam model. The tall building will be simplified as a fixed strut to which an uniformly distributed wind load has been applied. Figure 6.1 shows the simplified model of the tall building. For the first calculation procedure, the outrigger systems are neglected and only the reinforced concrete core will be taken into account. The foundation at the base of the structure is assumed to be rigid. Taken these conditions into consideration the following equations can be used to calculate the maximum lateral displacement of the structure:

$$\delta_{bending} = \frac{q_w \cdot H^4}{8 \cdot (EI)_{eff}} \quad and \quad \delta_{shear} = \frac{q_w \cdot H^2}{2 \cdot (GA)_{eff}} \tag{6.2}$$

q_w is an uniformly distributed lateral wind load $[kN/m]$
H is the total height of the structure $[m]$
$(EI)_{eff}$ is the bending stiffness of the structure $[kNm^2]$
$(GA)_{eff}$ is the shear stiffness of the structure $[kN]$
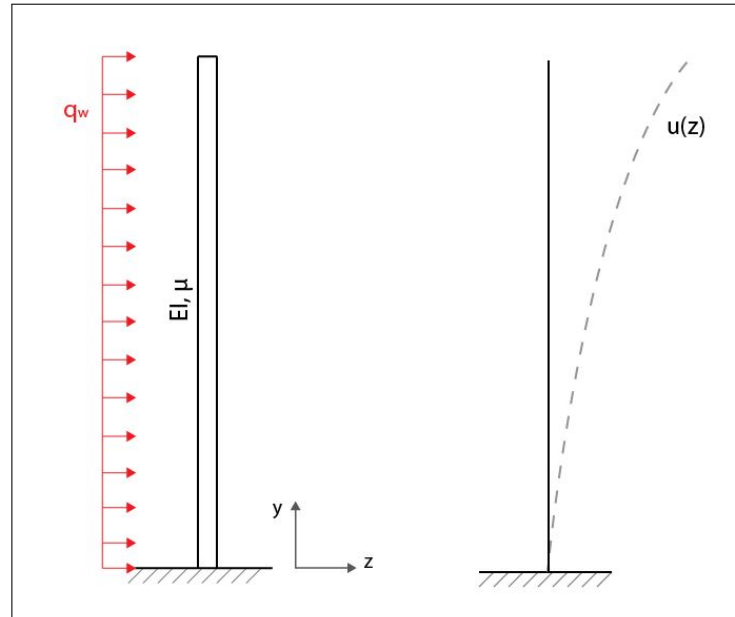
Figure 6.1: Cantilever beam model

Table 6.1 shows the results of the cantilever beam model under an uniformly distributed wind load. The contribution of the shear deformation to the total deformation is small compared to the deformation due to bending. This is due to the fact that the tall building is very slender. If outrigger/belt-truss system has been included, the shear stiffness in the structure will increase and should not be neglected.

'van Oosterhout' Method

Van Oosterhout (1996) developed a method to also include the additional stiffness due to the outrigger/belt-truss system. The maximum lateral displacement at the top story level with an outrigger system at three story levels can be calculated as follows:

$$\delta_{top,max} = \frac{q_w \cdot H^4}{8(EI)_{eff}} - \frac{1}{2(EI)_{eff}}[M_{r,1}(H^2 - x_1^2) + M_{r,2}(H^2 - x_2^2) + M_{r,3}(H^2 - x_3^2)] \qquad (6.3)$$

Where:

$M_{r,i}$ is the restraining moment due tot the outrigger/belt-truss systems $[kNm]$
x_i is the distance from the top of the structure to the the outrigger level $[m]$
$(EI)_{eff}$ is the effective bending stiffness of the structure $[kNm^2]$

The building has an outrigger level at three positions over the height of the building, and this means there will be a total of three restraining moments. Figure 6.2 shows the schematic view of the outrigger/belt-truss levels and the bending moments over the height of the structure. The outrigger levels will activate the perimeter columns in tension or compression, and the global stiffness of the building will be increased. As can be seen in table 6.1 the outrigger system reduces the maximum lateral displacement significantly. The horizontal displacement has been almost reduced to two-thirds of the displacement without an outrigger system. On the other hand, the axial forces in the columns due to lateral wind loading will increase, and the uplift forces at the foundation should be carefully checked.

The natural frequency is dependent on the global stiffness of the structure. The outrigger/belt-truss system increases the structure's stiffness, and therefore the natural frequency will also change. Oosterhout suggests the following formula to determine the natural frequency for a tall building including an outrigger system:
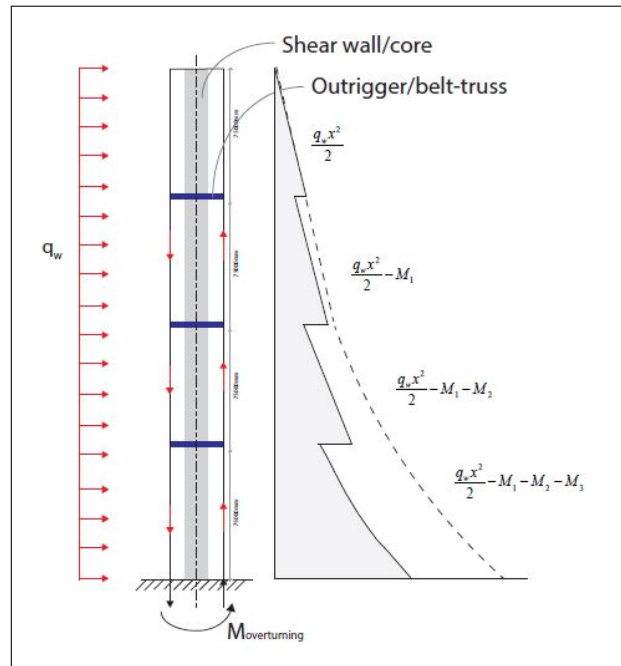
Figure 6.2: Schematic view and bending moment of structure including 3 outrigger/belt-truss levels

$$n_{1,x} = f(\alpha H) \sqrt{\frac{q_w \cdot H}{\mu \cdot \delta_{max}}} \qquad (6.4)$$

Where the function $f(\alpha H)$ takes into account the mode shape of the structure in the first mode, and is formulated by Oosterhout as follows:

$$f(\alpha H) = \sqrt{\left[\frac{0.2365}{(\alpha H - 0.3)^{1.22}} + \frac{1}{16}\right]\left[\frac{-1 - \alpha H \sinh(\alpha H) + \cosh(\alpha H)}{(\alpha H)^2 \cosh(\alpha H)} + \frac{1}{2}\right]} \qquad (6.5)$$

$$\alpha^2 = \frac{(GA)_{tot}}{(EI)_{tot}} \qquad (6.6)$$

μ is the distributed mass over the height $[kg/m]$
δ_{max} is the maximum lateral displacement $[m]$

Table 6.3 shows the results from the natural frequency analysis, and it can be seen that the method of 'van Oosterhout' gives an eigenfrequency of $0.154\ Hz$. It should be kept in mind that the foundation stiffness has not been included yet for the method described above. Including the rotational stiffness of the foundation will lower the natural frequency of the structure.

Table 6.1: Cantilever beam model: lateral response displacements

Input			
Uniform wind load	q_w	63.0	kN/m
Distributed mass	μ	245164	kg/m
Bending stiffness	$(EI)_{core}$	4.73E10	kNm^2
Shear stiffness	$(GA)_{core}$	3.27E9	kN
Bending stiffness including outriggers	$(EI)_{rigger}$	1.14E11	kNm^2
Shear stiffness including outriggers	$(GA)_{rigger}$	3.87E9	kN
Output			
Max. horizontal displacement	δ_{max}	1349	mm
Max. horizontal displacement (incl. outriggers)	$\delta_{max,outrigger}$	560	mm
Bending moment at the base	M_{max}	2.84E6	kNm
Bending moment at the base (incl. outrigger)	$M_{max,outrigger}$	2.03E6	kNm

6.2. Modal analysis

A modal analysis will be done in order to study the dynamic behaviour of the structure in the frequency domain. The modal analysis can be done for a single degree of freedom (SDOF) system or a multi degree of freedom (MDOF) system. The SDOF system only has one degree of freedom and is therefore characterized by a single rotation or displacement. As a consequence, only one mode shape can occur in the system. In reality multiple mode shapes will occur in the structure, and this can be represented by a MDOF system. First, the SDOF system will be discussed, and secondly, the modal analysis of the finite element model will be described in this section.

6.2.1. Single degree of freedom system

The tall building can be represented as an SDOF system, and could be used to get an estimation of the wind-induced behaviour of the structure. The spectral wind analysis by Davenport is also based on an SDOF system. Figure 6.3 shows the schematization of the structure as a SDOF system. The equation of motion of the SDOF system is defined as follows:

$$m\ddot{u} + c\dot{u} + ku = F(t) \tag{6.7}$$

Where, m is the mass, k the stiffness, and c the damping in the structure. $F(t)$ is the external dynamic wind loading on the system. The dynamic properties of the structure can be described with the angular frequency, ω, mode shape, ϕ, and damping ratio, ζ.

$$\omega_n = \sqrt{\frac{k}{m}} \tag{6.8}$$

$$[k - \omega_n^2 m]\phi_n = 0 \tag{6.9}$$

$$\zeta = \frac{c}{2m\omega_n} \tag{6.10}$$

At first, the structure will be schematized as a fixed strut model with an uniformly distributed stiffness and mass over the height of the structure. In reality the stiffness and mass will not be uniformly distributed due to the taper down of the cross-sectional dimensions of the structural components over the height of the building. Therefore, the model will be a simplification of the real structure. The uniformly distributed wind load is assumed as a concentrated force applied at the top of the structure. To translate the continuous fixed strut model to an SDOF system the mass has to be lumped at the top of the building. The translational stiffness property, k, can be calculated using the concentrated force and the maximum lateral displacement calculated earlier on. The additional stiffness of the outrigger system is also included in the stiffness property, k.

$$F = \int_0^H q_w(y)dy = q_w \cdot H \tag{6.11}$$

$$k = \frac{F}{u_{max}} \tag{6.12}$$

$$m_{eq} = \int_0^H m(y)dy \tag{6.13}$$
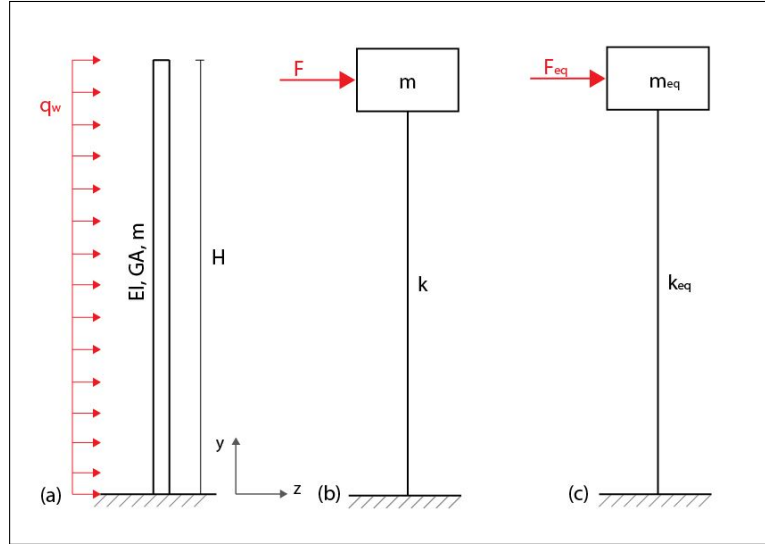
Figure 6.3: (a) Continuous cantilever beam model, (b) Non-equivalent SDOF model, (c) Equivalent SDOF model

The next step is to get the equivalent single degree of freedom (ESDOF) model, and this will give a good representation of the continuous model of the tall building. Figure 6.3 shows the continuous, non-equivalent SDOF, and ESDOF model, respectively. The equivalent properties can be calculated using the Rayleigh energy method and is based on the principle of conservation of energy. The conversion factors, φ_L, φ_M and φ_R are needed to calculate the equivalent properties for the loading, mass and stiffness, respectively. The non-equivalent and the equivalent SDOF model should both have the same lateral displacement and therefore the following can be stated:

$$u_{max} = \frac{F_{eq}}{k_{eq}} = \frac{\varphi_L F}{\varphi_R k} = \frac{F}{k} \tag{6.14}$$

From the above equation it can be seen that $\varphi_L = \varphi_R$, and therefore only the mass conversion factor, φ_M, will be required to get the equivalent SDOF system properties for the loading and mass. The natural angular frequency can be calculated as follows:

$$\omega_n = \sqrt{\frac{k_{eq}}{m_{eq}}} = \sqrt{\frac{\varphi_L k}{\varphi_M m}} = \sqrt{\frac{k}{\varphi_{LM} m}} \tag{6.15}$$

Where, φ_{LM} is the load-mass conversion factor. This φ_{LM}-factor is dependent on the slenderness and stiffness of the structure. The shear stiffness of the structure should not be neglected due to the fact that an outrigger system is going to be applied in the structure. The load-mass factor for a tall-building including an outrigger system can be found with the following formula (Boellaard, 2012):

$$\varphi_{LM} = \frac{4 \cdot (3024 + 999\alpha + 91\alpha^2)}{189 \cdot (80 + 32\alpha + 3\alpha^2)} \tag{6.16}$$

The α-factor includes the material and geometrical properties, and is equal to the ratio between the slenderness ratio, s^2, and the stiffness ratio, γ^2.

$$\alpha = \frac{s^2}{\gamma^2} \tag{6.17}$$

$$s^2 = \frac{H^2 A}{I_{core}} \quad ; \quad \gamma^2 = \frac{E}{G} \tag{6.18}$$

The damping of the structure should also be included in the calculation, and this will influence the natural frequency of the structure. The damped angular frequency, ω_d, is given by Eq.(6.19).

$$\omega_d = \omega_n \cdot \sqrt{1 - \zeta^2} \tag{6.19}$$

ω_1 is the natural angular frequency $[rad/s]$
ζ is the fraction of the critical damping

Table 6.2 shows the input and output for the SDOF system calculation. The maximum lateral displacement will be taken as 600mm and the foundation stiffness will be included in the effective stiffness. It can be seen that the calculated damped eigenfrequency of the SDOF system is equal to 0.130 Hz. It should be noted that this is the same result as for the natural frequency of the system without damping. Therefore, the effect of the damping of the structure on the natural frequency will be negligible. This could already been expected because Chopra (1995) stated that the effect of damping on the natural angular frequency is negligible for damping ratios equal and below 2 percent. A more detailed explanation on the influence of the damping on the natural frequency can be found in section 10.2 of Chapter 2, Literature Study.

The SDOF system can also be used to get an estimation of the peak response acceleration at the top of the structure. This could be done by a spectral wind analysis, which is a common approach to estimate the wind-induced response of a structure. The response spectrum method will be described in section 6.3 further on.

Table 6.2: SDOF system calculation

Input			
Wind load	q_w	$6.30 \cdot 10^4$	N/m
Distributed mass	$\mu(y)$	245164	kg/m
Max. lateral displacement	u_{max}	0.600	m
Effective stiffness	k_{ef}	$3.15 \cdot 10^7$	N/m
Damping ratio	ζ	2.15	%
Viscous damping	c	$2.53 \cdot 10^6$	$[N \cdot s/m]$
Building height	H	300.0	m
Output			
Load-mass conversion factor	φ_{LM}	0.642	
Natural angular frequency	ω_n	0.817	rad/s
Damped natural angular frequency	ω_d	0.817	rad/s
Natural frequency	f_n	0.130	Hz
Damped natural frequency	f_d	0.130	Hz

6.2.2. Modal analysis finite element model

The natural frequency of the structure can also be found using the 3D-finite element model in the structural analysis software CSi ETABS. The SDOF will be used as a verification of the found natural frequency. The natural frequency of the structure from the modal analysis

in CSi ETABS with a rigid foundation is equal to 0.149 Hz, and if the rotations of the foundations are included this results in a natural frequency of 0.130 Hz. The natural frequency found using a SDOF system gave the same result and the model is verified.

Figure 6.4 shows the modal analysis results for the first two modes of the 3D-finite element model. It can be seen that the modes are translational. The first mode is translational in the direction of the y-axis, and the second mode is translational in the direction of the x-axis. The first mode occurs in the y-axis and from this it can be concluded that the stiffness capacity in y-direction is a bit less compared to the stiffness in direction of the x-axis. Figure A.1 shows the floor plan, and it can be seen that the core of the structure is less stiff in the y-direction due to openings in the core walls. For the SDOF system calculation only the first and second translational mode will be taken into account.
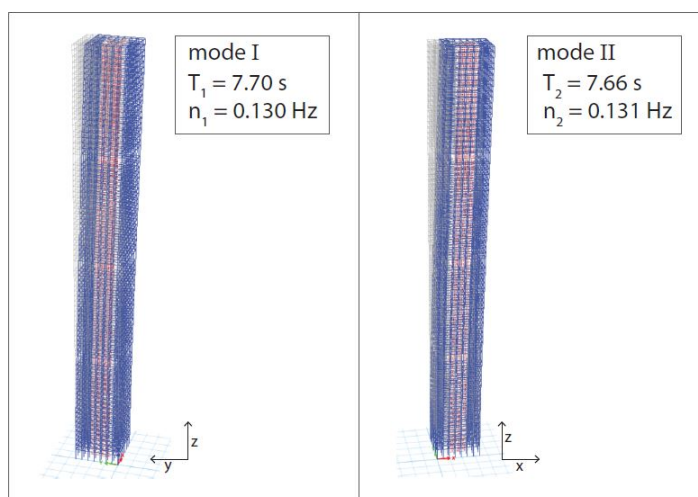
Figure 6.4: The first two modes of the 3D finite element model in CSi ETABS

Table 6.3: Results of frequency analysis

Method	Natural frequency, $n_{1,x}$	Natural period, T_s
Eurocode (NEN-EN1991-1-4 Annex F)	0.153 Hz	6.6 s
van Oosterhout	0.154 Hz	6.5 s
CSi ETABS	0.149 Hz	6.7 s
ESDOF Rayleigh (incl. foundation)	0.130 Hz	7.7 s
CSi ETABS (incl. foundation)	0.130 Hz	7.7 s

6.3. Spectral analysis

The wind load in along- and in across-wind direction are evaluated separately. This is convenient due to the different excitation mechanisms that apply for the along- and across-wind direction (Tamura and Kareem, 2013). It is valid to do so due to the fact that the maximum wind loads in both directions do not occur at the same time (Tamura and Kareem, 2013). First, the method of the spectral analysis by Davenport will be described for the along-wind response. Secondly, the method to determine the equivalent across-wind spectrum suggested by Liang in 2002 will be described. The along-wind response spectrum is dependent on the buffeting of the wind in along-wind direction, and the across-wind spectrum is for the most part dependent on the vortex shedding behaviour of the tall building.

6.3.1. Along-wind response spectrum

To get to the response spectrum, a variance spectrum of the fluctuating wind velocity should be determined first. Several spectra are suggested by researchers such as Davenport, Harris, Solari and Karman. In the Eurocode1-1-4 it is suggested to use the variance spectrum by Solari. An comparison of the spectra can be found in section 2.10 of the Literature Study. The spectrum by Solari is given by Eq.(6.20).

$$S_{v;Solari}(f_L) = \frac{6.8 \cdot f_L}{(1 + 10.2 \cdot f_L)^{5/3}} \tag{6.20}$$

Where the non-dimensional frequency, f_L, is defined by:

$$f_L = \frac{f \cdot L}{\bar{v}} \tag{6.21}$$

The non-dimensional frequency is dependent on the turbulence length scale, L, and the mean wind velocity at reference height, $\bar{v}$. In the case of wind tunnel tests it is more common to use the breadth/width of the building, B, instead of the turbulence length scale, L, to determine the non-dimensional frequency. The non-dimensional frequency is often used in combination with a reduced or normalised spectrum. The shape of the reduced spectrum is independent of the dimensions of the building. The reduced spectrum can be acquired by multiplying the spectrum by the frequency and dividing it by the variance of the spectrum. Figure 6.7 shows the variance spectrum of the fluctuating wind velocity. The main expected wind gust will have a frequency of 0.12 Hz. The area underneath the spectrum is equal to the variance of the fluctuating wind velocity, σ_v^2, and can be be determined by Eq.(6.22). If a variance spectrum of fluctuating wind is known, a random vibration of the wind velocity can be generated. Figure 6.5 shows a time history of the fluctuating wind velocity and next to it the probability density function.

$$\sigma_v^2 = \int_0^\infty S_v(f) \ df \tag{6.22}$$
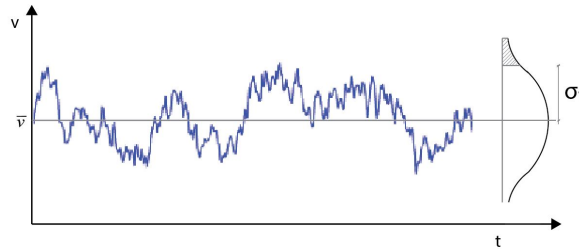
Figure 6.5: Time history of fluctuating wind velocity and its probability density function

The next step will be to determine a power density spectrum of force, S_F. For this the relation between the fluctuating wind and and the dynamic force on the façade will be required. The wind force in the along-wind direction can be determined as follows:

$$F(t) = C_D \cdot A \cdot \frac{1}{2} \cdot \rho \cdot v^2(t) \tag{6.23}$$

Where:

C_D is the drag coefficient
A is the area of the facade in along-wind direction $[m^2]$
ρ is the density of the air $[kg/m^3]$
$v(t)$ is the wind velocity $[m/s^2]$

The wind velocity, $v(t)$, can be split up in two parts, a mean wind velocity, $\bar{v}$, and a fluctuating part, $v'(t)$.

$$v(t) = \bar{v} + v'(t) \tag{6.24}$$

The wind force function can now be rewritten with Eq.(6.25), and the mean value of $F(t)$ is given by Eq.(6.26).

$$F(t) = C_D \cdot A \cdot \frac{1}{2} \cdot \rho \cdot (\bar{v}^2 + 2\bar{v}v'(t) + v'(t)^2) \tag{6.25}$$

$$\bar{F} = C_D \cdot A \cdot \frac{1}{2} \cdot \rho \cdot \overline{(\bar{v}^2 + 2\bar{v}v'(t) + v'(t)^2)} \tag{6.26}$$

Now this equation can be simplified as follows:

$$\bar{F} = C_D \cdot A \cdot \frac{1}{2}\left(\bar{v}^2 + \overline{v'(t)^2}\right) \tag{6.27}$$

In which the $\overline{v'^2(t)}$ term is very small, and could be neglected. The fluctuating part of the wind force can be found by subtracting the mean wind force off the total wind force.

$$F'(t) = F(t) - \bar{F} = C_D A \frac{1}{2}\rho\left(\bar{v}^2 + 2\bar{v}v'(t) + v'(t)^2 - \bar{v}^2 - \overline{v'(t)^2}\right) \tag{6.28}$$

$$F'(t) = C_D A \rho \bar{v}v'(t) + C_D A \frac{1}{2}\rho\left(v'(t)^2 - \overline{v'(t)^2}\right) \tag{6.29}$$

For low turbulence intensity, the second term of the equation can be ignored.(Tamura and Kareem, 2013) This due to the fact that the term, $v'(t)^2 - \overline{v'(t)^2}$, is normally small. The turbulence intensity at reference height will equal to 0.17 for the designed tall building. If the second term on the right-hand side is ignored Eq.(6.30) can be acquired.

$$F'(t) = (C_D \cdot A \cdot \rho \cdot \bar{v}) \cdot v'(t) \tag{6.30}$$

This linear approximation can be used to obtain a spectrum of the fluctuating wind using the Fourier transform. The Fourier transform can be used to get from an expression in the time domain to an expression in the frequency domain. The power density spectrum, S_F, can be calculated from the spectrum of the fluctuating wind velocity, S_v.

$$S_F(f) = (C_D \cdot A \cdot \rho \cdot \bar{v})^2 \cdot S_v(f) \tag{6.31}$$

In which the term, $(C_D \cdot A \cdot \rho \cdot \bar{v})^2$, comes from the first term in the Eq.(6.30), and this term is a constant. The power density spectrum, S_F, will have the dimensions of $[N^2/Hz]$. The acquired spectrum is quite satisfactory for wind on small objects and the wind gusts will completely envelope the structure. However, for larger structures the gusts will not envelope the entire façade any more. The force of the small wind gusts on a large surface are not completely correlated and therefore this 'lack of correlation' should be taken into account(Tamura and Kareem, 2013). To do this the concept of 'aerodynamic admittance' has been introduced by Vickery and Davenport in the late 1960's. The aerodynamic admittance function, χ^2, is given by Eq.(6.32).

$$\chi^2\left(\frac{f\sqrt{A}}{\bar{v}}\right) = \left[\frac{1}{1 + \left(\frac{2f\sqrt{A}}{\bar{v}}\right)^{4/3}}\right]^2 \tag{6.32}$$

Where:

f is the frequency [Hz]
A is the surface area of the façade $[m^2]$
$\bar{v}$ is the mean wind velocity $[m/s^2]$

Figure 6.8 shows the aerodynamic admittance function, $\chi^2(f)$. From the graph it can be seen that for wind gusts with a low frequency the aerodynamic admittance function is equal to one, and for high frequencies the function becomes equal to zero. This means that for high frequencies of the fluctuating wind velocity there will be a 'lack of correlation' of the wind gusts on the building façade. To acquire the spectrum of wind force the spectrum for small objects should be multiplied with the aerodynamic admittance function, χ^2.

$$S_F(f) = (C_D \cdot A \cdot \rho \cdot \bar{v})^2 \cdot \ S_v(f) \cdot \chi^2\left(\frac{f\sqrt{A}}{\bar{v}}\right) \tag{6.33}$$

Figure 6.9 shows the spectrum of force, $S_F(f)$. The wind force on the structure will cause lateral displacements and accelerations. The response of the structure depends on the range of wind excitation frequencies in relation to the natural frequency of the structure (Tamura and Kareem, 2013). The natural frequency of the structure is dependent on its stiffness and mass. A single degree of freedom (SDOF) system can be used to determine the dynamic amplification factor. In wind engineering this is often called the 'mechanical admittance function', $H(f)$. A detailed derivation of the dynamic amplification factor for the SDOF system can be found in chapter 6.4 of the book 'Advanced structural wind engineering' by Tamura and Kareem. The mechanical admittance function, $H(f)$, is given by Eq.(6.34).

$$H(f) = \frac{1}{\left(\left(1 - (\frac{\omega}{\omega_n})^2\right)^2 + \left(2\zeta\frac{\omega}{\omega_n}\right)^2\right)^{1/2}} \tag{6.34}$$

Where:

ω is the angular frequency in $[rad/s]$
ω_n is the natural angular frequency $[rad/s]$
ζ is the damping ratio of the structure

Figure 6.10 shows the mechanical admittance function, $H^2(f)$. The graph shows a peak at the natural frequency of the structure, which is equal to 0.130 Hz for the designed tall building. The mechanical admittance describes the dynamic properties of the structure, and if the mechanical admittance function will be reduced this will in its turn improve the wind-induced dynamic behaviour of the structure. The influence of a tuned mass damper system on the mechanical admittance will be discussed later on in Chapter 7, Parametric study and Optimization.

The response spectrum of displacements of the structure, S_x, can now be determined.

$$S_x(f) = \frac{1}{k^2} \cdot S_F(f) \cdot |H(f)|^2 \tag{6.35}$$

Where:

k is the stiffness of the structure $[N/m]$
$S_F(f)$ is the spectrum of the force $[N^2/Hz]$
$|H(f)|^2$ is the mechanical admittance function $[N^2/m^2Hz]$

A response spectrum of accelerations of the structure can also be determined. A spectrum of accelerations can be related to the displacement spectrum approximately through equation 6.36.

$$S_a(f) = S_x(f) \cdot (2\pi f)^4 \tag{6.36}$$

As can be seen in Eq.(6.36), the displacement spectrum should be multiplied by $2\pi f$ to the power 4 to get the estimate of the response acceleration spectrum. Figure 6.6 shows this relationship between the displacement and acceleration spectrum. For low frequencies ($f \leq 0.63Hz$) the intensity of the spectrum will decrease, and for higher frequency the spectrum will increase compared to the displacement spectrum. The response accelerations are
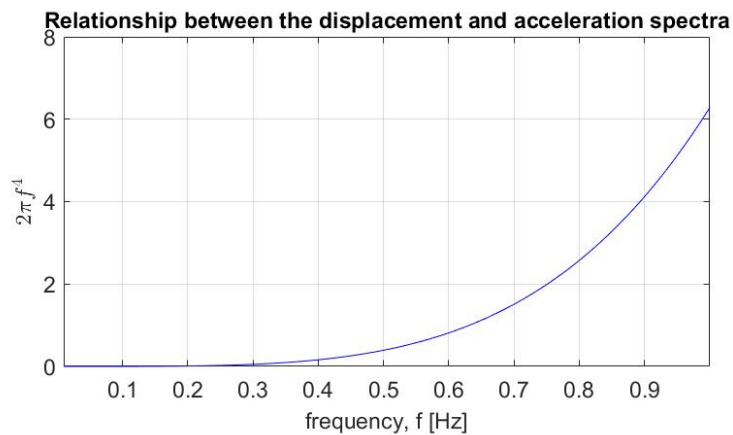
Figure 6.6: Relationship between the response displacement and acceleration spectrum, $(2\pi f)^4$

dependent on the wind gust frequencies and the response amplitude of the structure.

Figure 6.11 and 6.12 show the spectrum of displacements and accelerations, respectively. It can be seen wind-induced response spectra have a large peak at the natural frequency of the structure. The response spectrum can be split up into a background response part and a resonant response part. The main contribution to the wind-induced response will be from the resonant response part, and the contribution of the background response part will be a smaller. The natural frequency is close to the main frequency of the fluctuating wind. Due to this, the background part cannot be distinguished from the resonance response part anymore, and as a consequence, they will have the same peak in the response spectrum. However, if the frequency of the wind gusts and the structure's natural frequency differ a lot, two peaks will arise in a response spectrum. For example, this would be the case for a short and stiff structure. The background part is independent of any dynamic behaviour of the structure, and contributes very little to the response accelerations.

Table 6.4 shows the results of the response spectrum method in the along-wind direction. The calculation procedure for the peak response accelerations will be explained in section 6.3.3.
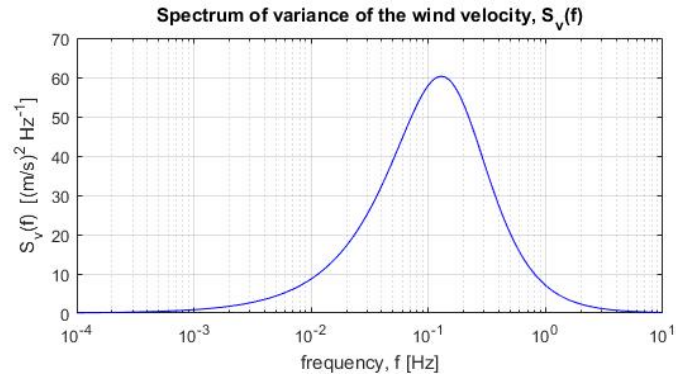
Figure 6.7: Spectrum of fluctuating wind velocity, $S_v(f)$
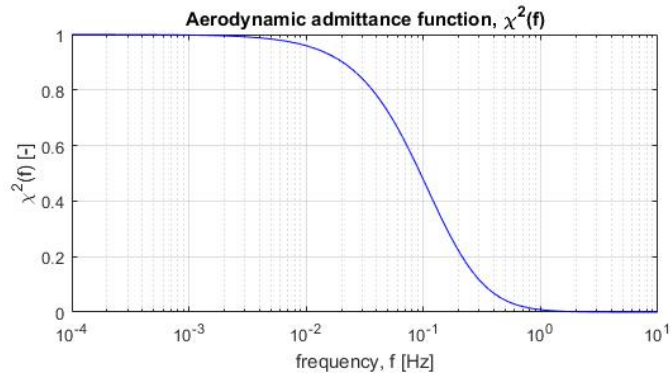
Figure 6.8: Aerodynamic admittance function, $\chi^2(f)$
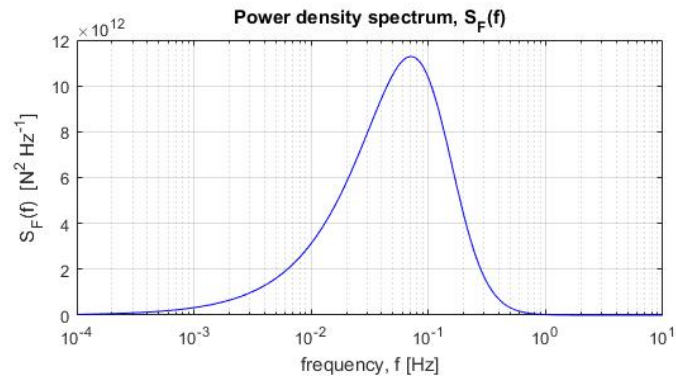
Figure 6.9: Power density spectrum, $S_F(f)$
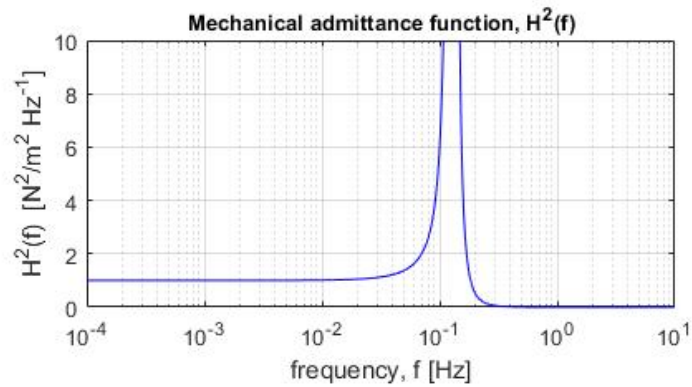
Figure 6.10: Mechanical admittance function, $H^2(f)$
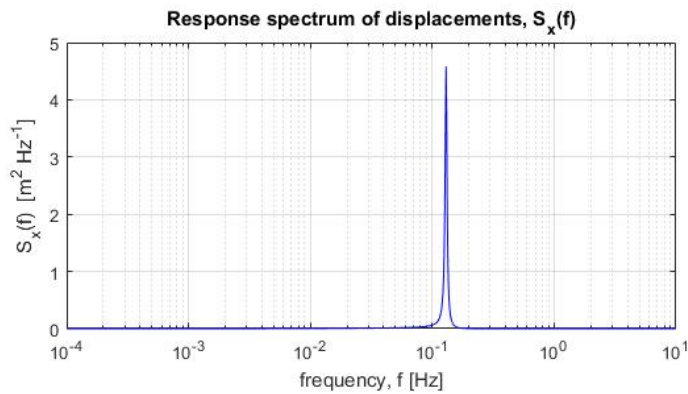
Figure 6.11: Response spectrum of displacements, $S_x(f)$
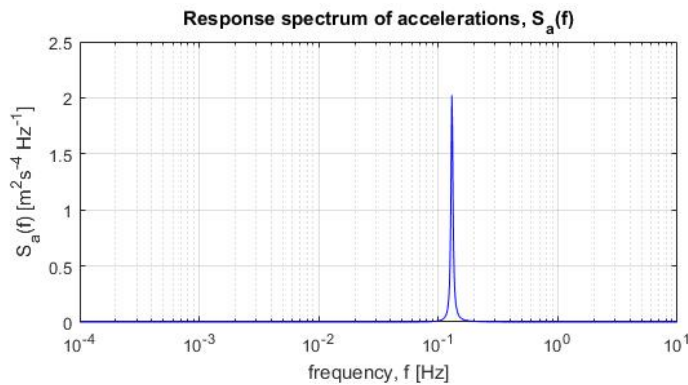
Figure 6.12: Response spectrum of accelerations, $S_a(f)$

Table 6.4: Results of spectral analysis in along-wind direction

Input			
Drag coefficient	C_D	1.46	-
Natural frequency	$f_{n,D}$	0.130	Hz
Gust peak factor	g_p	3.15	-
Turbulence length scale	$L(z_s)$	216.9	m
Mean wind velocity	$\bar{v}(z_s)$	35.5	m/s
Standard deviation of wind velocity	σ_v	6.03	m/s
Global stiffness of structure	k_{ef}	$3.15 \cdot 10^7$	N/m
Fraction of the critical damping	ζ	0.0215	-
Output			
Spectrum of force at the natural frequency	$S_F(f_n)$	$1.13 \cdot 10^{13}$	N^2/Hz
Response spectrum of acceleration at the natural frequency	$S_{a,D}(f_n)$	2.02	$m^2 s^{-4}/Hz$
Standard deviation of acceleration	$\sigma_{a,D}$	0.134	m/s^2
Peak acceleration response	$a_{D,max}$	0.421	m/s^2

6.3.2. Across-wind response spectrum

A combination of mechanisms is responsible for the across-wind excitations and accelerations. This makes acquiring the across-wind response spectrum a bit more complex compared to the method for acquiring the along-wind response. The dynamic wind load in across-wind direction is induced by three mechanisms: across-wind turbulence, along-wind turbulence, and the wake excitation. The wake excitation has the largest contribution of the three mechanisms and is induced by vortex formation and shedding.

A spectrum of force in the across-wind direction is also known as a lift force spectrum. This expression is especially common in aerospace engineering. For example, the wings of an

aircraft experience a lift force in the across-wind direction. For tall buildings the across-wind direction is horizontally orientated, in contrast to an aircraft wing, in which the lift force is in vertical direction. A formula to determine the across-wind force spectrum for circular tall buildings is given by Eq.(6.37) which has been introduced by Vickery and Clark in 1972. This formula is based on the assumption that the turbulent flow can be described as a Gaussian process, and it is dependent on physical parameters, such as the vortex shedding frequency, f_{s1}, and the spectral bandwidth, B_{e1}.

$$\frac{fS_L(f)}{\sigma_L^2} = \frac{(f/f_{s1})}{\sqrt{\pi}B_{e1}}exp\left[-\left(\frac{1-(f/f_{s1})}{B_{e1}}\right)^2\right] \tag{6.37}$$

However, for rectangular shaped tall buildings it will be more difficult to formulate the lift force spectrum in a similar way. This because the lateral turbulence and reattachment phenomenon become to play an important role in the across-wind loading for rectangular shaped buildings. These wind effects can be ignored for circular shaped tall buildings. Several studies are done to formulate the across-wind force spectra for rectangular shaped buildings, and most of them have been based on empirical results from wind tunnel tests. Liang et al. (2002) has proposed a mathematical model to describe the acrosswind force spectrum. This method will now be briefly discussed.

At first, a distinction has to be made between buildings with a side ratio $D/B < 3$, and side ratios $D/B > 3$. For structures with a long after body the reattachment phenomenon of the fluctuating wind becomes an important factor for the across-wind force. For larger side ratios ($D/B > 3$), the curve of the lift force spectrum will show two peaks. The second peak occurs due to the reattachment phenomenon of the fluctuating wind. The reattachment of separated flow will lead to the appearance of sub-vortices. The second peak of the force spectrum will correspond with the dominant frequency of the sub-vortex behaviour. However, for structures with a short after body the reattachment wind mechanism can be neglected. For a side ratio $D/B < 3$, the spectrum will show only a single peak located at the reduced vortex shedding frequency. This reduced frequency is also known as the Strouhal number.

The lift force spectrum can be calculated with the following equation:

$$\frac{fS_L(f)}{\sigma_L^2} = A\frac{H(C_1)\bar{f}^2}{(1-\bar{f}^2)^2 + C_1\bar{f}^2} + (1-A)\frac{C_2^{0.50}\bar{f}^3}{1.56[(1-\bar{f}^2)^2 + C_2\bar{f}^2]} \tag{6.38}$$

In the model of Liang the smallest side ratio that has been tested and verified in the wind tunnel test is for $D/B = \frac{1}{4}$, and therefore Eq.(6.38) should only be applied for side ratios $\frac{1}{4} \leq D/B < 3$. For larger side ratios the reattachment phenomenon should be taken into account, and a different formula should be used to calculate the lift force spectrum which can be found in the research paper of Liang et al. The designed tall building has a side ratio $D/B = 1$, and this means the formula above can be applied.

The parameters H, C_1, C_2, and A in Eq.(6.38) can be calculated as follows:

$$H(C_1) = 0.179C_1 + 0.65\sqrt{C_1} \tag{6.39}$$

$$C_1 = [0.47(D/B)^{2.8} - 0.52(D/B)^{1.4} + 0.24]/(H\sqrt{B \cdot D}) \tag{6.40}$$

$$C_2 = 2 \tag{6.41}$$

$$A = (H\sqrt{B \cdot D})[-0.6(D/B)^2 + 0.29(D/B) - 0.06] \\ + [9.84(D/B)^2 - 5.86(D/B) + 1.25] \tag{6.42}$$

C_1 is correlated to the bandwidth of the spectrum. The parameter, A, is correlated to the magnitude of the acrosswind force intensity, and is dependent on the side ratio of the structure.

For side ratios, $\frac{1}{4} \leq D/B \leq 1$, A, will increase along with the side ratio, and for larger side ratios ($D/B > 1$), A, will decrease when the side ratio increases. From this it can be concluded that a structure with a short after body will be more vulnerable to vortex shedding than a structure with a long after body.

The frequency ratio, $\bar{f}$, is the ratio of the frequency of the fluctuating wind over the dominant frequency of the vortex shedding: $\bar{f} = f/f_{s1}$. The centre frequency of the vortex shedding can be calculated with the following equation:

$$f_{s1} = \frac{S_t \cdot \bar{v}_H}{B} \tag{6.43}$$

In which, S_t, is the Strouhal number, $\bar{v}_H$, is the mean wind velocity, and B, is the breadth of the structure. The Strouhal number is a dimensionless frequency and can be used to analyse fluctuating wind flow mechanisms. If the Strouhal number is used to describe the vortex shedding mechanism, the frequency for determining the Strouhal number will be equal to the vortex shedding frequency. The Strouhal number can also be defined as a function of the Reynolds number. The Strouhal number for tall buildings with a side ratio of $\frac{1}{2} < D/B \leq 4$ is given by Eq.(6.44) (Liang et al., 2002). A Strouhal number equal to 0.084 is acquired for the designed tall building using this equation. Figure 6.13 shows the comparison of the Strouhal number from the empirical formula and the experimental results. It can be seen that for the side ratio equal to one the Strouhal number from the experimental results is equal to 0.088, instead of the calculated 0.084. The proposed formula fits quite well with the experimental data, and a maximum difference of 5 percent is found. The Strouhal number acquired with the empirical formula will be used for the calculation of the lift force spectrum for the designed tall building.

$$S_t = \begin{cases} 0.094 & \frac{1}{4} \leq D/B \leq \frac{1}{2}, \\ 0.002(D/B)^2 - 0.023(D/B) + 0.105, & \frac{1}{2} \leq D/B \leq 4. \end{cases} \tag{6.44}$$
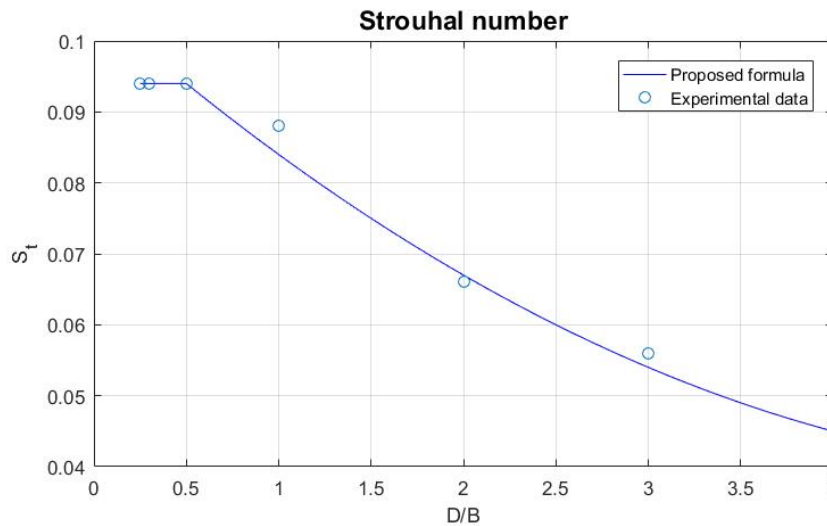
Figure 6.13: Comparison of Strouhal number, St, from empirical formula and experimental results.(Liang et al., 2002)

Figure 6.14 shows the across-wind force spectrum using the method by Liang et al. It can be seen that force spectrum only has one peak which is located near 10^{-1}, and this is close to the Strouhal number of the structure. It should be noted that for the non-dimensional frequency the breadth, B, instead of the turbulence length scale, L is used and this is common for spectra based on wind tunnel tests.
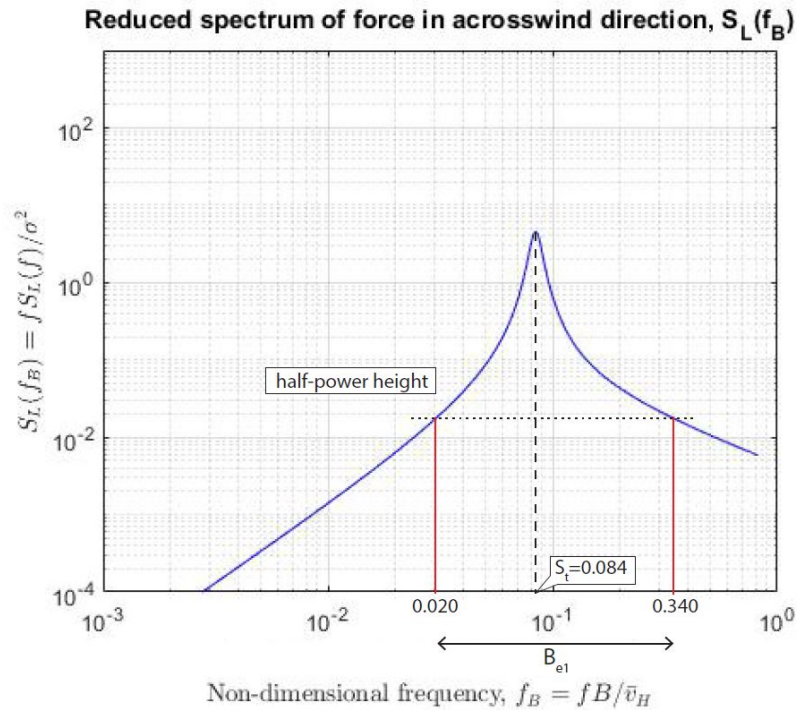
Figure 6.14: Reduced across-wind force spectrum, $S_L(f_B)$ with indication of spectral bandwidth, B_{e1}

.

The spectral bandwidth of the vortex shedding is an important physical parameter for the structure's across-wind behaviour, and is defined as the width of a spectrum at half-power height of the peak maximum. The spectral bandwidth of vortex shedding varies significantly between a short rectangular shape and a long rectangular shape (Cheng et al., 2016). Structures with a short after body will show a larger spectral bandwidth than structures with a long after body. In figure 6.14 the spectral bandwidth of the across-wind spectrum has been indicated. It can also be seen that the peak of the across-wind force spectrum is located at the Strouhal number. The spectral bandwidth of the vortex shedding is equal to 0.320 for the designed structure and the spectral bandwidth, B_{e1}, can be verified by the following formula which is based on empirical results:

$$B_{e1} = 6.28 \cdot \left(D/B\right)^{0.4} \cdot \left(I_v\right)^{1.71} \tag{6.45}$$

In which, I_v, is the longitudinal turbulence intensity at the reference height, and is equal to 0.17 for the designed tall building. The calculated spectral bandwidth using Eq.(6.45) is equal to 0.303. This value differs only 5% from the spectral bandwidth determined from the spectrum, and therefore the spectral bandwidth of the reduced across-wind force spectrum is verified.

To determine the wind-induced response of the structure the same calculation procedure as applied for the along-wind direction can be followed. The structure's dynamic amplification factor, $H(f)$, can be applied for both the along- and acrosswind direction. Table 6.5 shows the results of the spectral analysis in across-wind direction. The wind spectra from the response spectrum analysis can be found in Appendix C.3.

6.3.3. Peak response accelerations
The wind response spectrum can be used to estimate the peak response. The spectrum of accelerations should be integrated to get the variance. The variance is equal to the total area underneath a spectrum. The peak acceleration can be found by multiplying the standard

Table 6.5: Results of spectral analysis in across-wind direction

Input			
Lift coefficient	C_L	0.404	-
Natural frequency	$f_{n,W}$	0.130	Hz
Gust peak factor	g_p	3.15	-
Mean wind velocity	$\bar{v}_H$	38.6	m/s
Standard deviation of wind velocity	σ_v	6.03	m/s
Fraction of the critical damping	ζ	0.0215	-
Global stiffness of structure	k_{ef}	$3.15 \cdot 10^7$	N/m
Output			
Natural frequency of vortex shedding	f_{s1}	0.103	Hz
Strouhal number	S_t	0.084	-
Spectral bandwidth of vortex shedding	Be_1	0.320	-
Spectrum of force at the natural frequency	$S_L(f_n)$	$2.78 \cdot 10^{14}$	N^2/Hz
Response spectrum of acceleration at the natural frequency	$S_{a,D}(f_n)$	4.68	$m^2 s^{-4}/Hz$
Standard deviation of acceleration	$\sigma_{a,W}$	0.214	m/s^2
Peak acceleration response	$a_{W,max}$	0.674	m/s^2

deviation of accelerations by an appropriate gust peak factor. Equations 6.46 and 6.47 give the peak acceleration and gust peak factor, respectively. Eq.(6.47) is given in the Eurocode1-1-4 Annex F, and the gust peak factor is there referred to as the peak factor, k_p.

$$a_{max} = g_p \sigma_a \tag{6.46}$$

$$g_p \cong \sqrt{2\ln(v \cdot T)} + \frac{0.6}{\sqrt{2\ln(v \cdot T)}} \geq 3 \tag{6.47}$$

g_p is the gust peak factor (range 3-4)
v is the frequency of a gust
σ_a are several standard deviations of the response accelerations
T is the average period of the reference wind velocity, ($T = 600$ seconds)

A gust peak factor, g_p, equal to 3.15 will be applied for the designed structure. Table 6.4 and 6.5 show the results of the wind spectral analysis for the designed tall building. The peak response acceleration in along-wind direction is equal to 0.421 m/s^2, and the peak response acceleration in across-wind direction is equal to 0.674 m/s^2. The serviceability criterion for the peak response acceleration is equal to 0.390 m/s^2. This means structure still needs to be optimized to fulfil the serviceability criteria for occupant comfort. In particular, the vortex shedding behaviour in the across-wind direction will be governing for the occupant comfort. This could be expected due to tall and slender shape of the structure, and due to the fact that the vortex shedding frequency is close to the structure's natural frequency.

6.4. Time History Analysis

A time history function of the fluctuating wind can be generated from the wind variance spectrum. A random vibration generated from a spectrum can be described as a sum of sinusoidal functions. The following expression can be used to determine the wind velocity function over time:

$$v(t) = \sum_{i=1}^{N} a_i \cdot \sin(f_i t + \phi_i) \tag{6.48}$$

$$a_i = \sqrt{2 S_i \Delta f_i} \tag{6.49}$$

In which, a_i, is the amplitude and should be derived from the wind variance spectrum. f_i is the frequency, ϕ_i is the random phase angle, S_i is the wind variance spectrum, and Δf_i is the bandwidth of the spectrum. For the random vibration the sinusoidal functions are generated in MatLab. The phase angle will be generated at random, and a time evolution of a thousand seconds will be evaluated. The fluctuating wind force can be determined from the wind gusts. The fluctuating wind force in along-wind direction is determined with Eq.(6.50), which is derived earlier on in section 6.3.1.

$$F'_D(t) = (C_D \cdot A \cdot \rho \cdot \bar{v}) \cdot v'(t) \tag{6.50}$$

For the time history analysis in across-wind direction a similar approach can be followed as for the along-wind direction. Next to the drag coefficient, C_D, the lift coefficient, C_L, should be determined to get the fluctuating wind force in across-wind direction. The lift coefficient, C_L, can be calculated with Eq.(6.51), and is dependent on the depth to breadth ratio.(Liang et al., 2002) The lift coefficient will increase when the side ratio of the tall building also increases. The calculated lift coefficient for the designed tall structure is equal to 0.404.

$$C_L = 0.045(D/B)^3 - 0.335(D/B)^2 + 0.868(D/B) - 0.174 \tag{6.51}$$

Figure 6.15 shows the fluctuating wind force at the top of the building in along-wind direction. The time history of this fluctuating wind force can be put into the finite element model as a dynamic wind load, and this is done for the along -and acrosswind direction. The global damping ratio of the structure will be assumed to 0.0215 of the critical damping, which is the same value applied for the wind response spectrum method. Figure 6.16 and 6.17 show the results of the response accelerations in along- and acrosswind direction, respectively. It can be seen that a peak response acceleration of 0.590 m/s^2 will occur at the top of the building in the across-wind direction. This response acceleration is too large to satisfy the serviceability criterion for occupant comfort.

The phase angle of the sinusoidal functions will be picked at random, and this results in a different position of the peak values of the fluctuating wind force for every generated time history function. Also, the peak response accelerations in along- and acrosswind direction will not occur at the same time due to the different wind mechanisms that apply in the separate directions. The dominant frequency of the vortex shedding will be different from the dominant frequency of the oncoming wind gusts. The largest response accelerations will occur just after a large dynamic wind load has been applied onto the structure. The global damping in the structure will influence how long it will take for the vibration to die out. However, this can only been seen in the time history function if a free vibration can occur in the system. This will not be the case due to the fact that a forced vibration has been evaluated over a short time period.
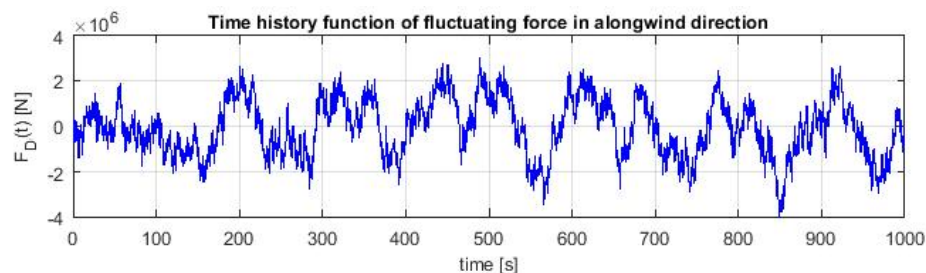
Figure 6.15: Time history of fluctuating wind force in along-wind direction
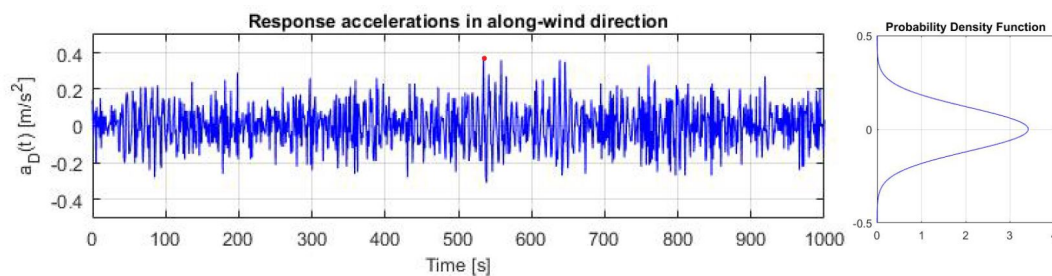
Figure 6.16: Time history of response accelerations in along-wind direction
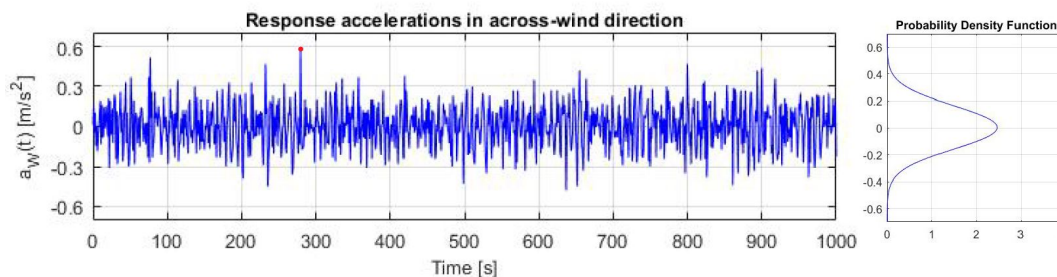
Figure 6.17: Time history of response accelerations in across-wind direction

6.5. Discussion of results

The natural frequency of the structure is equal to $0.130\ Hz$, and this frequency can be acquired from the modal analysis in the finite element model. This natural frequency is also verified with an SDOF system. The natural frequency determined from the cantilever beam model using the van Oosterhout method is equal to $0.154\ Hz$. The cantilever beam model including the outriggers turns out to be stiffer than the finite element model, and this can be explained by the fact that the cantilever beam model has a rigid foundation and the beam will be clamped at the base. The frequency calculated with the Ellis formula ($n_{1,x} = 46/H$) given in the Eurocode is equal to $0.153\ Hz$. The calculated frequency turns out to be too high, which was expected because this formula is based on experimental data from tall buildings done in concrete and steel. However, it gives a rough estimate for a hybrid wood-concrete tall building and it will give an idea of the expected natural frequency of the structure in the early design stage. The global damping in the structure has not much influence on the natural frequency for the designed tall building, and the effect of damping can be neglected for the global damping value of 2%. However, for higher damping values the effect of the damping on the structure's eigenfrequency should be taken into account.

The response spectrum method by Davenport is a commonly used approach to analyse the wind-induced response of a structure. The results of the response spectrum method have been compared by the response acquired from the time history analysis in the structural analysis software CSi ETABS. The peak response accelerations for the structure with sharp corners and no auxiliary damping have been calculated. The wind response spectrum method gives a peak response acceleration in the along-wind direction of $0.421\ m/s^2$, and the peak acceleration in the across-wind direction is equal to $0.674\ m/s^2$. The time history response from the finite element model gives a peak acceleration in along-wind direction of $0.393\ m/s^2$, and the peak acceleration in across-wind direction is equal to $0.590\ m/s^2$. The peak response accelerations acquired from the time history analysis are smaller than the acceleration acquired from the spectral analysis and the difference in results for the two applied methods stays below 12%. The difference in results can be explained by the fact that the time history analysis gives the response for the MDOF system and the response spectrum analysis gives the peak response of an SDOF system. The time history analysis will give the response over a certain time period and from the response spectrum analysis only the peak response in the structure can be determined. The determination of the peak response acceleration varies for

both methods. For the wind response spectrum method the peak acceleration is found by multiplying the standard deviation of the spectrum of response acceleration by a gust peak factor. This gust peak factor has been determined according to the building code, and is dependent on the average period of the reference wind velocity and the frequency of the wind gust. The peak response acceleration using the time history analysis is found by evaluating the time series of the response acceleration over a certain time period. The wind response spectrum analysis is a commonly accepted method for determining the dynamic wind load on a structure. Therefore, the results from the response spectrum analysis will be used for the design and optimization of the structure. Also, this method gave the largest peak response accelerations, so therefore this will be a more conservative approach. The final peak response accelerations are checked for the occupant comfort criteria and the dynamic behaviour of the structure will be optimized based on the wind response spectrum method.

The response peak acceleration in across-wind direction turns out to be critical for the occupant comfort. Due to the tall and slender shape of the structure the vortex shedding intensity could become large. The lift force spectrum has a high peak at the vortex shedding frequency, which is close to the eigenfrequency of the structure. If the natural frequency of the structure is further away from the dominant vortex shedding frequency, the wind-induced response would be less critical. The lift force spectrum can also be reduced by optimizing the shape of the building. For example, adding fins to the façade or recessed corners can improve the vortex shedding behaviour significantly. The recessed corners are also applied for the 508m tall Tapei-101 building (Poon et al., 2014).

The structure should be optimized to satisfy the serviceability criterion for occupant comfort. This can be done with the application of an auxiliary damping device and/or shape optimization of the building. To optimize the wind-induced behaviour it is decided to apply a tuned mass damper (TMD) at the top of the structure, and to apply a horizontal shape optimization. The tuning of the TMD system and shape optimization of the designed structure will be explained in more detail in the next chapter.

7

Parametric study and optimization

This chapter describes the parametric study that has been done to optimize the structural design of the tall building. The design choices will be explained which are made during the design process. First, the finite element model of the structure will be described and secondly, the parametric study and optimization will be discussed in more detail.

7.1. Finite element model

A finite element model of the design has been made in the structural analysis software CSi ETABS. This software is very useful for the design of tall buildings with a repetitive floor plan in particular. The finite element model is used for the parametric study.

7.1.1. Element discretization

The element discretization is the process of translating the material domain of an object-based model into an analytical model which is suitable for analysis (Kalny, 2017). The beams and columns have been modelled as beam elements. In CSi ETABS these elements are called frame elements and can be applied in the planar and three-dimensional analysis. The beam element consists of a bar element with two nodes, and each node has six degrees of freedom (three displacements and three rotations). Therefore the total number of degrees of freedom for the elements equals 12. The stiffness matrix will have a size of 12x12. Figure 7.2 shows a representation of the three-dimensional beam element. The floor slabs and walls have been modelled as thin shell elements. The Kirchoff-Love theory has been used for these thin shell elements. The Mindlin-Reissner theory should be applied for thick shells and should be applied on structural components in which the shear deformations tend to be important. The shell elements take into account the effect of the Poisson's ratio

Figure 7.1: 3D-view of finite element model

which is not the case for the beam elements. Figure 7.3 shows a representation of the linear quadrilateral shell element. Each node has six degrees of freedom (three translational displacements and three rotational deformations), and the stiffness matrix of the shell element has the size 24x24. Another possibility is to use membrane shell elements for the floor slabs which has the advantage of decreasing the analysis run time. If the slab is modelled as a membrane it only transfers forces to the supporting beams and does not have any out-of-plane stiffness. Figure 7.1 shows the three-dimensional view of the model in CSi ETABS.

Figure 7.2: (a) 3D beam element, (b) Beam element sign conventions CSi Etabs (Kalny, 2017)
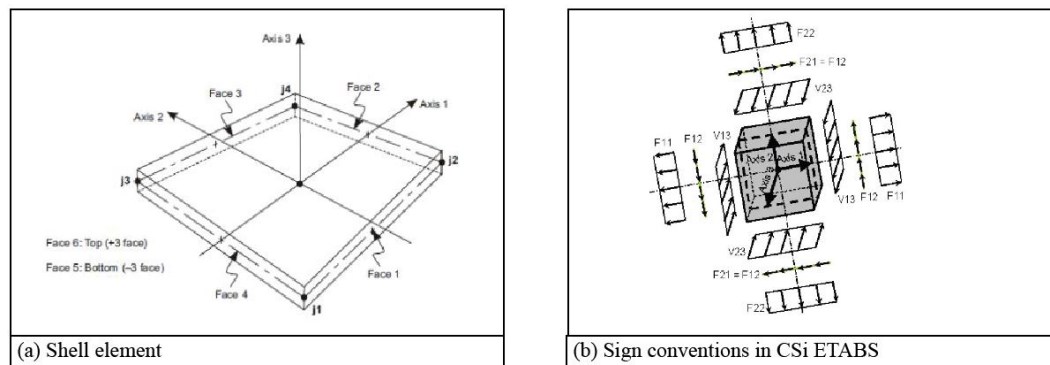
Figure 7.3: (a) Linear quadrilateral shell element, (b) Shell element sign conventions CSi Etabs (Kalny, 2017)

7.1.2. Mesh

CSi ETABS includes an auto meshing option which is easy to use but should be carefully checked. To have more control on the meshing process it is decided to do the meshing of the model manually. The beam and column element are meshed at intermediate points and at the joint intersections. The floor slab is meshed into small rectangles as shown in figure 7.4. In the case the floor slab is meshed fine enough the flat linear quadrilateral shell elements can give a good representation of the curvature. Figure 7.5 shows the meshing of the core wall. Another possibility is the use of quadratic shell elements which can simulate parabolic curvature in each element. However, due to computational speed the flat linear quadrilateral shell elements are more commonly used in finite element software. In the case membrane shell elements are used the mesh can be more coarse and the edges of the element should be supported by wall or beam elements.

7.1.3. Connections

The end releases of the columns and beams can be modelled as rigid, semi-rigid or hinged. It is possible to model the stiffness of the structural connections with the use of translational and rotational springs. In the case the frame is modelled as rigid no end release is applied to the structural components and all forces and moments are transferred. The moments are released at the end of the structural components for the hinged frame. The connections in the frame are modelled as rigid as usual for conventional all-concrete tall buildings.

7.1.4. Section modifiers

The stiffness of the concrete will be reduced so that it will also account for cracks occurring in the concrete. In the analysis software CSi ETABS this can be done with the help of section modifiers, which reduce the elastic flexural and shear stiffness properties of the concrete elements. In the case the concrete is cracked the modulus of elasticity will be reduced to one third of the original modulus of elasticity. According to the Eurocode 8 (NEN-EN1998-3)
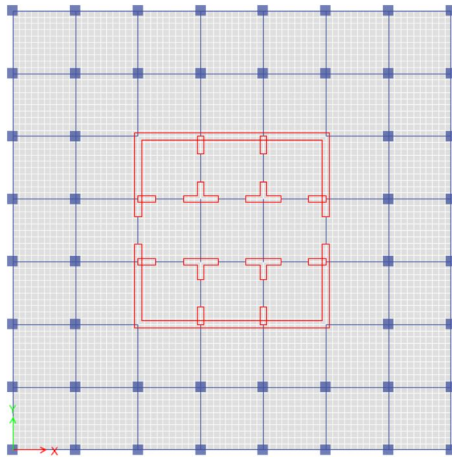
Figure 7.4: Floor mesh   Figure 7.5: Wall mesh
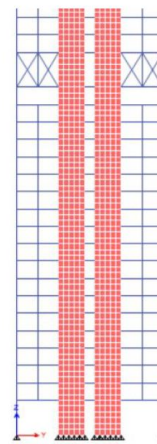
it is recommended that the elastic flexural and shear stiffness properties are taken as 50 percent of the corresponding stiffness of the uncracked element (Wong et al., 2017). Wong presented a literature study about the effective stiffness for modeling reinforced concrete and the results are presented in figure 7.6. For the shear walls the section properties are reduced by a factor 0.5 and the link beams in the core are reduced by a factor 0.35. This is based on the guidelines for wind loading of the 2012 International Building Codes (IBC) and the Eurocode.

	Elements	ACI 318-11 10.10.4.1 / ACI 318-14 6.6.3.1.1	ASCE 41-13 Table 10-5	PEER TBI Guidelines Service Level	LATBSDC MCE-Level Non Linear Models (2014)	LATBSDC Servicability & Wind (2014)	FEMA 356 Table 6-5	NZS 3101: Part 2:2006 Ultimate Limit State (fy=300Mpa)	NZS 3101: Part 2:2006 Servicability Limit State (μ=3) (Note 3)	CSA A23.3-14	EuroCode	TS 500-2000	Paulay & Priestley (1992)	Priestly, Calvi & Kowalsky (2007)
Beams	Conventional Beams (L/H > 4)	0.35Ig	0.30Ig	0.50Ig	0.35Ig	0.70Ig	0.50Ig	0.40Ig (rectangular) 0.35Ig (T and L beams)	0.70Ig (rectangular) 0.60Ig (T and L beams)	0.35Ig	0.50Ig	0.40Ig	0.40Ig	0.17Ig-0.44Ig
	Prestressed Beams (L/H > 4)	n/a	1.00Ig	1.00Ig	n/a	n/a	1.00Ig	n/a	n/a	0.35Ig	0.50Ig	0.40Ig	n/a	n/a
	Coupling Beams (L/H ≤ 4)		n/a	n/a	0.20Ig	0.30Ig	n/a	0.60Ig (diagonally reinforced)	0.75Ig				(9)	n/a
Columns	Columns - Pu ≥ 0.5Agfc	0.70Ig	0.70Ig	0.50Ig	0.70Ig	0.90Ig	0.70Ig	0.80Ig	1.00Ig	0.70Ig	0.50Ig	0.80Ig (Note 6)	0.80Ig	0.12Ig-0.86Ig
	Columns - Pu ≤ 0.3Agfc		0.70Ig	0.50Ig	0.70Ig	0.90Ig		0.55Ig	0.80Ig	0.70Ig	0.50Ig		0.60Ig	
	Columns - Pu ≤ 0.1Agfc	0.70Ig	0.30Ig		n/a	n/a	0.50Ig	0.40Ig	0.70Ig			0.40Ig	(9)	
	Columns - tension		n/a		n/a	n/a		n/a	n/a			n/a		
Walls (4)	Walls - uncracked	0.70Ig	n/a	0.75Ig	n/a	n/a	0.80Ig	n/a	n/a	0.7Ig	0.50Ig	n/a	(9)	n/a
	Walls - cracked	0.35Ig	0.50Ig		1.00Ec (1)	0.75Ig	0.50Ig	0.32Ig-0.48Ig	0.50Ig-0.70Ig	0.35Ig	0.50Ig	0.40Ig - 0.80Ig (Note 6)		0.20Ig-0.30Ig
	Walls - shear	n/a	0.40EcAw (10	n/a	0.50Ag	1.00Ag	n/a	n/a	n/a	n/a	n/a	n/a	(9)	n/a
Slabs	Conventional flat plates and flat slabs	0.25Ig	See 10.4.4.2	0.50Ig	0.25Ig	0.50Ig	n/a	n/a	n/a	0.25Ig	0.50Ig	n/a	(9)	n/a
	Post tensioned flat plates and flat slabs	n/a	See 10.4.4.2		0.25Ig	0.50Ig	n/a	n/a	n/a			n/a	n/a	n/a
	In-plane Shear	n/a	n/a	n/a	0.25Ag	0.80Ag	n/a	n/a	n/a	n/a	n/a	n/a	n/a	n/a
Notes		(5)	(2)	(2)	(2)				(3)			(7)		

Notes
(1) Non-linear fiber elements automatically account for cracking of concrete because the concrete fibers have zero tension stiffness.
(2) Elastic modulus may be computed using expected material strengths.
(3) μ is ductility capacity.
(4) Wall stiffness is intended for in-plane wall behavior.
(5) ACI 318-11 Section 8.8 (ACI 318-14, Section 6.6) permits the assumption of 0.50Ig for all elements under factored lateral load analysis.
(6) TS 500-2000 specifies the use of 0.4Ig for Pu/Acf'c < 0.1 and the use of 0.8Ig for Pu/Acf'c > 0.4; interpolate for all values in between 0.1 and 0.4.
(7) T and L beams should use recommended values of 0.35 Ig. For columns, categories are P = 0.2 f'c Ag and P = -0.05 f'c Ag
(8) Shear stifness properties are unmodified unless specifically noted otherwise.
(9) Effective stiffness per equation. See reference for more information.
(10) Note that G = 0.4*I, so ASCE 41-13 is recommending that a modifier of 1.0 be used for the shear stiffness of concrete shear walls; that is, they recommmend no reduction in shear stiffness.

Definitions
Ig = Gross moment of inertia
L = Clear span of coupling beam
H = Height of coupling beam
Pu = Factored axial load
Ag = Ac = Gross (uncracked) area
f'c = Compressive strength of concrete
Ec = Modulus of elasticity of concrete
fy = Yield stress of reinforcing steel
MPa = Megapascals
Aw = Horizontal area

Figure 7.6: Overview effective stiffness for modeling reinforced concrete (Wong et al., 2017).

7.1.5. Load cases

The load cases and combinations that are applied can be found in Appendix B.6. The lateral wind load case has been put in according to the Eurocode. The wind spectrum by Solari is used for the dynamic wind load. The time history of the fluctuating wind velocity has

been put in as point loads on the façade. This way the accelerations in the structure can be analysed over time and compared to the results from the wind response spectrum method.

7.1.6. Second order effect
The global second order effect should be considered for a tall and slender building and is also known as the $P - \Delta$ effect. The lateral wind load causes large moments and vertical forces at the base of the structure. The wind load will cause the structure to deflect horizontally and due to these lateral deflections the centre of mass of the building will shift. The shift in the centre of mass will result in an additional moment at the base and this causes an increase in lateral deflection. This effect is known as the second order effect. For high-rise buildings the second order effect can result in an additional deflection up to 20%. For a linear analysis the shift of the centre of mass is not taken into account, and therefore the second order effect is not taken into account automatically.

A simplified second order analysis is applied for the finite element model. For this case only the gravity loading is taken into account for the second order effect. The second order analysis resulted in an additional deflection of about 10% at the top of the structure.

7.1.7. Damping
The damping of the structure is taken into account with a global damping ratio. The global damping ratio is a fraction of the critical damping in the structure and is based on experimental results. The structural damping, ζ_s, and the aerodynamic damping, ζ_a, are included into the global damping ratio. The aerodynamic damping is dependent on the properties of the structure and the oncoming wind load. If an auxiliary damping device is applied its additional damping should also be added to the global damping ratio.

7.2. Parametric study

During the design process the concept design is constantly changing and evolving. Design choices have to be made based on a parametric study. By optimizing the design the characteristics of the structure are changing. Therefore, the results that are presented in this chapter do not represent the final lateral displacements and drifts. The results show the influence of a parameter on the behaviour of the structure. For each parameter study that is done, only the studied parameter is the variable and the other design characteristics are kept constant. In the sections described below, the iterative design process will be discussed which has led to the final concept design.

7.2.1. Outrigger/belt-truss systems

The effect of the outrigger/belt-truss system on the lateral inter-storey drift has been analysed and the following four cases are studied: no outrigger, one outrigger, two and three outrigger levels. The case of more than three outrigger levels has not be analysed due to the fact that the design would than become impractical and too much office space would be lost. The efficiency of the outriggers will also go down while the costs for an additional outrigger level stay the same. Figure 7.7 and 7.8 show the lateral displacements and drifts due to the wind loading for varying number of outrigger levels, respectively. The lateral inter-storey drifts presented in the graph are already divided by the storey height. It can be seen that the effect of adding one outrigger level compared to none shows a quite significant improvement of the lateral inter-storey drifts, and by adding one outrigger level this can already result in 37% reduction of the lateral inter-storey drifts. The implementation of two additional outrigger levels gives a total reduction of 54% on the lateral inter-storey drifts. To satisfy the lateral drift criterion an increase of stiffness in the structure is required. It shows that the outrigger system is an effective measure to accomplish the additional stiffness. The outrigger levels cannot be used as office space, and to limit the loss of usable office space the maximum number of outrigger levels is set to three. Therefore, it is chosen to apply the outrigger/belt-truss system at three positions over the height of the building.

Another aspect of the outrigger/belt-truss system that will be investigated is the layout of the outrigger trusses. The outrigger trusses transfer the forces from the core to the belt-truss and perimeter columns. Two outrigger designs are compared: the first option has four timber trusses which span from the core wall to the corner column, and the second option has eight timber trusses which are placed orthogonal from the core walls to the perimeter columns. Both variants have the same belt-truss design. Figure 7.9 and 7.10 show the plan view of the two different outrigger designs. The orthogonal layout gives a reduction of about 15% on the maximum lateral inter-storey drift compared to the diagonal layout of the outrigger trusses. The outrigger levels will become a lot stiffer with the use of eight trusses, and therefore more forces are transferred to the perimeter columns. Based on this, the design choice is made to use the orthogonal outriggers system layout instead of the diagonal variant.

7.2.2. Number of column rows

The effect of a second interior column row has been analysed. The advantage of adding an additional column row is that the floor span decreases and the stiffness of the structure will increase. However, it should be kept in mind that the interior columns row will decrease the open layout of the office space. This measurement is purely taken from a structural point of view. Figure 7.13 shows the lateral displacement due to the wind loading for a design with only perimeter columns, and a design including an additional interior column row. Figure 7.14 shows the lateral inter-storey drift for the different column layout options. It can be seen that the maximum lateral inter-storey drift can be reduced by 10% in the case a second column row is included. It should be noted that for this comparison the second column row is also part of the outrigger system. Due to the need for additional stiffness to the structure and the advantage of decreasing the floor span, it has been decided to add the interior column row in the structural design. Later on in the design process it was decided to let only the perimeter columns participate in the outrigger/belt-truss system. This because the second
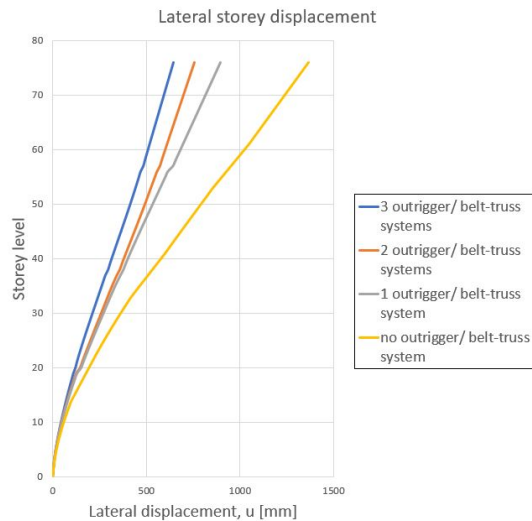
Figure 7.7: Influence of number of outrigger systems on lateral displacement
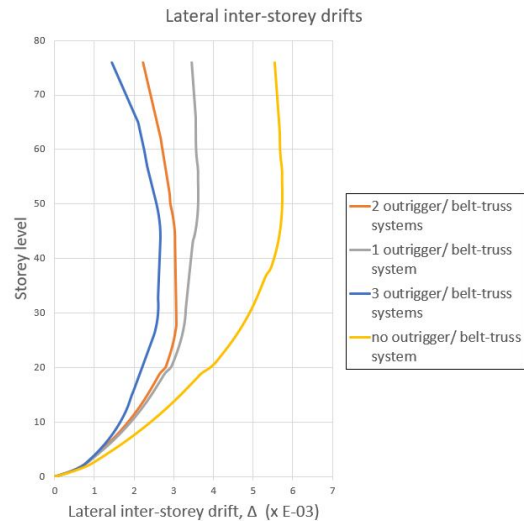
Figure 7.8: Influence of number of outrigger systems on lateral inter-storey drifts
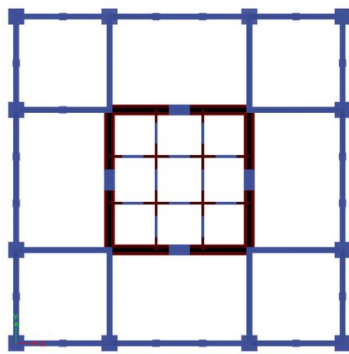
Figure 7.9: Plan view of orthogonal oriented outrigger trusses
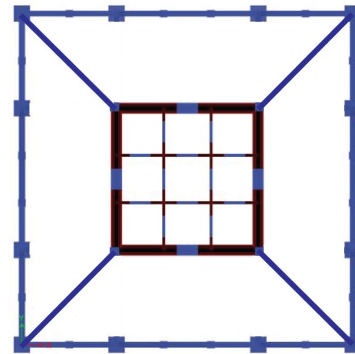
Figure 7.10: Plan view of diagonal oriented outrigger trusses

column row will already take on more vertical floor loading than the perimeter columns. As a consequence, the axial force will only be increased in the perimeter columns due to the lateral wind loading. The shorter floor span is also important for the accidental load design. An alternative load path should be possible in the case a column fails. If the floor spans are very large the accidental load design could become governing. Another advantage of decreasing the floor span is that the floor thickness can be reduced, and therefore the overall material use in the building. In tall building design the floors largely contribute to the total material use in the building.

7.2.3. Stiffness of connections

The connection details of the timber frame can be modelled as rigid, semi-rigid or hinged. First, in this study, the outer bounds of the stiffness parameter have been analysed. This means the timber frame is modelled as a hinged and also as a rigid frame. Figure 7.15 shows the lateral storey displacements of the hinged and rigid frame option. It can be seen that rigid beam-to-column connections decrease the lateral displacements significantly. A rigid frame reduces the maximum lateral displacement at the top of the building with about 20% compared to a hinged timber frame. However, it is quite difficult and expensive to make all timber frame connections moment resistant. Therefore, it is decided to model the beam-to-column and column-to-column connections as hinges. This will be a conservative approach because in reality the connections will have some rotational stiffness. In addition, it can be
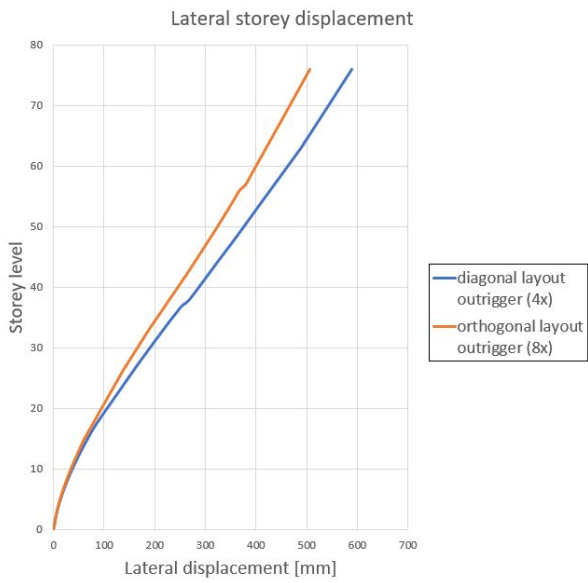
Figure 7.11: Layout trusses outrigger system
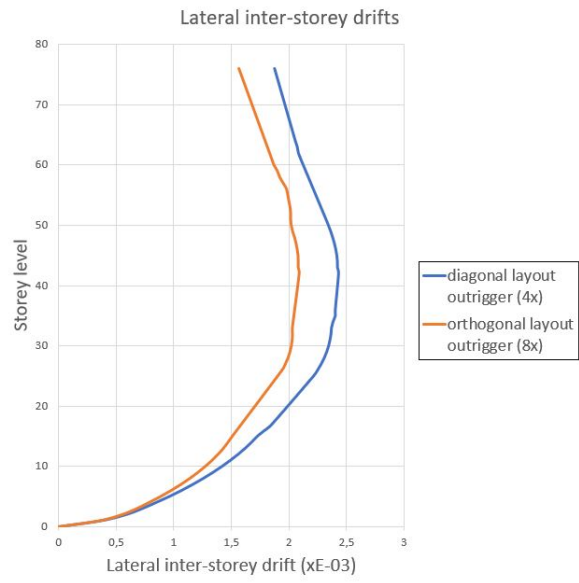
Figure 7.12: Layout trusses outrigger system
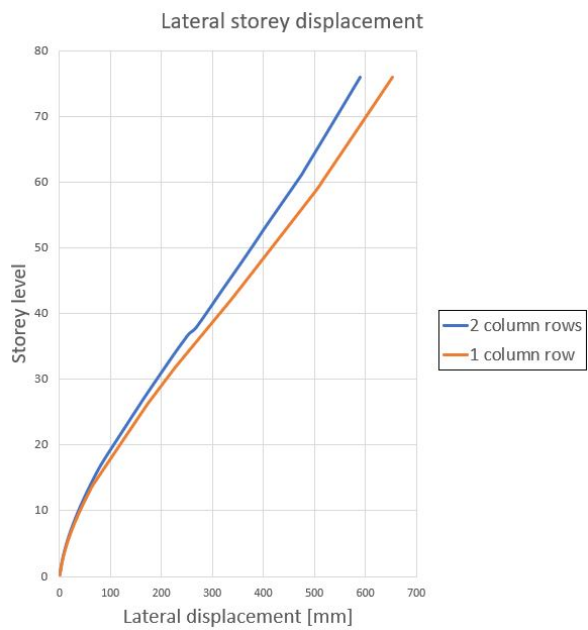
Figure 7.13: Influence of an interior column row on the lateral displacements
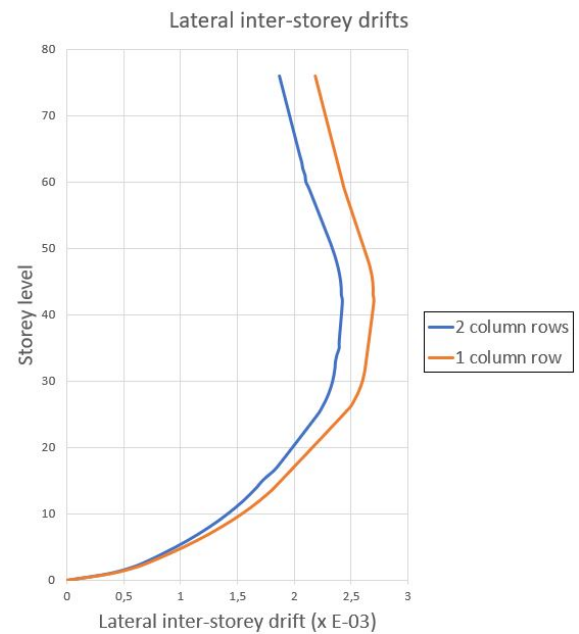
Figure 7.14: Influence of an interior column row on the lateral inter-storey drifts
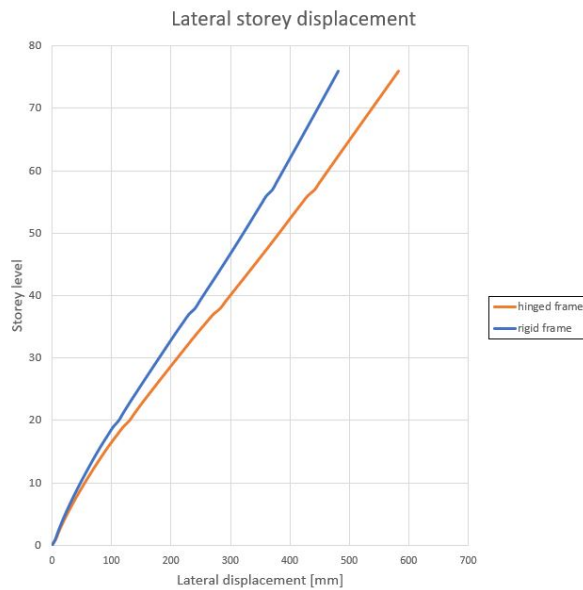
Figure 7.15: Stiffness connections
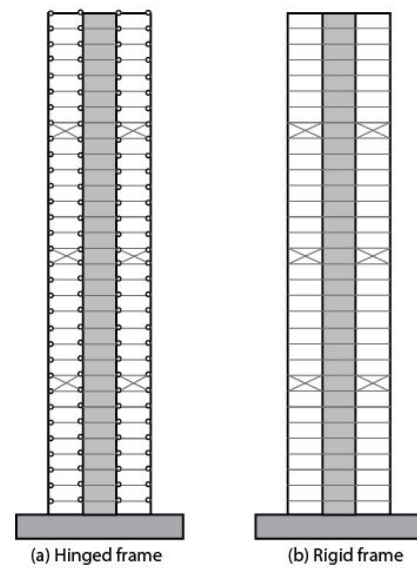
Figure 7.16: Schematic elevation views of hinged and rigid frame

concluded that the outrigger/belt-truss system already is quite efficient for a hinged frame and therefore a rigid frame is not required for this type of lateral stability system.

7.2.4. Core wall and column dimensions

In this section the iterative process of optimizing the lateral stability design by changing the core wall and column dimensions is described. The iterative process of increasing the dimensions of the structural members has been repeated until the serviceability criteria for the maximum lateral displacement and drift are fulfilled.

At first, the structure is designed for the ultimate limit state and this structural concept design is called option A. For the options B till F the dimensions of the structural elements will be further increased to make the structure stiffer. Table 7.1 shows the dimensions of the core wall and the GLT-columns for the several options. For option A, the maximum lateral displacement at the top is equal to $720mm$, and the maximum lateral inter-storey drift is equal to 3.16E-03. The limit for the lateral displacement is $H/500$, which gives an maximum allowed lateral displacement at the top of the building of $600mm$. The serviceability criterion for the maximum lateral storey drift is $h/300$, which gives a drift limit of 12.5E-03m. The inter-storey drift results shown in table 7.1 are already divided by their storey height, h, and therefore the inter-storey drift limit becomes 3.33E-03.

For the options B and C the core wall dimensions are increased and the column dimensions are kept constant. Option C has the smallest lateral displacement compared to option A and B. However, for this option the core wall thickness becomes quite large at the lower storey levels. Therefore, it is decided to not use option C for the core wall dimension, and instead option B is chosen for further optimization. For this option the reduction on the lateral storey drifts is already 7% compared to option A. The next step will be to increase the stiffness of the building by using larger column dimensions. For the options D, E, F and G the core wall dimensions are kept the same as in option B and the column dimensions will be increased. Option D is the first option that almost fulfils the serviceability criteria for both the lateral storey displacements and drifts. The maximum lateral displacement is equal to $602mm$ and the maximum lateral inter-storey drift is equal to 2.55E-03. The reduction of the lateral displacement for option D is 16% compared to option A. The column and core wall dimension for option D are chosen to be used in the final design. To satisfy the lateral displacement criterion the structure's stiffness should still be increased a bit more. This

Table 7.1: Overview of structural components for several options in the iterative design process

	Option A	Option B	Option C	Option D	Option E	Option F	Option G
Core exterior walls thickness [mm]							
Story 1 till 19	1000	1200	1400	1200	1200	1200	1200
Story 20 till 37	800	1000	1200	1000	1000	1000	1000
Story 38 till 56	500	800	900	800	800	800	800
Story 57 till 76	300	500	600	500	500	500	500
Core interior walls thickness [mm]							
Story 1 till 19	600	800	1000	800	800	800	800
Story 20 till 37	500	700	800	700	700	700	700
Story 38 till 56	400	600	600	600	600	600	600
Story 57 till 76	300	500	500	500	500	500	500
Columns dimension [mm^2]							
Story 2 till 19	1000x1000	1000x1000	1000x1000	1200x1200	1400x1400	1600x1600	1800x1800
Story 20 till 37	900x900	900x900	900x900	1100x1100	1300x1300	1500x1500	1700x1700
Story 38 till 56	800x800	800x800	800x800	900x900	1100x1100	1200x1200	1500x1500
Story 57 till 76	600x600	600x600	600x600	750x750	900x900	1000x1000	1200x1200
u_{max} [mm]	720	667	628	602	561	540	510
Δ_{max} [$-$]	3.16 E-03	3.00 E-03	2.75 E-03	2.55 E-03	2.34 E-03	2.26 E-03	2.11 E-03

Table 7.2: Parametric study of belt-truss dimension for option D

	Option D.1	Option D.2	Option D.3
Dimension belt-truss bracing [mm^2]	600 x 600	800 x 800	1000 x 1000
u_{max} [mm]	602	585	574
Δ_{max} [$-$]	2.55 E-03	2.51 E-03	2.48 E-03

increase of stiffness could be accomplished by small adjustments to the other structural components such as the outrigger and belt-trusses.

The structure's stiffness can still be increased by changing the stiffness in the outrigger levels. For example, the cross-sectional dimension of the belt-truss bracing can be increased from $600mm$x$600mm$ to $800mm$x$800mm$. This change ensures that the wind-induced lateral load is better distributed to all the perimeter columns. Table 7.2 shows the results for an increasing dimension for the belt-truss bracing. The use of a belt-truss bracing with a cross-sectional dimension of $800mm$x$800mm$ results in a reduction of 3% on the lateral displacement at the top. For this option the maximum lateral displacement is equal to $582mm$, and a maximum lateral inter-storey drift equal to 2.51E-03. This is below the serviceability limit of $600mm$ for the lateral storey displacement and also the serviceability criterion for the lateral inter-storey drift is fulfilled. Option D.2 has been further analysed and the dynamic behaviour will be optimized for this structural design.

7.2.5. Mega bracing

The mega-bracing has not been included at the beginning of the design process. First, it has been investigated whether the outrigger/belt-truss system can already give sufficient additional stiffness to the structure, and if the structure's stiffness is still insufficient the mega-bracing could be included to the structural design. Figure 7.3 shows the layout of mega-bracing over the height of the building. The diagonals will be included on all four sides of the structure's perimeter. The diagonals will have a span of 46 metres and therefore the bracing has to subdivided in smaller timber elements. Special attention should be given to the connection details of these elements. From table 7.3 it can be seen that the mega-bracing has a large influence on the wind-induced lateral displacements. It shows that mega-bracing is an effective method to increase the stiffness of the structure, and thereby the lateral stability design is improved. A reduction on the lateral inter-storey drifts of about 30% can be achieved. The mega-bracing stiffens the perimeter of the building and forms a stiff tube. In combination with the concrete core the structural design is also known as a tube-in-tube system. The structure including the outrigger system already has sufficient stiffness (see section 4.2.4) and therefore it is decided not to include the mega-bracing at the perimeter of the structure.
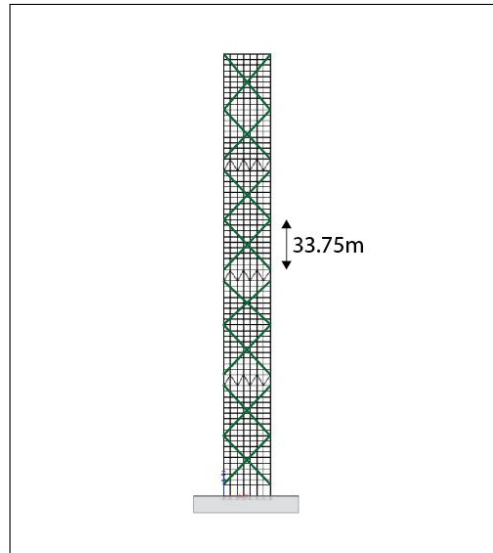
Figure 7.17: Elevation view including mega bracing

Table 7.3: Parametric study of dimensions of mega bracing for option D

	I	II	III
Dimension mega bracing $[mm^2]$	none	1000 x 1000	1200 x 1200
u_{max} $[mm]$	585	413	400
Δ_{max} $[-]$	2.51 E-03	1.74 E-03	1.70 E-03

7.2.6. Shape optimization

There are several ways to reduce the wind load of the building by shape optimization. For example, this could be done with corner modifications, tapering down over the height of the structure, including fins at the façade, or making openings in the structure. The aerodynamic treatments can be split up into two categories, the horizontal shape modifications which include adjustments in the plane of the floor plan, and the vertical shape modifications, which include adjustments over the height of the building. In this report, the focus will be especially on the corner modifications of the building. This because the effect of the rounded corners on the lateral wind load is included in the Eurocode and corner modifications can be applied at a later design stage compared to vertical shape modifications. The other shape optimizations will be more complex to analyse, and the best way to do this is by a wind tunnel test or computational fluid dynamics (CFD) studies.

Horizontal shape modification

Corner modifications can reduce the drag coefficient of the fluctuating wind and this will lead to a reduction of the lateral wind load on the structure. The drag coefficient consists of the friction and pressure drag. The pressure drag will have the largest contribution to the drag coefficient for the designed tall and slender building. This is due to the fact that the structure has a bluff body and is not streamlined. The Reynolds number (Re) becomes an important factor to explain the reduction in drag. The Reynolds number is the ratio between the inertia forces and the viscous forces. The Reynolds number indicates if the dynamic pressure or the viscous friction dominates in the air flow around a building. A low Reynolds number means a laminar wind flow is occurring, and this is normally the case for buildings with sharp corners. For a cylindrical building a more turbulent wind flow will occur, and the Reynolds number will be higher. Figure 7.18 shows the drag coefficient, C_D, versus the Reynolds number, Re for a tall building with sharp and rounded corners. It can be seen that there is an optimum Reynolds number for a building with rounded corners to get the lowest wind drag coefficient. The Reynolds number can be calculated as follows:

$$Re = \frac{\rho v L}{\eta} \tag{7.1}$$

Where:

L is the characteristic length of the building $[m]$
ρ is the density of air ($= 1.25\ kg/m^3$)
v is the characteristic wind velocity $[m/s]$
η is the dynamic viscosity ($= 17 \cdot 10^{-6}\ Ns/m^2$)

The Reynolds number has been calculated for the designed tall building with sharp corners and is equal to about $6.0 \cdot 10^8$. The Eurocode NEN-EN1991-1-4 includes a reduction factor, ψ_r, for buildings with a rectangular footprint and rounded corners. Figure 7.19 shows the reduction factor dependent on the corner radius. The reduction factor for the rounded corners will lower the wind drag coefficient, C_D, which in its turn will reduce peak response accelerations. From figure 7.19 it can be seen that for a rounded corner radius of 5 metres a reduction factor of 0.6 can be applied. Figure D.3 in Appendix D shows the floor plan layout of the tall building with the rounded corner modification. The reduction factor, ψ_r, will lower the force coefficient, and the latter can be determined as follows:

$$c_f = c_{f,0} \cdot \psi_r \cdot \psi_\lambda \tag{7.2}$$

In which, $c_{f,0}$, is the force coefficient without reductions, and ψ_λ is the reduction factor accounting for the end effects. The end effect factor takes into account the reduced resistance of the building due to the wind flow at the end of the structure. The factor for end effects is dependent on the grade of fullness of the façade of the building. The designed tall building has no openings in the façade, and this means the grade of fullness will be equal to one. The force coefficient is used to determine the characteristic global wind load, and also to determine the peak response accelerations. The aerodynamic properties of the structure will

also change due to the shape optimization. The background response factor, B, will remain constant, but the resonance response factor, R, will change due to the shape optimization. The aerodynamic damping, ζ_a, will be lower due to the corner modification, and as a consequence, the resonance response factor will increase. The resonance response factor will only increase by 8% for a corner radius of 5m while the reduction on the force coefficient is 40%. This confirms that the corner modification is an effective way for reducing the wind-induced response of the structure. The global damping in the structure becomes equal to 1.96% due to the reduction of the aerodynamic damping. The peak response acceleration has been calculated again for a structure with r=5m and the acceleration becomes equal to 0.257 m/s^2. This means a reduction of 36% of the peak acceleration in along-wind direction compared to the structure without any modifications. The calculation of the peak response acceleration for the rounded corner optimization can be found in Appendix D.2.
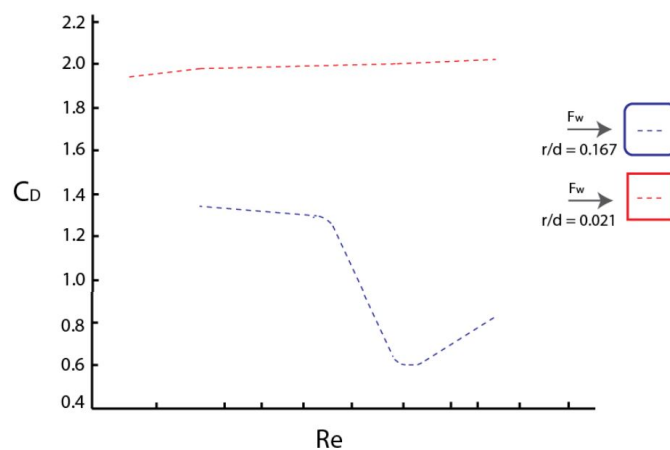
Figure 7.18: The relation between the Reynolds number and the drag coefficient for building with sharp edges and rounded corners (Tamura and Kareem, 2013).
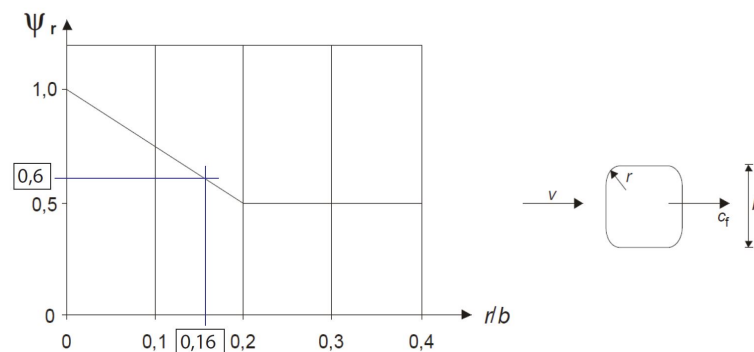
Figure 7.19: Reduction factor, ψ_r, for buildings with rounded corners (NEN-EN1991, 2002).

The rounded corners will also reduce the wind-induced accelerations in across-wind direction. However, how much the across-wind force will reduce due to the corner modification will be difficult to predict with an analytical model and this is not included in the Eurocode. (Li et al., 2018) have done a research on the influence of corner modifications on the across-wind force. From the research it was found that shape adjustment of the corners can have a significant influence on the across-wind forces on the structure. Several tall building models with and without corner shape modification have been put in the wind tunnel test. The tested square building models have a width of 0.1m and a height of 0.8m, and the geometric scale

that is used for the wind tunnel test is equal to 1/500. This means the represented tall building has a width of 50m and a height of 400m. The tall building has been tested for an urban terrain and the turbulence length, L, is 230m. The models with corner modifications have a corner cut-off rate of 10%. Figure 7.21 shows the different corner modifications and figure 7.20 shows the influence of the aerodynamic treatments on the wind force in across-wind direction. It can be seen that the lift coefficient varies over the height of the structure, and that the rounded corners will only reduce the lift coefficient at the top of the building by a factor of 0.9. If chamfered or recessed corners are applied than the lift coefficient can even be reduced by a factor 0.60 and 0.52, respectively. From this it can be concluded that the chamfered and recessed corner modifications will be more efficient in reducing the across-wind dynamic loads than the rounded corner modification.

Based on the research from Li et al. (2018) it is decided to use chamfered corners for the final design. The corners are chamfered on the grid lines of the floor plan, and this results in a corner cut rate of 14%. The reduction factor for the drag coefficient, C_D, will be roughly the same for the chamfered and rounded corners. Therefore, the calculated reduction factor, ψ_r=0.6, determined with the Eurocode can still be used for the design with chamfered corners. Figure 7.22 shows the wind flow around a tall building with straight and chamfered corners. It can be seen that the airflow around the chamfered corners is more streamlined and this reduces the drag coefficient of the wind compared to the structure with no corner modification. Wind vortices will be generated in the wake of the structure. The chamfered corners will 'confuse' the wind flow and as a result the intensity of the vortex shedding will be less than for the structure with straight corners. The straight corners encourage separation, and vortex shedding of the wind will occur no matter what the Reynolds number (Tamura and Kareem, 2013).

The peak response acceleration in along-wind direction is already below the serviceability limit, and therefore only the vortex shedding behaviour of the structure needs to be optimized. The application of a tuned mass damper could further reduce the wind-induced response accelerations, and this will be studied in section 7.2.8.
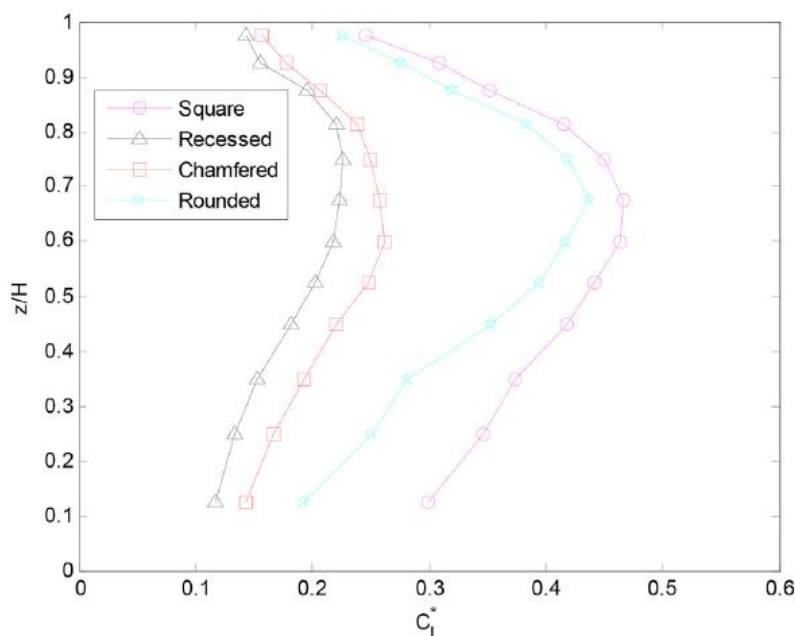
Figure 7.20: Lift force coefficients over the height of the building in across-wind direction for rounded, chamfered and recessed corner modifications (Li et al., 2018).
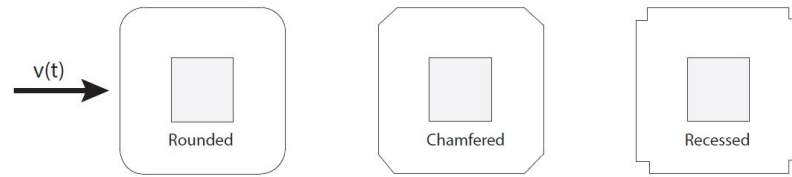
Figure 7.21: Plan views of rounded, chamfered and recessed corner modification.
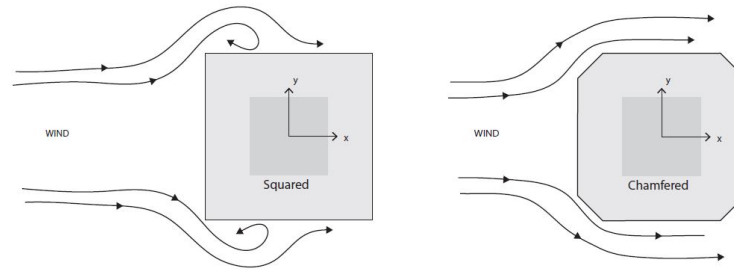
Figure 7.22: Wind flow on a squared and a chamfered tall building.

Vertical shape optimization

Vertical shape optimization can also improve the wind-induced behaviour of the structure. Examples of these aerodynamic treatments are tapering down, changing the cross-section over the height of the structure, and openings in the façade. These shape optimization can have a larger impact on the architectural design, and therefore a close joint architect-engineer involvement is recommended at an early design phase of the building project. Reference projects in which such an approach has been applied are the Burj Khalifa in Dubai, and the 432 Park Avenue in New York. The Burj Khalifa has been shape tailored in the wind tunnel test and vertical and horizontal shape optimization has been applied for this project. It was even achieved that no additional damping devices were necessary for the final design.

Figure 7.23 shows the 424m tall building 432 Park Avenue located in New York. It can be seen that openings in the façade are made at five levels along the building height. The architect did not want any horizontal shape optimizations applied in the floor plan, and therefore it has been decided to apply openings in the façade (Galsworthy et al., 2016). From the wind tunnel test it was found out that this is an effective way to break up the coherence of the vortex shedding. The across-wind forces can be reduced considerably by these openings, and especially the opening near the top of the structure will be very effective. A tuned mass damper system was still required to improve the wind-induced behaviour of the 432 Park Avenue building. This because the square shape of the building has a poor vortex-shedding behaviour.

A similar approach could be applied to the designed hybrid wood-concrete tall building. A possible location for these openings would be at the outrigger levels. In this case there will be three openings with a double storey height of $7.5m$ along the façade of the tall building. Another advantage of these openings will be that the timber outrigger/belt-trusses can kept in sight of the occupants of the building, however, this also means new locations for the MEP installations needs to be found.

Figure 7.23: 432 Park Avenue with double story openings at five levels (Galsworthy et al., 2016).

7.2.7. Global damping

The global damping that has been applied for the hybrid wood-concrete tall building is equal to 2.15% of critical damping, and this damping value has been calculated according to the Eurocode. The global damping ratio can be subdivided in the structural damping, the aerodynamic damping, and the damping due to auxiliary damping devices. The Eurocode recommends a structural damping in the range of 0.96-1.91% for timber structures and this is based on field measurements. Following from this a structural damping of 1.43% has been chosen to apply for the designed structure. The calculated aerodynamic damping using the NEN-EN1991-1-4 is equal to 0.72%, and this means the aerodynamic damping will contribute for one-third to the global damping. The damping measurements on full-scale buildings is the only way to determine the structural damping in the structure with certainty. The substructure in the tall building is likely to also contribute to the global damping. In addition, the designed structure has a concrete core which will also influence the global damping ratio. Therefore, it is important to have a good understanding of the influence of the damping in the structure on the aerodynamic behaviour. To study the effect on the wind-induced accelerations various global damping ratios have been applied for the designed structure.

The dynamic amplification factor describes the structure's response under dynamic loading and is dependent on the global damping in the structure. The dynamic amplification factor is equal to the ratio of the dynamic response to the static response. In wind engineering this factor is also known as the 'mechanical admittance' function, and is given by Eq.(7.3).

$$\left|\frac{X}{x_{stat}}\right| = H\left(\frac{\omega}{\omega_n}\right) = \frac{1}{\left(1 - \left(\frac{\omega}{\omega_n}\right)^2\right)^2 + \left(2\zeta\frac{\omega}{\omega_n}\right)^2\right)^{1/2}} \tag{7.3}$$

$$x_{stat} = \frac{F_0}{k} \qquad \text{so} \qquad |X| = \frac{F_0}{k}|H(\beta)| \tag{7.4}$$

The global damping ratio has a direct influence on the dynamic amplification factor. By increasing the global damping ratio the wind-induced accelerations will decrease. The dy-

namic amplification factor should be multiplied by the wind force spectrum to obtain the structure's response due to the dynamic wind loading. Figure 7.24 shows the dynamic amplification factor for several global damping ratios and it can be seen that for damping equal to zero the structure's response at the natural frequency will go to infinity. This is a theoretical case and in reality there will always be a certain damping present. The peak response accelerations have been calculated using the wind spectrum method by Davenport and the effect of the global damping on the wind-induced response of the structure has been studied. Figure 7.25 shows the peak acceleration in along- and acrosswind direction plotted against the global damping ratio. It can be seen that for a global damping of 10% of the critical damping the peak accelerations satisfy the occupant comfort criterion in both directions ($a_{max} \leq 0.390$ m/s^2). The existing global damping ratio of 2.15% in the structure will not be sufficient to fulfil the serviceability criterion and to get the required damping an additional damping device should be applied.
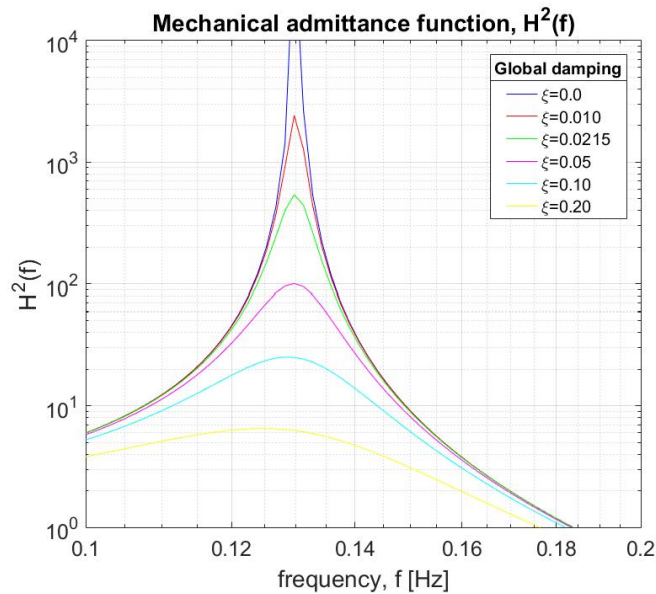
Figure 7.24: Mechanical admittance function, $H^2(f)$

A large contribution of the structural damping in timber comes from the timber connections and the substructure. It would be helpful to determine the stiffness and damping properties of the structural timber connection and substructure for further studies. This will lead to a more accurate estimation of the structural damping.

The estimation for the global damping of 2.15% is expected to be a bit conservative. The structural damping is based on damping measurements of timber bridges, and is equal to 1.43%. However, the contribution of the substructure to the structural damping will probably be larger for tall buildings than for bridge designs. Feldmann et al. have done a research on the dynamic properties of tall timber structures under wind-induced vibration in 2016. During this research several on-site ambient vibration measurements have been done on tall timber structures. The average damping ratio found from the experimental data is around 2.0%. The tallest structure that has been tested is 100m tall timber wind turbine. Therefore, no conclusions can be made for buildings above this height. Although, the research will help to make a better estimation for the structural damping for the 300m tall building.

The peak response accelerations will now be calculated again for a structural damping of 2.0%. The aerodynamic damping will stay the same ($\zeta_a = 0.72\%$), and this will result in a global damping of 2.72%. The increase in global damping will decrease the mechanical admittance of the structure. The peak response accelerations in along- and acrosswind direction

become equal to 0.374 m/s^2 and 0.606 m/s^2, respectively. From this it can be concluded that the damping in the structure is an effective way for optimizing the wind-induced behaviour. The global damping could be further increased by the addition of a tuned mass damper.
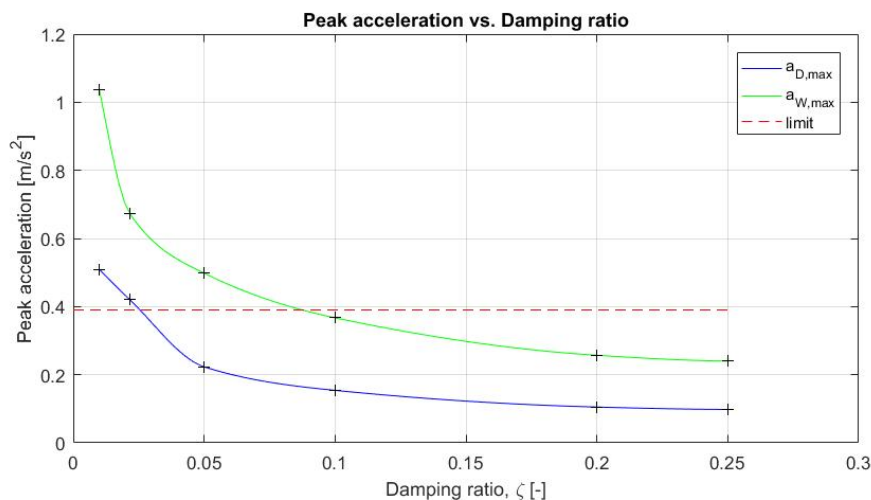
Figure 7.25: Peak accelerations in along- and acrosswind direction plotted against the global damping ratio of the structure

7.2.8. Tuned mass damper

The auxiliary damping devices can significantly reduce the peak response acceleration in the structure. A common auxiliary damping device in tall buildings is the tuned mass damper (TMD). A tuned mass damper can provide an additional damping to the structure up to 20% of critical damping. An other possibility would be to include visco-elastic dampers to the braces at the outrigger levels. The visco-elastic dampers can provide an additional damping of around 10% of critical damping (Oosterhout, 1996). In this section the focus will be on the TMD design, and the TMD will be tuned for the designed hybrid wood-concrete tall building.

A distinction can be made between a passive and active TMD. The parameters of the vibrating system can be changed and controlled for an active damper system. This way the wind-induced response can be counteracted more efficiently and this can lead to a mass reduction of the damper. The passive TMD can be seen as a pendulum device hanging at the top of the building. It should be kept in mind that the swaying of the pendulum stays in between the available space and the amplitude of the system will be limited by the surrounding structural components. The active TMD, also known as an active mass damper (AMD), will be more costly than a passive TMD. The choice to use an AMD or passive TMD will be dependent on the specific project, and the decision should be based on the required additional damping in the structure and the overall costs. The different applications and the effectiveness of tuned mass dampers will be discussed in more detail further on.

Undamped TMD

The structure including the TMD has been schematised as a 2 degree of freedom (2DOF) system. Figure 7.26 shows the 2DOF system, and it can be seen that the damper is only connected with a spring to the primary structure. The auxiliary damping system is not attached with a viscous damper to the main structure, and therefore this system is called an undamped TMD. To represent the wind loading a harmonic external force is applied on the primary structure. The equations of motion of the 2DOF system will be solved, and this will give insight in the efficiency and effect of the TMD on the wind-induced behaviour.

The equations of motion of the DOF system are:
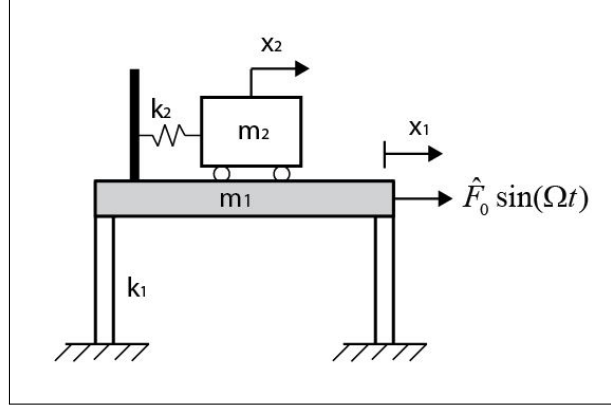
Figure 7.26: 2DOF system for an undamped TMD

$$m_1\ddot{x}_1 + k_1 x_1 + k_2 x_1 - k_2 x_2 = \widehat{F}_0 sin(\Omega t)$$
$$m_2\ddot{x}_2 + k_2 x_2 - k_2 x_1 = 0 \tag{7.5}$$

Let's assume a harmonic external force, and a particular solution formulated as follows:

$$x_1 = \widehat{X}_1 sin(\Omega t)$$
$$x_2 = \widehat{X}_2 sin(\Omega t) \tag{7.6}$$

Now substitute the steady-state solution into the equations of motion. This will give the following result:

$$\frac{\widehat{X}_1}{x_{stat}} = \frac{1 - \dfrac{\Omega^2}{\omega_2^2}}{\left(1 - \dfrac{\Omega^2}{\omega_2^2}\right)\left(1 + \dfrac{m_2}{m_1} - \dfrac{\Omega^2}{\omega_1^2}\right) + \dfrac{m_2}{m_1}} \tag{7.7}$$

$$\frac{\widehat{X}_2}{x_{stat}} = \frac{1}{\left(1 - \dfrac{\Omega^2}{\omega_2^2}\right)\left(1 + \dfrac{m_2}{m_1} - \dfrac{\Omega^2}{\omega_1^2}\right) - \dfrac{m_2}{m_1}} \tag{7.8}$$

The above expressions are valid for any ratio of Ω/ω, in which Ω is the angular frequency of the applied force and ω the angular frequency of the mass. However, the addition of a TMD is not of much use unless the primary structure is near resonance (Den Hartog, 1956). Therefore, a closer look is taken at a damper with an eigenfrequency equal to that of the structure and resonance can occur ($\Omega = \omega_1 = \omega_2$). If the structure is in resonance the amplitude of the response will get infinitely large. On the other hand, if the frequency of the force is equal to that of the damper ($\Omega = \omega_2$, $\omega_1 \neq \omega_2$), than this will give a zero amplitude to the primary mass. A closer look is taken at the last case, and $\Omega = \omega_2$ is put into Eq.(7.7) which results in:

$$\widehat{X}_2 = -\frac{\widehat{F}_0}{k_2} \tag{7.9}$$

$$x_2 = -\frac{\widehat{F}_0 \sin(\Omega t)}{k_2} \tag{7.10}$$

$$F_2 = x_2 k_2 = -\widehat{F}_0 \sin(\Omega t) \tag{7.11}$$

The reaction force of the TMD, F_2, is equal to the applied external force but in opposite direction. From this it follows that the efficiency of the damper is optimum and no vibration will occur in the primary system.

The dynamic amplification factor is determined to study the effect of the TMD on the response of the structure. The dynamic amplification factor is equal to the ratio of the dynamic response and the static response. Figure 7.27 shows the dynamic amplification function for a TMD system which is tuned to the natural frequency of the primary structure ($\omega_2 = \omega_1$), and resonance could occur in the primary system. Equations 7.12 and 7.13 can now be rewritten as follows:

$$\left|\frac{\widehat{X}_1}{x_{stat}}\right| = \frac{1 - \dfrac{\Omega^2}{\omega_2^2}}{\left(1 - \dfrac{\Omega^2}{\omega_2^2}\right)\left(1 + \dfrac{m_2}{m_1} - \dfrac{\Omega^2}{\omega_2^2}\right) - \dfrac{m_2}{m_1}} \tag{7.12}$$

$$\left|\frac{\widehat{X}_2}{x_{stat}}\right| = \frac{1}{\left(1 - \dfrac{\Omega^2}{\omega_2^2}\right)\left(1 + \dfrac{m_2}{m_1} - \dfrac{\Omega^2}{\omega_2^2}\right) - \dfrac{m_2}{m_1}} \tag{7.13}$$
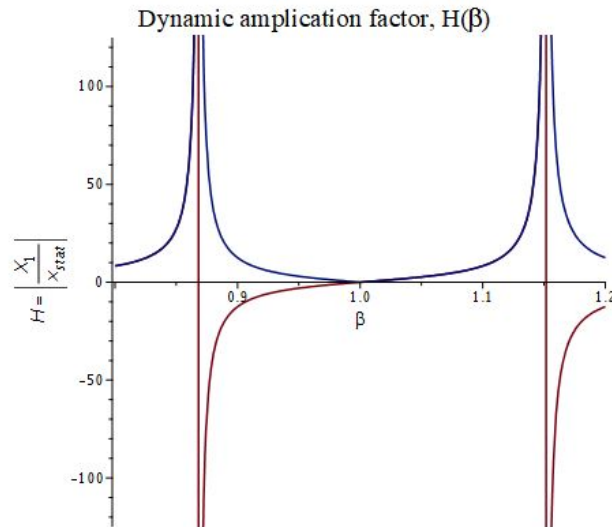
Figure 7.27: Dynamic amplification factor, $H(\beta)$, for an undamped TMD system

The mass ratio and frequency ratio are now introduced, respectively:

$$\mu = \frac{m_2}{m_1} \tag{7.14}$$

$$\beta = \frac{\Omega}{\omega_n} \tag{7.15}$$

A mass ratio of, $\mu = 0.02$, will be applied for further calculations and this is a typical ratio for a TMD system in high-rise structures. The lateral displacements of the TMD could become large if a minimum response in the structure is achieved. In most cases, such large lateral displacements are not possible in tall buildings due to obstruction by the main structural elements. The dampers and springs connected at the sides of the TMD will help to keep the secondary mass in place. In figure 7.27 it can be seen that the dynamic amplification function has two peaks. The two peaks will be located on each side of $\beta = 1$, and will have an infinite amplitude for an undamped TMD.

Damped TMD
The damped TMD has been connected to the primary structure with a spring and a dash-pot
in parallel. Ormondroyd and Den Hartog (1928) introduced the concept of the damped TMD
in 1928. In their research it was found that there is an optimum ratio of the eigenfrequency
of the damper and the eigenfrequency of the primary system. This optimum ratio is also
known as the tuning ratio. The optimum tuning ratio can be determined with Eq.(7.16).

$$f_{opt} = \frac{\omega_2}{\omega_1} = \frac{1}{1+\mu} \tag{7.16}$$

Figure 7.28 shows the 2DOF system for a damped TMD and an undamped primary structure.
The equations of motion for this 2DOF system can be formulated as follows:

$$m_1\ddot{x}_1 + c_2(\dot{x}_1 - \dot{x}_2) + k_1x_1 + k_2(x_1 - x_2) = \widehat{F}_0 sin(\Omega t)$$
$$m_2\ddot{x}_2 - c_2(\dot{x}_2 - \dot{x}_1) + k_2(x_2 - x_1) = 0 \tag{7.17}$$
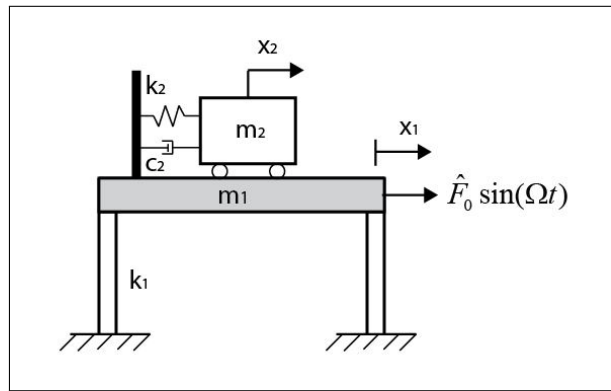
Figure 7.28: 2 degree of freedom system of damped TMD

The steady-state solution is assumed as:

$$x_1 = \text{Im}(\hat{X}_1 e^{i\omega t})$$
$$x_2 = \text{Im}(\hat{X}_2 e^{i\omega t}) \tag{7.18}$$

Substituting the steady-state solution into the equations of motion gives the following result:

$$\left|\frac{\widehat{X}_1}{x_{stat}}\right| = \sqrt{\frac{\left(2\frac{c_2}{c_c}\beta\right)^2 + \left(\beta^2 - f^2\right)^2}{\left(2\frac{c_2}{c_c}\beta\right)^2\left(\beta^2 - 1 + \mu\beta^2\right)^2 + \left(\mu f^2\beta^2 - (\beta^2 - 1)(\beta^2 - f^2)\right)^2}} \tag{7.19}$$

Where:

β is the frequency ratio ($= \Omega/\omega_n$)
c_c is the critical damping ($= 2m\omega_n$)
f is the tuning ratio ($= \omega_2/\omega_1$)
μ is the mass ratio ($= m_2/m_1$)

Figure 7.29 shows the dynamic amplification factor for several damping values. In this case
it is assumed that the mass ratio, $\mu = 0.02$, and the tuning ratio, $f = 1$. The frequency of the
TMD is the same as the frequency of the primary structure for this tuning tuning ratio and
this means the optimum tuning ratio has not been applied yet. The two peaks will approach

each other for an increase of the damping of the TMD and will merge into a single peak located at $\beta = 1$ (Connor, 2002). The green line represents the dynamic amplification function for a damping equal to zero and this gives the same dynamic amplification factor as for the undamped TMD system. The magenta coloured line is for an infinitely large damping. The TMD has a rigid connection with the primary structure for this case, and as a consequence, the system will behave as a SDOF system.

The dynamic amplification functions all intersect each other at two points and these points are known as the 'locked' points. In figure 7.29 the location of the 'locked' points are indicated with the letters Q and R. All the functions pass the two 'locked' points independent of the damping. To acquire the optimum damping of the TMD the two peaks of the dynamic amplification function should be located at the 'locked' points. The curve that passes with a horizontal tangent through the 'locked' points will be most favourable (Den Hartog, 1956). The 'locked' points should also have the same height and the height of the locked points can be adjusted by changing the frequency ratio. The optimum tuning ratio should be found to obtain two peaks of equal height and this ratio can be calculated with Eq.(7.16). A parametric study for the damping coefficient has been done to get the peaks of the dynamic amplification function at the 'locked' points. The optimum damping that has been found from the parametric study is equal to 0.10 for a TMD design with a mass ratio of 0.02. Both peaks of the dynamic amplification function are located at the 'locked' points Q and R for this damping ratio. The optimum tuning ratio for this TMD design would be $f = 0.98$.
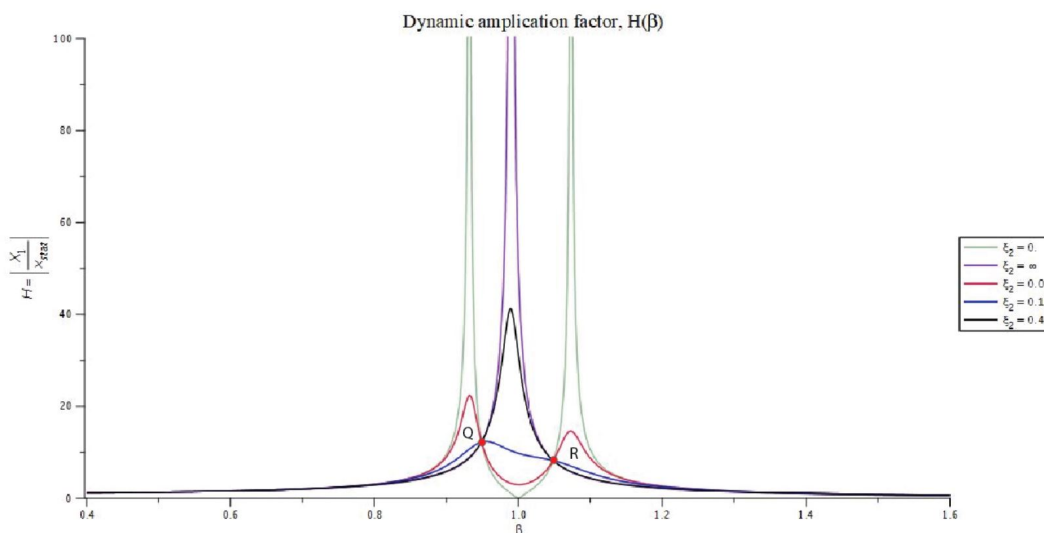
Figure 7.29: Dynamic amplification factor (for $f = 1$)

The mechanical admittance of the structure is equal to the dynamic amplification function to the power 2. The mechanical admittance will be determined again for a structure including a passive TMD and no corner modifications will be applied yet. The following three mass ratios are assumed: $\mu = \frac{1}{100}$, $\frac{1}{50}$, and $\frac{1}{20}$. The optimum viscous damping value and the optimum tuning ratio should be determined for each TMD design. The tuning has been done by an iterative process in MatLab. The optimum damping will be equal to 0.07 and the optimum tuning ratio will be equal to 0.99 for the TMD design with a mass ratio of 0.01. The optimum properties for the other TMD designs can be found in Appendix D.2.

Figure 7.30 shows the mechanical admittance function for the structure with and without the application of a passive TMD. It can be seen that the addition of the TMD reduces the mechanical admittance significantly. The mechanical admittance function including the TMD shows that the two peaks are located at the same height, which is the most optimum as
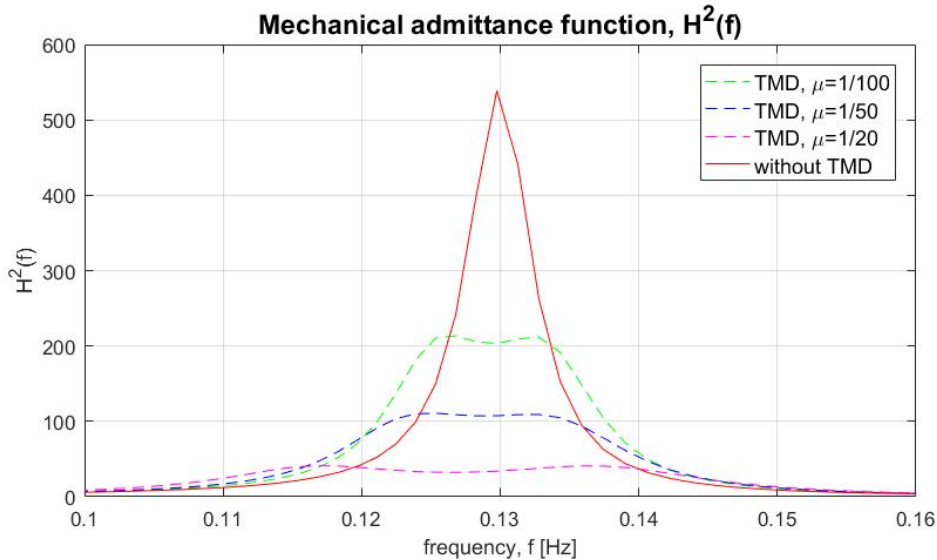
Figure 7.30: Mechanical admittance function, $H^2(f)$, for structure including a passive TMD with mass ratio μ= 0.01, 0.02 and 0.05

discussed earlier on. The mechanical admittance function will be used to determine the structure's wind-induced response accelerations. For a TMD with $\mu = \frac{1}{50}$ the peak response accelerations in along- and acrosswind direction are equal to 0.331 m/s^2 and 0.524 m/s^2, respectively. The peak acceleration has been reduced by 22% compared to the peak acceleration for the structure without a TMD. An increase in the mass of the TMD would further reduce the peak acceleration, however, a larger mass ratio would become impractical. The response accelerations determined above are based on the tall building with squared corners. An other alternative would be to apply shape modifications to reduce the shedding of the vortices and thereby the across-wind response accelerations.

Active Mass Damper
The active TMD (AMD) can be more effective in damping the vibrations than a passive TMD. The damper system is tuned to the incoming gust frequencies with an actuator. Sensors will be registering the external excitation or/and the structural response and based on these measurements the required control forces are computed (Chu et al., 2005). The actuator produces the required forces to the damping device based on the measurements.

The passive TMD has some disadvantages compared to an AMD and the following weak points can be stated (Nishimura et al., 1992):

- The efficiency of the TMD depends on the mass ratio, μ. For a tall building, the mass ratio cannot be very high due to the large weight of the primary structure.

- If the mass ratio is low this also means the optimum damping is low. Therefore, it is difficult to adjust the natural frequency of the damper to the optimum frequency. For a low damping it will take longer for the system to reach the steady-state response. At the start the disturbance vibration is not suppressed yet, and the TMD will be less effective.

The application of an AMD will save damper space and the mass can be reduced. It should kept in mind that one of the disadvantages of an AMD is the required power supply to the actuator. Especially, during a hazard event the probability that the main power source to the building may fail will be large. There also exist hybrid mass dampers (HMD) which are a combination of the AMD and passive TMD. The passive TMD could be seen as a backup in the case of the event of power supply failure.

Combination of TMD and chamfered corner modification

The chamfered corner modification turned out to be an effective measure to improve the wind-induced dynamic behaviour. However, the peak acceleration did not satisfy the occupant comfort criterion yet, and the peak response acceleration should be below the limit of 0.390 m/s^2 for a structure with a natural frequency of 0.130 Hz. A passive TMD with a mass ratio of 0.01 and the chamfered corner modification will be applied for the final design of the tall building. A combination of these measurements is necessary to improve the wind-induced behaviour so that the peak response acceleration satisfies the occupant comfort criterion. The peak response accelerations have been calculated again and are equal to 0.249 m/s^2 and 0.371 m/s^2 in along- and acrosswind direction, respectively. The occupant comfort criterion for the peak response acceleration has now been satisfied.

7.2.9. Discussion of results

Stiffness optimization

Three outrigger levels have been applied for the lateral stability for the final design. The addition of one outrigger level already showed a significant improvement on the lateral inter-storey drifts and a reduction of 37% can be achieved. The tall building design with three outrigger levels gives a total reduction of 54% on the lateral inter-storey drifts. The layout of the outrigger trusses turns out to be an important factor for the lateral displacement of the structure as well. The orthogonal layout gives a reduction of about 15% on the maximum lateral inter-storey drift compared to the diagonal layout of the outrigger trusses. The outrigger levels will become a lot stiffer for the option with the orthogonal placement, and therefore more forces are transferred to the perimeter columns.

A second column row has been added to the final design of the structure. In the case the interior columns are part of the outrigger/belt-truss system then the maximum lateral inter-storey drifts can be reduced by 10%. It should be noted that the second column row will reduce the openness of the floor plan. The main reason for the addition of the interior column row has been to reduce the cross-sectional dimensions of the GLT columns. For a super tall all-concrete building the span of 9 metres from the core to the perimeter could possibly be accomplished with still acceptable column dimensions. However, for a super tall timber frame the required column dimensions would become impractical. In addition, the interior column row reduces the floor span from 9 metres to 4.5. Subsequently, this will reduce the thickness of the floor slab, and therefore the overall material use in the building. Later on in the design process it has been decided to not let the interior columns participate in the outrigger/belt-truss system. This due to the fact that the vertical loading on the interior columns turned out to be already quite large and would only increase more when participating in the lateral stability system. The perimeter columns are more effective in increasing the lateral stiffness due to the larger lever arm from the core wall to the perimeter columns. As a consequence, the axial force will only increase in the perimeter columns due to the lateral wind load. The addition of the interior column row is one of design choices which belongs specifically to the design of a super tall hybrid wood-concrete building, and this measure will be less likely to be applied in a super tall all-concrete building.

The effect of a rigid frame compared to a hinged timber frame has been studied. A rigid frame will reduce the maximum lateral displacement at the top of the building with about 20% compared to a hinged timber frame. However, it is quite difficult and expensive to make all timber beam-to-column connections moment resistant. Therefore, it is decided to assume the beam-to-column connections as hinges for the final design.

The column and core wall dimensions have been optimized to increase the stiffness and mass capacity of the structure. The dimensions of the columns and walls have been increased until the serviceability criteria for lateral displacement and drift were met. The core wall thickness at the base is equal to 1200mm in the final design, and the thickness of the walls have been tapered down three times along the height of the structure to a thickness of 500mm at the top. The column dimensions have also been tapered down over the height of the structure, have been tapered down from 1200x1200 mm^2 to 750x750 mm^2 at the top of the structure in the final design. The dimensions of the belt-truss diagonal have been increased to 800x800 mm^2. The larger belt-truss dimension turned out to give more stiffness to the outrigger level and ensures that the wind-induced lateral load is better distributed to all the perimeter columns.

The stiffness optimization described above resulted in a maximum lateral drift of 8.33mm and a maximum lateral displacement of 585mm. This means that the serviceability criteria for lateral displacement and lateral inter-storey drift have both been satisfied. Figure 7.31 and 7.32 show the lateral displacements and inter-storey drifts for the final design of the hybrid wood-concrete tall building, respectively.

The addition of mega bracing at the perimeter has been studied as well. The mega bracing stiffens the perimeter of the building and forms a stiff tube. The combination with the concrete core the structural design is also known as a tube-in-tube system. From the para-
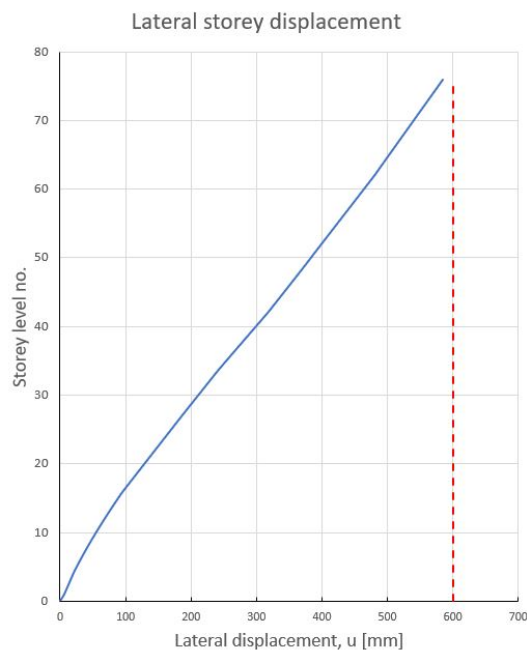
Figure 7.31: Lateral displacements along the height of the building for the final design
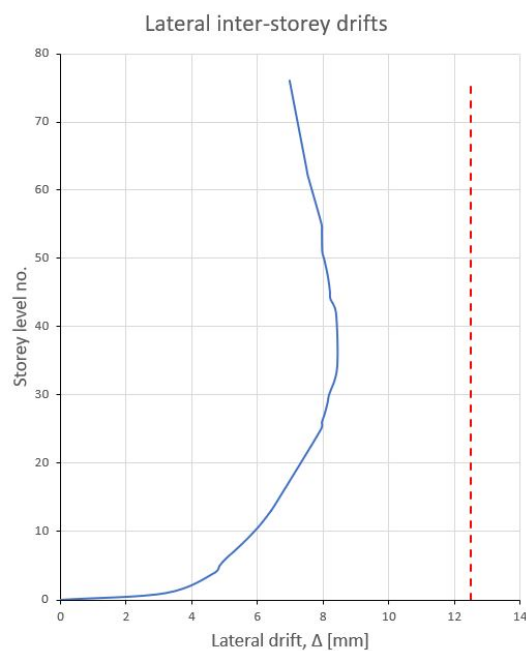
Figure 7.32: Lateral inter-storey drifts along the height of the building for the final design

metric study it showed that mega bracing is an effective method to increase the stiffness of the structure and the lateral inter-storey drifts can be reduced by a factor of 0.7. The stiffness serviceability criteria have already been met for the structure with three outriggers and therefore it is decided not to include the mega bracing.

Aerodynamic treatments
A rounded corner modification reduces the drag force in the along-wind direction in particular. However, the rounded corners will be less effective in reducing the lift force in across-wind direction. The chamfered corner modification turned out to be an effective measure to reduce the dynamic wind load both in along -and acrosswind direction. The chamfered corners break up the vortices at the wake of the building and also streamline the building in along-wind direction. The lift coefficient can be reduced by a factor of 0.6 for the designed structure with chamfered corners and a cut-off rate of 14%. The peak response acceleration has been calculated again with the response spectrum method and this resulted in an acceleration of 0.404 m/s^2 in the across-wind direction.

Vertical shape optimization can also be an effective measure to reduce the across-wind force. The vertical shape optimizations require larger changes to the design compared to the minor horizontal modifications such as corner adjustments. Therefore, the horizontal shape modifications will be easier to apply in a later phase of the design process. Openings at the façade located at the outrigger levels would be a good solution for a vertical shape optimization for the designed tall building.

Damping
The tall building already has a certain structural damping capacity. The estimated structural damping for the 300m hybrid wood-concrete tall building is equal to 1.43%, and the aerodynamic damping is equal to 0.72%. Therefore, the total global damping in the structure becomes equal to 2.15%. This damping value has been based on the Eurocode. The research of Feldmann et al. showed an average structural damping ratio of 2.0% for tall timber structures up to 100m. Based on this it could be expected that the structural damping of the designed hybrid wood-concrete tall building will be a bit higher than assumed at first. A parametric study for the global damping of the structure has been done to see the effect

on the peak response accelerations. This study showed that for a global damping of 10% the serviceability criterion for peak accelerations will be satisfied. The additional damping can be acquired by the application of a tuned mass damper (TMD).

A distinction should be made between a passive and an active TMD. The active tuned mass damper (AMD) can reach a higher efficiency with a lower mass than a passive TMD. Disadvantages of an AMD are that it is dependent on the power supply and the auxiliary device is more expensive than a passive TMD. A passive TMD with a mass ratio of $\frac{1}{50}$ can reduce the peak response accelerations by a factor of 0.78. A larger mass for the TMD will reduce the response acceleration even more, however, an increase in the mass of the damper will become impractical for the design.

7.3. Comparison with traditional structural system in concrete

The design of the tall building has also been done for the main structure fully designed in concrete. This is done to be able to make a comparison with the hybrid wood-concrete design. The concrete design has the same layout as the hybrid structural design and also three outrigger systems will be applied. The core wall design has been kept identical, and the timber frame is replaced by a moment-resistant concrete frame. The floor slabs consist of hollow core slabs and its dimensions are estimated with a rule-of-thumb. The concrete frame is designed according to the Eurocode using the concrete frame design in the analysis software CSi ETABS. The tuned mass damper system and shape optimization will be disregarded up to now for both design options.

The structure of the concrete design should satisfy the serviceability criteria for lateral inter-storey drift and displacements, and should be designed to just satisfy this criterion in order to achieve an economical design. The cross-sectional dimensions of the concrete structural elements can be reduced compared to the structural components in the hybrid wood-concrete design. The dimensions of the structural dimension can be found in the Appendix A.5. The stiffness capacity should be about the same for both the concrete and hybrid design because the same stiffness criterion of H/500 is followed for the structural design. On the other hand, the concrete design has a higher mass capacity compared to the hybrid wood-concrete design and this will result in a better wind-induced dynamic behaviour. A natural period of 8.3 seconds is achieved for the concrete design and the wind-induced accelerations will be lower compared to the hybrid design which has a natural period of 7.7 seconds.

Table 7.4: Comparison of concrete tall building and hybrid wood-concrete tall building

	Hybrid structure	Concrete structure
Maximum lateral displacement, δ_{max}	$0.585\ m$	$0.403\ m$
Maximum lateral inter-storey drift, Δ_{max}	$8.33\ mm$	$6.53\ mm$
Natural frequency, $n_{1,x}$	$0.130\ Hz$	$0.122\ Hz$
Global damping, ζ	2.15%	1.89%
Peak response acceleration, $a_{W,max}$	$0.674\ m/s^2$	$0.487\ m/s^2$
Weight, W	$7.5 \cdot 10^7\ kg$	$12.6 \cdot 10^7\ kg$

The mass capacity is for the concrete structure higher than for the hybrid wood-concrete structure and this will improve the wind-induced dynamic behaviour of the structure. The stiffness capacity is also larger than for the hybrid design. This is due to the fact that the same core wall thickness and also the second column row have been applied in the design. This results in a concrete tall building which has a maximum displacement of 0.403m at the top (see Figure 7.33). To optimize the design, the stiffness could be further reduced till the serviceability limit of 0.600m is reached. Table 7.4 shows the comparison of the maximum lateral inter-storey drift and displacement for the concrete and hybrid design. It can be seen that the hybrid wood-concrete structure will have a higher damping capacity compared to the concrete structure, and this is advantageous for the wind-induced dynamic behaviour. A global damping ratio of 2.15% is applied for the hybrid structure and for the concrete structure a lower global damping ratio of 1.89% is used, which are based on the Eurocode
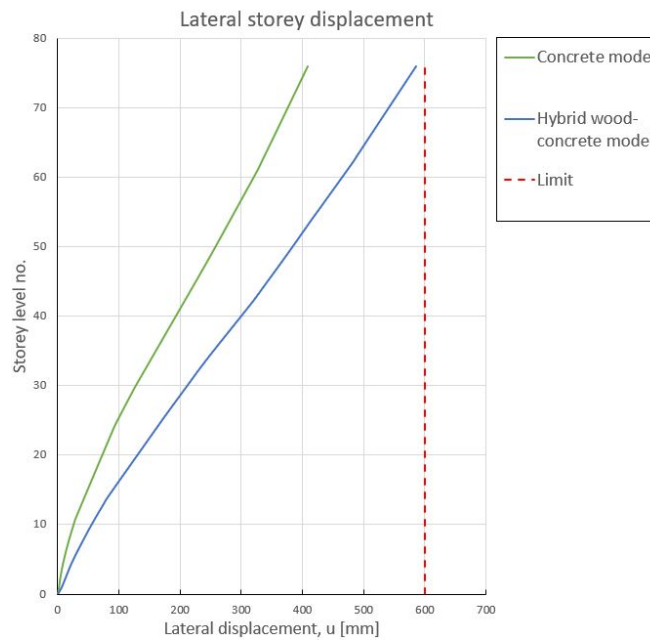
Figure 7.33: Comparison lateral storey displacements of concrete and wood-concrete tall building design

NEN-EN1991-1-4. The determined damping ratios are found from experimental tests on existing buildings and could differ from the designed structure. The applied damping ratio for the all-concrete structure is expected to be more reliable than the damping ratio for the hybrid wood-concrete structure due to the fact that more measurements have been done on concrete tall buildings. The peak acceleration for the concrete design is lower due to the larger mass. However, it should be noted that the damping ratio for the hybrid wood-concrete structure has been taken a bit conservative. Therefore, in the case the structure would have a higher structural damping ratio then the peak response acceleration would also get reduced.

7.4. Final design

The final design of the hybrid wood-concrete tall building consists of a reinforced concrete core and a mass timber frame around its core. The building has a total of 76 storey levels and a height of 300 metres. The footprint of the building is equal to 31.5 by 31.5 metres, and the central reinforced core has the dimensions of 13.5 by 13.5 metres. The timber frame has two column rows which have been placed on the structure's grid of 4.5 metres. An outrigger/belt-truss system has been applied on three levels over the height of the structure. Each outrigger level consists of eight outrigger trusses placed orthogonally with respect to the reinforced concrete core. The outriggers transfer the forces to the perimeter columns, and a belt-truss has been placed along the perimeter of the building at each outrigger level. Furthermore, the column dimensions and core wall thickness have been tapered down over the height. This because less strength has been required at the top of the building. Due to the tapering down the weight of the building can be reduced, and this also ensures a more economical design.
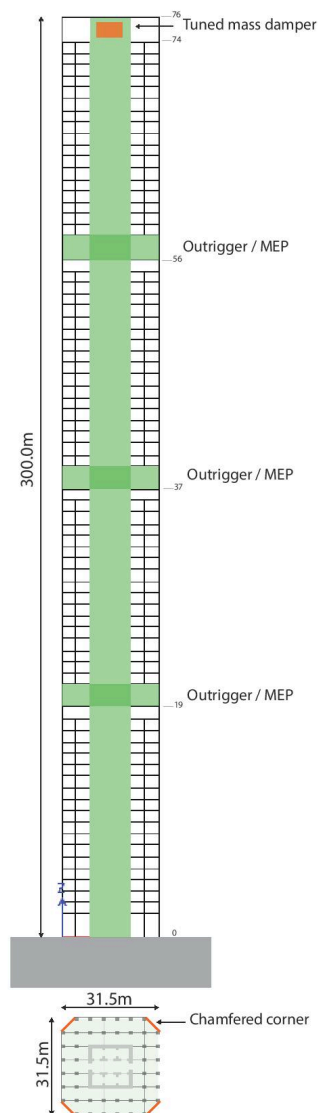
Figure 7.34: Schematic overview of final design including optimizations

Based on the Eurocode, the global damping as fraction of the critical damping has been taken equal to 2.15%. The global damping can be subdivided into a structural damping of 1.43% and an aerodynamic damping of 0.72%. The natural frequency of the structure is equal to 0.130 Hz, which is equivalent to a natural period of 7.7 seconds.

Figure 7.34 shows an overview of the optimization measurements that are applied to improve the wind-induced behaviour of the structure. A passive TMD in combination with a chamfered corner modification have been applied in the final design of the hybrid wood-concrete tall building. The cut-off rate of the chamfer is equal to 14% and the TMD will have a mass ratio of 0.01. These measurements will improve the structure's wind-induced behaviour and the peak response acceleration in along- and acrosswind direction will get reduced to 0.249 m/s^2 and 0.371 m/s^2, respectively. Figure 7.35 shows the occupant criterion for office buildings and the peak response acceleration for the designed tall building are indicated in the graph with red dots. It can be seen that the peak acceleration due to the vortex shedding is now also below the serviceability limit of 0.390 m/s^2 and the occupant comfort criterion has been satisfied.
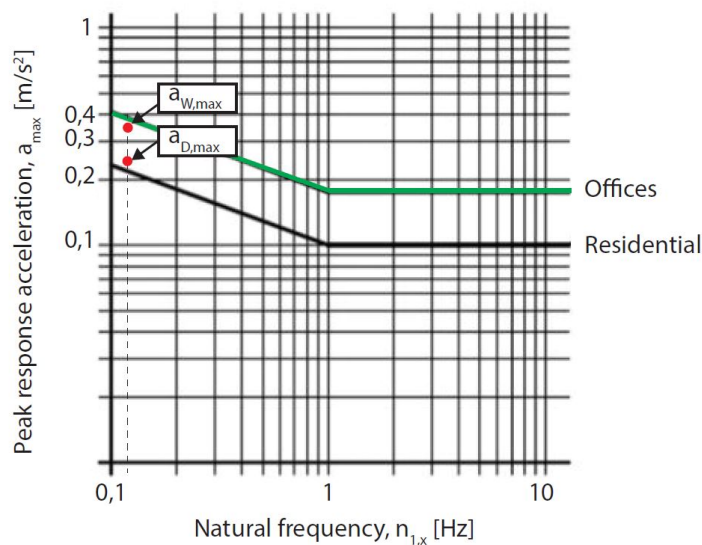
Figure 7.35: Occupant criteria according to Dutch Annex on the NEN-EN-1991-1-4 with indication of the peak response accelerations in along- and acrosswind direction.

8
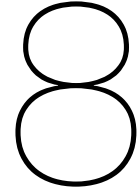
Discussion

In this chapter the findings are discussed, and aspects that might have an impact on the results of this research will be described. First, the design, research and results of the case study will be discussed. Subsequently, the design of a super tall hybrid wood-concrete building in general will be discussed based on the observations from the case study.

8.1. Design, research and results

In this case study, a complete and integral design of a 300m tall wood-concrete hybrid building was made. Design aspects such as the floor plan, core layout, lateral stability system and timber frame were designed first. The floor plan layout and storey height were based on a typical office building, which resulted in a length from the perimeter to the core of the building equal to 9 metres and a storey height of 3.75 metres. These dimensions also ensured that enough sunlight would fall into the office spaces. The entrance level with double storey height was performed in reinforced concrete to create a more open layout and to achieve a higher safety in the case of accidental blast loading.

The serviceability criteria for lateral displacements and accelerations were governing for the final structural design. The maximum lateral inter-storey drift should be below 12.5 mm and the maximum lateral displacement should be below 600 mm according to the Eurocode. The lateral displacements due to the wind loading were computed using a finite element model of the designed case in the structural analysis software CSi ETABS. An increase in stiffness capacity turned out to be required to satisfy the serviceability criteria mentioned earlier. Therefore, a parametric study of the cross-sectional dimension of the columns, the reinforced concrete core wall thickness, and the outrigger/belt-truss layout and dimensions was performed.

The cross-sectional dimension of the columns and the reinforced concrete core wall thickness were tapered down over the height of the structure. Subsequently, the column and core wall dimensions were modified in order to improve the stiffness capacity of the structure. For the lateral stability design, an outrigger/belt-truss system turned out to be adequate and efficient for the designed hybrid structure. A parametric study was performed to determine the required number of outrigger levels. A maximum of three outrigger levels were considered, as more would result in loss of too much office space. For the final design, the outrigger system was applied on three storey levels along the height of the structure, resulting in an about 2-fold reduction of lateral inter-storey drifts. However, the efficiency of the outriggers would go down while the costs for an additional outrigger level stays the same.

Furthermore, a diagonally- and orthogonally-oriented layout of the outrigger trusses were compared. For the final design, the orthogonally-oriented layout was applied, because it resulted in more lateral stiffness of the structure. Each outrigger level consists of 8 outrigger trusses which are orthogonally oriented with respect to the reinforced concrete core, and a belt-truss surrounds the perimeter of the structure. The outrigger levels with double storey

height were also designed as mechanical, electrical and public health system (MEP) levels.

The stiffness optimization resulted in a design that satisfied the lateral drift and displacement criteria. The maximum lateral inter-storey drift was computed to be equal to 8.33mm and the maximum lateral displacement was computed to be equal to 585mm. These results were acquired from the structure in which shape optimization and auxiliary damping were not applied yet.

A model analysis of the finite element model in CSi ETABS determined the natural frequency of the structure to be 0.130 Hz, which was was verified with a SDOF system. Based on the natural frequency and office function, the peak response acceleration should be below 0.390 m/s^2 with a return period of 50 years. For the designed case, the peak acceleration was computed to be equal to 0.674 m/s^2 and did not satisfy the occupant comfort criterion yet. The peak response acceleration occurred in across-wind direction due to the vortex shedding of the wind.

Consequently, improvements and optimization of the stiffness, structural damping and shape were required. The dynamic response of a structure is governed by its mass, stiffness and damping capacity. Adjustments to these properties change the wind-induced response and can help to optimize the structure's dynamic behaviour. Increasing the damping capacity of the structure is an effective way to reduce the wind-induced accelerations. Based on the Eurocode, the structure's global damping ratio was 2.15%. In addition, several damping ratios were analysed, and it was determined that a global damping ratio of 10% would result in a peak acceleration satisfying the occupant comfort criterion. Therefore, an auxiliary damping device and a shape optimization were required to reduce the peak acceleration in the structure. A passive tuned mass damper (TMD) with a mass ratio of 0.01 was applied at the top of the structure, which reduced peak acceleration by counteracting the dynamic response of the structure.

In addition, the wind load on the façade in the along-wind direction was reduced by a corner modification. This corner modification also limited shedding of the vortices, thereby reducing the dynamic wind load in across-wind direction. A chamfered corner modification was applied, since it reduces the lift force coefficient more efficiently than a rounded corner modification (Li et al., 2018), resulting in a reduction of the lift force coefficient by a factor of 0.6. Applying the TMD system and corner modification to the designed structure reduced the peak acceleration to 0.371 m/s^2 in the across-wind direction and 0.249 m/s^2 in the along-wind direction, thereby satisfying the occupant comfort criterion.

While most of the frame was designed in glued laminated timber (GLT), laminated veneer lumber (LVL) was used for the outrigger and belt trusses to resist the tension forces due to the lateral wind load. To resist these tension forces, the connections in the outrigger and belt truss were designed and engineered with two slotted-in steel plates and dowels. Beam-to-column and beam-to-wall connections were carried out with one slotted-in steel plate and dowels. The column splice connections were carried out with glued-in rods, steel plates and bolts. Furthermore, the connection details were designed to be repeatable over all the storey levels.

For the dowel-type connections, pre-drilling of the holes will be done in the factory, and the openings in the beams for the slotted-in steel plates will be sawn during the manufacturing process. The end plates in the column splice connection will be connected to the column with glued-in rods, which are glued with epoxy to the columns in the factory under controlled climate conditions. It is important that the glueing process occurs under controlled condition so that connection strength can be guaranteed. The connection of the column end plates with the bolts can be done on site. For the belt-truss connection, horizontal holes in the columns will be pre-drilled. The bolts will be placed through these holes on site, and the bolts will connect the belt-truss brace to the column.

Vertical differential shortening occurs between the timber frame and the reinforce concrete

walls. To compensate for this, adjustment devices at the column splice connections were installed, and a steel plate with the required adjustment thickness can be placed between the bolted steel plates of the column splice connection. Alternatively, the differential shortening could be taken into account by adjusting the length of the columns in the factory.

The uplift forces at the base of the structure were checked. Tension forces could occur in the foundation piles for light-weight structures due to the lateral wind loading. For the designed case, a maximum uplift force of 590 kN for the governing load combination occurred in the foundation piles, and the longitudinal reinforcement in the pile should be able to resist these tension forces.

The structure was checked for accidental loading, and in the case of a column failure a second load path was possible. During such an event, the structure would start to hang onto the stiff outrigger level. Most of the tension force would be transferred through the columns to the outrigger level and, to a lesser extent, through the beams. Deflections in the beam and floor slab would increase a lot and the maximum deflection due to column failure was computed to be equal to 27 mm. However, the serviceability criterion for the deflections can be neglected for the accidental load combinations. The connection in the timber frame were checked for the accidental load combination and were able to resist the occurring forces.

Protective cladding around the timber structural components and connections was designed to withstand 120 minutes of fire loading. During 120 minutes of intense fire, the cladding would eventually fall off and the timber would char to a depth computed to be equal to 34 mm. Therefore, all the steel plates, connectors and dowels were placed at a minimum distance of 40 mm from the outer surface of the timber beam element. For the timber columns, the plate thickness of the protective cladding can be less due to its larger cross-sectional dimensions.

A more conventional all-concrete tall building with a similar program of requirements was designed in order to compare the results to the hybrid wood-concrete tall building. The all-concrete structure was designed with the same grid and floor plan layout, and outrigger/belt-truss system for the lateral stability. The design of the core walls was kept identical, and the timber frame was replaced by a moment-resistant reinforced concrete frame. The tuned mass damper system and shape optimization were disregarded for this design. The serviceability criteria for lateral inter-storey drift and displacement were easier to satisfy, and as a consequence the cross-sectional dimensions of the concrete beams and columns were reduced. Another alternative would be to remove the interior column row. This second column row proved only to be necessary for the mass timber frame in order to reduce the dimensions of the columns at the lower storey levels.

Overall, the mass for the concrete structure was larger than for the hybrid wood-concrete structure, which resulted in a better dynamic behaviour. However, the global damping ratio of the concrete structure was lower, which negatively influences the wind-induced behaviour. In addition, the damping ratio for the hybrid wood-concrete structure was taken a bit conservative, and in the case a higher damping ratio was applied the wind-induced accelerations would be reduced.

8.2. Design choices and limitations

This research determined that a slender and tall hybrid wood-concrete building can satisfy the serviceability criteria for lateral displacements and accelerations. However, the serviceability criterion for the peak response acceleration could only be satisfied if both a tuned mass damper system and shape optimization were applied to the structure. Shape optimization was an effective measure to improve the wind-induced behaviour of the structure and could even lead to a design without need for additional damping devices. However, during this research the shape optimization was applied at the end of the design process, making only small shape modifications possible. For the super tall timber building proposals such as Oakwood tower and the W350 building, the shape has not yet been optimized. If the dy-

namic behaviour of these buildings were checked, a shape optimization would probably be necessary to reduce the dynamic wind load in across-wind direction.

The global damping ratio of the structure was difficult to estimate. Normally, the structural damping is estimated based on measurements on similar existing structures. However, only a handful of measurements on tall hybrid wood-concrete buildings have been taken place up to now. The research of Feldmann et al. (2016) showed an average structural damping ratio of 2.0% for tall timber structures up to 100m. In this study, the structural damping of the 300m hybrid wood-concrete tall building was estimated as 1.43%, based on measurements on timber bridges found in NEN-EN1991-1-4. However, a timber bridge has almost no sub-structure and less connections, which contribute to global damping. Therefore, the structural damping ratio of 1.43% may be a bit conservative and the necessity for a TMD and/or shape modification may have been overestimated as a result.

A passive TMD with a mass ratio of 0.01 was applied at the top of the structure. The damper mass could be reduced by using an active mass damper (AMD). An external force sets the frequency of the AMD, and the efficiency of the damper system is not dependent on the mass ratio. The disadvantage of an AMD is the required power supply. In the case of a hazard event the power supply can fail, and the damper system will not be tuned anymore. A solution for this problem could be the application of a hybrid mass damper, which is a combination of an AMD and a passive TMD. The damper system has a fail-safe and can still behave as a passive TMD if the actuator does not work (Chu et al., 2005).

For the designed structure, corner modifications were only researched as part of the shape optimization since they have no major implication for the floor plan design. In addition, Li et al. (2018) have done research on the effect of corner modifications on tall buildings and have been studied in the wind tunnel test. The vertical shape modifications have a larger impact on the architectural design and should be implemented at an early design stage. The effect of the vertical shape modification on the dynamic wind load is difficult to estimate with an analytical model as the building shape varies for each project. Therefore, the vertical shape optimization should be studied in the wind tunnel test or with a computational fluid dynamic (CFD) simulation.

The tall hybrid building was designed to satisfy the serviceability criteria for lateral inter-storey drift and displacement. The lateral displacement limit of $H/500$ was followed strictly. However, by using a more flexible lateral displacement limit, the cross-sectional dimensions of the structural components could be reduced, leading to a more economical design. For example, the 432 Park Avenue building in New York has a more flexible stiffness criterion of $H/275$, which allows the building to move 1.5m at the top (Snoek, 2016). The focus in the research has been on the structural feasibility and less on the functionality. The lateral displacement criterion of $H/500$ led to a stiff structure with large cross-sectional dimensions of the structural components. A more flexible stiffness criterion would enable an increase in the net floor area, improving the functionality of the office building. The reduction in stiffness would also lower the natural frequency, which can have a positive influence on the wind-induced dynamic behaviour of the structure. If a more flexible stiffness criterion was followed, the peak response acceleration could be optimized further in the design. In contrast, the serviceability criterion for peak acceleration should be followed more strictly because it can cause discomfort and nausea to occupants.

9

Conclusion

In this chapter, the main research question will be answered and this is done by answering the sub-questions of the research first. A summary is given, after which the important design issues and results will be described. Subsequently, the main conclusions are drawn.

In this thesis, the technical feasibility of a super tall hybrid wood-concrete building was evaluated and its wind-induced dynamic behaviour was improved. To this end a 300m tall hybrid building of timber and concrete was designed for construction in the city-centre of Rotterdam, The Netherlands. The designed hybrid wood-concrete structure provided guidance and support to the feasibility study, the research of the connection design, and the optimization of the wind-induced dynamic behaviour.

The design and research showed that important design issues such as the lateral stability design, fire safety design, uplift forces, vertical differential shortening, manufacturability, alternative load path design, connection design, and the wind-induced dynamic behaviour should be addressed for a hybrid wood-concrete tall building. Hence, these design aspects were all addressed, with a focus on the connection design and the wind-induced dynamic behaviour.

For the case study, the structural design was optimized to satisfy the serviceability criteria for lateral drift and occupant comfort. For the lateral stability design of a super tall hybrid wood-concrete building an outrigger/belt-truss was an adequate and efficient lateral stability system. A significant increase of the global stiffness in the structure was accomplished. Further stiffness optimization of the structure was carried out in order to satisfy the serviceability criteria for lateral inter-storey drift and displacement. Therefore, a parametric study of the cross-sectional dimension of the columns, the reinforced concrete core wall thickness, and the outrigger/belt-truss layout was performed.

The cross-sectional dimension of the columns and the core wall thickness were tapered down over the height of the structure. Furthermore, an orthogonally-oriented layout of the outrigger trusses was applied, which provided more lateral stiffness than the diagonally-oriented layout. Each outrigger level consists of 8 outrigger trusses with a belt-truss surrounding the perimeter of the structure. For the final design, the outrigger system was applied on three levels along the height of the structure. The outrigger levels were also designed to accommodate the mechanical, electrical and public health system (MEP) facilities.

The connection design of the mass timber frame was paramount for the feasibility of a hybrid wood-concrete tall building due to the large tension forces caused by the lateral wind loading. The outrigger trusses transfer large tension and compression forces to the perimeter columns, and to resist these tension forces, the connections in the outrigger and belt truss were designed and engineered with two slotted-in steel plates and dowels. Column splice connections were carried out with glued-in rods, steel plates and bolts. The connections

were designed to be repeatable over the height of the structure. The GLT columns were designed to be continuous over 4-storey levels, and the maximum length of the columns was determined by transportation limits.

Analysis of the designed tall and slender hybrid wood-concrete structure indicated that the serviceability criteria for lateral displacements and accelerations can be satisfied. However, the 300m tall hybrid wood-concrete building required shape optimization and a tuned mass damper to avoid peak acceleration levels exceeding the occupant comfort criterion. The peak acceleration due to vortex shedding was critical for this design, and made optimization of the wind-induced dynamic behaviour necessary.

In order to benchmark the hybrid wood-concrete tall building, an equivalent all-concrete building was designed. The all-concrete building included the same grid, floor plan layout, and outrigger/belt-truss system for lateral stability. The higher strength and stiffness of reinforced concrete enabled the use of smaller cross-sections for the beams and columns. In addition, the all-concrete structure did not require an interior column row, resulting in more net floor space. Therefore, obtaining sufficient net floor space for a functional design was more challenging for the wood-concrete hybrid building. Finally, the higher mass of the concrete structure resulted in superior wind-induced dynamic behaviour than the hybrid wood-concrete structure.

The design process for a super tall hybrid wood-concrete building was complex due to the absence of prior designs of super tall buildings using mass timber. Therefore, a more extensive optimization of the structure's wind-induced behaviour was required, potentially requiring higher design expenses. In the future, standardized design practices based on experience could result in a simplification of the process. In addition, normalization of hybrid wood-concrete buildings could lead to cheaper standardized production of structural components, such as the large cross-sectional timber dimensions and steel-timber connections. The combination of simplification of the design process and standardisation of structural components could increase the economic viability of future super tall hybrid wood-concrete buildings.

In this case study, a design strategy was established in response to the current trend towards mass timber tall buildings. The popularity of mass timber is due to its low environmental impact, to its interesting architectural features, and to the reduction of construction time. However, the low mass and high flexibility of timber pose novel limitations on serviceability requirements of the building. Therefore, in addition to defining a basic structural design, this strategy addressed specific challenges associated with the use of mass timber. In particular the wind-induced displacements and accelerations, the connection detailing, and fire safety measures were addressed. While this case study resulted in a design for a specific super tall wood-concrete building, the established design process could be applied as a roadmap for similar designs in the future.

10

Recommendations

An outrigger/belt-truss system has been applied for the lateral stability design. However, the parametric study of the mega bracing showed that a diagonal braced tube-in-tube system could also reduce lateral displacements for a 300m tall building. For further research, the hybrid wood-concrete super tall building could be designed as a diagonal braced tube-in-tube system. This possibly may also lead to a feasible structural design that satisfies the serviceability criteria for lateral displacements and accelerations.

A recessed corner modification could also be an effective measure to reduce the dynamic wind load. Recessed corner modifications are commonly applied in current tall building design and is even a bit more efficient in reducing the across-wind force than the chamfered corner modification (Li et al., 2018). The choice between a chamfered or recessed corner modification can also be based on the preference from the architect. Furthermore, vertical shape modifications could also be applied. These vertical shape modifications should be included in an early design phase because these can cause significant changes to the design.

The decision has been made to apply a reinforced concrete core for lateral stability, making the design a hybrid wood-concrete building instead of an all-timber building. It might be interesting to research an all-timber super tall building, which could lead to a more sustainable structural design. For example, this could be achieved by using cross-laminated timber (CLT) shear walls. However, it is expected that a slenderness ratio of 1:10 will be difficult to achieve. The all-timber building will be even more light-weight and more vulnerable to the wind-induced accelerations. Another issue is the realisation of moment-resistant connection of the CLT core walls in which large bending moments will occur. The slenderness should probably be reduced, and a more flexible stiffness criterion should be followed for the design of an all-timber super tall building.

In this research, the focus has been on the technical feasibility of a hybrid wood-concrete super tall building. The economic feasibility has not been assessed. A cost comparison with a conventional tall building would be a point of interest. A structural design will be chosen for its efficiency and economical point of view most of the times. The sustainability of the structure can also be a decisive factor nowadays. The carbon footprint of a hybrid wood-concrete building can be compared with the carbon footprint of a similar all-concrete building. More material is needed for the hybrid wood-concrete building, and it will be interesting to see if the carbon footprint is indeed lower than for the traditional concrete tall building.

Bibliography

R.B. Abrahamsen and K.A. Malo. Structural design and assembly of treet: A 14-storey timber residential building in norway. *New Zealand Timber Design Journal Vol.22-3*, 2014.

S.M. Auta, A.M. Maslennikov, and K. Street. Dynamic analysis of tall building under pulsation wind excitation. 2006.

G. Barney. Vertical transportation in tall buildings. *Elevator World 51 (50)66-75*, 2003.

H.J. Blass. Facts you should know about timber engineering. *World conference on timber engineering WCTE*, 2010.

H.J. Blass, P. Aune, B.S. Choo, R. Gorlacher, D.R. Griffiths, B.O. Hilson, P. Racher, and G. Steck. *Timber Engineering STEP 1*. Centrum Hout, 1995.

B.J.H. Boellaard. Design of an outrigger structure for tall timber buildings. Master's thesis, Eindhoven University of Technology, 2012.

D. Boggs. Acceleration indexes for human comfort in tall buildings—peak or rms? *CTBUH*, 1995.

D. Boggs and J. Dragovich. The nature of wind loads and dynamic response. *ACI*, 2006.

A.M. Buchanan and R.H. Fairweather. Seismic design of glulam beams. *Bulletin of the New Zealand national society for earthquake engineering*, 1993.

C. Cheng, J. Wang, T. Lai, and M. Tsai. An acrosswind equivalent static wind load model for rectangular shaped tall buildings. *Journal of Wind Engineering and Industrial Aerodynamics (90) 1757-1770*, 2016.

A.K. Chopra. *Dynamics of structures: Theory and application to earthquake engineering.* Prentice-Hall, 1995.

S.Y. Chu, T.T. Soong, and A.M. Reinhorn. *Active, Hybrid, and Semi-active Structural Control: A design and implementation handbook.* John Wiley and Sons, LTD, 2005.

J.J. Connor. *Introduction to Structural Motion Control.* MIT-Prentice Hall series on civil, environmental, and systems engineering, 2002.

CSi-ETABS. Integrated analysis, design and drafting of building systems user guide. *Version 13 Berkeley, CA Computers and Structures, Inc.*, 2013.

CTBUH. *Tall Buildings in Numbers Tall Timber: A Global Audit*, 2018. `http://global.ctbuh.org/resources/papers/3350-TBIN.pdf` [Accessed: 14/08/2018].

Canadian Wood Council CWC. *Glulam sizes, CWC*, 2018. `http://cwc.ca/wood-products/glulam/sizes-available/` [Accessed: 27/06/2018].

J.P. Den Hartog. *Mechanical Vibrations.* New York: Dover Publication Inc., 1956.

J.X. Deng. *Strength of Epoxy Bonded Steel Connections in Glue Laminated Timber.* PhD thesis, University of Canterbury, 1997.

A.M.P.G. Dias. *Mechanical behaviour of timber-concrete joints.* PhD thesis, Delft University of Technology, 2005.

Municipality Dubai. Dubai wind code [3833]. 2013.

A. Feldmann, H. Huang, W. Chang, R. Harris, P. Dietsch, M. Gräfe, and C. Hein. Dynamic properties of tall timber structures under wind-induced vibration. *WCTE,* 2016.

A. Frangi. Workshop structural fire design of buildings according to the eurocodes. *ETH Zurich Institute of Structural Engineering*, 2012.

S. Gagnon and C. Pirvu. *CLT Handbook.* FPInnovations, Quebec, 2011.

J. Galsworthy, J. Kilpatrick, and D. Kelly. Form follows physics. *STRUCTURE magazine*, 2016.

E. Hallebrand and W. Jakobsson. Structural design of high-rise buildings. Master's thesis, Faculty of Engineering LTH, Lund University, 2016.

J.D. Holmes. *Wind Loading of Structures.* CRC Press, 2007.

A.W. Irwin. Wind issues in the design of tall buildings. *RWDI*, 2010.

International Organization for Standardization ISO. Bases for design of structures - serviceability of buildings and walkways against vibration. *ISO 10137:2007,* 2007.

A. Just, J. Schmid, and J. König. Gypsum plasterboards used as fire protection - analysis of a database. *SP Technical Research Institute of Sweden*, 2010.

O. Kalny. Etabs analysis reference manual. *CSi Knowledge Base*, 2017.

M. Kryh and M. Nilsson. Wind-induced vibrations of a multi-storey residential building in cross-laminated timber in the serviceability limit state. Master's thesis, Chalmers University of Technology, Goteborg, Sweden, 2012.

L.C. La Gasse. Structural reliability assesment of buildings subjected to wind loading. Master's thesis, Delft University of Technology, 2017.

Y. Li, X. Tian, K.F. Tee, Q.S. Li, and Y.G. Li. Aerodynamic treatments for reduction of wind loads on high-rise buildings. *Journal of Wind Engineering and Industrial Aerodynamics*, 2018.

S. Liang, S. Liu, Q. Li, L. Zhang, and M. Gu. Mathematical model of across-wind dynamic loads on rectangular tall buildings. *Journal of Wind Engineering and Industrial Aerodynamics 90 1757-1770*, 2002.

J. Mayo. *Solid Wood: Case Studies in Mass Timber Architecture, Technology and Design.* London: Routledge, 2015.

W.H. Melbourne and T.R. Palmer. Acceleration and comfort criteria for buildings undergoing complex motions. *Journal of Wind Engineering and Industrial Aerodynamics 41-44 (1992) 105-116 Elsevier*, 1992.

Nederlands Normalisatie instituut NEN-EN14080. *Timber structures - Glued laminated timber and glued solid timber - Requirements.* 2013.

Nederlands Normalisatie instituut NEN-EN1991. *Eurocode 1-4. Belastingen op constructies. Deel 1-4: algemene belastingen - Windbelasting. NEN-EN1991-1-4.* 2002.

Nederlands Normalisatie instituut NEN-EN1995. *Eurocode 5-1. Design of timber structures. NEN-EN1995-1-1.* 1995.

I. Nishimura, T. Kobori, M. Sakamoto, N. Koshika, K. Sasaki, and S. Ohrui. Active tuned mass damper. *Smart Materials and Structures, 1(4):306–311*, 1992.

G. van. Oosterhout. *Wind-induced Dynamic Behaviour of Tall Buildings.* PhD thesis, Delft University of Technology, 1996.

J. Ormondroyd and J.P. Den Hartog. The theory of the dynamic vibration absorber. *Transactions of the American Society of Mechanical Engineers, 50, pp. A9-A22*, 1928.

C. Petersen. *Dynamik der Baukonstruktionen.* Braunschweig / Wiesbaden, 2000.

A. Pilon, A. Utimati, and J. Jin. Design and preconstruction of a tall wood building - brock commons phase 1: Overview. *Naturally:wood*, 2016.

PLP-architecture. *Oakwood Timber Tower London, UK*, 2017. `http://www.plparchitecture.com/oakwood-timber-tower.html` [Accessed: 30/11/2017].

D. Poon, S. Shieh, L. Joseph, and C. Chang. Structural design of tapei-101, the world's tallest building. *CTBUH*, 2014.

H.G. Poulos. *Tall building foundations: design methods and applications.* Springer International Publishing, 2016.

Rethink-Wood. *Wood a natural choice*, 2018. `https://www.thinkwood.com/` [Accessed: 05/02/2018].

H. Riberholt. Glued bolts in glulam. *Report no. 10, Department of Structural Engineering, Technical University Denmark*, 1986.

M. Sarkisian. *Designing Tall Buildings: Structure as Architecture.* New York Routledge, 2016.

A. Sev and A. Özgen. Space efficiency in high-rise office buildings. *METU Journal of the Faculty of Architecture 26(2)*, 2009.

T.G. Sitharam. Advanced foundation engineering. *Indian Institute of Science, Bangalore*, 2013.

B.S. Smith and A. Coull. *Tall Building Structures: Analysis and Design.* USA Wiley-Interscience publication, 1991.

I. Smith and A. Frangi. Overview of design issues for tall timber buildings. *Structural Engineering International*, 2008.

R. Snoek. Grenzen in slankheid verlegd. *Cement*, 2016.

Skidmore Owings Merill SOM. Timber tower research projects. *SOM Timber tower system report 1*, 2014.

C.C.B. Stathopoulos. Wind effects on buildings and structures. *Nature*, 2007.

Forestry Sumitomo. New development concept w350 plan for wooden high-rise building. *Sumitomo Forestry Co. Ltd*, 2018.

X. Sun, H. Liu, N. Su, and Y. Wu. Investigation on wind tunnel tests of the kilometer skyscraper. *Engineering Structures, Vol 148*, 2017.

Y. Tamura and A. Kareem. *Advanced Structural Wind Engineering.* Springer, 2013.

B.S. Taranath. *Reinforced Concrete Design of Tall Buildings.* CRC Press, 2010.

S. Thelandersson and H.J. Larsen. *Timber Engineering.* John Wiley and Sons, LTD, 2003.

J.P. Van der Windt. De constructeur in het hoogbouwontwerpproces: Een factor van betekenis. *Cement*, 2006.

J. Vessby. *Experimental study of cross-laminated timber wall panels.* PhD thesis, Växjö University, 2010.

J. Wong, A. Sommer, K. Briggs, and C. Ergin. Effective stiffness for modeling reinforced concrete. *Structure*, 2017.

A
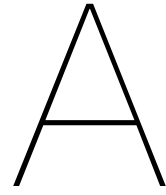
Annex A - Structural design

A.1. Elevation drawings
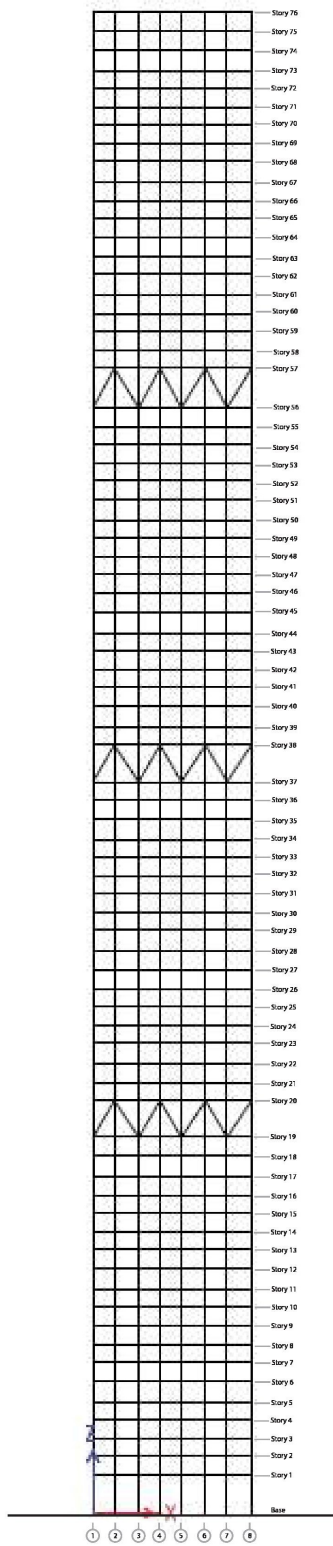
Figure A.1: Elevation view 1
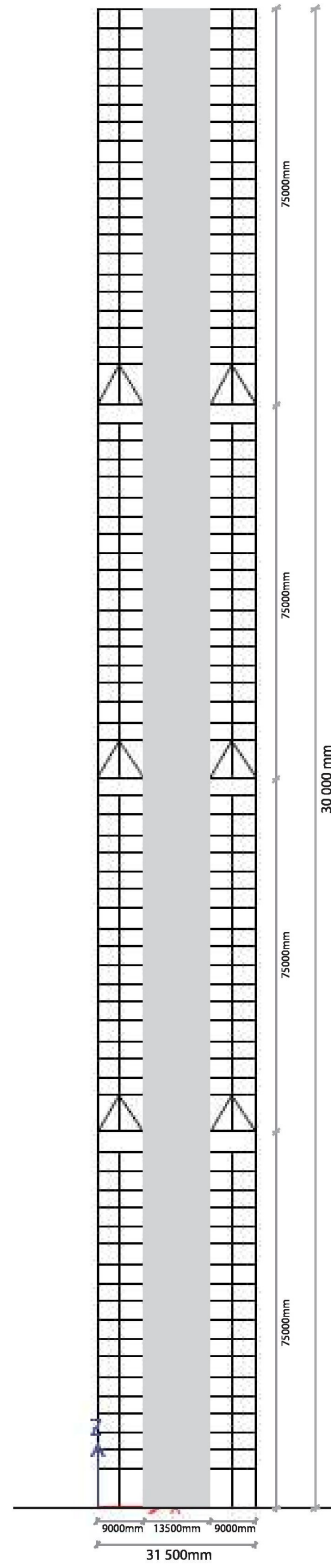
Figure A.2: Section view 3

A.2. Floor plan
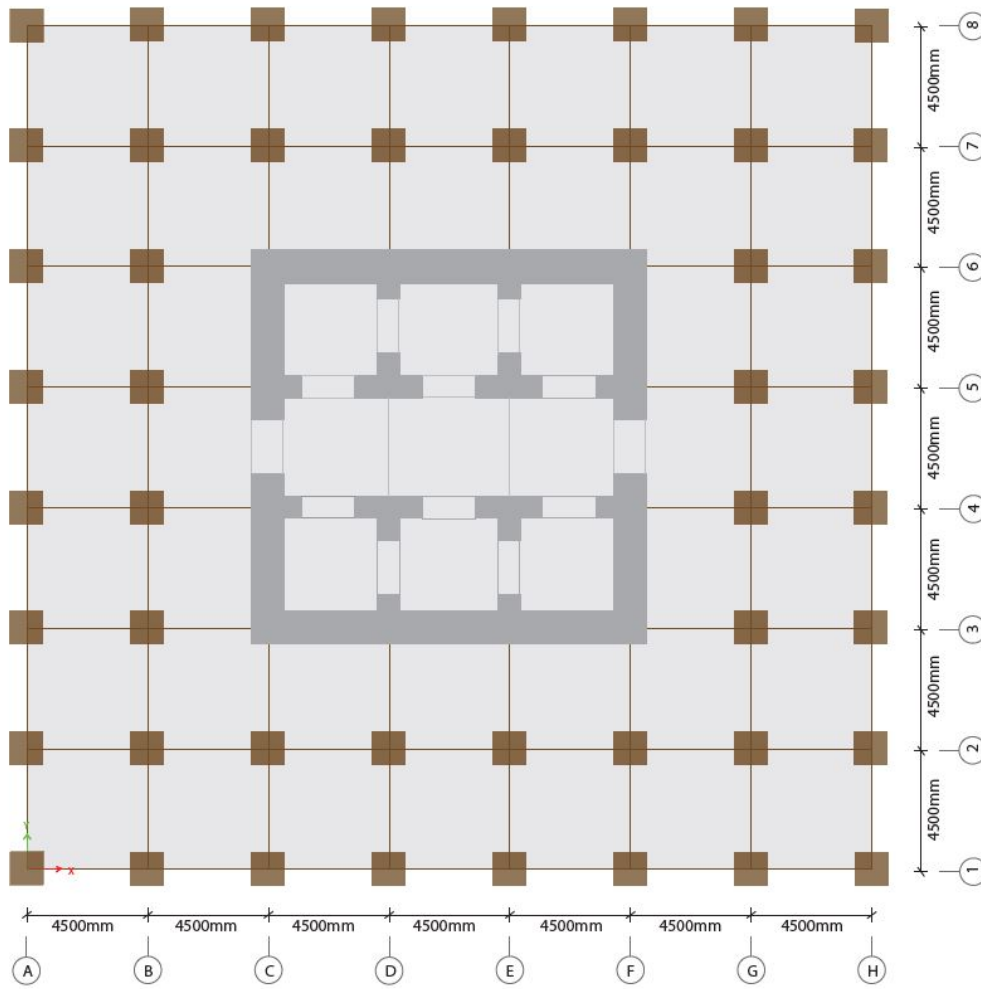
Figure A.3: Floor plan of Storey level 2-19
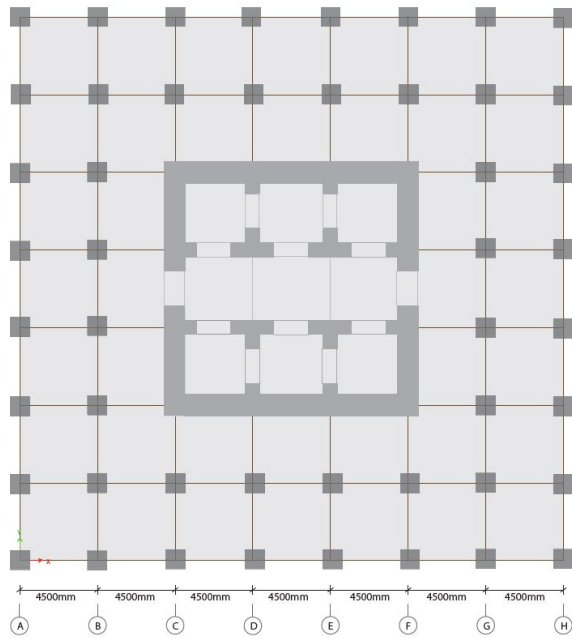
Figure A.4: Plan view of Storey level 1 - Entrance
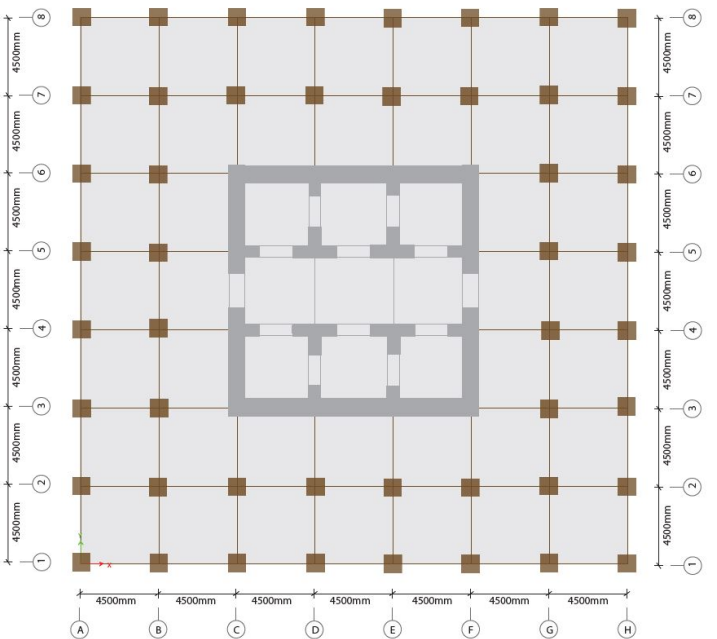
Figure A.5: Plan view of Storey level 20-37
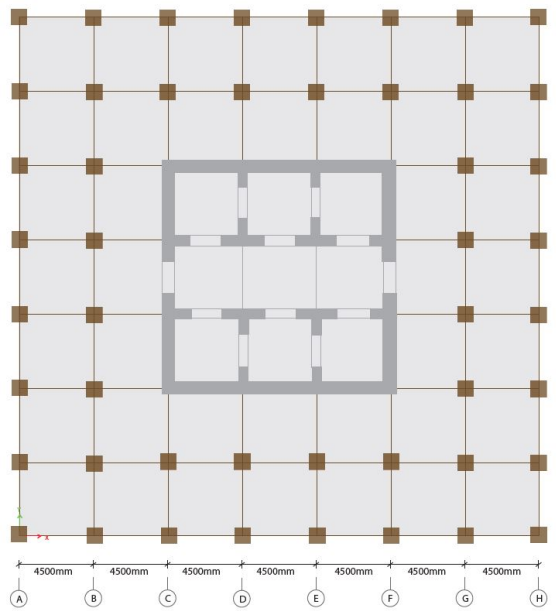
Figure A.6: Plan view of Storey level 38-56
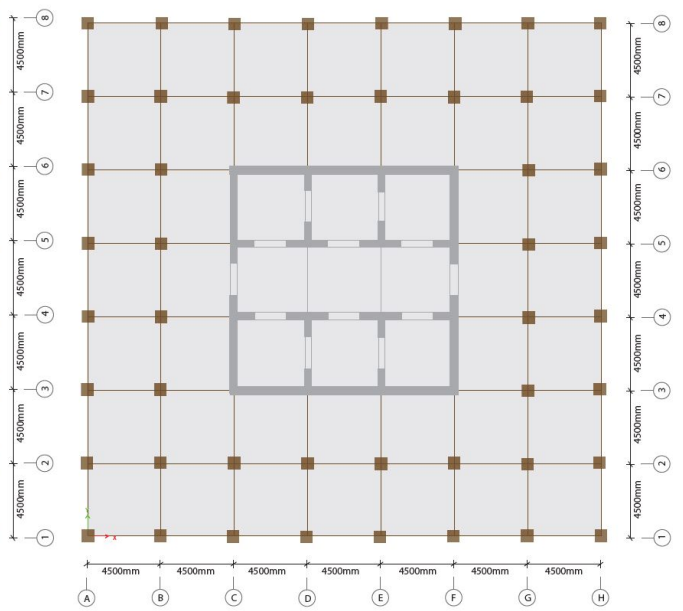
Figure A.7: Plan view of Storey level 57-76

A.3. Three-dimensional view

Figure A.8: 3D-view
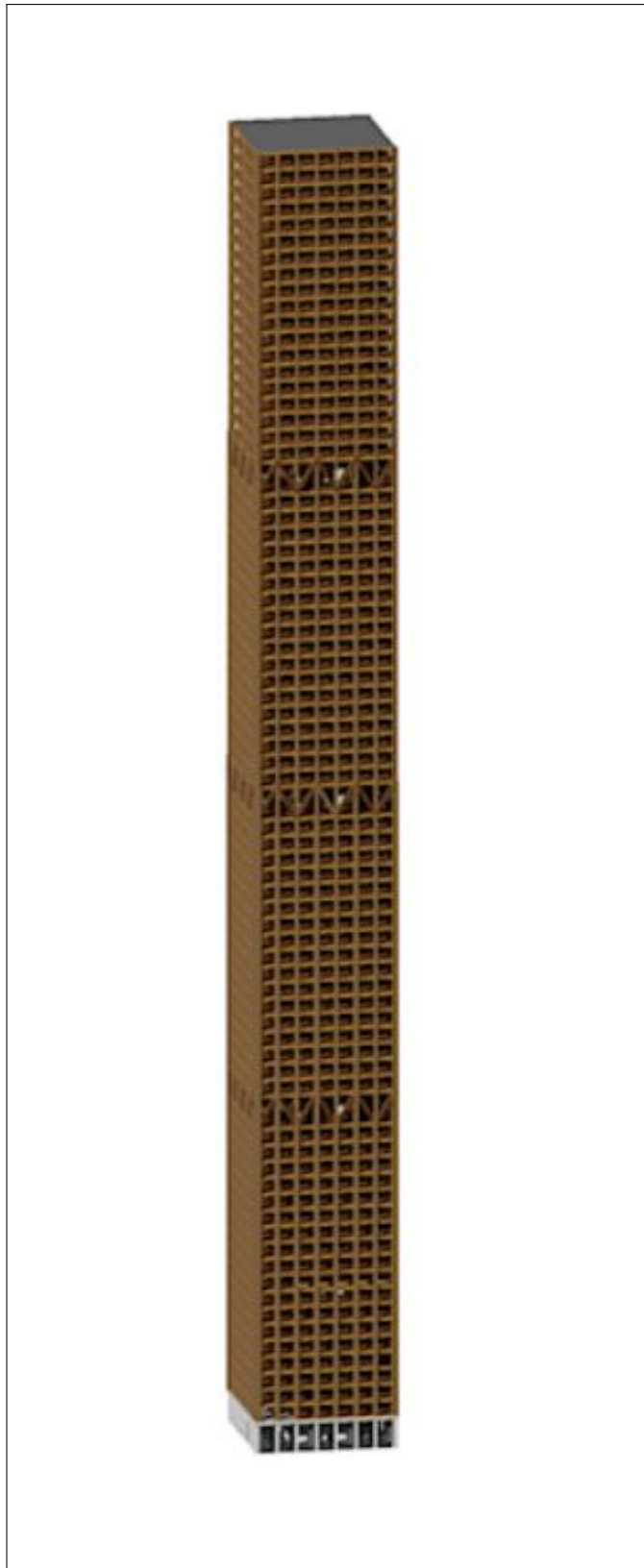
A.3. Three-dimensional view
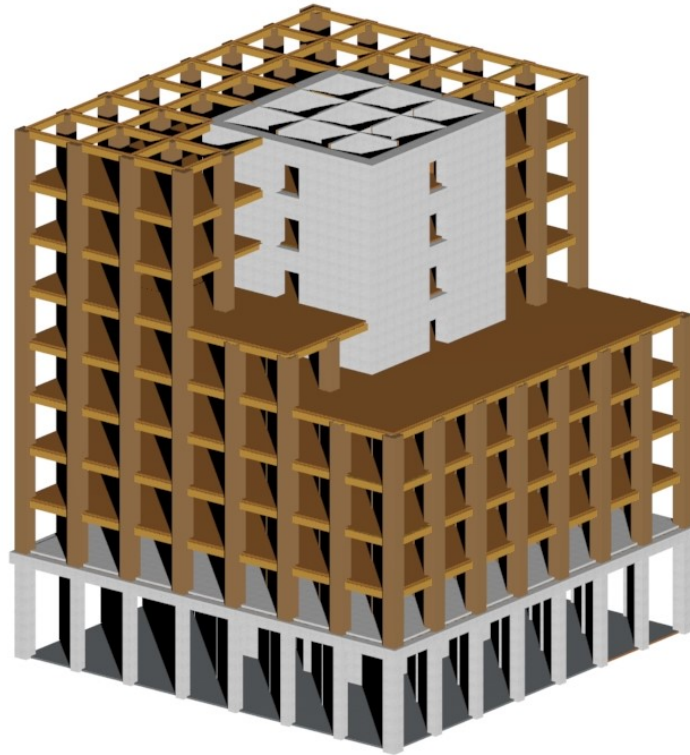
Figure A.9: Open cut 3D-view
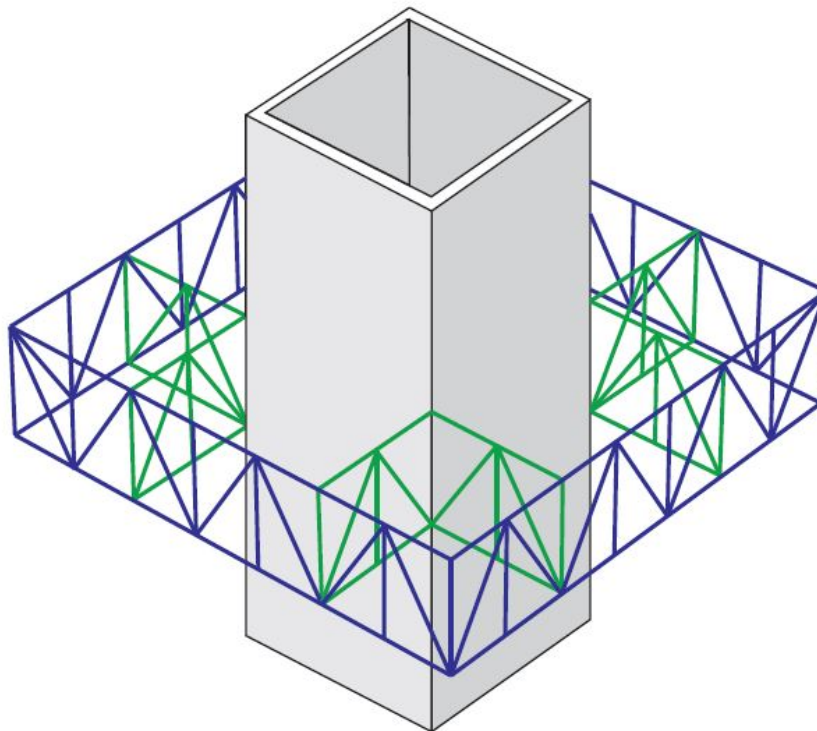
Figure A.10: Schematic view of outrigger/belt-truss level
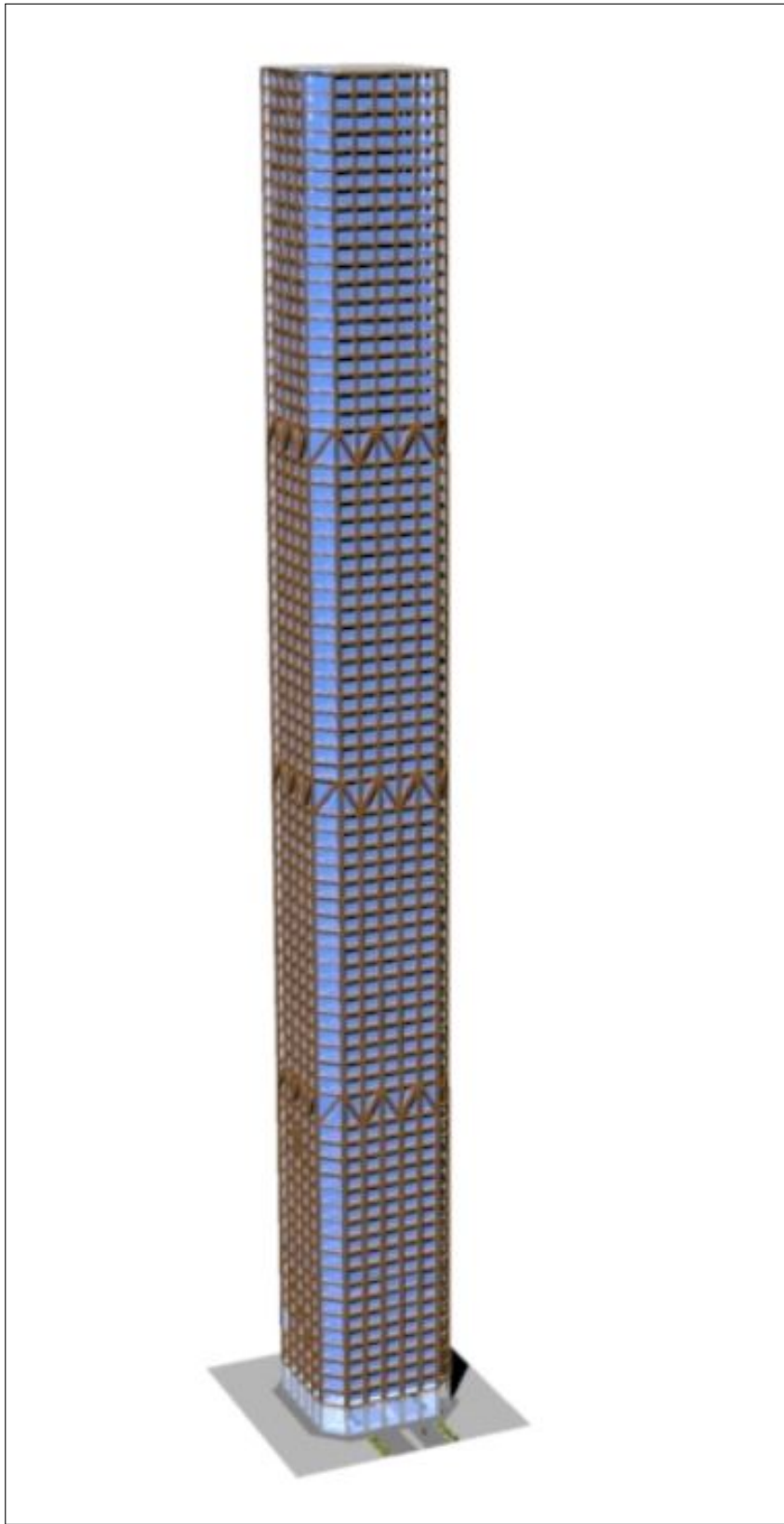
Figure A.11: 3D view of structure with chamfered corner modification

A.4. Connection details
A.4.1. Column-to-beam detail

Column GL32H (1000mm x1000mm)

Concrete screed top layer

CLT floor panel (2250mm x 4500mm)

Beam GL32H 500mm x 300mm

Slotted steel plate S355 t= 10mm

Dowels Ø16mm (7x)

Screws LBS, d1=7mm, l=70mm (24x)
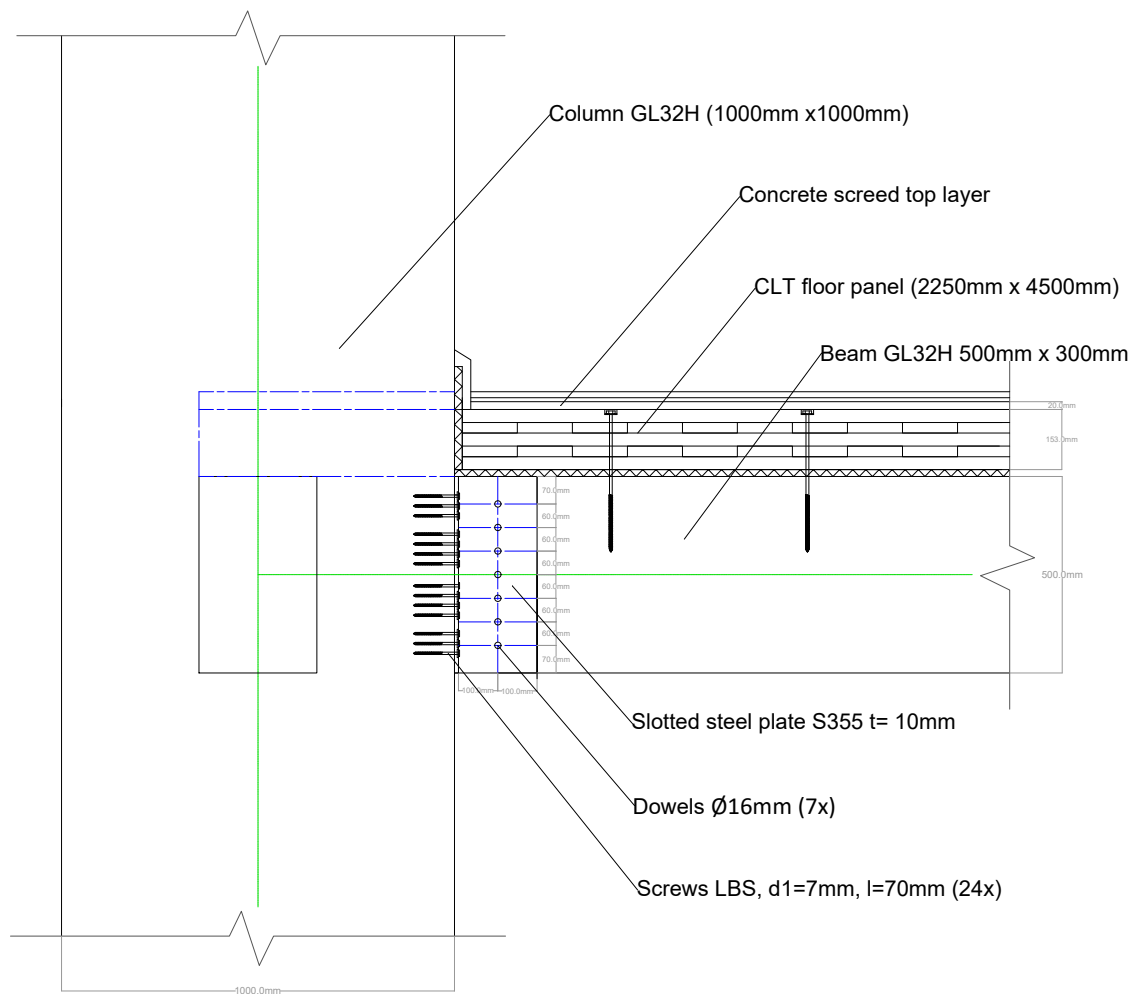
A.4.2. Column-to-column detail

Column GL32H (1000mm x1000mm)

Steel plate S355 t=30mm

Resin adjustment layer t=4mm

Bolts M24 8.8 (12x)

Glued-in rods Ø56-800 mm (4x)

Opening for epoxy

A.4.3. Outrigger truss detail A

Diagonal LVL 80mm x 800mm

Dowels Ø24mm (38x)

Dowels Ø24mm (30x)

Beam LVL 800mm x 800mm

Dowels Ø24mm (20x)

Slotted steel plate (2x) t=25mm

Column GL32H 1000mm x 1000mm
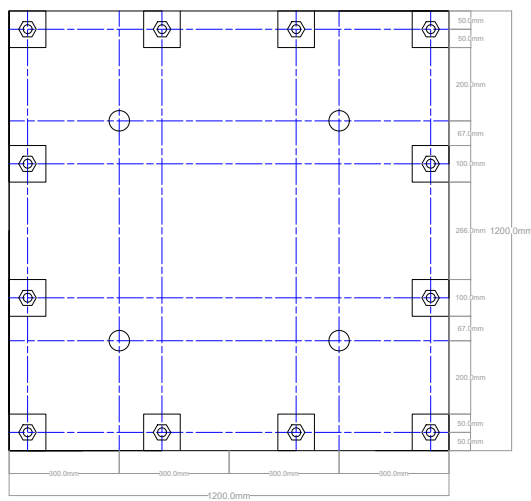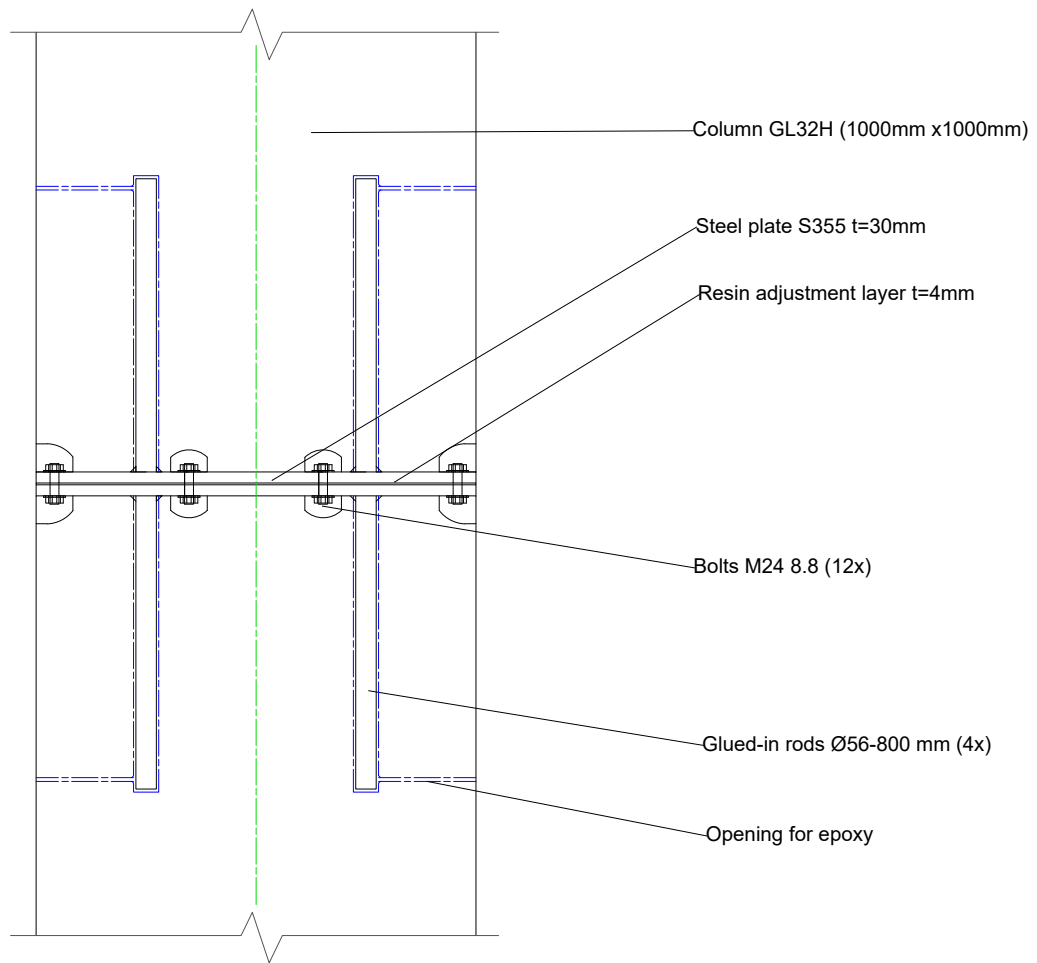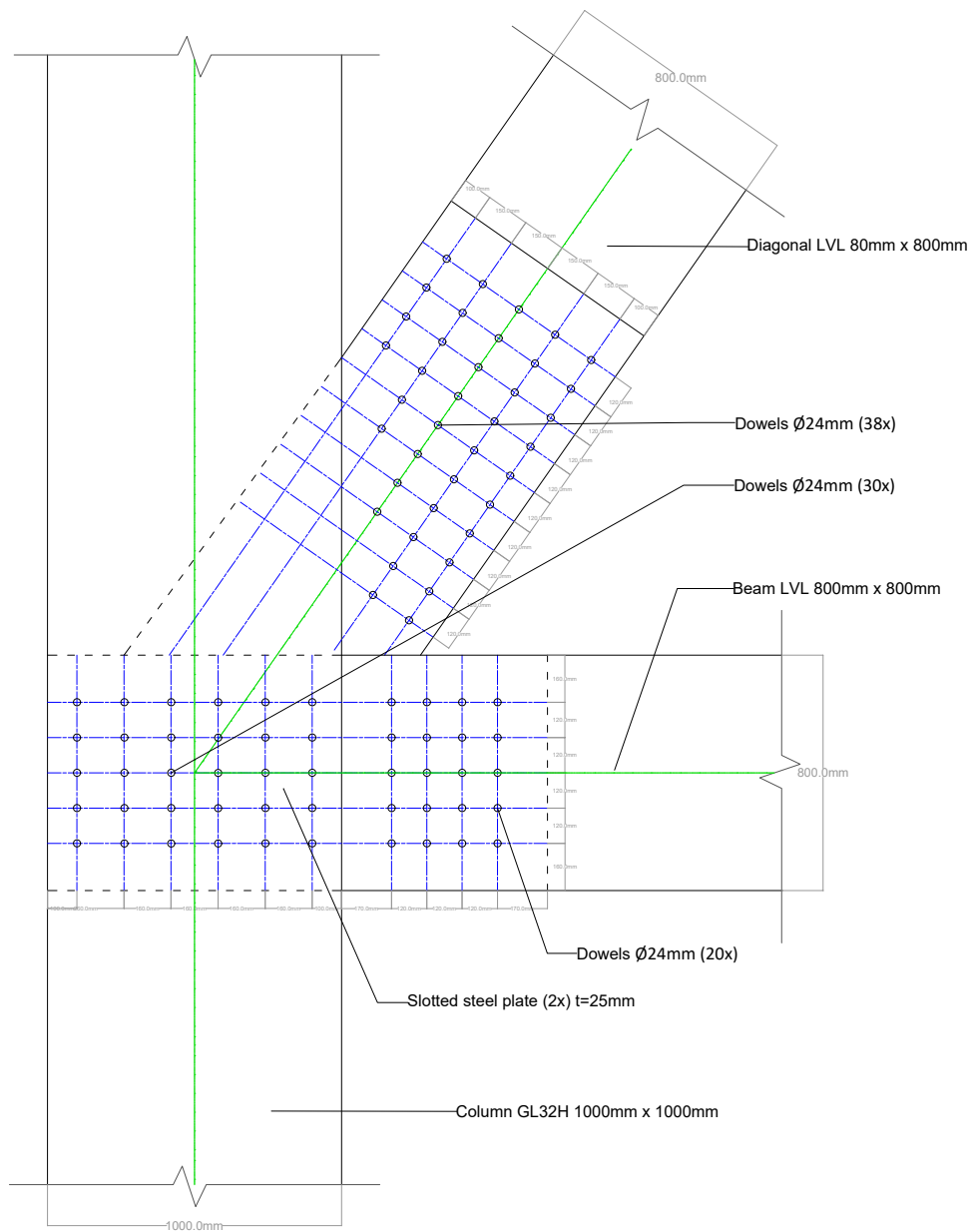
A.4.4. Outrigger truss detail B

A.4.5. Belt-truss detail

Steel plate S460 t=30mm

Bolts M24 10.9 (10x)

Dowels Ø24mm (28x)

Slotted steel plates (2x) t=25mm

Diagonal LVL 800x800mm

1540,0mm

800,0mm

1540,0mm

Steel block S235 1200x150x70mm

Steel plate S460 t=30 mm

Column GL32H 1200x1200mm

A.4.6. Beam-to-concrete wall detail

Concrete screed top layer

CLT floor panel (2250x4500x153mm)

Beam GL32H 500mm x 300mm

Steel anchor plate S355 t=25mm

Headed studs Ø22mm

Slotted steel plate S355 t= 10mm

Dowels Ø16mm (7x)

A.5. Overview Structural elements

Table A.1: Overview of structural components for hybrid timber-concrete design

Design assemblies and connections	Material type	Dimensions
Roof	CLT-Beech	thickness 170mm
Floor	CLT-Beech	thickness 153mm
Beams at perimeter		
Story 2 till 19	Glulam32h	500mm x 300mm
Story 20 till 37	Glulam32h	500mm x 300mm
Story 38 till 56	Glulam32h	500mm x 300mm
Story 57 till 76	Glulam32h	500mm x 300mm
Interior beams		
Story 2 till 19	Glulam32h	500mm x 300mm
Story 20 till 37	Glulam32h	500mm x 300mm
Story 38 till 56	Glulam32h	500mm x 300mm
Story 57 till 76	Glulam32h	500mm x 300mm
Columns		
Story 2 till 19	Glulam32h	1200mm x 1200mm
Story 20 till 37	Glulam32h	1100mm x 1100mm
Story 38 till 56	Glulam32h	900m x 900mm
Story 57 till 76	Glulam32h	750m x 750mm
Outrigger beams		
Story 19	Glulam32h	800mm x 800mm
Story 37	Glulam32h	800mm x 800mm
Story 57	Glulam32h	800mm x 800mm
Outrigger interior columns		
Story 19	LVL-Kerto-S	800mm x 800mm
Story 37	LVL-Kerto-S	800mm x 800mm
Story 57	LVL-Kerto-S	800mm x 800mm
Outrigger braces		
Story 19	LVL-Kerto-S	800mm x 800mm
Story 37	LVL-Kerto-S	800mm x 800mm
Story 57	LVL-Kerto-S	800mm x 800mm
Belt truss braces		
Story 19	LVL-Kerto-S	800mm x 800mm
Story 37	LVL-Kerto-S	800mm x 800mm
Story 57	LVL-Kerto-S	800mm x 800mm
Core exterior walls		
Story 1 till 19	C55/67	thickness 1200mm
Story 20 till 37	C55/67	thickness 1000mm
Story 38 till 56	C50/60	thickness 800mm
Story 57 till 76	C45/55	thickness 500mm
Core interior walls		
Story 1 till 19	C55/67	thickness 800mm
Story 20 till 37	C55/67	thickness 700mm
Story 38 till 56	C50/60	thickness 600mm
Story 57 till 76	C45/55	thickness 500mm
Link beams at exterior core wall		
Story 1 till 19	C55/67	1200mm x 1500mm
Story 20 till 37	C55/67	1000mm x 1500mm
Story 38 till 56	C50/60	800mm x 1500mm
Story 57 till 76	C45/55	500mm x 1500mm
Link beams at interior core wall		
Story 1 till 19	C55/67	800mm x 1500mm
Story 20 till 37	C55/67	700mm x 1500mm
Story 38 till 56	C50/60	600mm x 1500mm
Story 57 till 76	C45/55	500mm x 1500mm
Concrete beams		
Entrance level	C55/67	300mm x 500mm
Concrete columns		
Entrance level	C55/67	1000mm x 1000mm

Table A.2: Overview of structural components for conventional concrete design

Design assemblies and connections	Material type	Dimensions
Roof	Hollow core slab	thickness 160mm
Floor	Hollow core slab	thickness 130mm
Beams		
Story 1 till 19	C45/55	500mm x 300mm
Story 20 till 37	C45/55	500mm x 300mm
Story 38 till 56	C45/55	500mm x 300mm
Story 57 till 76	C45/55	500mm x 300mm
Columns		
Story 1 till 19	C55/67	1000mm x 1000mm
Story 20 till 37	C55/67	800mm x 800mm
Story 38 till 56	C50/60	700mm x 700mm
Story 57 till 76	C45/55	500mm x 500mm
Outrigger beams		
Story 19	C55/67	700mm x 400mm
Story 37	C55/67	700mm x 400mm
Story 57	C55/67	700mm x 400mm
Outrigger interior columns		
Story 19	C55/67	700mm x 400mm
Story 37	C55/67	700mm x 400mm
Story 57	C55/67	700mm x 400mm
Outrigger braces		
Story 19	C55/67	700mm x 400mm
Story 37	C55/67	700mm x 400mm
Story 57	C55/67	700mm x 400mm
Belt truss braces		
Story 19	C55/67	700mm x 400mm
Story 37	C55/67	700mm x 400mm
Story 57	C55/67	700mm x 400mm
Core exterior walls		
Story 1 till 19	C55/67	thickness 1200mm
Story 20 till 37	C55/67	thickness 1000mm
Story 38 till 56	C50/60	thickness 800mm
Story 57 till 76	C45/55	thickness 500mm
Core interior walls		
Story 1 till 19	C55/67	thickness 800mm
Story 20 till 37	C55/67	thickness 700mm
Story 38 till 56	C50/60	thickness 600mm
Story 57 till 76	C45/55	thickness 500mm
Link beams at exterior core wall		
Story 1 till 19	C55/67	1200mm x 1500mm
Story 20 till 37	C55/67	1000mm x 1500mm
Story 38 till 56	C50/60	800mm x 1500mm
Story 57 till 76	C45/55	500mm x 1500mm
Link beams at interior core wall		
Story 1 till 19	C55/67	800mm x 1500mm
Story 20 till 37	C55/67	700mm x 1500mm
Story 38 till 56	C50/60	600mm x 1500mm
Story 57 till 76	C45/55	500mm x 1500mm
Concrete beam		
Entrance level	C55/67	300mm x 500mm
Concrete column		
Entrance level	C55/67	1000mm x 1000mm

B

Annex B - Design and Verification

B.1. Verification timber frame

The glued-laminated structural members will be verified according to the EC5 and the NEN-EN14080. The design strength of a structural timber element can be calculated as follows:

$$R_d = \frac{k_{mod} \cdot R_k}{\gamma_M} \tag{B.1}$$

Where, k_{mod}, is the modification factor which takes into account the service class and the duration of the load. The stresses perpendicular to the grain should be avoided in the design.

In the serviceability limit state the timber elements have different time-dependent properties. The moisture content and the load-duration will influence the deformation, and should be taken into account to calculate the final deformation of the timber element. The final mean value of modulus of elasticity, the final shear modulus, and the final slip modulus are time-dependent properties which can be calculated with Eq.(B.2), Eq.(B.3), and Eq.(B.4), respectively. The timber used in for the designed structure will lay inside the perimeter of the building and is protected by the facade elements, and therefore a service class 1 will be used for the timber design.

$$E_{mean,fin} = \frac{E_{mean}}{(1 + k_{def})} \tag{B.2}$$

$$G_{mean,fin} = \frac{G_{mean}}{(1 + k_{def})} \tag{B.3}$$

$$K_{ser,fin} = \frac{K_{ser}}{(1 + k_{def})} \tag{B.4}$$

The deformation factor, k_{def}, takes into account the service class of the structure. For service class 1 the moisture content in the timber is corresponding to a temperature of 20 degrees Celsius, and the relative humidity of the surrounding air is most of the time below 65 percent. For service class 2 the moisture content in the timber is corresponding to a temperature of 20 degrees Celsius, and the relative humidity of the surrounding air is most of the time below 85 percent. Service class 3 is for outdoor applications, and should be used for moisture contents that are higher than in service class 2.

In this chapter first the ultimate limit design will be discussed, and secondly the serviceability limit design will be explained in more detail.

B.1.1. Tension parallel to the grain
For the tension force parallel to the grain the following expression should be satisfied:

$$\sigma_{t,0,d} \leq f_{t,0,d} \tag{B.5}$$

Where:

$\sigma_{t,0,d}$ is the design tensile stress along the grain
$f_{t,0,d}$ is the design tensile strength along the grain

For glued laminated timber sections with a width smaller than 600mm a factor k_h should be applied.

B.1.2. Compression parallel to the grain
For the compression force parallel to the grain the following expression should be satisfied:

$$\sigma_{c,0,d} \leq f_{c,0,d} \tag{B.6}$$

Where:

$\sigma_{c,0,d}$ is the design compressive stress along the grain
$f_{c,0,d}$ is the design compressive strength along the grain

The compression capacity is dependent on the wood crushing or buckling. The failure of the timber in compression will be gradual, and this is in contrast with the brittle failure of the timber in tension.

B.1.3. Bending
The bending capacity of the timber element should be checked as follows:

$$\frac{\sigma_{m,y,d}}{f_{m,y,d}} + k_m \frac{\sigma_{m,z,d}}{f_{m,z,d}} \leq 1 \tag{B.7}$$

$$\frac{\sigma_{m,z,d}}{f_{m,z,d}} + k_m \frac{\sigma_{m,y,d}}{f_{m,y,d}} \leq 1 \tag{B.8}$$

Where:

$\sigma_{m,y,d}$ and $\sigma_{m,z,d}$ are the design bending stresses about the principal axes
$f_{m,y,d}$ and $f_{m,z,d}$ are the design bending strengths

In the case bi-axial bending occurs a factor k_m should be applied. This factor accounts for inhomogeneity in the cross-section, and allows for the re-distribution of the stresses. For a rectangular glued laminated timber cross-section $k_m = 0.7$.

B.1.4. Shear
The shear stress is verified with the following expression:

$$\tau_d \leq f_{v,d} \tag{B.9}$$

Where:

τ_d the design shear stress
$f_{v,d}$ is the design shear strength for the actual condition

B.1.5. Combined bending and axial tension
For the combined bending and axial tension check the following expressions should be satisfied:

$$\frac{\sigma_{t,0,d}}{f_{t,0,d}} + k_m \frac{\sigma_{m,y,d}}{f_{m,y,d}} + \frac{\sigma_{m,z,d}}{f_{m,z,d}} \leq 1 \tag{B.10}$$

$$\frac{\sigma_{t,0,d}}{f_{t,0,d}} + \frac{\sigma_{m,y,d}}{f_{m,y,d}} + k_m \frac{\sigma_{m,z,d}}{f_{m,z,d}} \leq 1 \tag{B.11}$$

B.1.6. Combined bending and axial compression

For the combined bending an axial compression check the following expressions should be satisfied:

$$\left(\frac{\sigma_{c,0,d}}{f_{c,0,d}}\right)^2 + \frac{\sigma_{m,y,d}}{f_{m,y,d}} + k_m \frac{\sigma_{m,z,d}}{f_{m,z,d}} \leq 1 \tag{B.12}$$

$$\left(\frac{\sigma_{c,0,d}}{f_{c,0,d}}\right)^2 + k_m \frac{\sigma_{m,y,d}}{f_{m,y,d}} + \frac{\sigma_{m,z,d}}{f_{m,z,d}} \leq 1 \tag{B.13}$$

B.1.7. Stability combined compression and bending

The columns should be checked for flexural buckling, and for the beams the stability should be checked for lateral-torsional buckling. First, the verification procedure for the glued-laminated columns will be described.

The relative slenderness ratios should be determined as follows:

$$\lambda_{rel,y} = \frac{\lambda_y}{\pi}\sqrt{\frac{f_{c,0,k}}{E_{0,05}}} \tag{B.14}$$

$$\lambda_{rel,z} = \frac{\lambda_z}{\pi}\sqrt{\frac{f_{c,0,k}}{E_{0,05}}} \tag{B.15}$$

Where:

λ_y and $\lambda_{rel,y}$ are the slenderness ratios about the y-axis
λ_z and $\lambda_{rel,z}$ are the slenderness ratios about the z-axis

In the case $\lambda_{rel,z} \leq 0.3$ and $\lambda_{rel,y} \leq 0.3$ the stresses should be checked with the combined bending and axial compression expressions. In all other cases the following expression should be satisfied:

$$\frac{\sigma_{c,0,d}}{k_{c,y}f_{c,0,d}} + \frac{\sigma_{m,y,d}}{f_{m,y,d}} + k_m \frac{\sigma_{m,z,d}}{f_{m,z,d}} \leq 1 \tag{B.16}$$

$$\frac{\sigma_{c,0,d}}{k_{c,z}f_{c,0,d}} + k_m \frac{\sigma_{m,y,d}}{f_{m,y,d}} + \frac{\sigma_{m,z,d}}{f_{m,z,d}} \leq 1 \tag{B.17}$$

Where:

$$k_{c,y} = \frac{1}{k_y + \sqrt{k_y^2 - \lambda rel,y^2}} \tag{B.18}$$

$$k_{c,z} = \frac{1}{k_z + \sqrt{k_z^2 - \lambda rel,z^2}} \tag{B.19}$$

$$k_y = 0.5(1 + \beta_c(\lambda_{rel,y} - 0.3) + \lambda_{rel,y}^2) \tag{B.20}$$

$$k_z = 0.5(1 + \beta_c(\lambda_{rel,z} - 0.3) + \lambda_{rel,z}^2) \tag{B.21}$$

The factor, β_c, is equal to 0.1 for glued-laminated timber and LVL.

The timber beam elements should be checked for lateral-torsional buckling. The relative slenderness ratio should be determined with Eq.(B.22).

$$\lambda_{rel,m} = \sqrt{\frac{f_{m,k}}{\sigma_{m,crit}}} \tag{B.22}$$

The critical bending, $\sigma_{m,crit}$, can be calculated as follows:

$$\sigma_{m,crit} = \frac{M_{y,crit}}{W_y} = \frac{\pi\sqrt{E_{0.05}I_z G_{0.05}I_{tor}}}{l_{ef}W_y} \tag{B.23}$$

Where:

$M_{y,crit}$	is the critical bending moment
W_y	is the section modulus about the major axis y
$E_{0.05}$	is the fifth percentile value of modulus of elasticity
I_z	is the second moment of area about the minor axis z
$G_{0.05}$	is the fifth percentile value of shear modulus
I_{tor}	is the torsional moment of inertia
l_{ef}	is the effective length of the beam

In the timber beam bending about the major axis y can occur, or a combined case of bending and compression can occur. The case for only bending should be checked with Eq.(B.24).

$$\sigma_{m,d} \leq k_{crit} \cdot f_{m,d} \tag{B.24}$$

Where:

$\sigma_{m,d}$	is the design bending stress
k_{crit}	is a factor which takes into account the lateral buckling which reduces the bending strength
$f_{m,d}$	is the design bending strength

For the case a combination of bending moment and compressive force occur, the beam should be checked as follows:

$$\left(\frac{\sigma_{m,d}}{k_{crit}f_{m,d}}\right)^2 + \frac{\sigma_{c,d}}{k_{c,z}f_{c,0,d}} \leq 1.0 \tag{B.25}$$

Where:

$\sigma_{c,d}$	is the design compression stress
$f_{c,0,d}$	is the design compression strength parallel to the grain
$k_{c,z}$	is the factor given by Eq.(B.19)

B.1.8. Deformations

The deflection of the timber beams should be limited. Due to the variable loading on the beam the deflection will vary considerably over time. For a beam on two supports the net deflection can be determined with:

$$w_{net,fin} = w_{inst} + w_{creep} \tag{B.26}$$

Where:

$w_{net,fin}$	is the net final deflection
w_{inst}	is the instantaneous deflection
w_{creep}	is the creep deflection

The deflection limit for beams on two supports is between $l/250$ and $l/350$.

B.1.9. Example design calculation timber frame

Beam design

Beam section properties

Depth	d	500	mm
Width	w	300	mm
Cross sectional Area	A	150000	mm2
Moment of inertia about the z-axis	I_z	1,13E+09	mm4
Moment of intertia about the y-axis	I_y	3,13E+09	mm4
Section modulus about the y-axis	W_z	7,50E+06	mm3
Section modulus about the z-axis	W_y	1,25E+07	mm3

GL32h properties

Bending strength	$f_{m,k}$	32	N/mm2
Tension strength	$f_{t,0,k}$	24	N/mm2
Tension strength perp. To grain	$f_{t,90,k}$	0,45	N/mm2
Compression strength	$f_{c,0,k}$	29	N/mm2
Compression strength perp. to grain	$f_{c,90,k}$	6	N/mm2
Shear strength	$f_{v,k}$	3,5	N/mm2
Mean modulus of elasticity	$E_{0,mean}$	13700	N/mm2
Lower 5-percentile modulus of elasticity	$E_{0,05}$	11100	N/mm2
Mean modulus of elasticity perp. to grain	$E_{90,mean}$	460	N/mm2
Shear modulus	G_{mean}	850	N/mm2
Characteristic density	ρ_k	440	kg/m3
Mean density	ρ_{mean}	500	kg/m3

Material factor	γ_m	1,25	
Service class	SC	1	
Modification factor (short-term, SC1)	k_{mod}	0,9	
Rectangular glulam section	k_m	0,7	
Size factor (for depth <600mm)	k_h	1,1	0,982
System strength factor	k_{sys}	1,1	section 6.6

Design strenght

Bending strength	fm,d	27,9	N/mm2
Tension strength	ft,0,d	20,9	N/mm2
Compression strength	fc,0,d	23,0	N/mm2
Shear strength	fv,d	2,5	N/mm2

ETABS results
Perimeter Beam B17 at Story 2

Tension force	Nt,d	73,3	kN
Compression force	Nc,d	158,1	kN
Shear force y	Vy,d	4,6	kN
Shear force z	Vz,d	106,1	kN
Moment about the y-axis	My,d	146,6	kNm
Moment about the z-axis	Mz,d	11,1	kNm

Compression parallel to the grain	
$\sigma_{c,0,d} \leq f_{c,0,d}$	Eq. 6.2
fc,0,d	23,0 N/mm2
σc,0,d	1,05 N/mm2
UC	0,046 ≤1.0

Tension parallel to the grain	
$\sigma_{t,0,d} \leq f_{t,0,d}$	Eq. 6.1
ft,0,d	20,9 N/mm2
σt,0,d	0,49 N/mm2
UC	0,023 ≤1.0
*when width is less than 600mm use kh factor	

Bending	
$\dfrac{\sigma_{m,y,d}}{f_{m,y,d}} + k_m \dfrac{\sigma_{m,z,d}}{f_{m,z,d}} \leq 1$ $k_m \dfrac{\sigma_{m,y,d}}{f_{m,y,d}} + \dfrac{\sigma_{m,z,d}}{f_{m,z,d}} \leq 1$	Eq. 6.11 + 6.12
fm,y,d	27,88 N/mm2
σm,y,d	19,55 N/mm2
fm,z,d	27,88 N/mm2
σm,z,d	0,89 N/mm2
km	0,7
UC	0,723 ≤1.0

Shear	
$\tau_d \leq f_{v,d}$	Eq. 6.13
fv,d	2,5 N/mm2
kcr	0,67
bef	201 mm
Aef	100500 mm2
τd	1,58 N/mm2
UC	0,628 ≤1.0

Combined bending and axial compression	
$\left(\dfrac{\sigma_{c,0,d}}{f_{c,0,d}}\right)^2 + \dfrac{\sigma_{m,y,d}}{f_{m,y,d}} + k_m \dfrac{\sigma_{m,z,d}}{f_{m,z,d}} \leq 1$ $\left(\dfrac{\sigma_{c,0,d}}{f_{c,0,d}}\right)^2 + k_m \dfrac{\sigma_{m,y,d}}{f_{m,y,d}} + \dfrac{\sigma_{m,z,d}}{f_{m,z,d}} \leq 1$	Eq. 6.19 + 6.20
fm,y,d	27,88 N/mm2
σm,y,d	19,55 N/mm2
fm,z,d	27,88 N/mm2
σm,z,d	0,89 N/mm2
km	0,7
fc,0,d	22,97 N/mm2
σc,0,d	1,05 N/mm2
UC	0,726 ≤1.0

Combined bending and axial tension	
$\dfrac{\sigma_{t,0,d}}{f_{t,0,d}} + \dfrac{\sigma_{m,y,d}}{f_{m,y,d}} + k_m \dfrac{\sigma_{m,z,d}}{f_{m,z,d}} \leq 1$ $\dfrac{\sigma_{t,0,d}}{f_{t,0,d}} + k_m \dfrac{\sigma_{m,y,d}}{f_{m,y,d}} + \dfrac{\sigma_{m,z,d}}{f_{m,z,d}} \leq 1$	Eq. 6.17 + 6.18
fm,y,d	27,88 N/mm2
σm,y,d	19,55 N/mm2
fm,z,d	27,88 N/mm2
σm,z,d	0,89 N/mm2
km	0,7
ft,0,d	20,91 N/mm2
σt,0,d	0,49 N/mm2
UC	0,506 ≤1.0

Stability combined bending and axial compression	
$\left(\dfrac{\sigma_{m,d}}{k_{crit} f_{m,d}}\right)^2 + \dfrac{\sigma_{c,0,d}}{k_{c,z} f_{c,0,d}} \leq 1$	Eq. 6.35
leff	4500 mm
σm,crit	333 N/mm2
λrel,m	0,310
kcrit	1
i	86,6
λz	51,96
kz	0,87
βc	0,10
λrel,z	0,85
kc,z	0,910
UC	0,542 ≤1.0

Deflections	
$u_{fin} = u_{fin,G} + u_{fin,Q1} + u_{fin,Qi}$	Eq.7.2
Fd,G	12,16 kN
uinst,G	0,47 mm
Qk1,offices	26,46 kN
uinst,Q1	0,92 mm
$u_{fin,G} = u_{inst,G}(1 + k_{def})$	
kdef	0,6
ufin,G	0,75 mm
$u_{fin,Q1} = u_{inst,Q1}(1 + \psi_{2,1} k_{def})$	
ψ2,1	0,3
ufin,Q1	1,09 mm
ufin,tot	1,83 mm
limit (l/250)	18 mm
	OK

Column design (Storey 2 till 20)

Column section properties

Depth	d	1200	mm
Width	w	1200	mm
Cross sectional Area	A	1440000	mm2
Moment of inertia about the y-axis	I_y	1,73E+11	mm4
Moment of inertia about the z-axis	I_z	1,73E+11	mm4
Section modulus about the y-axis	W_y	2,88E+08	mm3
Section modulus about the z-axis	W_z	2,88E+08	mm3

GL32h properties

Bending strength	$f_{m,k}$	32	N/mm2
Tension strength	$f_{t,0,k}$	24	N/mm2
Tension strength perp. To grain	$f_{t,90,k}$	0,45	N/mm2
Compression strength	$f_{c,0,k}$	29	N/mm2
Compression strength perp. to grain	$f_{c,90,k}$	6	N/mm2
Shear strength	$f_{v,k}$	3,5	N/mm2
Mean modulus of elasticity	$E_{0,mean}$	13700	N/mm2
Lower 5-percentile modulus of elasticity	$E_{0,05}$	11100	N/mm2
Mean modulus of elasticity perp. to grain	$E_{90,mean}$	460	N/mm2
Shear modulus	G_{mean}	850	N/mm2
Characteristic density	ρ_k	440	kg/m3
Mean density	ρ_{mean}	500	kg/m3

Material factor	γ_M	1,25
Service class	SC	1
Modification factor	k_{mod}	0,9
Rectangular glulam section	k_m	0,7

Design strenght

Bending strength	fm,d	23,04	N/mm2
Tension strength	ft,0,d	17,28	N/mm2
Compression strength	fc,0,d	20,88	N/mm2
Shear strength	fv,d	2,52	N/mm2

ETABS results

Column C1 at storey level 2			
Tension force	Nt,d	1260	kN
Compression force	Nc,d	21,2	MN
Shear force y	Vy,d	73	kN
Shear force z	Vz,d	6,5	kN
Moment about the y-axis	My,d	45,2	kNm
Moment about the z-axis	Mz,d	152,3	kNm

Tension parallel to the grain

	Eq. 6.1
$\sigma_{t,0,d} \leq f_{t,0,d}$	

ft,0,d	17,28 N/mm2
σt,0,d	0,88 N/mm2
UC	0,051 ≤1.0
*when width is less than 600mm use kh factor	

Compression parallel to the grain

	Eq. 6.2
$\sigma_{c,0,d} \leq f_{c,0,d}$	

fc,0,d	20,88 N/mm2
σc,0,d	14,72 N/mm2
UC	0,705 ≤1.0

Bending

	Eq. 6.11 + 6.12
$\frac{\sigma_{m,y,d}}{f_{m,y,d}} + k_m \frac{\sigma_{m,z,d}}{f_{m,z,d}} \leq 1$	
$k_m \frac{\sigma_{m,y,d}}{f_{m,y,d}} + \frac{\sigma_{m,z,d}}{f_{m,z,d}} \leq 1$	

fm,y,d	23,04 N/mm2
σm,y,d	0,16 N/mm2
fm,z,d	23,04 N/mm2
σm,z,d	0,53 N/mm2
km	0,7
UC	0,023 ≤1.0

Shear

	Eq. 6.13
$\tau_d \leq f_{v,d}$	

fv,d	2,52 N/mm2
kcr	0,67
bef	804 mm
Aef	964800 mm2
τd	0,11 N/mm2
UC	0,045 ≤1.0

Combined bending and axial tension

	Eq. 6.17 + 6.18
$\frac{\sigma_{t,0,d}}{f_{t,0,d}} + \frac{\sigma_{m,y,d}}{f_{m,y,d}} + k_m \frac{\sigma_{m,z,d}}{f_{m,z,d}} \leq 1$	
$\frac{\sigma_{t,0,d}}{f_{t,0,d}} + k_m \frac{\sigma_{m,y,d}}{f_{m,y,d}} + \frac{\sigma_{m,z,d}}{f_{m,z,d}} \leq 1$	

fm,y,d	23,04 N/mm2
σm,y,d	0,16 N/mm2
fm,z,d	23,04 N/mm2
σm,z,d	0,53 N/mm2
km	0,7
ft,0,d	17,28 N/mm2
σt,0,d	0,88 N/mm2
UC	0,078 ≤1.0

Combined bending and axial compression	
$$\left(\frac{\sigma_{c,0,d}}{f_{c,0,d}}\right)^2 + \frac{\sigma_{m,y,d}}{f_{m,y,d}} + k_m \frac{\sigma_{m,z,d}}{f_{m,z,d}} \leq 1$$ $$\left(\frac{\sigma_{c,0,d}}{f_{c,0,d}}\right)^2 + k_m \frac{\sigma_{m,y,d}}{f_{m,y,d}} + \frac{\sigma_{m,z,d}}{f_{m,z,d}} \leq 1$$	Eq. 6.19 + 6.20
fm,y,d	23,04 N/mm2
σm,y,d	0,16 N/mm2
fm,z,d	23,04 N/mm2
σm,z,d	0,53 N/mm2
km	0,7
fc,0,d	20,88 N/mm2
σc,0,d	14,72 N/mm2
UC	0,520 ≤1.0

Stability compression and bending		
$$\frac{\sigma_{c,0,d}}{k_{c,y} f_{c,0,d}} + \frac{\sigma_{m,y,d}}{f_{m,y,d}} + k_m \frac{\sigma_{m,z,d}}{f_{m,z,d}} \leq 1$$ $$\frac{\sigma_{c,0,d}}{k_{c,z} f_{c,0,d}} + k_m \frac{\sigma_{m,y,d}}{f_{m,y,d}} + \frac{\sigma_{m,z,d}}{f_{m,z,d}} \leq 1$$	$$\lambda_{rel,z} = \frac{\lambda_z}{\pi} \sqrt{\frac{f_{c,0,k}}{E_{0,05}}}$$ $$\lambda_{rel,y} = \frac{\lambda_y}{\pi} \sqrt{\frac{f_{c,0,k}}{E_{0,05}}}$$	Eq. 6.21 + 6.22
leff	3750 mm	
i	346,4	
λy	10,8	
λrel,y	0,18	
βc	0,10	
ky	0,50	
kc,y	1	1,03
fm,y,d	23,04 N/mm2	
UC	0,704 ≤1.0	
UC	0,709 ≤1.0	

Outrigger-truss diagonal (Storey level 21)

Diagonal section properties

Depth	d	800	mm
Width	w	800	mm
Cross sectional Area	A	640000	mm2
Moment of inertia about the z-axis	I_z	3,41E+10	mm4
Moment of intertia about the y-axis	I_y	3,41E+10	mm4
Section modulus about the y-axis	W_z	8,53E+07	mm3
Section modulus about the z-axis	W_y	8,53E+07	mm3

LVL-Kerto-S properties

Bending strength	$f_{m,k}$	51	N/mm2
Tension strength	$f_{t,0,k}$	42	N/mm2
Tension strength perp. To grain	$f_{t,90,k}$	0,6	N/mm2
Compression strength	$f_{c,0,k}$	42	N/mm2
Compression strength perp. to grain	$f_{c,90,k}$	9	N/mm2
Shear strength	$f_{v,k}$	5,1	N/mm2
Mean modulus of elasticity	$E_{0,mean}$	14000	N/mm2
Lower 5-percentile modulus of elasticity	$E_{0,05}$	12400	N/mm2
Mean modulus of elasticity perp. edgewise	$E_{90,edge,mean}$	430	N/mm2
Mean modulus of elasticity perp. flatwise	$E_{90,flat,mean}$	130	N/mm2
Mean shear modulus	$G_{0,mean}$	850	N/mm2
5 % shear modulus	$G_{0,05}$	820	N/mm2
Poisson ration	v	0,3	
Characteristic density	ρ_k	480	kg/m3

Material factor	γm	1,25	
Service class	SC	1	
Modification factor (short-term, SC1)	kmod	0,9	
Rectangular glulam section	km	0,7	
Size factor (for depth <600mm)	kh	1,1	1,03
System strength factor	ksys	1,1	

Design strenght

Bending strength	fm,d	44,43	N/mm2
Tension strength	ft,0,d	36,59	N/mm2
Compression strength	fc,0,d	33,26	N/mm2
Shear strength	fv,d	3,67	N/mm2

ETABS results

Tension force	Nt,d	4247	kN
Compression force	Nc,d	8380	kN
Shear force y	Vy,d	10	kN
Shear force z	Vz,d	0	kN
Moment about the y-axis	My,d	20	kNm
Moment about the z-axis	Mz,d	0	kNm

Compression parallel to the grain	
$\sigma_{c,0,d} \le f_{c,0,d}$	Eq. 6.2
fc,0,d	33,26 N/mm2
σc,0,d	13,09 N/mm2
UC	0,394 ≤1.0

Tension parallel to the grain	
$\sigma_{t,0,d} \le f_{t,0,d}$	Eq. 6.1
ft,0,d	36,59 N/mm2
σt,0,d	6,6359375 N/mm2
UC	0,181 ≤1.0
*when width is less than 600mm use kh factor	

Bending	
$\dfrac{\sigma_{m,y,d}}{f_{m,y,d}} + k_m \dfrac{\sigma_{m,z,d}}{f_{m,z,d}} \le 1$ $k_m \dfrac{\sigma_{m,y,d}}{f_{m,y,d}} + \dfrac{\sigma_{m,z,d}}{f_{m,z,d}} \le 1$	Eq. 6.11 + 6.12
fm,y,d	44,43 N/mm2
σm,y,d	0,23 N/mm2
fm,z,d	44,43 N/mm2
σm,z,d	0,00 N/mm2
km	0,7
UC	0,005 ≤1.0

Shear	
$\tau_d \le f_{v,d}$	Eq. 6.13
fv,d	3,67 N/mm2
kcr	0,67
bef	536 mm
Aef	428800 mm2
τd	0,035 N/mm2
UC	0,010 ≤1.0

Combined bending and axial compression	
$\left(\dfrac{\sigma_{c,0,d}}{f_{c,0,d}}\right)^2 + \dfrac{\sigma_{m,y,d}}{f_{m,y,d}} + k_m \dfrac{\sigma_{m,z,d}}{f_{m,z,d}} \le 1$ $\left(\dfrac{\sigma_{c,0,d}}{f_{c,0,d}}\right)^2 + k_m \dfrac{\sigma_{m,y,d}}{f_{m,y,d}} + \dfrac{\sigma_{m,z,d}}{f_{m,z,d}} \le 1$	Eq. 6.19 + 6.20
fm,y,d	44,43 N/mm2
σm,y,d	0,23 N/mm2
fm,z,d	44,43 N/mm2
σm,z,d	0,00 N/mm2
km	0,7
fc,0,d	33,26 N/mm2
σc,0,d	13,09 N/mm2

UC	0,160 ≤1.0

Combined bending and axial tension

$\dfrac{\sigma_{t,0,d}}{f_{t,0,d}} + \dfrac{\sigma_{m,y,d}}{f_{m,y,d}} + k_m \dfrac{\sigma_{m,z,d}}{f_{m,z,d}} \leq 1$ $\dfrac{\sigma_{t,0,d}}{f_{t,0,d}} + k_m \dfrac{\sigma_{m,y,d}}{f_{m,y,d}} + \dfrac{\sigma_{m,z,d}}{f_{m,z,d}} \leq 1$	Eq. 6.17 + 6.18
fm,y,d	44,43 N/mm2
σm,y,d	0,23 N/mm2
fm,z,d	44,43 N/mm2
σm,z,d	0,00 N/mm2
km	0,7
ft,0,d	36,59 N/mm2
σt,0,d	6,64 N/mm2
UC	0,187 ≤1.0

Stability combined bending and axial compression

$\left(\dfrac{\sigma_{m,d}}{k_{crit} f_{m,d}}\right)^2 + \dfrac{\sigma_{c,0,d}}{k_{c,z} f_{c,0,d}} \leq 1$	Eq. 6.35
leff	4500 mm
σm,crit	1653 N/mm2
λrel,m	0,176
kcrit	1
i	230,9
λz	19,49
kz	0,56
βc	0,10
λrel,z	0,36
kc,z	1,016
UC	0,387 ≤1.0

Belt-truss diagonal design (Storey level 21)

Diagonal section properties

Depth	d	800	mm
Width	w	800	mm
Cross sectional Area	A	640000	mm2
Moment of inertia about the z-axis	Iz	3,41E+10	mm4
Moment of intertia about the y-axis	Iy	3,41E+10	mm4
Section modulus about the y-axis	Wz	8,53E+07	mm3
Section modulus about the z-axis	Wy	8,53E+07	mm3

LVL-Kerto-S properties

Bending strength	$f_{m,k}$	51	N/mm2
Tension strength	$f_{t,0,k}$	42	N/mm2
Tension strength perp. To grain	$f_{t,90,k}$	0,6	N/mm2
Compression strength	$f_{c,0,k}$	42	N/mm2
Compression strength perp. to grain	$f_{c,90,k}$	9	N/mm2
Shear strength	$f_{v,k}$	5,1	N/mm2
Mean modulus of elasticity	$E_{0,mean}$	14000	N/mm2
Lower 5-percentile modulus of elasticity	$E_{0,05}$	12400	N/mm2
Mean modulus of elasticity perp. edgewise	$E_{90,edge,mean}$	430	N/mm2
Mean modulus of elasticity perp. flatwise	$E_{90,flat,mean}$	130	N/mm2
Mean shear modulus	$G_{0,mean}$	850	N/mm2
5 % shear modulus	$G_{0,05}$	820	N/mm2
Poisson ration	v	0,3	
Characteristic density	ρ_k	480	kg/m3

Material factor	γ_M	1,25	
Service class	SC	1	
Modification factor (short-term, SC1)	k_{mod}	0,9	
Rectangular glulam section	k_m	0,7	
Size factor (for depth <600mm)	k_h	1,1	1,03
System strength factor	k_{sys}	1,1	

Design strenght

Bending strength	fm,d	44,43	N/mm2
Tension strength	ft,0,d	36,59	N/mm2
Compression strength	fc,0,d	33,26	N/mm2
Shear strength	fv,d	3,67	N/mm2

ETABS results

Tension force	Nt,d	3602	kN
Compression force	Nc,d	2517	kN
Shear force y	Vy,d	9	kN
Shear force z	Vz,d	0	kN
Moment about the y-axis	My,d	22	kNm
Moment about the z-axis	Mz,d	0	kNm

Compression parallel to the grain

$\sigma_{c,0,d} \leq f_{c,0,d}$	Eq. 6.2
fc,0,d	33,26 N/mm2
σc,0,d	3,93 N/mm2
UC	0,118 ≤1.0

Tension parallel to the grain

$\sigma_{t,0,d} \leq f_{t,0,d}$	Eq. 6.1
ft,0,d	36,59 N/mm2
σt,0,d	5,63 N/mm2
UC	0,154 ≤1.0
*when width is less than 600mm use kh factor	

Bending

$\dfrac{\sigma_{m,y,d}}{f_{m,y,d}} + k_m \dfrac{\sigma_{m,z,d}}{f_{m,z,d}} \leq 1$ $k_m \dfrac{\sigma_{m,y,d}}{f_{m,y,d}} + \dfrac{\sigma_{m,z,d}}{f_{m,z,d}} \leq 1$	Eq. 6.11 + 6.12
fm,y,d	44,43 N/mm2
σm,y,d	0,26 N/mm2
fm,z,d	44,43 N/mm2
σm,z,d	0,000 N/mm2
km	0,7
UC	0,006 ≤1.0

Shear

$\tau_d \leq f_{v,d}$	Eq. 6.13
fv,d	3,67 N/mm2
kcr	0,67
bef	536 mm
Aef	428800 mm2
τd	0,031 N/mm2
UC	0,009 ≤1.0

Combined bending and axial compression

$\left(\dfrac{\sigma_{c,0,d}}{f_{c,0,d}}\right)^2 + \dfrac{\sigma_{m,y,d}}{f_{m,y,d}} + k_m \dfrac{\sigma_{m,z,d}}{f_{m,z,d}} \leq 1$ $\left(\dfrac{\sigma_{c,0,d}}{f_{c,0,d}}\right)^2 + k_m \dfrac{\sigma_{m,y,d}}{f_{m,y,d}} + \dfrac{\sigma_{m,z,d}}{f_{m,z,d}} \leq 1$	Eq. 6.19 + 6.20
fm,y,d	44,43 N/mm2
σm,y,d	0,26 N/mm2
fm,z,d	44,43 N/mm2
σm,z,d	0,00 N/mm2
km	0,7
fc,0,d	33,26 N/mm2
σc,0,d	3,93 N/mm2
UC	0,020 ≤1.0

Combined bending and axial tension

$$\frac{\sigma_{t,0,d}}{f_{t,0,d}} + \frac{\sigma_{m,y,d}}{f_{m,y,d}} + k_m \frac{\sigma_{m,z,d}}{f_{m,z,d}} \leq 1$$ $$\frac{\sigma_{t,0,d}}{f_{t,0,d}} + k_m \frac{\sigma_{m,y,d}}{f_{m,y,d}} + \frac{\sigma_{m,z,d}}{f_{m,z,d}} \leq 1$$	Eq. 6.17 + 6.18
fm,y,d	44,43 N/mm2
σm,y,d	0,26 N/mm2
fm,z,d	44,43 N/mm2
σm,z,d	0,00 N/mm2
km	0,7
ft,0,d	36,59 N/mm2
σt,0,d	5,63 N/mm2
UC	0,160 ≤1.0

Stability combined bending and axial compression

$$\left(\frac{\sigma_{m,d}}{k_{crit} f_{m,d}}\right)^2 + \frac{\sigma_{c,0,d}}{k_{c,z} f_{c,0,d}} \leq 1$$	Eq. 6.35
leff	4500 mm
σm,crit	1653,3 N/mm2
λrel,m	0,176
kcrit	1
i	230,9
λz	19,49
kz	0,56
βc	0,10
λrel,z	0,36
kc,z	1,016
UC	0,116 ≤1.0

B.2. Floor slab design

Floor slab calculation

CLT panel properties		
Thickness panel	d	153 mm
Build-up layers	33-27-33-27-33	mm
Span	l	4500 mm
Effective width	b_{eff}	1000 mm
Panel thickness parallel	$h_{1,2,3}$	33 mm
Panel thickness perpendicular	$h_{4,5}$	27 mm
Bending stiffness parallel to grain	$E_{0,mean}$	12000 Mpa
Bending stiffness perpendicular to grain	$E_{90,mean}$	370 Mpa
Shear stiffness parallel to grain	$G_{0,mean}$	250 Mpa
Rolling shear stiffness	G_R	50 Mpa
Connection efficiency factor	γ	0,91
Effective bending stiffness	$(EI)_{eff}$	2,48E+12 Nmm2
Effective second moment of area	I_{eff}	2,26E+08 mm4
Effective shear stiffness	$(GA)_{eff}$	1,89E+07 N
Characteristic bending strength	f_{mk}	24 Mpa
Characteristic shear strength	f_{vk}	2,7 Mpa
Characteristic rolling shear	f_{rk}	1,5 Mpa
Modification factor	k_{mod}	0,8
System factor	k_{sys}	1,1
Material factor	γ_M	1,3
Characteristic density of concrete	ρ_c	2500 kg/m3
Characteristic density of CLT	$\rho_{k,CLT}$	350 kg/m3
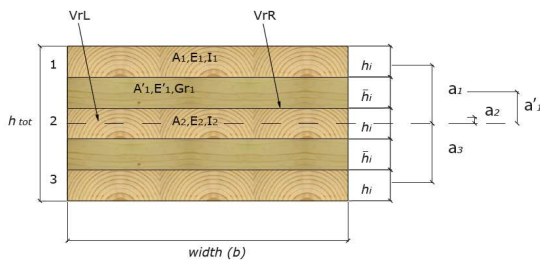
Cross-section of CLT panel with 5 layers   (Gagnon S. and Pirvu C. - CLT Handbook, 2011)

ETABS results		
Design bending moment	$M_{y,d}$	14,25 kNm
Design shear force	$V_{y,d}$	12,66 kNm

Flexural strenght design		
Design bending moment resistance	$$M_{y,Rd} = f_{md} \cdot \frac{I_{eff}}{(\gamma_1 a_1 + 0.5 h_1)}$$	
Design bending strength	f_{md}	16,25 N/mm2
	a_1	60,00 mm
	M_{Rd}	51,64 kNm
Max design bending moment	$$\sigma_{y,d,max} = \frac{\gamma_1 E_1 a_1 M_{y,d}}{(EI)_{eff}} + \frac{0.5 E_1 h_1 M_{y,d}}{(EI)_{eff}}$$	
	$\sigma_{y,d,max}$	4,89 N/mm2
	UC	0,28

Shear strength design		
Maximum design shear stress	$\tau_{d,max} = \dfrac{V_{d,max} \cdot (EQ)}{(EI)_{eff} \cdot b}$	
Static moment of area	$(EQ) = \gamma_1 E_1 A_1 a_1 + E_1' A_1' a_1' + \gamma_2 E_2 \cdot \dfrac{A_2}{2} \cdot \dfrac{h_2}{4}$	
	EQ	2,34E+10 Nmm^5
	$\tau_{d,max}$	0,12 N/mm2
Longitudinal shear resistance	$V_{rL} = \dfrac{f_{v,d} \cdot (EI)_{eff} \cdot b}{\gamma_1 E_1 A_1 a_1 + E_1' A_1' a_1' + \gamma_2 E_2 \cdot \dfrac{A_2}{2} \cdot \dfrac{h_2}{4}}$	
Design shear resistance	$f_{v,d}$	1,83 N/mm2
	$V_{d,rL}$	194 kN
	UC	0,07

Deflections		
Instanteneous deflection due to permanent loading	$u_{inst,G} = \dfrac{5 \cdot q_G \cdot l^4}{384 \cdot (EI)_{eff}} + \dfrac{q_G \cdot l^2}{8 \cdot (GA)_{eff}}$	
	q_G	1,14 kN/m
	$u_{inst,G}$	2,60 mm
Instanteneous deflection due to variable loading	$u_{inst,Q} = \dfrac{5 \cdot q_Q \cdot l^4}{384 \cdot (EI)_{eff}} + \dfrac{q_Q \cdot l^2}{8 \cdot (GA)_{eff}}$	
	q_Q	2,5 kN/m
	$u_{inst,Q}$	5,71 mm
Final deflection due to permanent loading	$u_{fin,G} = u_{inst,G}(1 + k_{def,G})$	
	$k_{def,G}$	0,6
	$u_{fin,G}$	4,16 mm
Final deflection due to variable loading	$u_{fin,Q} = u_{inst,Q}(1 + \varphi_2 k_{def,Q})$	
	$k_{def,Q}$	0,8
	$\psi_{2,1}$	0,3
	$u_{fin,Q}$	7,08 mm
Total instanteneous deflection	$u_{inst,tot}$	8,31 mm
Total final deflection	$u_{fin,tot}$	11,24 mm
Maximum deflection	u_{limit}	18,00 mm
	UC	0,62

Vibrations		
Fundamental frequency of floor slab	$n_{1,x} = \dfrac{\pi}{2l^2} \sqrt{\dfrac{(EI)_{eff}^{1m}}{\rho A}}$	
	$n_{1,x}$	11,35 Hz
	$n_{1,min}$	9,0 Hz
	OK	
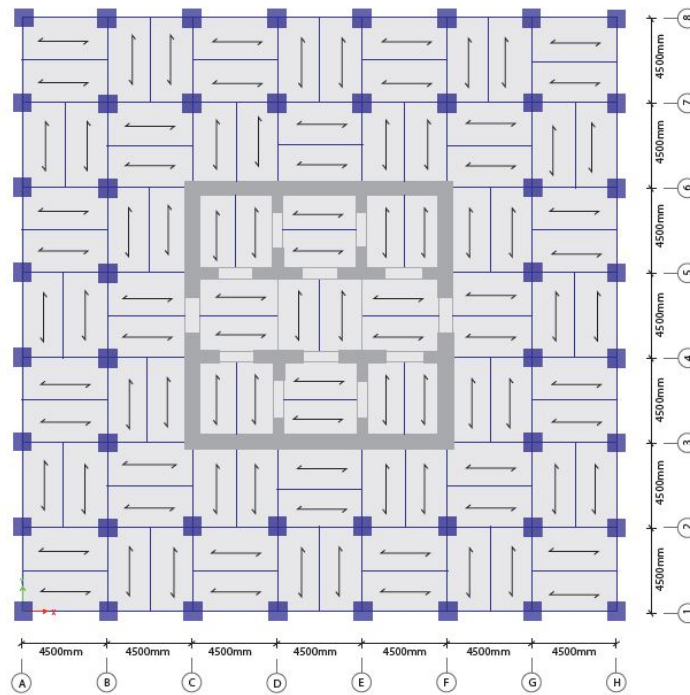
Figure B.1: CLT floor spans in principal dir. (panels with dimensions of 4.5m x 2.25m)

The floor slabs should be able to transfer the lateral wind load subjected on the façade of the building. The floor slab transfers the horizontal load to the shear walls at the core. The shear resistance of the CLT floor panels should be checked. The glued laminated beams will also cooperate in transferring the lateral wind load. The shear strength will be checked with a simplified model in which only the floor slabs are included, and is therefore a conservative approach. Figure B.2 shows how the floor slab behaves as a deep beam, and how the shear forces are transferred to the core.
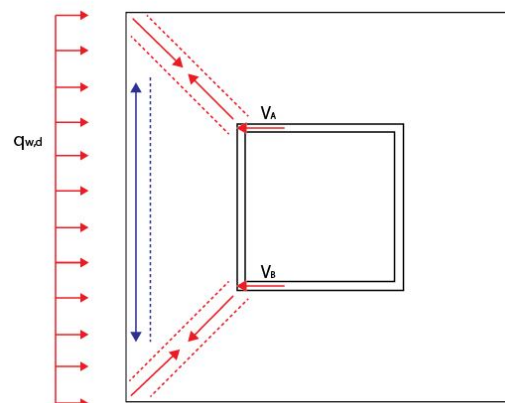
Figure B.2: Simplified force flow in the floor diaphragm

Lateral floor design

Floor slab properties

Thickness, d	d	153 mm
Build-up layers	33-27-33-27-33	mm
Width	w	2250 mm
Span	l	4500 mm
Effective width	b_{eff}	1000 mm
Cross sectional Area	A	153000 mm2

CLT-Beech properties

Bending strength	$f_{m,k}$	24 N/mm2
Rolling shear strength	$f_{r,k}$	1,5 N/mm2
In plane compression strength	$f_{c,0,k}$	30 N/mm2
Compression strength perp. to grain	$f_{c,90,k}$	2,7 N/mm2
In plane tension strength	$f_{t,0,k}$	16,5 N/mm2
Shear strength	$f_{v,k}$	2,7 N/mm2
Mean modulus of elasticity	$E_{0,mean}$	12000 N/mm2
Shear modulus	G_{mean}	250 N/mm2
Characteristic density	ρ_k	350 kg/m3

Material factor	γ_M	1,25
Service class	SC	1
Modification factor	k_{mod}	0,9

Design strenght

Bending strength	$f_{m,d}$	17,3 N/mm2
Tension strength	$f_{t,0,d}$	11,9 N/mm2
Compression strength	$f_{c,0,d}$	21,6 N/mm2
Shear strength	$f_{v,d}$	1,9 N/mm2

Uniformly distributed wind load

wind load at top	q	2,7 kN/m2
wind load at top	q_d	4,05 kN/m2
	q_d	15,2 kN/m

Distribution length of shear force	l	1500 mm
	A_{gros}	229500 mm2

Lateral reaction force core at A	V_A	239,2 kN
Lateral reaction force core at A	V_B	239,2 kN

Shear strength

Design shear stress	τ_d	1,04 N/mm2
Design shear strength	$f_{v,d}$	1,9 N/mm2
	UC	0,54

B.3. Concrete wall design

Wall design (Storey level 1-20)		
Wall element section properties		
Length	l	13500 mm
Thickness	t	1200 mm
Height	h	7500 mm
Cross-sectional area of concrete	A_c	16200000 mm2

C55/67 properties		
Tension strength	f_{ctm}	4,4 N/mm2
Compression strength	$f_{c,k}$	55 N/mm2
Modulus of elasticity	E_{cm}	38000 MPa
Modified modulus of elasticity	E_{mod}	12667 MPa

Design strength		
Tension design strenght	$f_{t,d}$	2,93 N/mm2
Compression design strength	$f_{c,d}$	36,7 N/mm2
Shear design strenght	$f_{v,d}$	0,4 N/mm2

FeB500 properties		
Yielding strength	f_{yk}	500,0 N/mm2
Design yielding strength	f_{yd}	435 N/mm2

ETABS results		
Wall (Storey level 1)		
Tension stress	$\sigma_{t,d}$ (Nmax)	12 MPa
Compression stress	$\sigma_{c,d}$ (Nmin)	26,9 MPa
Shear stress	$\tau_{z,max}$	5,4 MPa

Flexural reinforcement design		
Top		
Design axial force	N_{Ed}	85261 kN
Design moment about y-axis	$M_{Ed,2}$	47795 kN
Design moment about z-axis	$M_{Ed,3}$	317411 kN
Bottom		
Design axial force	N_{Ed}	92270 kNm
Design moment about y-axis	$M_{Ed,2}$	77481 kNm
Design moment about z-axis	$M_{Ed,3}$	337299 kNm

Min. reinforcement	$A_{s,min}$ (0.25%)	40500 mm2
Max. reinforcement	$A_{s,max}$ (4%)	648000 mm2
Required reinf. at top	$A_{s,req,top}$	140873 mm2
Required reinf. at bottom	$A_{s,req,bottom}$	316329 mm2
Reinforcement ratio top		0,0087
Reinforcement ratio bottom		0,0195
Top		
Reinforcement bar diameter	$\varnothing$	28 mm
Reinforcement spacing	s	110 mm
Reinforcement cover	c	35 mm
	2x	114 bars

Demand/Capacity ratio	D/C	0,885
Bottom		
Reinforcement bar diameter	Ø	40 mm
Reinforcement spacing	s	110 mm
Reinforcement cover	c	60 mm
	2x	126 bars
Demand/Capacity ratio	D/C	0,926

Shear reinforcement design		
Top		
Design axial force	N_{Ed}	85261 kN
Design shear force	V_{Ed}	7321 kN
Required reinf. top	$A_{s,v,top}$	2609 mm2/m
Design shear resistance	V_{Rd}	10135 kN
Bottom		
Design axial force	N_{Ed}	92270 kN
Design shear force	V_{Ed}	4343 kN
Required reinf. bottom	$A_{s,v,bottom}$	5858 mm2/m
Design shear resistance	V_{Rd}	22758 kN

Unity check compressive stress	
0,73	<1.0

Interior wall design (Storey level 38-57)			

Wall element section properties			
Length	l	7500	mm
Thickness	t	600	mm
Height	h	3750	mm
Cross sectional area of concrete	Ac	4500000	mm2

C50/60 properties			
Tension strength	fctm	4,2	N/mm2
Compression strength	fc,k	50	N/mm2
Modulus of elasticity	Ecm	37000	MPa
Modified modulus of elasticity	Emod	12333	MPa

Design strength			
Tension design strenght	ft,d	2,8	N/mm2
Compression design strength	fc,d	33,3	N/mm2
Shear design strenght	fv,d	0,4	N/mm2

FeB500 properties			
Yielding strength	fyk	500,0	N/mm2
Design yielding strength	fyd	435	N/mm2

ETABS results			
Tension stress	σt,d (Nmax)	-	MPa
Compression stress	σc,d (Nmin)	9,5	MPa
Shear stress	τz,max	0,9	MPa

Flexural reinforcement design			
Top			
Design axial force	NEd	38575	kN
Design moment about y-axis	MEd,2	900	kN
Design moment about z-axis	MEd,3	17355	kN
Bottom			
Design axial force	NEd	38271	kNm
Design moment about y-axis	MEd,2	892	kNm
Design moment about z-axis	MEd,3	17222	kNm

Min. reinforcement	As,min (0.25%)	11250	mm2
Max. reinforcement	As,max (4%)	180000	mm2
Required reinf. at top	As,req,top	9375	mm2
Required reinf. at bottom	As,req,bottom	9375	mm2
Reinforcement ratio top		0,0021	
Reinforcement ratio bottom		0,0021	

Shear reinforcement design			
Top			
Design axial force	NEd	4393	kN
Design shear force	VEd	192	kN

Required reinf. top	$A_{s,v,top}$	600 mm2/m
Design shear resistance	V_{Rd}	432 kN
Bottom		
Design axial force	N_{Ed}	4335 kN
Design shear force	V_{Ed}	175 kN
Required reinf. bottom	$A_{s,v,bottom}$	600 mm2/m
Design shear resistance	V_{Rd}	432 kN

Unity check compressive stress	
	0,29 <1.0

B.4. Façade load

Table B.1: Façade load calculation

Façade panel loading		
Volumetric weight glass	25	kN/m^3
Width	4.5	m
Height	3.75	m
Total area	16.88	m^2
Thickness glass (2x10mm)	20	mm
Total weight	8.4	kN
Characteristic façade load	0.5	kN/m^2
Line load façade	1.9	kN/m

B.5. Foundation design

Table B.2: Foundation design: translational spring stiffness

Foundation design			
Thickness concrete raft	t_{raft}	2.0	m
$K_{p,z} = SWL/(0.01 \cdot d)$			
Average working load on pile	SWL	16000	kN
Diameter of piles	d	1.2	m
Number of piles	n	64	
Axial stiffness of pile	$K_{p,z}$	1920000	kN/m

B.6. Connection design
B.6.1. Beam-to-column design

Connection: beam-column detail

Input parameters		
Beam	500x300	mm2
Column	1000x1000	mm2
Material	Glulam32h	
Conceiled beam hanger	Rothoblaas Alumaxi	
Screws	Rothoblaas LBS	
Smooth dowels	Rothoblaas STA	

Beam B8 at story level 2		
Design tension force	$N_{t,d}$	73 kN
Design compression force	$N_{c,d}$	158 kN
Design shear force	V_d	106 kN
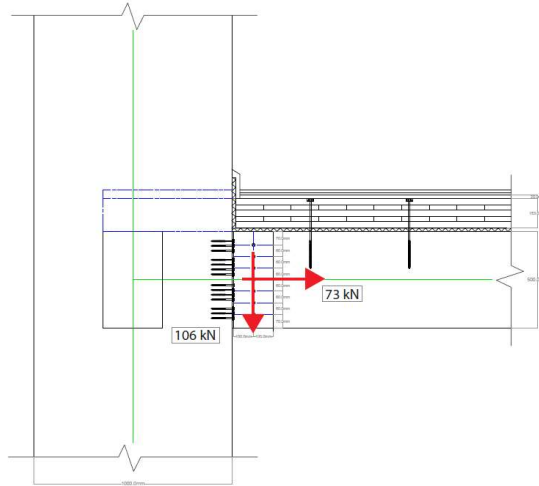
1. Check load-carrying capacity dowel type connection		
Dowel type connection		
diameter of fastener	d	16 mm
density of timber	ρ_k	440 kg/m3
number of bolts	n_b	7
thickness steel plate	t_2	10 mm
thickness timber	t_1	145 mm
kdef for service class 1	kdef	0,6
kmod short-term	kmod	0,9
characteristic tensile strenght fastener	$f_{u,k}$	800 N/mm2

1.1 Check tension and compression strength (parallel to grain)	
Characteristic load-carrying capacity (for central plate double shear connection)	$$F_{v,Rk} = \min \begin{cases} f_{h,1,k}\, t_1\, d & \text{(f)} \\ f_{h,1,k}\, t_1\, d\left[\sqrt{2 + \dfrac{4M_{y,Rk}}{f_{h,1,k}\, d\, t_1^2}} - 1\right] + \dfrac{F_{ax,Rk}}{4} & \text{(g)} \\ 2{,}3\sqrt{M_{y,Rk}\, f_{h,1,k}\, d} + \dfrac{F_{ax,Rk}}{4} & \text{(h)} \end{cases}$$
Characteristic embedment strength	$f_{h,k} = 0{,}082(1 - 0{,}01d) \cdot \rho_k$
	$f_{h,k}$ 30,31 N/mm2

		$f_{h,d}$	20,98 N/mm2
Characteristic fastener yield moment	$M_{y,Rk} = 0.3 \cdot f_{u,k} \cdot d^{2.6}$		
		$M_{y,Rk}$	324282 Nmm
		$M_{y,d}$	294802 Nmm
		f	48678 N
		g	22981 N
		h	22881 N
		$F_{v,Rd}$	22881 N
Required number of fasteners	$n_{required} = \dfrac{N_d}{F_{V,Rd}}$		
		n_{req}	3,2
		n_{ef}	3,2
Design load-carrying capacity of the joint	$R_{d,joint} = n * F_{V,Rd} \geq N_d$		
		$R_{d,joint}$	160,2 kN
Minimum spacings and distances			
Spacing parallel to the grain	$a_1 = (3 + 2 \cdot \cos\alpha)d$		
		a_1	80 mm
Spacing perpendicular to the grain	$a_2 = 3d$		
		a_2	48 mm
End distance (loaded end)	$a_{3,t} = 7d \ (\geq 80mm)$		
		$a_{3,t}$	112 mm
End distance edge (unloaded edge)	$\alpha_{4,c} = 3d$		
		$a_{4,c}$	48 mm
Serviceability limit state design			
Fser per shear plane per dowel		$F_{ser,c}$	8 kN
Stiffness modulus of fastener	$K_{ser} = \rho_m^{1.5} \cdot \dfrac{d}{23}$		
		K_{ser}	6421 N/mm
		K_{ser}	12841 N/mm
Stiffness modulus of joint	$K_{ser,connection} = n \cdot K_{ser}$		
		$K_{ser,joint,dowels}$	89887 N/mm
Instantaneous slip	$u_{inst} = \dfrac{F_{ser}}{K_{ser}}$		
		u_{inst}	0,7 mm
Final joint slip	$u_{fin} = u_{inst}\sqrt{(1+k_{def,1})(1+k_{def,2})}$		
		u_{fin}	0,8 mm

1.2 Check shear strength (perpendicular to grain)	
Characteristic load-carrying capacity (for central plate double shear connection)	$F_{v,Rk} = \min \begin{cases} f_{h,1,k}\, t_1\, d & \text{(f)} \\ f_{h,1,k}\, t_1\, d \left[\sqrt{2 + \dfrac{4M_{y,Rk}}{f_{h,1,k}\, d\, t_1^2}} - 1 \right] + \dfrac{F_{ax,Rk}}{4} & \text{(g)} \\ 2,3\sqrt{M_{y,Rk}\, f_{h,1,k}\, d} + \dfrac{F_{ax,Rk}}{4} & \text{(h)} \end{cases}$
Characteristic embedment strength	$f_{h,k} = 0.082(1 - 0.01 \cdot d) \cdot \rho_k$

	$f_{h,\alpha,k} = \dfrac{f_{h,0,k}}{k_{90}\sin^2\alpha + \cos^2\alpha}$	
	k_{90}	1,54
	$f_{h,0,k}$	30,31 N/mm2
	$f_{h,90,k}$	19,68 N/mm2
	$f_{h,90,d}$	13,62 N/mm2
Characteristic fastener yield moment	$M_{y,Rk}$	324282 Nmm
	$M_{y,d}$	294802 Nmm
	f	31609 N
	g	15881 N
	h	18438 N
	$F_{v,Rd}$	15881 N
Required number of fasteners	$n_{required} = \dfrac{N_d}{F_{V,Rd}}$	
	n_{req}	6,7
Design load-carrying capacity of the joint	$R_{d,joint} = n * F_{V,Rd} \geq N_d$	
	$R_{d,joint}$	111,2 kN
Minimum spacings and distances		
Spacing parallel to the grain	$a_1 = (3 + 2\cdot\cos\alpha)d$	
	a_1	48 mm
Spacing perpendicular to the grain	$a_2 = 3d$	
	a_2	48 mm
End distance (unloaded end)	$a_{3,c} = (1 + 6\sin\alpha)d$	
	$a_{3,c}$	112 mm
End distance edge (loaded edge)	$a_{4,t} = (2 + 2\sin\alpha)d \ (\geq 3d)$	
	$a_{4,t}$	64 mm
Serviceability limit state design		
Fser per shear plane per dowel	$F_{ser,v}$	6 kN
Stiffness modulus of fastener per shear plane	$K_{ser} = \rho_m^{1.5}\cdot\dfrac{d}{23}$	
	K_{ser}	7384 N/mm
Doubled slip modulus for steel-timber connection	K_{ser}	14767 N/mm
Stiffness modulus of joint	$K_{ser,connection} = n\cdot K_{ser}$	
	$K_{ser,joint,dowels}$	51685 N/mm
Instantaneous slip	$u_{inst} = \dfrac{F_{ser}}{K_{ser}}$	
	u_{inst}	0,4 mm
Final joint slip	$u_{fin} = u_{inst}\sqrt{(1+k_{def,1})(1+k_{def,2})}$	
	u_{fin}	0,5 mm

2. Check load-carrying capacity screws type connection		
Screw type connection		
Connection, steel plate to column		
Screw - LBS Rothoblaas		
nominal diameter of screw	d_1	7 mm
length of screw	l	70 mm
effective length of screw	l_{ef}	66 mm
density of timber	ρ_k	440 kg/m3
number of screws	n	24
thickness steel plate	t	10 mm
headside thickness of timber	t_1	70 mm
kdef permanent for service class 1	k_{def}	0,6
kdef short-term for service class 1	k_{def}	0,9
characteristic yield moment	$M_{y,k}$	5417 Nmm
characteristic head pull-through parameter	$f_{head,k}$	10,5 N/mm2
characteristic tensile strenght fastener	$f_{u,k}$	790 N/mm2

2.1 Check axial capacity screws
Check:
Withdrawal failure
Pull through of the head
Tensile failure of the screw
Group effect (neff number of effective fasteners)

Axially loaded screws		
Characteristic withdrawal strenght	$f_{ax,k} = 3,6 \times 10^{-3} \rho_k^{1,5}$	
	$f_{ax,k}$	33,2 N/mm2
Characteristic withdrawal capacity for single screw	$F_{ax,\alpha,Rk} = (\pi d l_{ef})^{0.8} f_{ax,\alpha,k}$	
	$F_{ax,90,Rk}$	11 kN
	$F_{ax,Rd}$	8 kN
Required number of fasteners	$n_{required} = \dfrac{N_{t,d}}{F_{ax,90,Rd}}$	
	n_{req}	9,4
Group effect		
Effective number of screws	n_{ef}	17
Resistance of joint	$R_{d,joint} = n_{ef} \cdot F_{ax,Rd}$	
	$R_{d,joint}$	136 kN
Check pull-through of the head	$f_{t,Rd} = \dfrac{N_{t,d}}{n} \leq f_{head,d}$	
	$f_{head,d}$	10 N/mm2
	$f_{t,Rd}$	3,0 N/mm2
Check tensile failure screw	$N_{t,d} \leq N_{t,Rd}$	
	$f_{u,d}$	718 N/mm2
	$A_{fasteners}$	924 mm2
	$N_{t,Rd}$	663 kN

Minimum spacing and edge distance screws		
Screws driven at right angle to grain		
Minimum spacing	a_1	28 mm

Minimum edge distance	a3	28 mm

2.2 Check lateral capacity screws		
Thickness steel plate	t	15 mm
Characteristic load-carrying capacity (for thick steel plate single shear connection) Rope effect is 100%	$$F_{v,Rk} = \min \begin{cases} f_{h,k}\, t_1\, d \left[\sqrt{2 + \dfrac{4 M_{y,Rk}}{f_{h,k}\, d\, t_1^2}} - 1 \right] + \dfrac{F_{ax,Rk}}{4} & (c) \\ 2,3 \sqrt{M_{y,Rk}\, f_{h,k}\, d} + \dfrac{F_{ax,Rk}}{4} & (d) \\ f_{h,k}\, t_1\, d & (e) \end{cases}$$	
Characteristic embedment strength	$f_{h,k} = 0.082(1 - 0.01 \cdot d) \cdot \rho_k$	
	fh,d	23,2 N/mm2
Characteristic fastener yield moment	$M_{y,Rk} = 0.3 \cdot f_u \cdot d^{2.6}$	
	My,Rk	37325 Nmm
	My,Rd	33932 Nmm
	c	5388 N
	d	5668 N
	e	11383 N
Design load-carrying capacity	Fv,Rd	5388 N
Required number of fasteners	$$n_{required} = \frac{N_d}{F_{V,Rd}}$$	
	nreq	20
Effective diameter screw	def	7,7 mm
Effective number of fasteners	$n_{ef} = n^{k_{ef}}$	
	kef	1
	nef	20
Design load carrying capacity of the joint	Rd,joint	129 kN

2.3 Combined laterally and axially loaded screws		
	$$\left(\frac{F_{ax,Ed}}{F_{ax,Rd}} \right)^2 + \left(\frac{F_{v,Ed}}{F_{v,Rd}} \right)^2 \le 1$$	
	UC	0,96

3. Check splitting capacity		
Design splitting capacity	$$F_{90,Rd} = 14 \cdot b \cdot w \cdot \sqrt{\frac{h_e}{(1 - \frac{h_e}{h})}}$$ $$F_{v,Ed} \le F_{90,Rd}$$	
Length from edge till furthest fastener	he	436 mm
Modification factor	w	1
Height of element	h	500 mm
Width	b	300 mm
	F90,Rd	245,1 kN

4. Check strength steel plate		
Characteristic yield strenght	fyk	355 N/mm2
Design yield strength	fyd	323 N/mm2
Surface area of steel plate	Asteelplate	3000 mm2
Design yield strength steel plate	$N_{t,d} \le N_{y,Rd,steelplate}$	
	Ny,Rd	968 kN

B.6.2. Column-to-column design

Connection: column-column detail	column splice design see EC3-1-8 (6.2.7)

Input parameters		
Column	1200x1200	mm2
Material	Glulam32h	
Bolts	M24	
Head plate	S355	

Axial forces for load combination:	$ULS\_STR\_8\_1.32 \cdot G + 1.65 \cdot Q_{k,wind} + 1,65(0,5 \cdot Q_{k,v,offices} + 0,25 \cdot Q_{k,v,JT})$
Elevation 6	
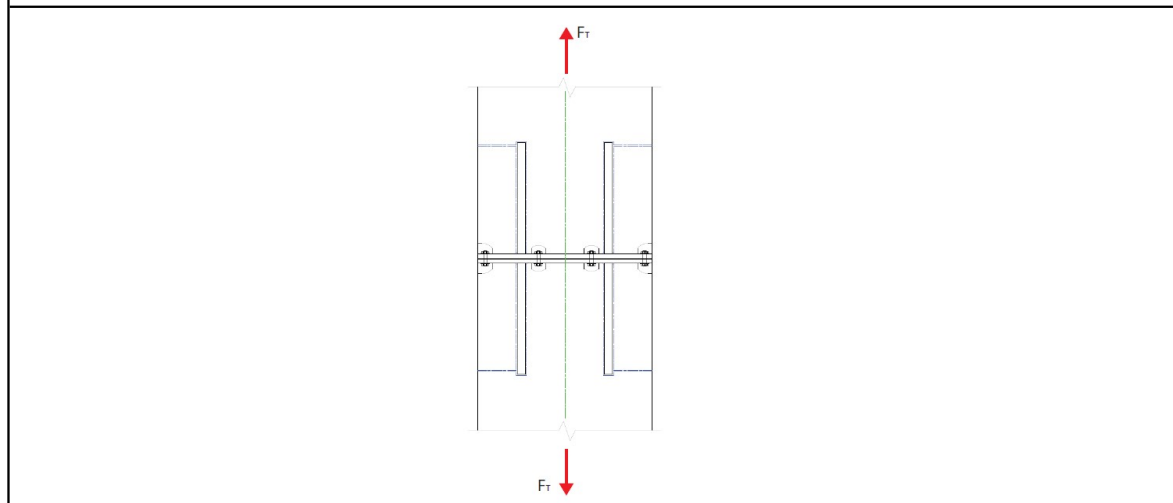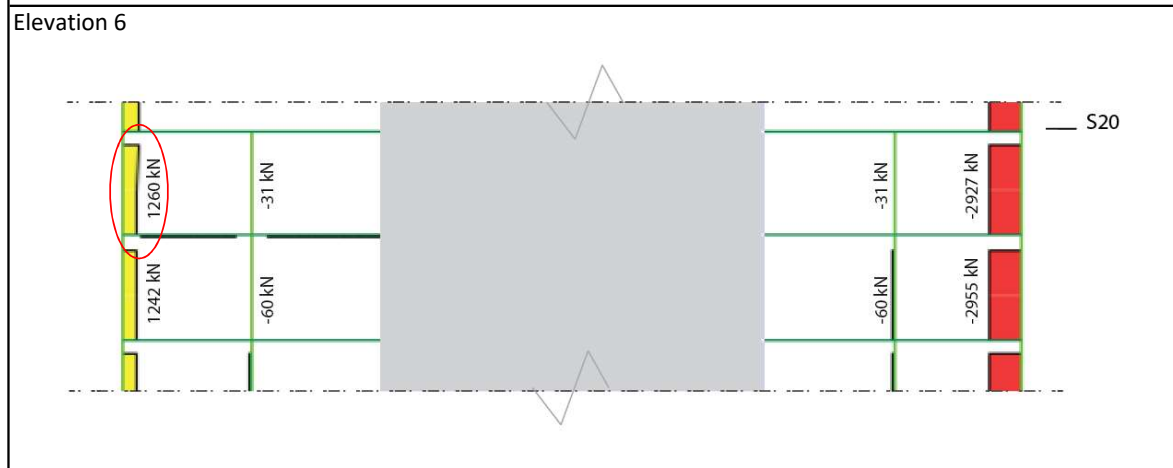
Column C28 at storey level 19		
Design tension force	$N_{t,d}$	1260 kN
Column C1 at storey level 1		
Design compression force	$N_{c,d}$	21171 kN

1. Check load-carrying capacity glued-in rod connection		
Glued-in rods		
diameter of fastener	d	56 mm
density of timber	ρk	480 kg/m3
number of bolts	n	4
thickness steel plate	t1	45 mm

characteristic tensile strenght fastener	fu,k	800 N/mm2
characteristic tensile strenght GLT	ft,0,k	24 N/mm2
characteristic compressive strength GLT	fc,0,k	29 N/mm2
characteristic bending strength GLT	fm,k	32 N/mm2

1.1 Check tension strength (parallel to grain)

Strength of glued-in rod in axial dir.	$F_{ax,Rk} = f_{ws} \cdot \rho_k \cdot d \cdot \sqrt{l_g}$	
embedment length of rod	lg	800 mm
strength parameter (for polyurethane adhesives)	fws	0,65 N/mm
diameter of rod	d	56 mm
	$F_{ax,Rk}$	494,2 kN

Design tensile strength	$F_{t,Rd} = k_{mod} \cdot \dfrac{F_{ax,Rk}}{\gamma_M}$	
	kmod	0,9
	γm	1,25
	$F_{t,Rd}$	355,8 kN

Design tensile strength rod		
	As	2463 mm2
	Ft,Rd	1576 kN

number of rods required	$n = \dfrac{N_{t,d}}{F_{t,Rd}}$	
	Nt,d	1260 kN
	nreq	3,54
	n	4
Total design tensile strength	Ft,Rd,total	1423 kN
	UC	0,89

Tensile stress in effective area	$\sigma_{t,0,d} = \dfrac{N_{t,d}/4}{A_w} \leq f_{t,0,d}$	
	Aw	40000 mm2
	$\sigma_{t,0,d}$	7,9 N/mm2
	$f_{t,0,d}$	17,3 N/mm2
	UC	0,5

1.2 Check compression strength (parallel to grain)

	$\sigma_{c,0,d} \leq f_{c,0,d}$	
design compressive stress	$\sigma_{c,0,d}$	14,7 N/mm2
design compressive strength	$f_{c,0,d}$	20,9 N/mm2
UC		0,70

1.3 Check lateral strength glued-in rods

Load carrying capacity per rod	$F_{v,Rk} = \left(\sqrt{e^2 + \dfrac{4M_{y,Rk}}{df_{h,k}}} - e \right) df_{h,k}$	
eccentricity	e	20 mm
characteristic fastener yield moment	$M_{y,Rk} = 0.3 \cdot f_{u,k} \cdot d^{2.6}$	
	My,Rk	8423646 Nmm
characteristic embedment strength	$f_{h,k} = (0.0023 + 0.75d^{-1.5})\rho_k$	
	fh,k	2,0 N/mm2
	Fv,Rk	58,7 kN

Design load carrying capacity per rod	$F_{V,Rd} = k_{mod} \cdot F_{V,Rk} / \gamma_M$	
	Fv,Rd	40,6 kN
Total design load carrying capacity	Fv,Rd,tot	162,6 kN

Minimum spacings and edge distances		
Minimum internal length rod	$l_{min;rod} \geq 10d$	
	lmin	560 mm
Min end distance (loaded end)	$a_{3,t} = 4d$	
	a3,t	224 mm

2. Check load carrying capacity of individual bolts (EC3-1-8 T.3.4)		
diameter of fastener	d	24 mm
number of bolts	n	12
thickness steel plate	t1	45 mm
characteristic tensile strenght fastener	fu,k	800 N/mm2

2.1 Tension resistance bolts		
	$F_{t,Rd} = k_2 \cdot f_{u,b} \cdot \dfrac{A_s}{\gamma_{M2}}$	
factor for countersunk bolt	k2	0,63
ultimate tensile strength	fu,b	800 N/mm2
tensile stress area of bolt	As	452,4 mm2
Material factor	ɣm2	1,25
Design tension resistance	Ft,Rd	182,4 kN
Design tension force	Nt,d	105,0 kN
	UC	0,58

2.2 Shear resistance bolts		
	$F_{v,Rd} = 0.6 \cdot f_{u,b} \cdot \dfrac{A}{\gamma_{M2}}$	
Gross area bolt	A	452,4 mm2
Design shear resistance	Fv,Rd	173,7 kN

2.3 Bearing resistance		
	$F_{b,Rd} = k_1 \cdot \alpha_b \cdot f_u \cdot \dfrac{dt}{\gamma_{M2}}$	
ultimate tensile strength plate	fu	470 N/mm2
factor for edge bolt	$k_1 = \min\left(2.8\dfrac{e_2}{d_0} - 1.7; 2.5\right)$	
diameter hole	d0	26 mm
edge distance	e2	40 mm
	k1	2,5
factor for end bolt	$\alpha_b = \min\left(\dfrac{e_1}{3d_0} ; \dfrac{f_{u,b}}{f_u} ; 1.0\right)$	
	e1	40 mm
	αb	0,51
Design bearing resistance per bolt	Fb,Rd	520,6 kN

2.4 Punching shear resistance		
	$B_{p,Rd} = 0.6\pi d_m t_p f_u / \gamma_{M2}$	
Nominal diameter bolt	dm	24 mm
Thickness plate	tp	20 mm
ultimate tensile strength plate	fu	470 N/mm2
	Bp,Rd	340,2 kN
Inertial axial force in the bolt	Nb,d	105,0 kN
	UC	0,3

3. Check load carrying capacity head plates		
Equivalent T-stub in tension (6.2.4)		
Steel plate thickness	tp	45 mm
Yield strength	fy	355 N/mm2
Bolt elongation length	Lb	65 mm

Effective lengths		
	e	50 mm
	e1	50 mm
	rc	5 mm
	p	367 mm
	m	118 mm
	n	50 mm
Individual end bolt-row	leff,cp	471 mm
	leff,np	317 mm
Group end-bolt row	leff,cp	467 mm
	leff,np	233,5 mm
Individual inner bolt-row	leff,cp	741 mm
	leff,np	535 mm
Group inner bolt-row	leff,cp	734 mm
	leff,np	367 mm
Mode 1 Individual bolt-row	leff,1	317 mm
Mode 1 Group bolt-row	leff,1	233,5 mm
Mode 2 Individual bolt-row	leff,2	317 mm
Mode 2 Group bolt-row	leff,2	233,5 mm

Design moment of plasticity	Mpl,1,Rd	57015773 Nmm
	Mpl,2,Rd	57015773 Nmm

Mode 1 Design tension resistance		
Prying forces may develop	FT,1,Rd	1933 kN
Mode 2 Design tension resistance		
Prying forces may develop	FT,2,Rd	1004 kN
Mode 3 Design tension resistance		
	FT,3,Rd	1094 kN
Design tension resistance for T-stub	FT,Rd	1004 kN
	Nt,d	630 kN
	UC	0,63

4. Welds rods to head plate		
Directional method (EC3 4.5.3.2)		
Ultimate tensile strength S355	f_u	500 N/mm2
Correlation factor	β_w	0,9
Throat thickness	a	14 mm
Partial safety factor weld	γ_{Mw}	1,25

Weld design for full resistance		
Fillet weld loading by normal connecting member		
Design tension load per rod	F_{Sd}	315000 N
Design tension stress	σ_{Sd}	127,9 N/mm2
	a_{min}	12,5 mm
circumference of rod	c	175,9 mm
height of weld	h_w	10,0 mm
effective area of weld	A_{eff}	1759,3 mm2
Design tension stress	σ_R	179,0 N/mm2
	σ_{max}	314,3 N/mm2
	UC	0,6

6. Serviceability limit state design

Determine the translational stiffness of the connection

Component method EC3-1-8

6.1 Stiffness coefficient of the bolts in tension

		$k_b = 1.6 \dfrac{A_s}{L_b}$
Diameter bolt	d_b	24 mm
Number of bolts	n	12
Area of bolt	A_b	452,4 mm2
Length of bolt	L_b	65 mm
Modulus of Elasticity	E_s	210000 N/mm2
Stiffness coefficient per bolt in mm	k_b	11,1 mm
Translational stiffness per bolt	K_b	2338505 N/mm
Total translational stiffness bolts	$K_{b,tot}$	28062059 N/mm

6.2 Stiffness of the steel plate

		$k_p = \dfrac{0.425 \cdot l_{eff} \cdot t^3}{m^3}$
Steel end-plate thickness	t_p	45 mm
Effective length of plate	l_{eff}	317 mm
	m	118 mm
Stiffness coefficient plate in mm	k_p	7,5 mm
Translational stiffness plate	K_p	1570368 N/mm

6.3 Stiffness of the rods

		$k_r = 1.6 \dfrac{A_s}{L_r}$
Diameter rod	d_r	56 mm
Number of rods	n	4
Area of rod	A_r	2463 mm2
Length of rod	L_r	800 mm
Stiffness coefficient per rod in mm	k_r	5 mm
Translational stiffness per rod	K_r	646540 N/mm
Translational stiffness rods	$K_{r,tot}$	2586159 N/mm

6.4 Total translational stiffness in joint

$\dfrac{1}{K_{tot,joint}} = \dfrac{1}{K_{b,tot,top}} + \dfrac{1}{K_{p,top}} + \dfrac{1}{K_{r,tot,top}} + \dfrac{1}{K_{b,tot,bot}} + \dfrac{1}{K_{p,bot}} + \dfrac{1}{K_{r,tot,bot}}$		
Translational stiffness in joint in top part	$K_{joint,tot,top}$	944196 N/mm
Translational stiffness in joint in bottom part	$K_{joint,tot,bot}$	944196 N/mm
Total translational stiffness in joint	$K_{joint,tot}$	472098 kN/m

Maximum design tensile load	$N_{t,d,max}$	1260 kN
Maximum translational slip	y	2,7 mm

Number of columns in plane		48
Number of storey levels with column splices		19

B.6.3. Beam-to-concrete wall design

Connection: beam-wall detail

Input parameters		
Beam	500x300	mm2
Column	1000x1000	mm2
Material	Glulam32h	
Conceiled beam hanger	Rothoblaas Alumaxi	
Smooth dowels	Rothoblaas STA	
Headed studs		

Beam B8 at story level 2		
Design tension force	Nt,d	73 kN
Design compression force	Nc,d	158 kN
Design shear force	Vd	106 kN
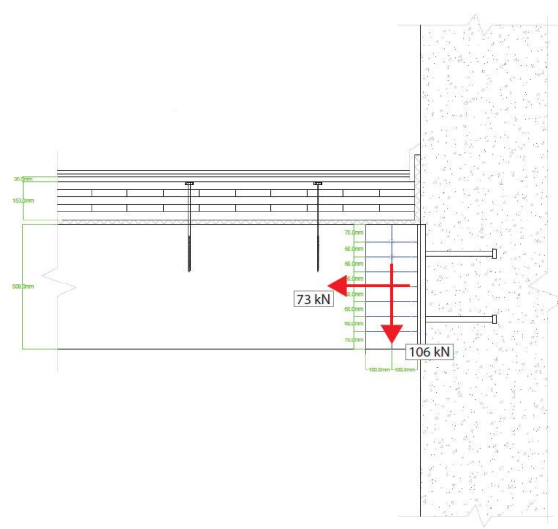
1. Check load-carrying capacity dowel type connection		
Dowel type connection		
diameter of fastener	d	16 mm
density of timber	ρk	440 kg/m3
number of bolts	n	7
thickness steel plate	t2	10 mm
thickness timber	t1	145 mm
kdef for service class 1	kdef	0,6
kmod short-term	kmod	0,9
characteristic tensile strenght fastener	fu,k	800 N/mm2

1.1 Check tension and compression strength (parallel to grain)	
Characteristic load-carrying capacity (for central plate double shear connection)	$$F_{v,Rk} = \min \begin{cases} f_{h,1,k}\, t_1\, d & \text{(f)} \\ f_{h,1,k}\, t_1\, d \left[\sqrt{2 + \dfrac{4M_{y,Rk}}{f_{h,1,k}\, d\, t_1^2}} - 1 \right] + \dfrac{F_{ax,Rk}}{4} & \text{(g)} \\ 2{,}3\sqrt{M_{y,Rk}\, f_{h,1,k}\, d} + \dfrac{F_{ax,Rk}}{4} & \text{(h)} \end{cases}$$
Characteristic embedment strength	$f_{h,k} = 0.082(1 - 0.01d) \cdot \rho_k$
	fh,k 30,31 N/mm2

	fh,d	20,98 N/mm2
Characteristic fastener yield moment	$M_{y,Rk} = 0.3 \cdot f_{u,k} \cdot d^{2.6}$	
	My,Rk	324282 Nmm
	My,d	294802 Nmm
	f	48678 N
	g	22981 N
	h	22881 N
	Fv,Rd	22881 N
Required number of fasteners	$n_{required} = \dfrac{N_d}{F_{V,Rd}}$	
	n_req	3,2
	n_ef	3,2
Design load-carrying capacity of the joint	$R_{d,joint} = n * F_{V,Rd} \geq N_d$	
	Rd,joint	160,2 kN
Minimum spacings and distances		
Spacing parallel to the grain	$a_1 = (3 + 2 \cdot \cos\alpha)d$	
	a1	80 mm
Spacing perpendicular to the grain	$a_2 = 3d$	
	a2	48 mm
End distance (loaded end)	$a_{3,t} = 7d \;(\geq 80mm)$	
	a3,t	112 mm
End distance edge (unloaded edge)	$\alpha_{4,c} = 3d$	
	a4,c	48 mm
Serviceability limit state design		
Fser per shear plane per dowel	Fser,c	8 kN
Stiffness modulus of fastener	$K_{ser} = \rho_m^{1.5} \cdot \dfrac{d}{23}$	
	Kser	6421 N/mm
	Kser	12841 N/mm
Stiffness modulus of joint	$K_{ser,connection} = n \cdot K_{ser}$	
	Kser,joint,dowels	89887 N/mm
Instantaneous slip	$u_{inst} = \dfrac{F_{ser}}{K_{ser}}$	
	u_inst	0,7 mm
Final joint slip	$u_{fin} = u_{inst}\sqrt{(1+k_{def,1})(1+k_{def,2})}$	
	u_fin	0,8 mm

1.2 Check shear strength (perpendicular to grain)	
Characteristic load-carrying capacity (for central plate double shear connection)	$F_{v,Rk} = \min \begin{cases} f_{h,1,k}\, t_1\, d & \text{(f)} \\ f_{h,1,k}\, t_1\, d \left[\sqrt{2 + \dfrac{4M_{y,Rk}}{f_{h,1,k}\, d\, t_1^2}} - 1 \right] + \dfrac{F_{ax,Rk}}{4} & \text{(g)} \\ 2{,}3\sqrt{M_{y,Rk}\, f_{h,1,k}\, d} + \dfrac{F_{ax,Rk}}{4} & \text{(h)} \end{cases}$

Characteristic embedment strength	$f_{h,k} = 0.082(1 - 0.01 \cdot d) \cdot \rho_k$	
	$f_{h,\alpha,k} = \dfrac{f_{h,0,k}}{k_{90} \sin^2 \alpha + \cos^2 \alpha}$	
	k90	1,54
	fh,0,k	30,31 N/mm2
	fh,90,k	19,68 N/mm2
	fh,90,d	13,62 N/mm2
Characteristic fastener yield moment	My,Rk	324282 Nmm
	My,d	294802 Nmm
	f	31609 N
	g	15881 N
	h	18438 N
	Fv,Rd	15881 N
Required number of fasteners	$n_{required} = \dfrac{N_d}{F_{V,Rd}}$	
	n_req	6,7
Design load-carrying capacity of the joint	$R_{d,joint} = n * F_{V,Rd} \geq N_d$	
	Rd,joint	111,2 kN
Minimum spacings and distances		
Spacing parallel to the grain	$a_1 = (3 + 2 \cdot \cos \alpha) d$	
	a1	48 mm
Spacing perpendicular to the grain	$a_2 = 3d$	
	a2	48 mm
End distance (unloaded end)	$a_{3,c} = (1 + 6 \sin \alpha) d$	
	a3,c	112 mm
End distance edge (loaded edge)	$a_{4,t} = (2 + 2 \sin \alpha) d \ (\geq 3d)$	
	a4,t	64 mm
Serviceability limit state design		
Fser per shear plane per dowel	Fser,v	6 kN
Stiffness modulus of fastener per shear plane	$K_{ser} = \rho_m^{1.5} \cdot \dfrac{d}{23}$	
	Kser	7384 N/mm
Doubled slip modulus for steel-timber connection	Kser	14767 N/mm
Stiffness modulus of joint	$K_{ser,connection} = n \cdot K_{ser}$	
	Kser,joint,dowels	51685 N/mm
Instantaneous slip	$u_{inst} = \dfrac{F_{ser}}{K_{ser}}$	
	u_inst	0,4 mm
Final joint slip	$u_{fin} = u_{inst} \sqrt{(1 + k_{def,1})(1 + k_{def,2})}$	
	u_fin	0,5 mm

2. Check load-carrying capacity of headed studs		
Headed stud type connection		
Connection, steel plate to concrete wall		
Nominal diameter of stud	d	22 mm
Diameter of head stud	d_h	35 mm
Length of stud	l	260 mm
Density of concrete	ρ_k	2320 kg/m3
Number of studs	n	4
Thickness steel anchor plate	t	25 mm
Characteristic tensile strenght fastener	$f_{u,k}$	470 N/mm2
Characteristic yield strength fastener	$f_{y,k}$	350 N/mm2

2.1 Check tension resistance studs		
Characterisitic ultimate tensile strength	$f_{u,k}$	470 N/mm2
Characteristic yield strength	$f_{y,k}$	350 N/mm2
Number of studs	n_s	4
Cross-sectional area of fastener	A_s	380 mm2
Partial safety factor	γ_{Mc}	1,5
Tension resistance	$N_{Rd,s}$	476,4 kN

2.2 Check pull-out failure		
Design pull-out resistance		$$N_{Rd,p} = n \cdot \frac{p_{uk}}{\gamma_{Mc}} \cdot A_h$$
Factor for head pressing	p_k	540
Partial safety factor concrete	γ_{Mc}	1,5
Characteristic strength concrete	f_{ck}	45 N/mm2
Cross-sectional area of effective head	A_h	582,0 mm2
Pull-out resistance	$N_{Rd,p}$	838,1 kN

2.3 Check shear resistance studs		
Number of studs	n_s	4
Characteristic ultimate strength	f_{uk}	470 N/mm2
Cross-sectional area of fastener	A_s	380 mm2
Partial safety factor	γ_{M2}	1,25
Shear resistance of studs	$F_{v,Rd}$	343,0 kN

2.4 Check combination tension and shear		
Design shear force	V_{Ed}	106 kN
Design shear resistance	V_{Rd}	343,0 kN
Design tension force	$N_{t,Ed}$	73 kN
Design tension resistance	$N_{Rd,s}$	476,4 kN
	UC	0,12

3. Check splitting capacity		
Design splitting capacity		$$F_{90,Rd} = 14 \cdot b \cdot w \cdot \sqrt{\frac{h_e}{(1 - \frac{h_e}{h})}}$$ $$F_{v,Ed} \leq F_{90,Rd}$$
Length from edge till furthest fastener	h_e	436 mm

Modification factor	w	1	
Height of element	h	500	mm
Width	b	300	mm
	$F_{90,Rd}$	245,1	kN

4. Check strength steel plate			
Characteristic yield strenght	f_{yk}	355	N/mm2
Design yield strength	f_{yd}	323	N/mm2
Surface area of steel plate	$A_{steelplate}$	3000	mm2
Design yield strength steel plate	$N_{t,d} \le N_{y,Rd,steelplate}$		
	$N_{y,Rd}$	968	kN

B.6.4. Outrigger truss design

Outrigger-truss design

Axial forces for load combination:	$ULS\_STR\_8\_1.32 \cdot G + 1.65 \cdot Q_{k,wind} + 1,65(0,5 \cdot Q_{k,v,offices} + 0,25 \cdot Q_{k,v,JT})$
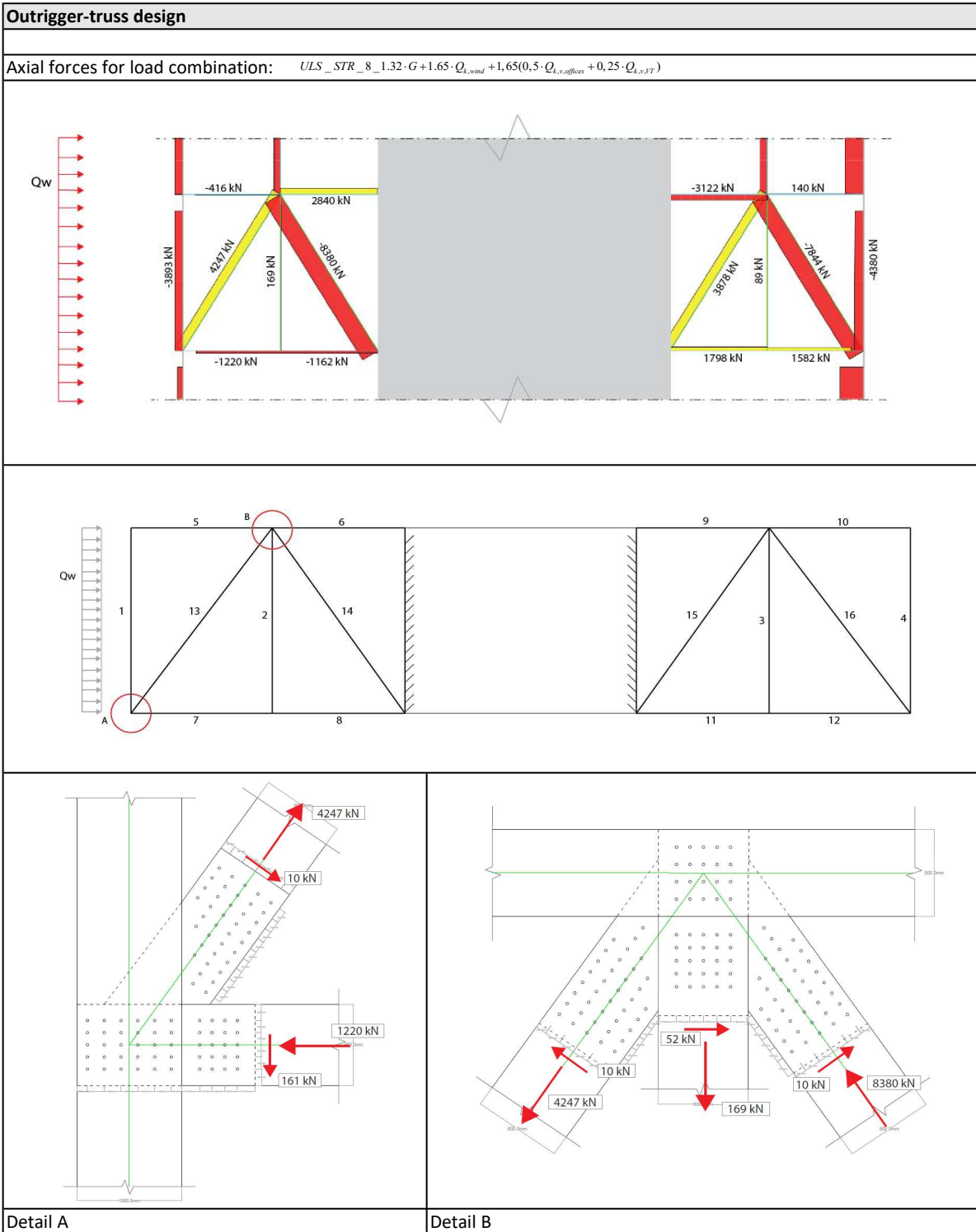
Detail A

Detail B

Connection: outrigger detail A

Beam-to-column

Input parameters			
Beam		800x800	mm2
Column		1000x1000	mm2
Material	LVL-Kerto-S		
Smooth dowels	Rothoblaas STA		
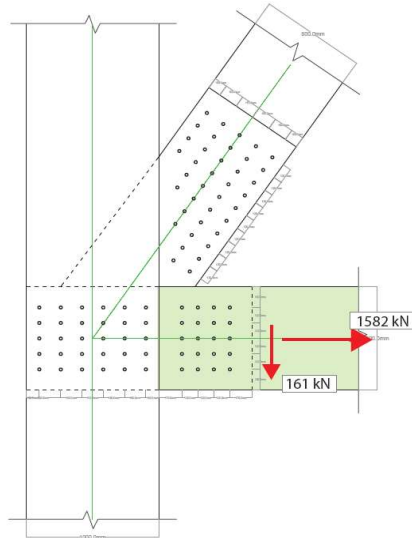
Beam-column element 7		
Beam B121 at story 20		
Design tension force	Nt,d	1582 kN
Design shear force y	Vy,d	161 kN

1. Check load-carrying capacity dowel type connection		
Dowel type connection		
diameter of fastener	d	24 mm
density of timber	ρk	480 kg/m3
number of fasteners	n	20
number of rows	n_rows	5
thickness steel plate	t2	25 mm
thickness timber	t1	250 mm
kdef for service class 1	kdef	0,6
kmod short-term	kmod	0,9
characteristic tensile strenght fastener	fu,k	1040 N/mm2

1.1 Check tension and compression strength (parallel to grain)		
Characteristic load-carrying capacity (for thick plate single shear connection)	$F_{v,Rk} = \min \begin{cases} f_{h,k}\, t_1\, d \left[\sqrt{2 + \dfrac{4 M_{y,Rk}}{f_{h,k}\, d\, t_1^2}} - 1 \right] + \dfrac{F_{ax,Rk}}{4} & (c) \\ 2,3 \sqrt{M_{y,Rk}\, f_{h,k}\, d} + \dfrac{F_{ax,Rk}}{4} & (d) \\ f_{h,k}\, t_1\, d & (e) \end{cases}$	
Characteristic embedment strength	$f_{h,k} = 0.082 (1 - 0.01 d) \cdot \rho_k$	
	fh,k	29,91 N/mm2

	fh,d	20,71	N/mm2
Characteristic fastener yield moment	$M_{y,Rk} = 0.3 \cdot f_{u,k} \cdot d^{2.6}$		
	My,Rk	1209773	Nmm
	My,d	1099793	Nmm
	c	57584	N
	d	53774	N
	e	124256	N
Design shear capacity per dowel per shear plane	Fv,Rd	53774	N
Design shear capacity per dowel	Fv,Rd,total	215096	N
Group effect	$n_{ef} = \min \left\{ \begin{array}{l} n \\ n^{0.9} \sqrt[3]{\frac{a_1}{13d}} \end{array} \right.$		
bolts per row	n	4,0	
	n_ef	2,7	
Effective design shear capacity per row	Fv,ef,Rd,row	590	kN
Required number of rows	$n_{required} = \dfrac{N_d}{F_{V,Rd}}$		
	n_req_rows	2,7	
Required number of fasteners	n_req	10,7	
Design load-carrying capacity of the joint	$R_{d,joint} = n * F_{V,Rd} \geq N_d$		
	Rd,joint	2949	kN
	UC	0,54	
Minimum spacings and distances			
spacing parallel to the grain	$a_1 = (3 + 2 \cdot \cos \alpha)d$		
	a1	120	mm
spacing perpendicular to the grain	$a_2 = 3d$		
	a2	72	mm
end distance (loaded end)	$a_{3,t} = 7d \ (\geq 80mm)$		
	a3,t	168	mm
end distance edge (unloaded edge)	$\alpha_{4,c} = 3d$		
	a4,c	72	mm
Serviceability limit state design			
Fser per shear plane per dowel	Fser,c	15	kN
Stiffness modulus of fastener	$K_{ser} = \rho_m^{1.5} \cdot \dfrac{d}{23}$		
	Kser	10974	N/mm
Doubled Kser for steel-timber connection	Kser	21947	N/mm
Instantaneous slip	$u_{inst} = \dfrac{F_{ser}}{K_{ser}}$		
	u_inst	0,7	mm
Final joint slip	$u_{fin} = u_{inst} \sqrt{(1 + k_{def,1})(1 + k_{def,2})}$		
	u_fin	0,8	mm
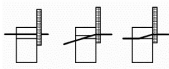
1.2 Check shear strength (perpendicular to grain)	
Characteristic load-carrying capacity (for thick plate single shear connection)	$F_{v,Rk} = \min \begin{cases} f_{h,k}\, t_1\, d \left[\sqrt{2 + \dfrac{4M_{y,Rk}}{f_{h,k}\, d\, t_1^2}} - 1 \right] + \dfrac{F_{ax,Rk}}{4} & (c) \\[2ex] 2,3 \sqrt{M_{y,Rk}\, f_{h,k}\, d} + \dfrac{F_{ax,Rk}}{4} & (d) \\[2ex] f_{h,k}\, t_1\, d & (e) \end{cases}$

Characteristic embedment strength	$f_{h,k} = 0.082(1 - 0.01 \cdot d) \cdot \rho_k \cdot \dfrac{k_{mod}}{\gamma_M}$		
	$f_{h,\alpha,k} = \dfrac{f_{h,0,k}}{k_{90} \sin^2 \alpha + \cos^2 \alpha}$		
	k90	1,66	
	fh,0,k	29,91	N/mm2
	fh,90,k	18,02	N/mm2
	fh,90,d	12,48	N/mm2
Characteristic fastener yield moment	My,Rk	1209773	Nmm
	My,d	1099793	Nmm
	c	37054	N
	d	41737	N
	e	74853	N
Design shear capacity per dowel per shear plane	Fv,Rd	37054	N
Design shear capacity per dowel	Fv,Rd,total	148215	N
Required number of fasteners	$n_{required} = \dfrac{N_d}{F_{V,Rd}}$		
	n_req	1,1	
Design load-carrying capacity of the joint	$R_{d,joint} = n * F_{V,Rd} \geq N_d$		
	Rd,joint	2964	kN
	UC	0,05	

1.3 Combined laterally and axially loaded connection	$\left(\dfrac{F_{ax,Ed}}{F_{ax,Rd}}\right) + \left(\dfrac{F_{v,Ed}}{F_{v,Rd}}\right) \leq 1$		
	UC	0,59	OK

Minimum spacings and distances			
spacing parallel to the grain	$a_1 = (3 + 2 \cdot \cos \alpha)d$		
	a1	72	mm
spacing perpendicular to the grain	$a_2 = 3d$		
	a2	72	mm
end distance (unloaded end)	$a_{3,c} = (1 + 6 \sin \alpha)d$		
	a3,c	168	mm
end distance edge (loaded edge)	$a_{4,t} = (2 + 2 \sin \alpha)d \ (\geq 3d)$		
	a4,t	96	mm

2. Check strength steel plates			
characteristic yield strenght	fyk	355	N/mm2
design yield strength	fyd	323	N/mm2
surface area of steel plates	Asteelplate	40000	mm2
	$N_{t,d} \leq N_{y,Rd,steelplate}$		
	Ny,Rd	12909	kN

Connection: outrigger detail A

Diagonal-to-column

Input parameters			
Diagonal		800x800	mm2
Column		1000x1000	mm2
Material	LVL-Kerto-S		
Smooth dowels	Rothoblaas STA		
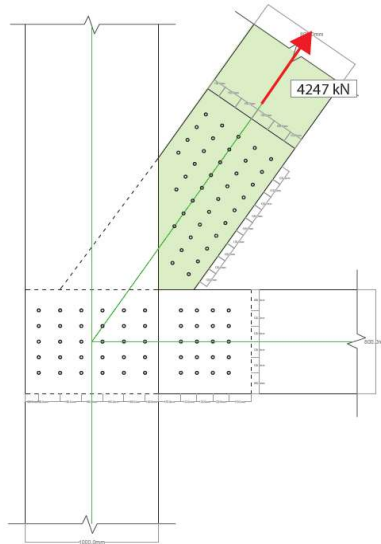
Diagonal element 13		
Diagonal D25 at story 20		
Design tension force	Nt,d	4247 kN

The self-weight of the beam will be neglected.

1. Check load-carrying capacity dowel type connection		
Dowel type connection		
diameter of fastener	d	24 mm
density of timber	ρk	480 kg/m3
number of fasteners	n	38
number of rows	n_rows	5
thickness steel plate	t2	25 mm
thickness timber	t1	250 mm
kdef for service class 1	kdef	0,6
kmod short-term	kmod	0,9
characteristic tensile strenght fastener	fu,k	1040 N/mm2

1.1 Check tension and compression strength (parallel to grain)		
Characteristic load-carrying capacity (for thick plate single shear connection)	$F_{v,Rk} = \min \begin{cases} f_{h,k}\, t_1\, d \left[\sqrt{2 + \dfrac{4 M_{y,Rk}}{f_{h,k}\, d\, t_1^2}} - 1 \right] + \dfrac{F_{ax,Rk}}{4} & \text{(c)} \\[2ex] 2,3 \sqrt{M_{y,Rk}\, f_{h,k}\, d} + \dfrac{F_{ax,Rk}}{4} & \text{(d)} \\[2ex] f_{h,k}\, t_1\, d & \text{(e)} \end{cases}$	
Characteristic embedment strength	fh,k	29,91 N/mm2
	fh,d	20,71 N/mm2

Characteristic fastener yield moment	My,Rk	1209773 Nmm
	My,d	1099793 Nmm
	c	57584 N
	d	53774 N
	e	124256 N
Design shear capacity per dowel per shear plane	Fv,Rd	53774 N
Design shear capacity per dowel	Fv,Rd,total	215096 N
Group effect	$n_{ef} = \min \begin{cases} n \\ n^{0.9} \sqrt[4]{\dfrac{a_1}{13d}} \end{cases}$	
bolts per row	n	7,6
	n_ef	4,9
Effective design shear capacity per row	Fv,ef,Rd,row	1051 kN
Required number of rows	$n_{required} = \dfrac{N_d}{F_{V,Rd}}$	
	n_req_rows	4,0
Required number of fasteners	n_req	30,7
Design load-carrying capacity of the joint	$R_{d,joint} = n * F_{V,Rd} \geq N_d$	
	Rd,joint	5255 kN
	UC	0,81
Minimum spacings and distances		
spacing parallel to the grain	$a_1 = (3 + 2 \cdot \cos\alpha)d$	
	a1	120 mm
spacing perpendicular to the grain	$a_2 = 3d$	
	a2	72 mm
end distance (loaded end)	$a_{3,t} = 7d \ (\geq 80mm)$	
	a3,t	168 mm
end distance edge (unloaded edge)	$\alpha_{4,c} = 3d$	
	a4,c	72 mm
Serviceability limit state design		
Fser per shear plane per dowel	Fser,c	21 kN
Stiffness modulus of fastener	$K_{ser} = \rho_m^{1.5} \cdot \dfrac{d}{23}$	
	Kser	10974 N/mm
Doubled Kser for steel-timber connection	Kser	21947 N/mm
Instantaneous slip	$u_{inst} = \dfrac{F_{ser}}{K_{ser}}$	
	u_inst	0,9 mm
Final joint slip	$u_{fin} = u_{inst} \sqrt{(1 + k_{def,1})(1 + k_{def,2})}$	
	u_fin	1,2 mm

Connection: outrigger detail A

Column

Input parameters			
Diagonal		800x800	mm2
Column		1000x1000	mm2
Material	Glulam32h		
Smooth dowels	Rothoblaas STA		
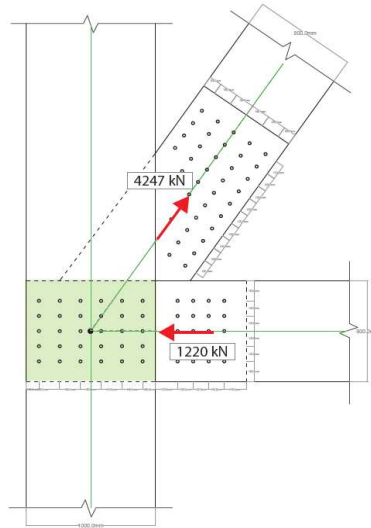
Column element 1			
Column C41 at story level 20			
Tension force in diagonal	Nt,diagonal	4247	kN
Compression force in beam	Nc,beam	1220	kN
Angle between diagonal and beam	α	53	degrees

1. Check load-carrying capacity dowel type connection			
Dowel type connection			
diameter of fastener	d	24	mm
density of timber	ρk	480	kg/m3
number of fasteners	n	30	
number of rows	n_rows	5	
thickness steel plate	t2	25	mm
thickness timber	t1	250	mm
kdef for service class 1	kdef	0,6	
kmod short-term	kmod	0,9	
characteristic tensile strenght fastener	fu,k	1040	N/mm2

1.1 Check tension strength at an angle to the grain	
Characteristic load-carrying capacity (for thick plate single shear connection)	$$F_{v,Rk} = \min \begin{cases} f_{h,k}\, t_1\, d \left[\sqrt{2 + \dfrac{4M_{y,Rk}}{f_{h,k}\, d\, t_1^{2}}} - 1 \right] + \dfrac{F_{ax,Rk}}{4} & \text{(c)} \\ 2,3\sqrt{M_{y,Rk}\, f_{h,k}\, d} + \dfrac{F_{ax,Rk}}{4} & \text{(d)} \\ f_{h,k}\, t_1\, d & \text{(e)} \end{cases}$$

Characteristic embedment strength	$f_{h,\alpha,k} = \dfrac{f_{h,0,k}}{k_{90}\sin^2\alpha + \cos^2\alpha}$	
	k90	1,66
	fh,0,k	29,91 N/mm2
	fh,α,k	21,05 N/mm2
	fh,α,d	14,57 N/mm2
Characteristic fastener yield moment	My,Rk	1209773 Nmm
	My,d	1099793 Nmm
	c	42293 N
	d	45111 N
	e	87445 N
Design shear capacity per dowel per shear plane	Fv,Rd	42293 N
Design shear capacity per dowel	Fv,Rd,total	169173 N
Required number of fasteners	$n_{required} = \dfrac{N_d \cdot}{F_{V,Rd}}$	
	n_req	7,2
Design load-carrying capacity of the joint	$R_{d,joint} = n * F_{V,Rd} \geq N_d$	
	Rd,joint	5075 kN
	UC	0,84
Minimum spacings and distances		
spacing parallel to the grain	$a_1 = (3 + 2\cdot\cos\alpha)d$	
	a1	72 mm
spacing perpendicular to the grain	$a_2 = 3d$	
	a2	72 mm
end distance (unloaded end)	$a_{3,c} = (1 + 6\sin\alpha)d$	
	a3,c	168 mm
end distance edge (loaded edge)	$a_{4,t} = (2 + 2\sin\alpha)d \ (\geq 3d)$	
	a4,t	96 mm
Serviceability limit state design		
Fser per shear plane per dowel	Fser,v	8 kN
Stiffness modulus of fastener	$K_{ser} = \rho_m^{1.5}\cdot\dfrac{d}{23}$	
	Kser	10974 N/mm
Doubles Kser for steel-timber connection	Kser	21947 N/mm
Stiffness modulus of joint	$K_{ser,connection} = n\cdot K_{ser}$	
	Kser,joint,dowels	329205 N/mm
Instantaneous slip	$u_{inst} = \dfrac{F_{ser}}{K_{ser}}$	
	u_inst	0,3 mm
Final joint slip	$u_{fin} = u_{inst}\sqrt{(1+k_{def,1})(1+k_{def,2})}$	
	u_fin	0,4 mm

3. Check splitting capacity		
Design splitting capacity	$F_{90,Rd} = 14\cdot b\cdot w\cdot\sqrt{\dfrac{h_e}{(1-\dfrac{h_e}{h})}}$ $F_{v,Ed} \leq F_{90,Rd}$	
Length from edge till furthest fastener	he	1100 mm
Modification factor	w	1

Height of element	h	1200	mm
Width	b	1000	mm
	$F_{v,Ed}$	1278	kN
	$F_{90,Rd}$	1608	kN

5. Check bearing strength column

	$\sigma_{c,90,d} \leq k_{c,90} \cdot f_{c,90,d}$	
	$k_{c,90}$	1,0
Effective area	A	640000 mm2
Design compression stress perp to grain	$\sigma_{c,90,d}$	1,9 N/mm2
Design compression strength perp to grain	$f_{c,90,d}$	6,0 N/mm2
	UC	0,3

6. Check strength steel plate

Characteristic yield strenght	f_{yk}	355	N/mm2
Design yield strength	f_{yd}	323	N/mm2
Surface area of steel plate	Asteelplate	40000	mm2
Design yield strength steel plate	$N_{t,d} \leq N_{y,Rd,steelplate}$		
	$N_{y,Rd}$	12909	kN

Connection: outrigger detail B

Diagonal

Input parameters			
Diagonal		800x800	mm2
Column		800x800	mm2
Material	LVL-Kerto-S		
Smooth dowels	Rothoblaas STA		
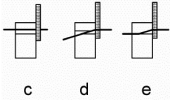
Diagonal element 15			
Diagonal D25 at story 20			
Design tension force	Nt,d	4247	kN
Design shear force y	Vd	10	kN

1. Check load-carrying capacity dowel type connection			
Dowel type connection			
diameter of fastener	d	24	mm
density of timber	ρk	480	kg/m3
number of fasteners	n	38	
number of rows	n_rows	5	
thickness steel plate	t2	25	mm
thickness timber	t1	250	mm
kdef for service class 1	kdef	0,6	
kmod short-term	kmod	0,9	
characteristic tensile strenght fastener	fu,k	1040	N/mm2

1.1 Check tension and compression strength (parallel to grain)

Characteristic load-carrying capacity (for thick plate single shear connection)	$$F_{v,Rk} = \min \begin{cases} f_{h,k}\, t_1\, d \left[\sqrt{2 + \dfrac{4 M_{y,Rk}}{f_{h,k}\, d\, t_1^2}} - 1 \right] + \dfrac{F_{ax,Rk}}{4} \quad (c) \\ 2{,}3 \sqrt{M_{y,Rk}\, f_{h,k}\, d} + \dfrac{F_{ax,Rk}}{4} \quad (d) \\ f_{h,k}\, t_1\, d \quad (e) \end{cases}$$		
Characteristic embedment strength	fh,k	29,91	N/mm2
	fh,d	20,71	N/mm2
Characteristic fastener yield moment	My,Rk	1209773	Nmm
	My,d	1099793	Nmm
	c	57584	N
	d	53774	N
	e	124256	N
Design shear capacity per dowel per shear plane	Fv,Rd	53774	N
Design shear capacity per dowel	Fv,Rd,total	215096	N
Group effect	$$n_{ef} = \min \begin{cases} n \\ n^{0,9} \sqrt[4]{\dfrac{a_1}{13d}} \end{cases}$$		
bolts per row	n	7,6	
	n_ef	4,9	
Effective design shear capacity per row	Fv,ef,Rd,row	1051	kN
Required number of rows	$$n_{required} = \dfrac{N_d}{F_{V,Rd}}$$		
	n_req_rows	4,0	

Required number of fasteners	n_req	30,7
Design load-carrying capacity of the joint	$R_{d,joint} = n * F_{V,Rd} \geq N_d$	
	Rd,joint	**5255** kN

Minimum spacings and distances		
spacing parallel to the grain	$a_1 = (3 + 2 \cdot \cos\alpha)d$	
	a1	120 mm
spacing perpendicular to the grain	$a_2 = 3d$	
	a2	72 mm
end distance (loaded end)	$a_{3,t} = 7d \ (\geq 80mm)$	
	a3,t	168 mm
end distance edge (unloaded edge)	$\alpha_{4,c} = 3d$	
	a4,c	72 mm

Serviceability limit state design		
Fser per shear plane per dowel	Fser,c	21 kN
Stiffness modulus of fastener	$K_{ser} = \rho_m^{1.5} \cdot \dfrac{d}{23}$	
	Kser	10974 N/mm
Doubled Kser for steel-timber connection	Kser	21947 N/mm
Instantaneous slip	$u_{inst} = \dfrac{F_{ser}}{K_{ser}}$	
	u_inst	0,9 mm
Final joint slip	$u_{fin} = u_{inst}\sqrt{(1 + k_{def,1})(1 + k_{def,2})}$	
	u_fin	1,2 mm

1.2 Check shear strength (perpendicular to grain)		
Characteristic load-carrying capacity (for thick plate single shear connection)	$F_{v,Rk} = \min \begin{cases} f_{h,k}\, t_1\, d\left[\sqrt{2 + \dfrac{4M_{y,Rk}}{f_{h,k}\, d\, t_1^2}} - 1\right] + \dfrac{F_{ax,Rk}}{4} & (c) \\ 2,3\sqrt{M_{y,Rk}\, f_{h,k}\, d} + \dfrac{F_{ax,Rk}}{4} & (d) \\ f_{h,k}\, t_1\, d & (e) \end{cases}$	
Characteristic embedment strength	$f_{h,\alpha,k} = \dfrac{f_{h,0,k}}{k_{90}\sin^2\alpha + \cos^2\alpha}$	
	k90	1,66
	fh,0,k	29,91 N/mm2
	fh,90,k	18,02 N/mm2
	fh,90,d	12,48 N/mm2
Characteristic fastener yield moment	My,Rk	1209773 Nmm
	My,d	1099793 Nmm
	c	37054 N
	d	41737 N
	e	74853 N
Design shear capacity per dowel per shear plane	Fv,Rd	37054 N
Design shear capacity per dowel	Fv,Rd,total	148215 N
Required number of fasteners	$n_{required} = \dfrac{N_d}{F_{V,Rd}}$	
	n_req	0,1

Design load-carrying capacity of the joint	$R_{d,joint} = n * F_{V,Rd} \geq N_d$	
	Rd,joint	5632 kN
Minimum spacings and distances		
spacing parallel to the grain	$a_1 = (3 + 2 \cdot \cos \alpha)d$	
	a1	72 mm
spacing perpendicular to the grain	$a_2 = 3d$	
	a2	72 mm
end distance (unloaded end)	$a_{3,c} = (1 + 6\sin \alpha)d$	
	a3,c	168 mm
end distance edge (loaded edge)	$a_{4,t} = (2 + 2\sin \alpha)d \ (\geq 3d)$	
	a4,t	96 mm

2. Check strength steel plates		
characteristic yield strenght	fyk	355 N/mm2
design yield strength	fyd	323 N/mm2
surface area of steel plates	Asteelplate	40000 mm2
	$N_{t,d} \leq N_{y,Rd,steelplate}$	
	Ny,Rd	12909 kN

Connection: outrigger detail B

Beam

Input parameters			
Diagonal		800x800	mm2
Column		800x800	mm2
Material	LVL-Kerto-S		
Smooth dowels	Rothoblaas STA		

Tension force in diagonal 15	Nt,diagonal	4247	kN
Compression force in diagonal 16	Nc,diagonal	-8380	kN
Tension force in column 3	Nc,column	169	kN
Angle between diagonal and beam	α	53	degrees
Horizontal component of force in diagonal 15	x15	2556	kN
Vertical component of force in diagonal 15	y15	3392	kN
Horizontal component of force in diagonal 16	x16	-5043	kN
Vertical component of force in diagonal 16	y16	-6693	kN
Horizontal resultant force	Fx,resultant	2556	kN
Vertical resultant force	Fy,resultant	3561	kN

Beam elements 9 and 10			
Design tension force (horizontal/ parallel to grain)	Nt,d	2556	kN
Design shear force (vertical/ perp to grain)	Vd	3561	kN
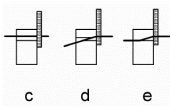
1. Check load-carrying capacity dowel type connection			
Dowel type connection			
diameter of fastener	d	24	mm
density of timber	ρk	480	kg/m3
number of fasteners	n	20	
number of rows	n_rows	5	
thickness steel plate	t2	25	mm
thickness timber	t1	250	mm
kdef for service class 1	kdef	0,6	
kmod short-term	kmod	0,9	
characteristic tensile strenght fastener	fu,k	1040	N/mm2

1.1 Check tension and compression strength (parallel to grain)			
Characteristic load-carrying capacity (for thick plate single shear connection)	$F_{v,Rk} = \min \begin{cases} f_{h,k}\,t_1\,d\left[\sqrt{2+\dfrac{4M_{y,Rk}}{f_{h,k}\,d\,t_1^2}}-1\right]+\dfrac{F_{ax,Rk}}{4} & \text{(c)} \\ 2,3\sqrt{M_{y,Rk}\,f_{h,k}\,d}+\dfrac{F_{ax,Rk}}{4} & \text{(d)} \\ f_{h,k}\,t_1\,d & \text{(e)} \end{cases}$			
Characteristic embedment strength	fh,k	29,91	N/mm2
	fh,d	20,71	N/mm2
Characteristic fastener yield moment	My,Rk	1209773	Nmm
	My,d	1099793	Nmm
	c	57584	N
	d	53774	N
	e	124256	N
Design shear capacity per dowel per shear plane	Fv,Rd	53774	N

Design shear capacity per dowel	Fv,Rd,total	215096 N
Group effect	$n_{ef} = \min \begin{cases} n \\ n^{0,9} \sqrt[4]{\dfrac{a_1}{13d}} \end{cases}$	
bolts per row	n	5,0
	n_ef	3,4
Effective design shear capacity per row	Fv,ef,Rd,row	721 kN
Required number of rows	$n_{required} = \dfrac{N_d}{F_{V,Rd}}$	
	n_req_rows	3,5
	n_req	17,7
Design load-carrying capacity of the joint	$R_{d,joint} = n * F_{V,Rd} \geq N_d$	
	Rd,joint	3605 kN
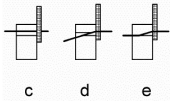
Minimum spacings and distances

spacing parallel to the grain	$a_1 = (3 + 2 \cdot \cos\alpha)d$	
	a1	120 mm
spacing perpendicular to the grain	$a_2 = 3d$	
	a2	72 mm
end distance (loaded end)	$a_{3,t} = 7d \ (\geq 80mm)$	
	a3,t	168 mm
end distance edge (unloaded edge)	$\alpha_{4,c} = 3d$	
	a4,c	72 mm

Serviceability limit state design

Fser per shear plane per dowel	Fser,c	24 kN
Stiffness modulus of fastener	$K_{ser} = \rho_m^{1,5} \cdot \dfrac{d}{23}$	
	Kser	10974 N/mm
Doubled Kser for steel-timber connection	Kser	21947 N/mm
Instantaneous slip	$u_{inst} = \dfrac{F_{ser}}{K_{ser}}$	
	u_inst	1,1 mm
Final joint slip	$u_{fin} = u_{inst}\sqrt{(1+k_{def,1})(1+k_{def,2})}$	
	u_fin	1,4 mm

1.2 Check shear strength (perpendicular to grain)		
Characteristic load-carrying capacity (for thick plate single shear connection)	$F_{v,Rk} = \min \begin{cases} f_{h,k}\,t_1\,d \left[\sqrt{2 + \dfrac{4M_{y,Rk}}{f_{h,k}\,d\,t_1^2}} - 1 \right] + \dfrac{F_{ax,Rk}}{4} & (c) \\ 2,3\sqrt{M_{y,Rk}\,f_{h,k}\,d} + \dfrac{F_{ax,Rk}}{4} & (d) \\ f_{h,k}\,t_1\,d & (e) \end{cases}$	
Characteristic embedment strength	$f_{h,\alpha,k} = \dfrac{f_{h,0,k}}{k_{90}\sin^2\alpha + \cos^2\alpha}$	
	k90	1,66
	fh,0,k	29,91 N/mm2
	fh,90,k	18,02 N/mm2
	fh,90,d	12,48 N/mm2

Characteristic fastener yield moment	My,Rk	1209773 Nmm
	My,d	1099793 Nmm
	c	37054 N
	d	41737 N
	e	74853 N
Design shear capacity per dowel per shear plane	Fv,Rd	37054 N
Design shear capacity per dowel	Fv,Rd,total	148215 N
Required number of fasteners	$n_{required} = \dfrac{N_d}{F_{V,Rd}}$	
	n_req	24,0
Number of dowels including effective dowels from column	neff	35
Design load-carrying capacity of the joint	$R_{d,joint} = n * F_{V,Rd} \geq N_d$	
	Rd,joint	5188 kN
Minimum spacings and distances		
spacing parallel to the grain	$a_1 = (3 + 2 \cdot \cos\alpha)d$	
	a1	72 mm
spacing perpendicular to the grain	$a_2 = 3d$	
	a2	72 mm
end distance (unloaded end)	$a_{3,c} = (1 + 6\sin\alpha)d$	
	a3,c	168 mm
end distance edge (loaded edge)	$a_{4,t} = (2 + 2\sin\alpha)d \ (\geq 3d)$	
	a4,t	96 mm
Serviceability limit state design		
Fser per shear plane per dowel	Fser,v	33 kN
Stiffness modulus of fastener	$K_{ser} = \rho_m^{1.5} \cdot \dfrac{d}{23}$	
	Kser	10974 N/mm
Doubles Kser for steel-timber connection	Kser	21947 N/mm
Stiffness modulus of joint	$K_{ser,connection} = n \cdot K_{ser}$	
	Kser,joint,dowels	219470 N/mm
Instantaneous slip	$u_{inst} = \dfrac{F_{ser}}{K_{ser}}$	
	u_inst	1,5 mm
Final joint slip	$u_{fin} = u_{inst}\sqrt{(1 + k_{def,1})(1 + k_{def,2})}$	
	u_fin	1,9 mm

Connection: outrigger detail B

Column

Input parameters			
Beam		800x800	mm2
Column		1000x1000	mm2
Material	LVL-Kerto-S		
Smooth dowels	Rothoblaas STA		
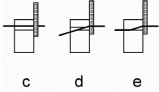
Column element 3			
Design tension force	Nt,d	1444	kN
Design shear force y	Vy,d	1645	kN

1. Check load-carrying capacity dowel type connection
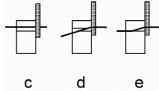
Dowel type connection			
diameter of fastener	d	24	mm
density of timber	ρk	480	kg/m3
number of fasteners	n	25	
number of rows	n_rows	5	
thickness steel plate	t2	25	mm
thickness timber	t1	250	mm
kdef for service class 1	kdef	0,6	
kmod short-term	kmod	0,9	
characteristic tensile strenght fastener	fu,k	1040	N/mm2

1.1 Check tension and compression strength (parallel to grain)

Characteristic load-carrying capacity (for thick plate single shear connection)		$F_{v,Rk} = \min \begin{cases} f_{h,k}\, t_1\, d \left[\sqrt{2 + \dfrac{4 M_{y,Rk}}{f_{h,k}\, d\, t_1^2}} - 1 \right] + \dfrac{F_{ax,Rk}}{4} & (c) \\ 2,3 \sqrt{M_{y,Rk}\, f_{h,k}\, d} + \dfrac{F_{ax,Rk}}{4} & (d) \\ f_{h,k}\, t_1\, d & (e) \end{cases}$	
c d e			
Characteristic embedment strength	fh,k	29,91	N/mm2
	fh,d	20,71	N/mm2
Characteristic fastener yield moment	My,Rk	1209773	Nmm
	My,d	1099793	Nmm
	c	57584	N
	d	53774	N
	e	124256	N
Design shear capacity per dowel per shear plane	Fv,Rd	53774	N
Design shear capacity per dowel	Fv,Rd,total	215096	N
Group effect		$n_{ef} = \min \begin{cases} n \\ n^{0,9} \sqrt[4]{\dfrac{a_1}{13d}} \end{cases}$	
bolts per row	n	5,0	
	n_ef	3,4	
Effective design shear capacity per row	Fv,ef,Rd,row	721	kN
Required number of rows		$n_{required} = \dfrac{N_d}{F_{V,Rd}}$	
	n_req_rows	2,0	
Required number of fasteners	n_req	10,0	
Design load-carrying capacity of the joint		$R_{d,joint} = n * F_{V,Rd} \geq N_d$	
	Rd,joint	3605	kN

Minimum spacings and distances		
spacing parallel to the grain	$a_1 = (3 + 2 \cdot \cos \alpha)d$	
	a1	120 mm
spacing perpendicular to the grain	$a_2 = 3d$	
	a2	72 mm
end distance (loaded end)	$a_{3,t} = 7d \; (\geq 80mm)$	
	a3,t	168 mm
end distance edge (unloaded edge)	$\alpha_{4,c} = 3d$	
	a4,c	72 mm
Serviceability limit state design		
Fser per shear plane per dowel	Fser,c	11 kN
Stiffness modulus of fastener	$K_{ser} = \rho_m^{1.5} \cdot \dfrac{d}{23}$	
	Kser	10974 N/mm
Doubled Kser for steel-timber connection	Kser	21947 N/mm
Instantaneous slip	$u_{inst} = \dfrac{F_{ser}}{K_{ser}}$	
	u_inst	0,5 mm
Final joint slip	$u_{fin} = u_{inst}\sqrt{(1+k_{def,1})(1+k_{def,2})}$	
	u_fin	0,6 mm

1.2 Check shear strength (perpendicular to grain)		
Characteristic load-carrying capacity (for thick plate single shear connection)	$F_{v,Rk} = \min \begin{cases} f_{h,k}\, t_1\, d\left[\sqrt{2 + \dfrac{4M_{y,Rk}}{f_{h,k}\, d\, t_1^2}} - 1\right] + \dfrac{F_{ax,Rk}}{4} & (c) \\ 2,3\sqrt{M_{y,Rk}\, f_{h,k}\, d} + \dfrac{F_{ax,Rk}}{4} & (d) \\ f_{h,k}\, t_1\, d & (e) \end{cases}$	
Characteristic embedment strength	$f_{h,\alpha,k} = \dfrac{f_{h,0,k}}{k_{90}\sin^2\alpha + \cos^2\alpha}$	
	k90	1,66
	fh,0,k	29,91 N/mm2
	fh,90,k	18,02 N/mm2
	fh,90,d	12,48 N/mm2
Characteristic fastener yield moment	My,Rk	1209773 Nmm
	My,d	1099793 Nmm
	c	37054 N
	d	41737 N
	e	74853 N
Design shear capacity per dowel per shear plane	Fv,Rd	37054 N
Design shear capacity per dowel	Fv,Rd,total	148215 N
Required number of fasteners	$n_{required} = \dfrac{N_d}{F_{V,Rd}}$	
	n_req	11,1
Design load-carrying capacity of the joint	$R_{d,joint} = n * F_{V,Rd} \geq N_d$	
	Rd,joint	3705 kN

2. Check splitting capacity

Design splitting capacity	$F_{90,Rd} = 14 \cdot b \cdot w \cdot \sqrt{\dfrac{h_e}{(1-\frac{h_e}{h})}}$ $F_{v,Ed} \leq F_{90,Rd}$	
	$F_{v,Ed}$	1193,4 kN
Length from edge till furthest fastener	h_e	640 mm
Modification factor	w	1
Height of element	h	800 mm
Width	b	800 mm
	$F_{90,Rd}$	633,6 kN

Minimum spacings and distances

spacing parallel to the grain	$a_1 = (3 + 2 \cdot \cos\alpha)d$	
	a1	72 mm
spacing perpendicular to the grain	$a_2 = 3d$	
	a2	72 mm
end distance (unloaded end)	$a_{3,c} = (1 + 6\sin\alpha)d$	
	a3,c	168 mm
end distance edge (loaded edge)	$a_{4,t} = (2 + 2\sin\alpha)d \ (\geq 3d)$	
	a4,t	96 mm

Serviceability limit state design

Fser per shear plane per dowel	$F_{ser,v}$	12 kN
Stiffness modulus of fastener	$K_{ser} = \rho_m^{1.5} \cdot \dfrac{d}{23}$	
	Kser	10974 N/mm
Doubles Kser for steel-timber connection	Kser	21947 N/mm
Stiffness modulus of joint	$K_{ser,connection} = n \cdot K_{ser}$	
	Kser,joint,dowels	274338 N/mm
Instantaneous slip	$u_{inst} = \dfrac{F_{ser}}{K_{ser}}$	
	u_inst	0,6 mm
Final joint slip	$u_{fin} = u_{inst} \sqrt{(1 + k_{def,1})(1 + k_{def,2})}$	
	u_fin	0,7 mm

B.6.5. Belt-truss design

Belt-truss design

Axial forces for load combination: $ULS\_STR\_8\_1.32 \cdot G + 1.65 \cdot Q_{k,wind} + 1,65(0,5 \cdot Q_{k,v,offices} + 0,25 \cdot Q_{k,v,VT})$
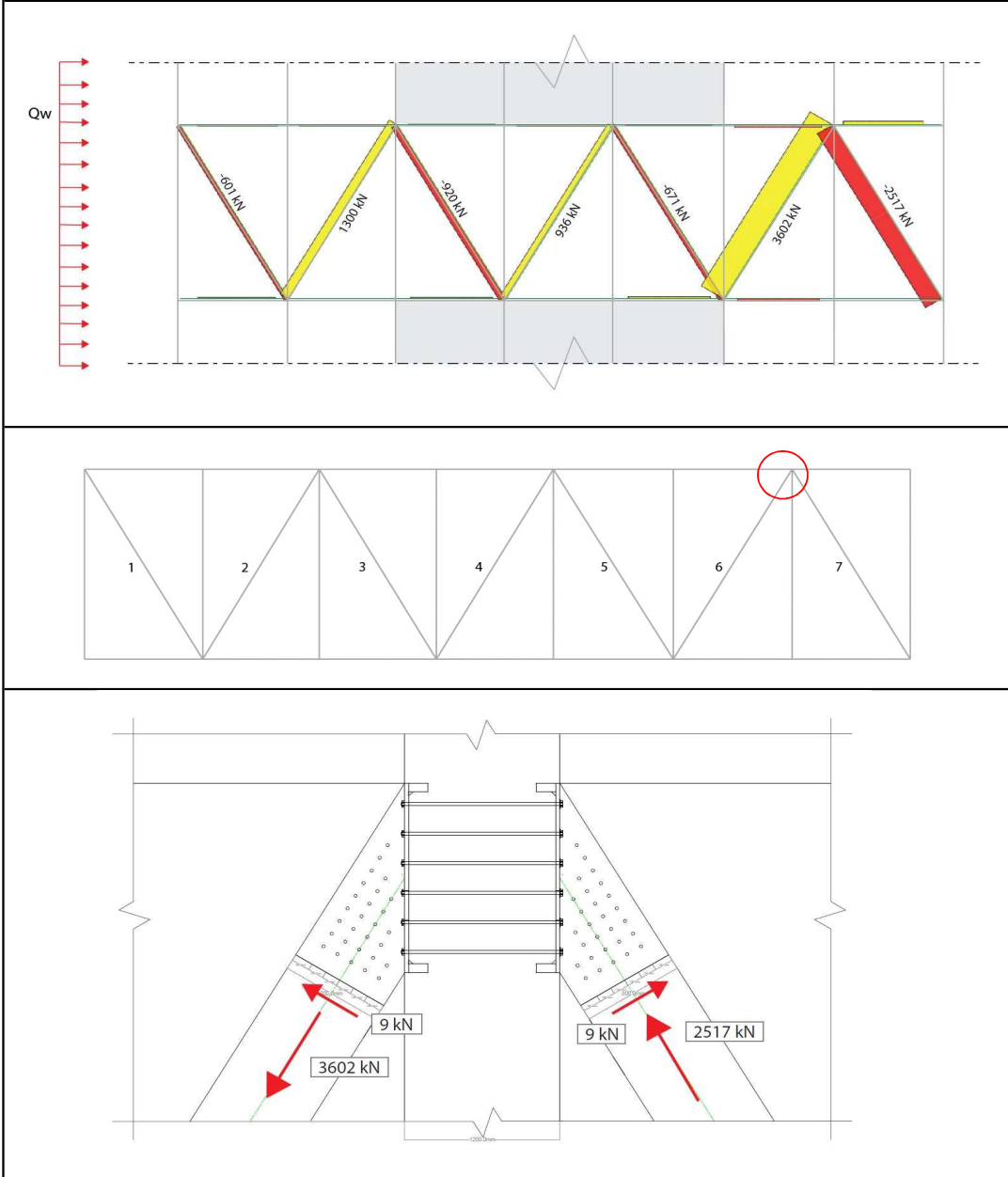
Connection: belt-truss diagonal

Diagonal

Input parameters			
Diagonal	800x800	mm2	
Column	1200x1200	mm2	
Material	LVL-Kerto-S		
Smooth dowels	Rothoblaas STA		

Diagional element 6			
Design tension force	$N_{t,d}$	3602	kN
Design shear force	V_d	9	kN
Diagonal element 7			
Design compression force	$N_{c,d}$	-2517	kN
Design shear force	V_d	9	kN

1. Check load-carrying capacity dowel type connection			
Dowel type connection			
diameter of fastener	d	24	mm
density of timber	ρ_k	480	kg/m3
number of fasteners	n	28	
number of rows	n_{rows}	5	
thickness steel plate	t_2	25	mm
thickness timber	t_1	250	mm
kdef for service class 1	k_{def}	0,6	
kmod short-term	k_{mod}	0,9	
characteristic tensile strenght fastener	$f_{u,k}$	1040	N/mm2

1.1 Check tension and compression strength (parallel to grain)			
Characteristic load-carrying capacity (for thick plate single shear connection)	$$F_{v,Rk} = \min \begin{cases} f_{h,k}\, t_1\, d \left[\sqrt{2 + \dfrac{4M_{y,Rk}}{f_{h,k}\, d\, t_1^2}} - 1 \right] + \dfrac{F_{ax,Rk}}{4} & \text{(c)} \\[2ex] 2,3\sqrt{M_{y,Rk}\, f_{h,k}\, d} + \dfrac{F_{ax,Rk}}{4} & \text{(d)} \\[2ex] f_{h,k}\, t_1\, d & \text{(e)} \end{cases}$$			
Characteristic embedment strength	$f_{h,k} = 0.082(1 - 0.01d) \cdot \rho_k$		
	fh,k	29,91	N/mm2
	fh,d	20,71	N/mm2
Characteristic fastener yield moment	$M_{y,Rk} = 0.3 \cdot f_{u,k} \cdot d^{2.6}$		
	My,Rk	1209773	Nmm
	My,d	1099793	Nmm
	c	57584	N
	d	53774	N
	e	124256	N
Design shear capacity per dowel per shear plane	Fv,Rd	53774	N
Design shear capacity per dowel	Fv,Rd,total	215096	N
Group effect	$$n_{ef} = \min \begin{cases} n \\ n^{0.9} \sqrt[4]{\dfrac{a_1}{13d}} \end{cases}$$		
	n	5,6	
	n_ef	3,7	

| Effective design shear capacity per row	$F_{v,ef,Rd,row}$	798 kN
Required number of rows	$n_{required} = \dfrac{N_d}{F_{V,Rd}}$	
	nreq,rows	4,5
Required number of fasteners	nreq	25,3
Design load-carrying capacity of the joint	$R_{d,joint} = n * F_{V,Rd} \geq N_d$	
	Rd,joint	3992 kN
Minimum spacings and distances		
spacing parallel to the grain	$a_1 = (3 + 2 \cdot \cos\alpha)d$	
	a1	120 mm
spacing perpendicular to the grain	$a_2 = 3d$	
	a2	72 mm
end distance (loaded end)	$a_{3,t} = 7d \ (\geq 80mm)$	
	a3,t	168 mm
end distance edge (unloaded edge)	$\alpha_{4,c} = 3d$	
	a4,c	72 mm
Serviceability limit state design		
Fser per shear plane per dowel	$F_{ser,c}$	24 kN
Stiffness modulus of fastener	$K_{ser} = \rho_m^{1.5} \cdot \dfrac{d}{23}$	
	Kser	10974 N/mm
Doubled Kser for steel-timber connection	Kser	21947 N/mm
Instantaneous slip	$u_{inst} = \dfrac{F_{ser}}{K_{ser}}$	
	Uinst	1,1 mm
Final joint slip	$u_{fin} = u_{inst}\sqrt{(1+k_{def,1})(1+k_{def,2})}$	
	Ufin	1,4 mm

2. Check splitting capacity		
Design splitting capacity	$F_{90,Rd} = 14 \cdot b \cdot w \cdot \sqrt{\dfrac{h_e}{(1 - \dfrac{h_e}{h})}}$ $F_{v,Ed} \leq F_{90,Rd}$	
length from edge till furthest fastener	he	700 mm
modification factor	w	1
height of element	h	800 mm
width	b	800 mm
	F90,Rd	838 kN

3. Check strength steel plates		
Characteristic yield strenght	fyk	460 N/mm2
Design yield strength	fyd	418 N/mm2
Surface area of steel plates	Asteelplate	77000 mm2
	$N_{t,d} \leq N_{y,Rd,steelplate}$	
	Ny,Rd	32200 kN

Connection: belt-truss column

Column

Input parameters			
Diagonal	800x800	mm2	
Column	1200x1200	mm2	
Material	LVL-Kerto-S		
Bolts	M24	10.9	
Steel plate	S355		

Diagional element 6		
Design tension force	$N_{t,d}$	3602 kN
Design shear force	V_d	9 kN
Angle diagonal	α	30,8 °
Design horizontal force	$F_{x,d}$	1843 kN
Design vertical force	$F_{y,d}$	3095 kN

1.1 Check tension resistance bolts		
Density of timber	ρ_k	480 kg/m3
Diameter of bolt	d	24 mm
Number of bolts	n	10
	$$F_{t,Rd} = k_2 \cdot f_{u,b} \cdot \frac{A_s}{\gamma_{M2}}$$	
factor for countersunk bolt	k2	0,63
ultimate tensile strength	fu,b	1040 N/mm2
tensile stress area of bolt	As	452,4 mm2
Material factor	γm2	1,25
Design tension resistance	Ft,Rd	237,1 kN
Total design tension resistance	Ft,Rd,tot	2371,2 kN
Design tension force	Nt,d	1842,8 kN
	UC	0,78

2.1 Check lateral capacity bolts		
Thickness steel plate	t2	30 mm
Thickness timber	t1	600 mm
Characteristic load-carrying capacity (for thick steel plate single shear connection) Rope effect is 25%	$$F_{v,Rk} = \min \begin{cases} f_{h,k}\, t_1\, d \left[\sqrt{2 + \frac{4 M_{y,Rk}}{f_{h,k}\, d\, t_1^2}} - 1 \right] + \frac{F_{ax,Rk}}{4} & (c) \\ 2.3\sqrt{M_{y,Rk}\, f_{h,k}\, d} + \frac{F_{ax,Rk}}{4} & (d) \\ f_{h,k}\, t_1\, d & (e) \end{cases}$$	
Characteristic embedment strength	$f_{h,k} = 0.082(1 - 0.01d) \cdot \rho_k$	
	fh,k	29,9 N/mm2
	fh,d	20,7 N/mm2
Characteristic fastener yield moment	$M_{y,Rk} = 0.3 \cdot f_{u,k} \cdot d^{2.6}$	
	My,Rk	1916928 Nmm
	My,Rd	1327104 Nmm
	c	127234 N
	d	59663 N
	e	298216 N
Design load-carrying capacity	Fv,Rd	59663 N

Required number of fasteners	$n_{required} = \dfrac{N_d}{F_{V,Rd}}$		
	nreq	51,9	
Number of bolt rows	rows	8,0	
Number of bolts in row	nrow	6,48	11
Effective number of fasteners	$n_{ef} = \min \left\{ \begin{array}{l} n \\ n^{0.9} \sqrt[4]{\dfrac{a_1}{13d}} \end{array} \right.$		
	nef	6,82	
	nef,tot	54,5	
Design load carrying capacity of the joint	Rd,joint	3253 kN	

Minimum spacings and distances		
Spacing parallel to the grain	$(4 + |\cos\alpha|)\, d$	
	a1	120 mm
Spacing perpendicular to the grain	$4\, d$	
	a2	96 mm
End distance (loaded end)	$\max(7\, d;\ 80\ \text{mm})$	
	a3,t	168 mm
End distance (unloaded end)	$\max[(1 + 6\sin\alpha)\, d;\ 4d]$	
	a3,c	145 mm
End distance edge (loaded edge)	$\max[(2 + 2\sin\alpha)\, d;\ 3d]$	
	a4,t	72 mm
End distance edge (unloaded edge)	$3\, d$	
	a4,c	72 mm

Serviceability limit state design		
Fser per shear plane per fastener	Fser,v	229 kN
Stiffness modulus of fastener per shear plane	$K_{ser} = \rho_m^{1.5} \cdot \dfrac{d}{23}$	
	Kser	10974 N/mm
Doubled slip modulus for steel-timber connection	Kser	21947 N/mm
Stiffness modulus of joint	$K_{ser,connection} = n \cdot K_{ser}$	
	Kser,joint	109735 N/mm
Instantaneous slip	$u_{inst} = \dfrac{F_{ser}}{K_{ser}}$	
	Uinst	10,4 mm
Final joint slip	$u_{fin} = u_{inst}\sqrt{(1 + k_{def,1})(1 + k_{def,2})}$	
	Ufin	18,2 mm

3. Check timber capacity on compression		
Addition of steel block to add lateral capacity to reduce the number of bolts		
Compression strength parallel to grain	fc,0,k	29,0 N/mm2
	fc,0,d	20,9 N/mm2
Area steel block (150mmx1200mm)	Asteel	180000 mm2
Compression force on timber surface	fc,d	17,2 N/mm2
The lateral capacity due to the additional steel blocks suffices, and the number of bolts		
will be reduced to n=10.		

4. Check load carrying capacity head plates		
Equivalent T-stub in tension (6.2.4)		
Steel plate thickness	tp	30 mm
Yield strength	fy	355 N/mm2
Bolt elongation length	Lb	600 mm

Effective lengths		
	e	150 mm
	e1	50 mm
	rc	5 mm
	p	240 mm
	m	146 mm
	n	50 mm
Individual end bolt-row	leff,cp	759 mm
	leff,np	536 mm
Group end-bolt row	leff,cp	340 mm
	leff,np	170 mm
Individual inner bolt-row	leff,cp	917 mm
	leff,np	772 mm
Group inner bolt-row	leff,cp	480 mm
	leff,np	240 mm
Mode 1 Individual bolt-row	leff,1	536 mm
Mode 1 Group bolt-row	leff,1	170 mm
Mode 2 Individual bolt-row	leff,2	536 mm
Mode 2 Group bolt-row	leff,2	170 mm

Design moment of plasticity	$M_{pl,1,Rd} = 0.25 \sum l_{eff,1} t_f^2 f_y / \gamma_{M0}$	
	Mpl,1,Rd	42793031 Nmm
	$M_{pl,2,Rd} = 0.25 \sum l_{eff,2} t_f^2 f_y / \gamma_{M0}$	
	Mpl,2,Rd	42793031 Nmm

Mode 1 Design tension resistance	$F_{T,1,Rd} = \dfrac{4 M_{pl,1,Rd}}{m}$	
(prying forces may develop)	FT,1,Rd	1172 kN
Mode 2 Design tension resistance	$F_{T,2,Rd} = \dfrac{2 M_{pl,2,Rd} + n \sum F_{t,Rd}}{m + n}$	
(prying forces may develop)	FT,2,Rd	1042 kN
Mode 3 Design tension resistance	$F_{T,3,Rd} = \sum F_{t,Rd}$	
	FT,3,Rd	2371 kN
Design tension resistance for T-stub	FT,Rd	1042 kN
	Nt,d	921 kN
	UC	0,88

B.7. Fire Safety Design

Fire safety design		
Column design (Storey 58 till 76)		

Column section properties		
Depth	d	750 mm
Width	w	750 mm
Cross sectional Area	A	562500 mm2

Fire resistance structural member		
Fire resistance time	R	120 min
Cladding	Gypsum plasterboard type A	
Thickness plate	h_p	20 mm
Charring rate	$\beta 0$	0,65 mm/min
Notional charring rate	βn	0,7 mm/min

Time start charring	t_{ch}	42 min
Time fall off cladding	t_f	42 min
Time limit when original GLT char rate starts	t_a	60 min
Post protection coefficient	$k3$	2
Required fire resistance time	$t_{fi,req}$	120 min
Required fire resistance time left after t_a	$t_{fi,2}$	60 min
Notianal charring rate (phase 1)	$\beta_{n,1}$	1,4 mm/min
Char depth at time t_a	$d_{char,ta}$	25 mm
Char depth at t=120min	$d_{char,tR120}$	67 mm

Reduced cross-section		
Depth zero strength layer	$d0$	7 mm
Effective charring depth	d_{ef}	74 mm
Reduced width	b_{fi}	602,0 mm
Reduced height	h_{fi}	602,0 mm
Reduced cross-sectional area	A_{fi}	362404 mm2

Column splice fire protection		
Gypsum plasterboard type F	$t_{ch} = 2.8 \cdot h_p - 23$	
Required time before charring starts	t_{ch}	120 min
Thickness of plasterboard	h_p	51,1 mm
Required additional plasterboard	$h_{p,req}$	32 mm

Fire safety design

Beam design

Beam section properties

Depth	d	500 mm
Width	w	300 mm
Cross sectional Area	A	150000 mm2

Fire resistance structural member

Fire resistance time	R	120 min
Cladding	Gypsum plasterboard type F	
Thickness plate	h_{p1}	25 mm
	h_{p2}	15 mm
Charring rate	$\beta 0$	0,65 mm/min
Notional charring rate	βn	0,7 mm/min

Time start charring	t_{ch}	89 min
Time fall off cladding	t_f	89 min
Time limit when original GLT char rate starts	t_a	107 min
Post protection coefficient	k3	2
Required fire resistance time	$t_{fi,req}$	120 min
Required fire resistance time left after t_a	$t_{fi,2}$	13 min
Notianal charring rate (phase 1)	$\beta_{n,1}$	1,4 mm/min
Char depth at time t_a	$d_{char,ta}$	25 mm
Char depth at t=120min	$d_{char,tR120}$	34,2 mm

Reduced cross-section

Depth zero strength layer	d0	7 mm
Effective charring depth	d_{ef}	41,2 mm
Reduced width	d_{fi}	417,6 mm
Reduced height	w_{fi}	217,6 mm
Reduced cross-sectional area	A_{fi}	90870 mm2

B.8. Alternative Load Path

Alternative load path

Accidental load combination			
G '+' P '+ (ψ1,1 or ψ2,1)Qk,1 + ψ2,1 Qk,wind			
Offices (Catogory B)		Wind load	
ψ0	0,7	ψ0	0,6
ψ1	0,5	ψ1	0,2
ψ2	0,3	ψ2	0
G '+' 0,5 Qk,offices + 0 Qk,wind	(a)		
G '+' 0,2 Qk,wind + 0,3 Ok,offices	(b)		
Tension force after column failure at ground level			

1) Check tensile capacity of column		
(column below belt-truss)		
Design tension force	$N_{t,d,max}$	1180 kN
Column dimensions		750mmx750mm
Cross-sectional area	A	562500 mm2
Characteristic tension strength	$f_{t,0,k}$	22,5 N/mm2
Design tension strength	$f_{t,0,d}$	16,2 N/mm2
Design tension resistance	$N_{t,Rd}$	9112,5 kN
	UC	0,13

2) Check column splice detail tensile capacity		
(beam below belt-truss)		
Design tension resistance	$N_{t,Rd}$	1423 kN
	UC	0,83

3) Check tensile capacity of beam			
Design tension force	$N_{t,d,max}$		70 kN
Column dimensions		500mmx300mm	
Cross-sectional area	A		150000 mm2
Characteristic tension strength	$f_{t,0,k}$		22,5 N/mm2
Design tension strength	$f_{t,0,d}$		16,2 N/mm2
Design tension resistance	$N_{t,Rd}$		2430 kN
	UC		0,03

4) Check tensile capacity of beam connection			
Design tension resistance	$N_{t,Rd}$		136 kN
	UC		0,51

B.9. Load combinations

Ultimate Limit State	Loading combination	k_{mod}
Limit State Failures, STR		
Floor structures	1.49G	0.6
	1.49G '+' 1.65$\psi_{0,i}Q_{k,v,offices}$	0.8
	1.32G '+' 1.65 $Q_{k,v,offices}$	0.8
Beams/ diagonals	1.49G	0.6
	1.49G '+' 1.65($\psi_{0,i}Q_{k,v,offices}$ '+' $\psi_{0,i}Q_{k,v,VT}$)	0.8
	1.32G '+' 1.65($Q_{k,v,offices}$ '+' $Q_{k,v,VT}$)	0.8
	1.32G '+' 1.65$Q_{k,snow}$ + 1.65($\psi_{0,i}Q_{k,v,offices}$ '+' $\psi_{0,i}Q_{k,v,VT}$)	0.9
	1.32G '+' 1.65$Q_{k,wind}$ + 1.65($\psi_{0,i}Q_{k,v,offices}$ '+' $\psi_{0,i}Q_{k,v},VT$)	0.9
Columns	1.49G	0.6
	1.49G '+' 1.65($\psi_{0,i}$ $\alpha_{n,1}$ $Q_{k,v,offices}$ '+' $\psi_{0,i}$ $\alpha_{n,2}$ $Q_{k,v}$,VT)	0.8
	1.32G '+' 1.65($\alpha_{n,1}$ $Q_{k,v,offices}$ '+' $\alpha_{n,2}$ $Q_{k,v,VT}$)	0.8
	1.32G '+' 1.65$Q_{k,snow}$ '+' 1.65($\psi_{0,i}$ $\alpha_{n,1}$ $Q_{k,v,offices}$ '+' $\psi_{0,i}$ $\alpha_{n,2}$ $Q_{k,v}$,VT)	0.9
	1.32G '+' 1.65$Q_{k,wind}$ '+' 1.65($\psi_{0,i}$ $\alpha_{n,1}$ $Q_{k,v,offices}$ '+' $\psi_{0,i}$ $\alpha_{n,2}$ $Q_{k,v}$,VT)	0.9
	0.9G	0.6
	0.9G '+' 1.65($\psi_{0,i}$ $\alpha_{n,1}$ $Q_{k,v}$,offices '+' $\psi_{0,i}$ $\alpha_{n,2}$ $Q_{k,v}$,VT)	0.8
	0.9G '+' 1.65($\alpha_{n,1}$ $Q_{k,v,offices}$ '+' $\alpha_{n,2}$ $Q_{k,v,VT}$)	0.8
	0.9G '+' 1.65$Q_{k,snow}$ '+' 1.65($\psi_{0,i}$ $\alpha_{n,1}$ $Q_{k,v}$,offices '+' $\psi_{0,i}$ $\alpha_{n,2}$ $Q_{k,v}$,VT)	0.9
	0.9G '+' 1.65$Q_{k,wind}$ '+' 1.65($\psi_{0,i}$ $\alpha_{n,1}$ $Q_{k,v}$,offices '+' $\psi_{0,i}$ $\alpha_{n,2}$ $Q_{k,v}$,VT)	0.9
Static equilibrium, EQU		
	0.9G '+'1.5$Q_{k,wind}$	0.6
	0.9G '+' 1.5$Q_{k,wind}$ '+' 1.5($\alpha_{n,1}$ $Q_{k,v}$,offices '+' $\alpha_{n,2}$ $Q_{k,v}$,VT)	0.9

*$Q_{k,v,VT}$ = variable load vertical transportation (stairs/elevators).

*$Q_{k,v,office}$ = variable load offices.

*α_n is the reduction value for imposed floor loading in multi-storey buildings which should only be used for vertical elements.

Figure B.3: ULS load combinations

Serviceability Limit State	Loading combination
Characteristic load combinations	
Floor/ beam deflections	G '+' $Q_{k,v,offices}$ '+' $Q_{k,v,VT}$
	G '+' $Q_{k,wind}$ '+' $\psi_{0,i} Q_{k,v,offices}$ '+' $\psi_{0,i} Q_{k,v,VT}$
	G '+' $Q_{k,snow}$ '+' $\psi_{0,i} Q_{k,v,offices}$ '+' $\psi_{0,i} Q_{k,v,VT}$
Lateral displacements	G '+' $Q_{k,wind}$ '+' $\psi_{0,i} Q_{k,v,offices}$ '+' $\psi_{0,i} Q_{k,v,VT}$
	G '+' $Q_{k,snow}$ '+' $\psi_{0,i} Q_{k,v,offices}$ '+' $\psi_{0,i} Q_{k,v,VT}$
Frequent load combinations	
Floor/ beam deflections	G '+' $\psi_{1,i} Q_{k,v,offices}$ '+' $\psi_{1,i} Q_{k,v,VT}$
	G '+' $\psi_{1,i} Q_{k,wind}$ '+' $\psi_{2,i} Q_{k,v,offices}$ '+' $\psi_{2,i} Q_{k,v,VT}$
	G '+' $\psi_{1,i} Q_{k,snow}$ '+' $\psi_{2,i} Q_{k,v,offices}$ '+' $\psi_{2,i} Q_{k,v,VT}$
Lateral displacements	G '+' $\psi_{1,i} Q_{k,wind}$
	G '+' $\psi_{1,i} Q_{k,wind}$ '+' $\psi_{2,i} Q_{k,v,offices}$ '+' $\psi_{2,i} Q_{k,v,VT}$
	G '+' $\psi_{1,i} Q_{k,snow}$ '+' $\psi_{2,i} Q_{k,v,offices}$ '+' $\psi_{2,i} Q_{k,v,VT}$
Quasi-static load combinations	
Floor/ beam deflections	G '+' $\psi_{2,i} Q_{k,v,offices}$ '+' $\psi_{2,i} Q_{k,v,VT}$

Figure B.4: SLS load combinations

C
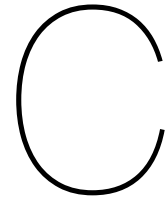
Annex C - Lateral wind calculation and dynamic analysis

C.1. Wind load calculation according to NEN-EN1991-1-4

The procedure of determining the wind load according to the Eurocode has been described in Chapter 5: *Lateral wind load according to building code.* In this section the input parameters and results of the wind load calculation are shown. Table C.1 shows the wind load input parameters. The Matlab script of the wind load calculation according to the Eurocode is presented in the Annex E.

Table C.1: Wind load input parameters

Wind input parameters			
Basis wind velocity	v_b	27	m/s
Height	H	300.0	m
Width	W	31.5	m
Depth	D	31.5	m
Terrain category	I-IV	III	-
Natural frequency (in along-wind dir.)	$n_{1,x}$	0.130	Hz
Logarithmic decrement of structural damping	δ_s	0.090	-

Table C.2: Wind and terrain properties according to Eurocode

Background response factor	B^2	0.381	-
Resonance response factor	R^2	0.753	-
Structural dynamic factor	$c_s c_d$	0.976	-
Force coefficient	c_f	1.46	-
Terrain factor	k_r	0.223	-
Turbulence length scale	$L(z_s)$	280.6	m

Table C.3: Damping

	Logarithmic decrement, δ	Damping ratio , ζ
Structural damping	0.0900	1.43 %
Aerodynamic damping	0.0451	0.72 %
Damping due to auxiliary devices	-	-
Total damping	0.1351	2.15 %

Table C.4: Results wind calculation according to Eurocode

Reference height h_{ref} [m]	Mean wind velocity $v_m(z)$ $[m/s^2]$	Turbulence intensity $I_v(z)$	Peak wind pressure $q_p(z)$ $[N/m^2]$
31.50	24.97	0.24	1048.22
41.38	26.62	0.23	1144.55
51.25	27.91	0.22	1222.52
61.13	28.97	0.21	1288.28
71.00	29.87	0.20	1345.27
80.88	30.65	0.20	1395.66
90.75	31.35	0.19	1440.88
100.63	31.97	0.19	1481.93
110.50	32.54	0.19	1519.56
120.38	33.05	0.18	1554.31
130.25	33.53	0.18	1586.62
140.13	33.97	0.18	1616.81
150.00	34.38	0.18	1645.17
159.88	34.76	0.17	1671.91
169.75	35.12	0.17	1697.21
179.63	35.46	0.17	1721.23
189.50	35.79	0.17	1744.10
199.38	36.09	0.17	1765.93
209.25	36.38	0.17	1786.81
219.13	36.66	0.16	1806.83
229.00	36.93	0.16	1826.06
238.88	37.18	0.16	1844.55
248.75	37.43	0.16	1862.38
258.63	37.66	0.16	1879.58
268.50	37.89	0.16	1896.20
268.50	37.89	0.16	1896.20
300.00	38.56	0.16	1945.77

C.2. Peak accelerations EC

The calculation procedure for the peak accelerations according to the Eurocode can be found in Chapter 5: *Lateral wind load according to building code.* Table C.6 shows the results for the peak response accelerations in the along-wind direction over the height of the building.

Table C.5: Wind load input parameters for peak acceleration calculation

Wind input parameters			
Basis wind velocity	v_b	27	m/s
Mean wind velocity at reference height	$v_m(z_s)$	35.5	m/s^2
Pressure coefficient	c_f	1.46	-
Turbulence intensity at reference heigth	$I_v(z_s)$	0.17	-
Resonant response factor	R	0.90	-
Background response factor	B	0.57	-
Natural frequency	$n_{1,x}$	0.130	Hz
Logarithmic decrement of structural damping	δ_s	0.090	-

Table C.6: Wind peak accelerations

Height, H [m]	Peak wind acceleration, a_{max} [m/s²]
31.50	0.000
41.38	0.005
51.25	0.008
61.13	0.012
71.00	0.017
80.88	0.023
90.75	0.029
100.63	0.037
110.50	0.045
120.38	0.054
130.25	0.065
140.13	0.076
150.00	0.088
159.88	0.100
169.75	0.114
179.63	0.128
189.50	0.144
199.38	0.160
209.25	0.177
219.13	0.195
229.00	0.214
238.88	0.234
248.75	0.254
258.63	0.276
268.50	0.298
268.50	0.321
300.00	0.402

C.3. Wind Response Spectrum Method

Spectrum of variance of the wind velocity, $S_v(f)$
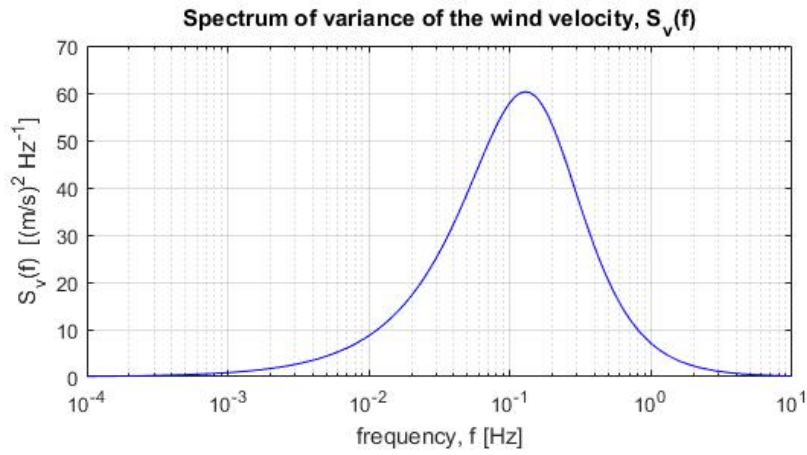
Figure C.1: Spectrum of fluctuating wind velocity, $S_v(f)$

Aerodynamic admittance function, $\chi^2(f)$
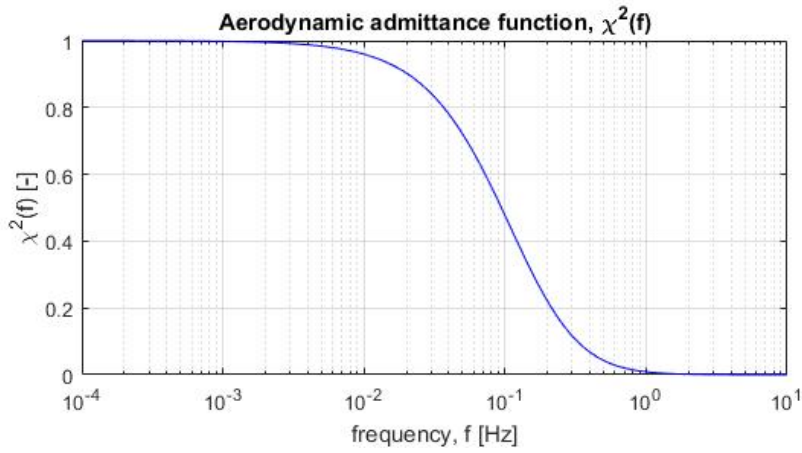
Figure C.2: Aerodynamic admittance function, $\chi^2(f)$

Power density spectrum, $S_F(f)$
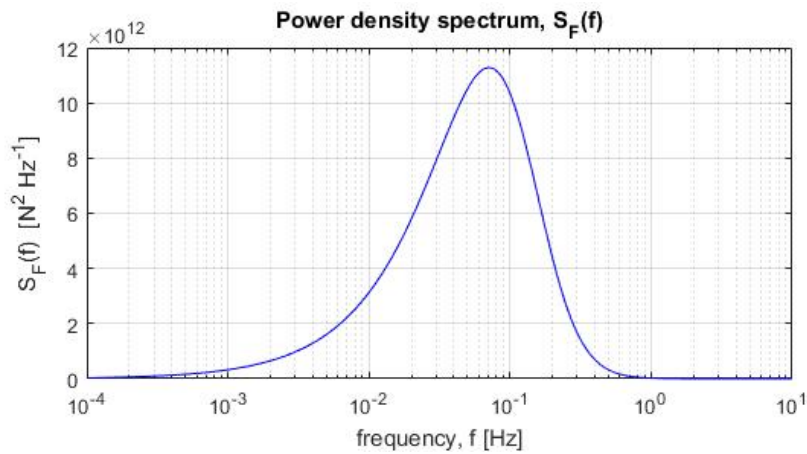
Figure C.3: Power density spectrum, $S_F(f)$
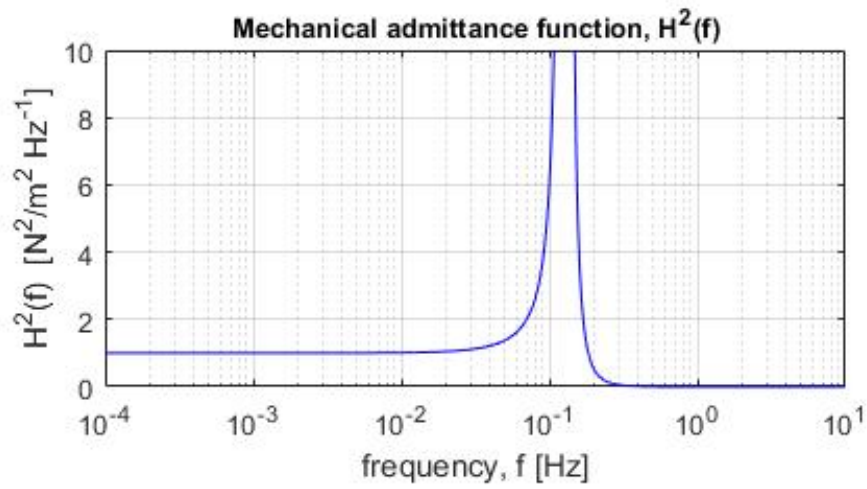
Figure C.4: Mechanical admittance function, $H^2(f)$
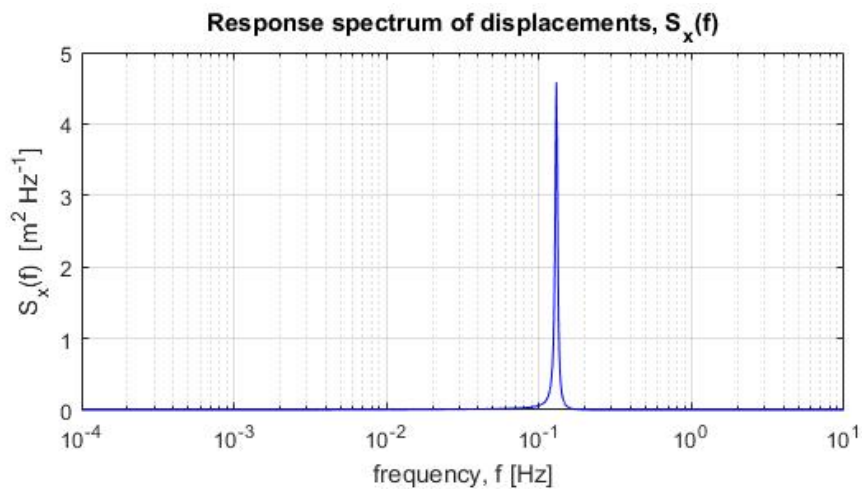
Figure C.5: Response spectrum of displacements in along-wind direction, $S_x(f)$
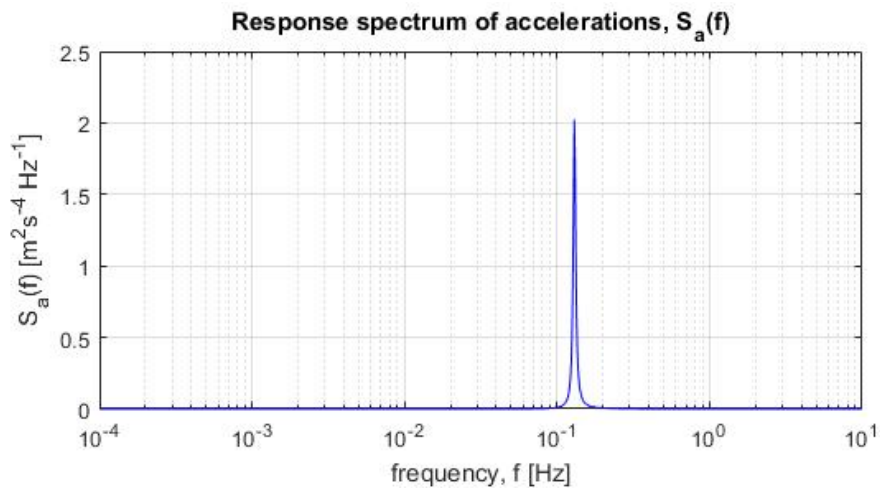
Figure C.6: Response spectrum of accelerations in along-wind direction, $S_a(f)$
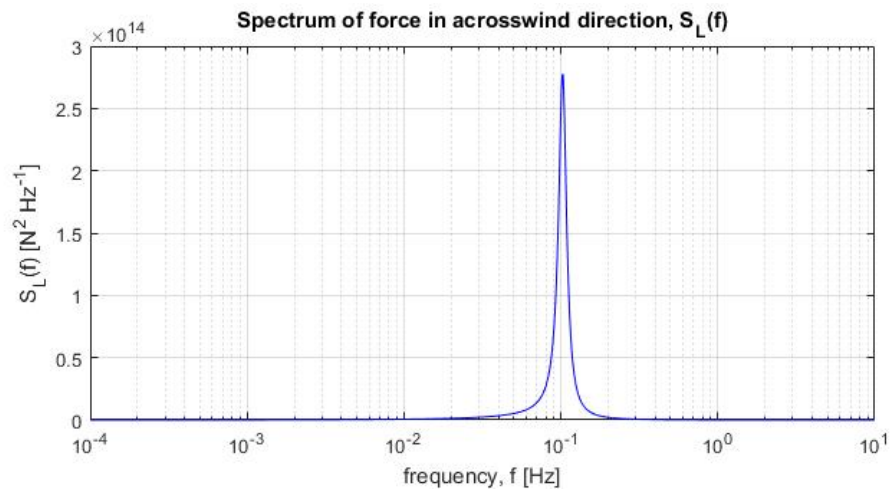
Figure C.7: Spectrum of force in across-wind direction, $S_L(f)$
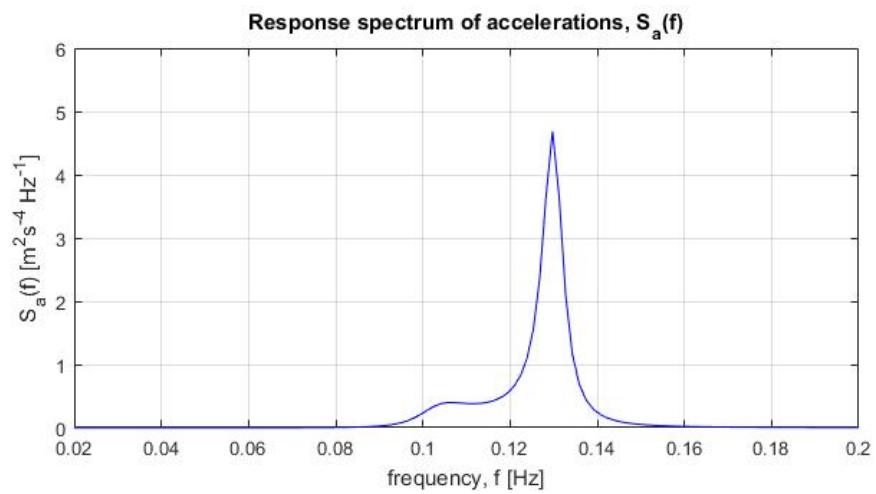
Figure C.8: Response spectrum of accelerations in across-wind direction, $S_a(f)$

C.4. Time History Analysis
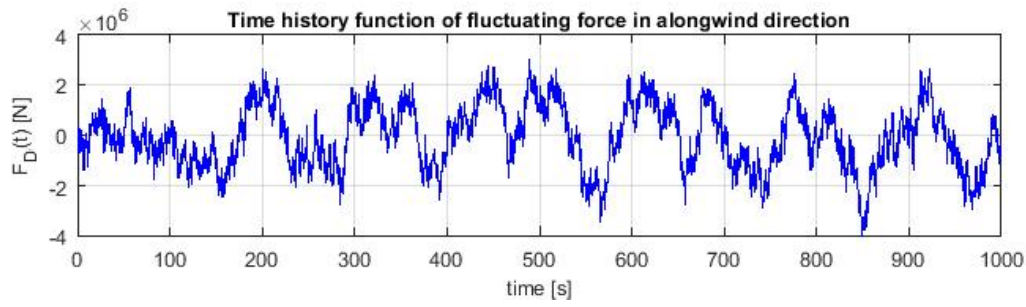
Figure C.9: Time history of fluctuating force in along-wind direction
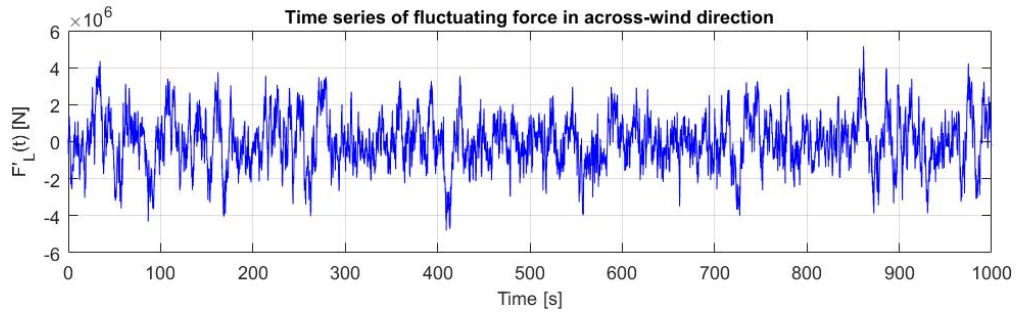
Figure C.10: Time history of fluctuating force in across-wind direction
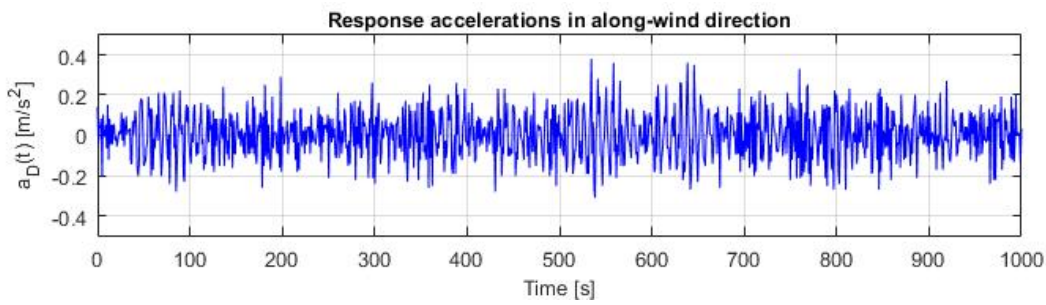
Figure C.11: Time history of response accelerations in along-wind direction
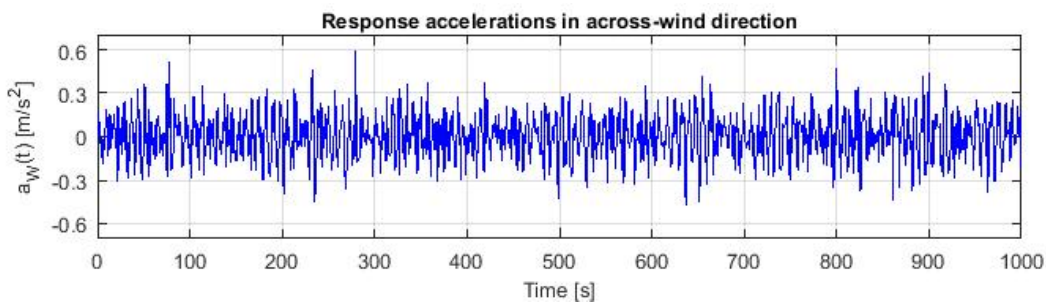
Figure C.12: Time history of response accelerations in across-wind direction

D
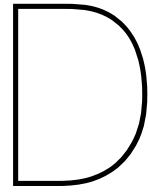
Annex D - Parametric study and Optimization

D.1. Stiffness optimization
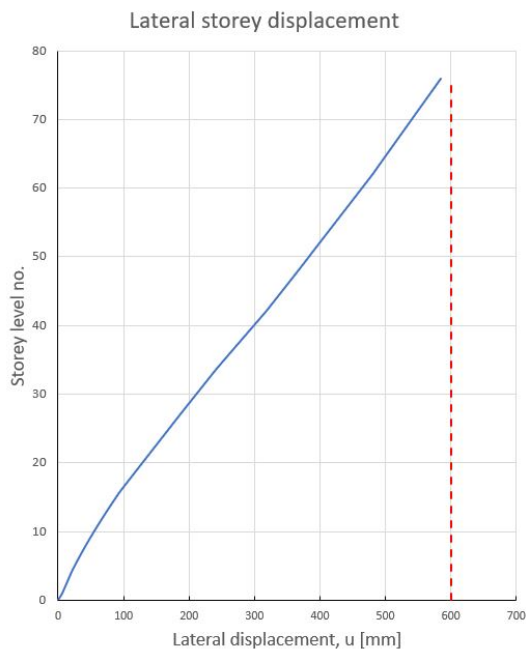
Figure D.1: Lateral displacements along the height of the building for the final design
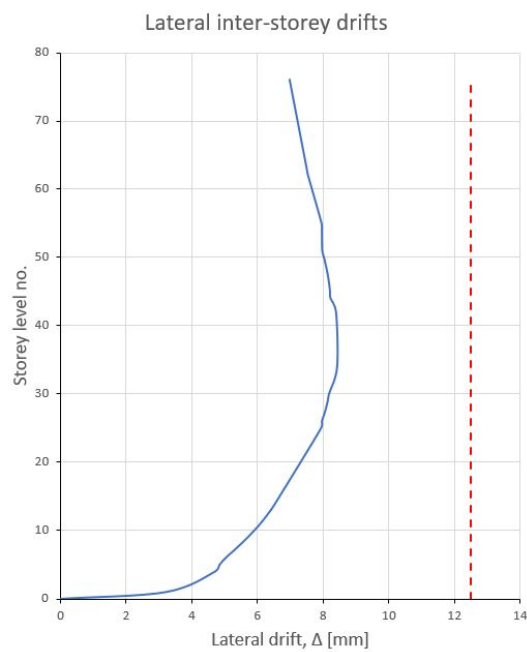
Figure D.2: Lateral inter-storey drifts along the height of the building for the final design

D.2. Shape optimization

Shape optimization

Rounded corners and end effect	NEN-EN1991-1-4	
Corners radius	r	5 m
Force coefficient	$c_f = c_{f,0} \cdot \psi_r \cdot \psi_\lambda$	
Reduction factor for rounded corners	ψ_r	0,60
Reduction factor for end effect	ψ_λ	0,72
Force coefficient without reduction	$c_{f,0}$	2,1
	c_f	0,91

Reduction factor for rounded corners	

	r/b	0,16
	ψ_r	0,90

Reduction factor for end effect	
The end effect factor is determined as a function of	
the effective slenderness ratio.	

Determination of the effective slenderness ratio		
$\lambda = \min(1.4 \cdot l / b\,; 70)$		13,3
		70
	λ	13,3
Grade of fullness	$\varphi = \dfrac{A}{A_c}$	

Reduction factor for end effect	ψ_λ	0,72

Resonance response factor	$R = \sqrt{\dfrac{\pi^2}{2\delta} \cdot S_L(z_s, n_{1x}) \cdot K_s(n_{1x})}$	
Aero-dynamic damping	$\delta_a = \dfrac{c_f \cdot \rho \cdot b \cdot v_m(z_s)}{2 \cdot n_{1,x} \cdot m_e}$	
Aerodynamic damping will change if the force coefficient will change. *Therefore, for the rounded corners optimimization the aerodynamic* *damping should be recalculated.*		
Aero-dynamic damping	δ_a	0,033
Structural damping	δ_s	0,090
Damping due to auxiliary device	δ_d	0,000
Total damping	δ_{tot}	0,123
Total damping as fraction of the critical damping	ζ_{tot}	0,0196

Peak accelerations in along-wind direction		
Standard deviation of peak response accelerations		
$\sigma_{a,x} = c_f \cdot \rho \cdot I_v(z_s) \cdot v_m^2(z_s) \cdot R \cdot \dfrac{K_y \cdot K_z \cdot \phi(y,z)}{\mu_{ref} \cdot \phi_{max}}$		
Characteristic density of air	ρ	1,25 kg/m3
Turbulence intensity	$I_v(z_s)$	0,17 -
Mean wind velocity	$v_m(z_s)$	35,5 m/s
Resonance response factor	R	0,97 -
Background response factro	B	0,32 -
Reference mass	μ_{ref}	4819,5 kg/m2
Mode at top	ϕ_{max}	1,00 -
Non-dimensional K_y-factor	K_y	1,00 -
Non-dimensional K_z-factor	K_z	1,67 -
Standard deviation of accelerations	$\sigma_{a,x}$	0,081 m/s^2
Peak response acceleration	$a_{max} = k_p \cdot \sigma_{a,x}$	
Gust peak factor	k_p	3,15
Peak response acceleration for building with sharp edges	$a_{D,max}$	0,421 m/s^2
Peak response acceleration for building with rounded corners	$a_{D,max}$	0,257 m/s^2
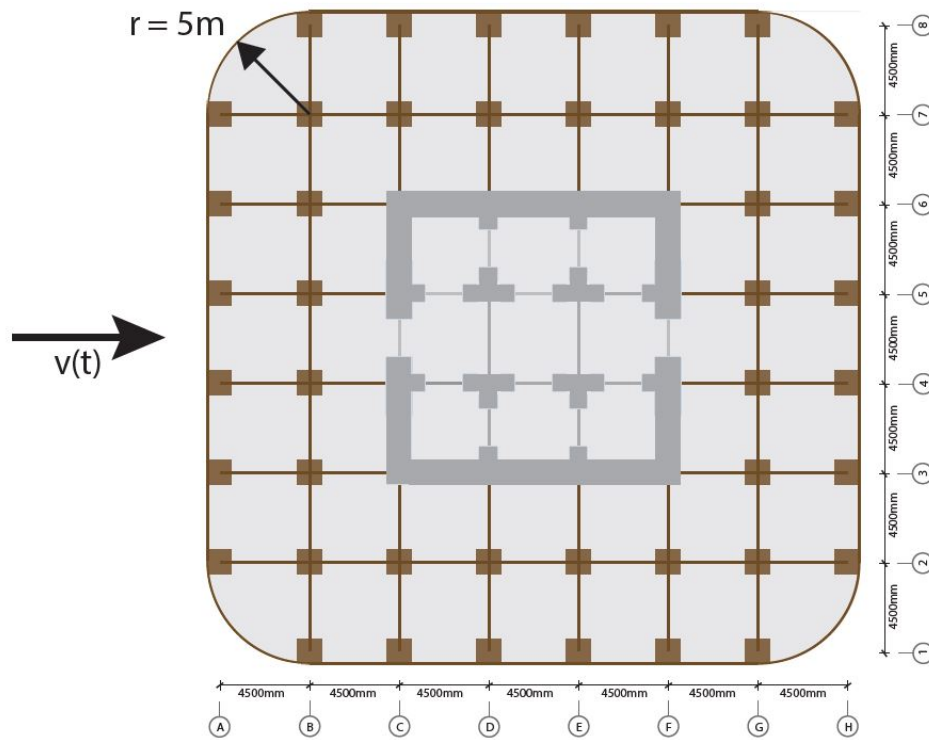
Figure D.3: Plan view of tall building with rounded corner modification, r=5m.
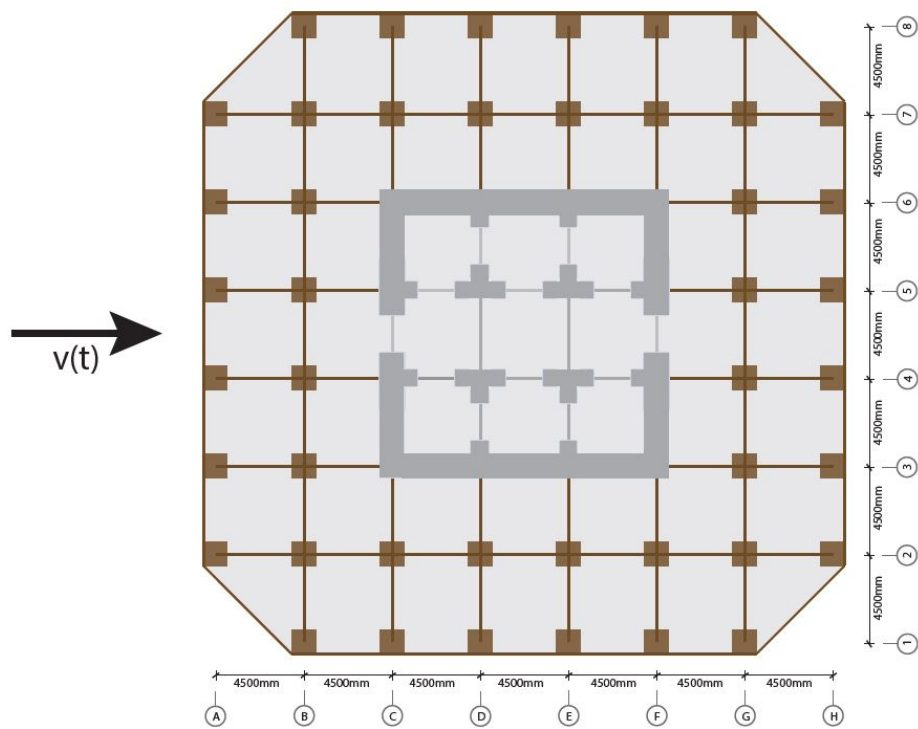
Figure D.4: Plan view of tall building with chamfered corner modification (cut-off rate 14%)

D.3. Damping optimization

Table D.1: TMD design: 2DOF system properties

		Case 1	**Case 2**	**Case 3:**	**Case 4:**	
Mass ratio	μ	-	1/100	1/50	1/20	-
Tuning ratio	f	-	100/101	50/51	20/21	-
Natural frequency of primary system	ω_1	0.817	0.817	0.817	0.817	Hz
Natural frequency of TMD	ω_2	-	0.809	0.801	0.778	Hz
Mass of primary system	m_1	$7.355 \cdot 10^7$	$7.355 \cdot 10^7$	$7.355 \cdot 10^7$	$7.355 \cdot 10^7$	kg
Mass of TMD	m_2	-	$7.355 \cdot 10^5$	$1.471 \cdot 10^6$	$3.678 \cdot 10^6$	kg
Stiffness of primary system	k_1	$3.150 \cdot 10^7$	$3.150 \cdot 10^7$	$3.150 \cdot 10^7$	$3.150 \cdot 10^7$	N/m
Stiffness of TMD	k_2	-	$4.810 \cdot 10^5$	$9.433 \cdot 10^5$	$2.225 \cdot 10^6$	N/m
Damping ratio of TMD	ζ_2	-	0.20	0.10	0.07	-
Damping of TMD	c_2	-	$2.379 \cdot 10^5$	$2.356 \cdot 10^5$	$4.005 \cdot 10^5$	$N \cdot s/m$
Peak acceleration in along-wind dir.	$a_{D,max}$	0.421	0.397	0.331	0.251	m/s^2
Peak acceleration in across-wind dir.	$a_{W,max}$	0.674	0.618	0.524	0.398	m/s^2

$$E$$
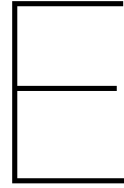
Annex E - Listings Matlab

Cantilever Beam Model: Lateral displacements

Listing E.1: Estimation of the maximum lateral displacement using the cantilever beam model

```matlab
clear all
close all
clc
%%%%%%%%%%%%%%%%%%%%%%%%%%%%%%%%%%%%%%%%%%%%%%%%%%%%%%%%%%%%%%%%
%                    Lateral displacements                   %
%%%%%%%%%%%%%%%%%%%%%%%%%%%%%%%%%%%%%%%%%%%%%%%%%%%%%%%%%%%%%%%%

% Input parameters
H=300; % [m]
qw=63; % (2 kN/m2) [kN/m]
E_cm=38000; % [MPa]
b=13500; % [mm]
h=13500; % [mm]
t1=1200; % [mm]
t2=700; % [mm]
x0=150; % [m]
A_column=10*10^5; % [mm2]
mu_concrete=0.15; % Poissons ratio

% Bending stiffness
I_core=(1/12*b*h^3-1/12*(b-t1)*(h-t1)^3)...
    +2*(1/12*b*t2^3+b*t2*2250^2)...
    +2*(1/12*t2*b^3)...
    +2*(A_column*15750^2+A_column*11250^2); % moment of inertia [mm^4]
E_core=E_cm; % modulus of elasticity [MPa]
EI_core=(E_core*I_core)*10^-9; % [kNm2]

G_core=E_core/(2*(1+mu_concrete)); % modulus of shear [MPa]
A_core=b*h-(b-(b-t1))*(h-(h-t1))+...
    4*(b*t2); %shear area [mm2]
GA_core=(G_core*A_core)/1000; % [kN]

% Stiffness of perimeter columns
E_pc=13700; % [MPa]
n=16; % number of outrigger trusses
z=15750; % lever arm [mm]
```

```matlab
A_pc=600*600*2; % [mm2]
EI_pc=(E_pc*n*2*z^2*A_pc)*10^-9; % [kNm2]

% Cross-sectional area contributing to stiffness
A_eff = A_core + A_column*28;

% Adjusted bending stiffness of outrigger structure
E_outrigger=14000; % [MPa]
A_beam=800*800; % [mm2]
h_outrigger=7500; % [mm]
j=2; % number of segments
EI_outrigger=(n*(j^2/(j^2-1))*...
    ((E_outrigger*A_beam*h_outrigger^2)/2))*10^-9; % [kNm2]

% Racking shear stiffness of outrigger
a=4500; % length beam [mm]
b=9000; % length outrigger [mm]
d=sqrt(a^2+h_outrigger^2); % length diagonal [mm]
A_diagonal=800*800; % [mm2]
GA_outrigger=(n*4*((2*a^2*h_outrigger*E_outrigger*A_diagonal)/d^3))...
    /1000; % [kN]
alpha=z/b;
Sv=H/EI_core+H/EI_pc; % char. parameter for flexibility [kN/m]
Sh=1/alpha^2*((b/1000)/(24*EI_outrigger)+...
    1/((h_outrigger/1000)*GA_outrigger)); % [kN/m]
omega=Sh/Sv;

% Restraining moment due to outrigger system
Mr=((qw*(H^3-x0^3))/(6*EI_core))*(H/((H-x0)*Sv+H*Sh)); % [kNm]

% Overturning moment on foundation
M=1/2*qw*H^2; % [kNm]
M_overturning = M - Mr; % [kNm]

% Reduction of the bending moment
M_red_percentage=(1-(M-Mr)/M)*100; % [%]

% Maximum lateral displacement at top storey level
u_max_outrigger=(qw*H^4)/(8*EI_core)+(qw*H^2)/(2*GA_core)...
    -(Mr*(H^2-x0^2))/(2*EI_core) % [m]
u_max_bending=(qw*H^4)/(8*EI_core); % [m]
u_max_shear=(qw*H^2)/(2*GA_core); % [m]
u_max_no_outrigger=(qw*H^4)/(8*EI_core)+(qw*H^2)/(2*GA_core) % [m]
u_max_red=(1-u_max_outrigger/u_max_no_outrigger)*100; % [%]

% Minimum required bending stiffness to satisfy limit building code
EI_min=(qw*H^4)/(8*0.4)

% Total effective stiffness
EI_tot = EI_core + EI_outrigger + EI_pc % [kNm2]
GA_tot = GA_core + GA_outrigger % [kN]

save('Cantilever_beam','GA_tot','EI_tot','EI_core','EI_outrigger',...
    'GA_core','GA_outrigger','A_eff','I_core')
```

Single Degree of Freedom system

Listing E.2: SDOF calculation

```matlab
clear all
close all
clc
%%%%%%%%%%%%%%%%%%%%%%%%%%%%%%%%%%%%%%%%%%%%%%%%%%%%%%%%%%%%%%%%%%%%%
%                      SDOF - Rayleigh                             %
%%%%%%%%%%%%%%%%%%%%%%%%%%%%%%%%%%%%%%%%%%%%%%%%%%%%%%%%%%%%%%%%%%%%%

% Input parameters
H=300; % [m]
B=31.5; % [m]
qw=63000; % [N/m]
E_cm=38000; % [MPa]
g=9.81; % [m/s2]
rho=1.25; % [kg/m^3]
m_z=245164; % equivalent mass per unit length [kg/m]
Z = load('Cantilever_beam','I_core','A_eff');
I_eff = Z.I_core*10^-12; % [m^4]
A_eff = Z.A_eff*10^-6; % [m^2]
u_max1=0.600; % [m]

% Concentrated load at top
F=qw*H; % [N]

% Lumped mass at top
m_tot=m_z*H; %[kg]

% Stiffness k
k_eff=F/u_max1; % [N/m]

EI_structure=k_eff*H^3/3; % [Nm2]

% Alpha (ratio of slenderness and stiffness ratio)
s_squared=(H^2*A_eff)/I_eff; % slenderness ratio
gamma_squared=(2*(1+0.15))/1; % stiffness ratio (=E/G)
alpha=s_squared/gamma_squared;

% Load-mass factor
k_lm=(4*(3024+999*alpha+91*alpha^2))/(189*(80+32*alpha+3*alpha^2));

% Fundamental frequency
omega_1=sqrt(k_eff/(k_lm*m_tot)); % [rad/s]
n_1x=omega_1/(2*pi); % [Hz]

% Input damping values
xi_s=0.0143; % structural damping ratio
xi_a=0.0072; % aerodynamic damping ratio
xi_d=0.0; % auxiliary device damping ratio
xi_tot=xi_s+xi_a+xi_d; % total damping ratio
c_cr=2*sqrt(k_eff*m_tot); % critical damping [N*s/m]
c= xi_tot*c_cr; % viscous damping [N*s/m]

% Fundamental freqency (incl damping)
omega_1damping=omega_1*sqrt(1-xi_tot^2) % [rad/s]
```

```matlab
n_1damping=omega_1damping/(2*pi) % [Hz]
T_d=1/n_1damping; % [s]

% Minimum time step
min_delta_t= T_d/10;

save('SDOF_output','k_eff','m_tot','c','c_cr','omega_1damping','xi_tot');
```

Eurocode wind calculation

Listing E.3: Wind calculation according to EN1991-1-1-4

```matlab
clear all
close all
clc
%%%%%%%%%%%%%%%%%%%%%%%%%%%%%%%%%%%%%%%%%%%%%%%%%%%%%%%%%%%%%%%%%%%%%%%%%%%%%
%                  Eurocode Wind Load Calculation                        %
%%%%%%%%%%%%%%%%%%%%%%%%%%%%%%%%%%%%%%%%%%%%%%%%%%%%%%%%%%%%%%%%%%%%%%%%%%%%%

% Input parameters
vb_0=27; % basic wind velocity [m/s2]
cat=3; % terrain category
h=300; % height
b=31.5; % width in direction orthogonal with wind load
l=31.5; % width in direction parallel with wind load
m_e=245167; % equivalent mass [kg/m]

f=0.13; % frequency in alongwind direction [Hz]

% Wind load distributed over the height
zstrip=(h-2*b)/24;
z=[b (b+zstrip) (b+2*zstrip) (b+3*zstrip) (b+4*zstrip) (b+5*zstrip)...
    (b+6*zstrip) (b+7*zstrip) (b+8*zstrip) (b+9*zstrip) (b+10*zstrip)...
    (b+11*zstrip) (b+12*zstrip) (b+13*zstrip) (b+14*zstrip)...
    (b+15*zstrip) (b+16*zstrip) (b+17*zstrip) (b+18*zstrip)...
    (b+19*zstrip) (b+20*zstrip) (b+21*zstrip) (b+22*zstrip)...
    (b+23*zstrip) (b+24*zstrip) (h-b) h];

% Wind constants
rho=1.25; %[kg/m3]
c_dir=1; % directional factor
c_season=1; %seasonal factor
c_prob=1; %probabilistic factor

z_0=0.5; %roughness length for cat3
z_min=7; % minimum height
k_r=0.19*(z_0/0.05)^0.07; % terrain factor

c_0=1; % orography
kl=1; % turbulence factor

% Basic wind pressure
v_b= c_dir*c_season*c_prob*vb_0;

% Roughness factor
if z<z_min
```

```matlab
        c_r=k_r*log(z_min/z_0);
else
        c_r=k_r*log(z/z_0);
end

% mean wind velocity
v_m=c_r*c_0*v_b;
v_mzs= v_m(16); %mean wind velocity at reference height zs=180 [m/s2]

% Turbulence intensity
if z<z_min
        I_v=kl./(c_0*log(z_min/z_0));
else
        I_v=kl./(c_0*log(z/z_0));
end


I_vzs= I_v(16);

% Peak wind pressure
q_p=(1+(7.*I_v))*0.5.*rho.*v_m.^2; % [N/m]

% Pressure coefficients (h/d>5)
psi_r= 1.0; %reduction factor for rounded corners
psi_lambda=0.63; %end effect factor
c_f0=2.1; %pressure coefficients without correction
c_f=c_f0*psi_r*psi_lambda;

% CsCd factor (Appendix C)
% Turbulence length
z_s=0.6*h;
alpha=0.67+0.05*log(z_0);
L_t=300; %reference length
z_t=300; %reference height
L_zs=L_t*(z_s/z_t)^alpha; %turbulence length scale
L_z=L_t*(z/z_t).^alpha; %turbulence length scale

% Background factor B^2
B2=1/(1+3/2*sqrt((b/L_zs)^2+(h/L_zs)^2+((b*h)/(L_zs*L_zs))^2));

% Resonance factor R^2
% non-dimensional spectral density
n_1x=0.13;
f_L=n_1x*L_zs/v_mzs; %non-dimensional frequency
S_L=(6.8*f_L)/((1+10.2*f_L)^(5/3)) ;% non-dimensional spectral
% density function

% damping logarithmic decrement
delta_s= 0.09;% logarithmic decrement of the structural damping
% (given for timber bridges)
delta_a=(c_f*rho*b*v_mzs)/(2*n_1x*m_e); %logarithmic decrement of the
%aerodynamic damping
lambda=1.4*h/b; %relative slenderness
phi=1.0; %degree of fullness
psi_lambda=0.73; %end effect factor
delta_d=0; %logarithmic decrement of the damping due to auxiliary devices
delta=delta_s+delta_a+delta_d; %logarithmic decrement of the total damping
```

```matlab
xi_s=delta_s/(sqrt((2*pi)^2+delta_s^2)); %damping ratio
xi_a=delta_a/(sqrt((2*pi)^2+delta_a^2));
xi_d=delta_d/(sqrt((2*pi)^2+delta_d^2));
xi=delta/(sqrt((2*pi)^2+delta^2));

% damping ratio
zeta=delta/(sqrt((2*pi)^2+delta^2));

%measure reduction function
phi_y=(11.5*b*n_1x)/v_mzs;
phi_z=(11.5*h*n_1x)/v_mzs;
G_y=1/2; %assumption uniform vibration mode over width
G_z=5/18; %assumption parabolic vibration mode over height
K_s=1./(1+sqrt((G_y.*phi_y).^2+(G_z.*phi_z).^2+...
    (2./pi.*G_y.*phi_y*G_z.*phi_z).^2)); %measure reduction function
R2=pi^2./(2*delta).*S_L.*K_s; %Resonance factor

%peak factor k_p
T=600;
nu=n_1x*sqrt(R2/(B2+R2)); %estimate of frequency during a wind gust
k_p=sqrt(2*log(nu*T))+0.6/sqrt(2*log(nu*T)); %peak value
if k_p < 3
    k_p=3
else
end

% Structural dynamic factor cscd
cscd=(1+2*k_p*I_v.*sqrt(B2+R2))/(1+7*I_v);

%Wind force on facade (alongwind)
z_y=[0 z];
no_strips=length(z_y);
F=zeros(1, length(z)); %make empty matrix
A=zeros(1, length(z));
for i=1:no_strips-1
    hi=z_y(i+1)-z_y(i);
    A(i)=hi*b; %A_ref
    F(i)=cscd*c_f*q_p(i)*A(i)/1000; %wind force
    f_w(i)=F(i)/A(i); %wind pressure
end

q_w=f_w*b; %wind load [kN/m]
```

Eurocode peak accelerations calculation

Listing E.4: Peak accelerations according to EN1991-1-1-4 Annex C

```matlab
clear all
close all
clc
%%%%%%%%%%%%%%%%%%%%%%%%%%%%%%%%%%%%%%%%%%%%%%%%%%%%%%%%%%%%%%%%%%%%%%%%%%%%%%%
%                  Eurocode maximum acceleration (Annex C)                  %
%%%%%%%%%%%%%%%%%%%%%%%%%%%%%%%%%%%%%%%%%%%%%%%%%%%%%%%%%%%%%%%%%%%%%%%%%%%%%%%

% Input parameters
```

```matlab
v_b0=27; %basic wind velocity [m/s2]
cat=3; %terrain category
rho=1.25; %air density [kg/m3]
b=31.5;
l=31.5;
h=300;
m_e=245164 ; % equivalent mass per unit length [kg/m]
X = load('Eurocode_variables','R2','B2','I_vzs','v_mzs','n_1x','c_f');
n_1x = X.n_1x; % Natural frequency [Hz]
c_f = X.c_f; % Pressure coefficient
I_vzs = X.I_vzs; % Turbulence intensity at height zs
v_mzs = X.v_mzs; % Mean wind velocity at height zs [m/s]
R2 = X.R2; % Resonance response factor
B2 = X.B2; % Background response factor

% Squareroot of Resonance Response factor
R=sqrt(R2);

%non-dimensional coefficient K_x and K_y
K_y=1; %for a horizontal uniform vibration mode
K_z=5/3; %for a vertical parabolic vibration mode

% Fundamental vibration mode
zstrip=(h-2*b)/24;
z=[b (b+zstrip) (b+2*zstrip) (b+3*zstrip) (b+4*zstrip) (b+5*zstrip)...
    (b+6*zstrip) (b+7*zstrip) (b+8*zstrip) (b+9*zstrip) (b+10*zstrip)...
    (b+11*zstrip) (b+12*zstrip) (b+13*zstrip) (b+14*zstrip)...
    (b+15*zstrip) (b+16*zstrip) (b+17*zstrip) (b+18*zstrip)...
    (b+19*zstrip) (b+20*zstrip) (b+21*zstrip) (b+22*zstrip)...
    (b+23*zstrip) (b+24*zstrip) (h-b) h];
Phi_1x=((z.^2)./h^2); %fundamental vibration mode

figure
plot(Phi_1x,z,'b');
title('Fundamental vibration mode');
xlabel('vibration mode');
ylabel('Height [m]');
plottools
print -deps vibrationmode

Phi_max = max(Phi_1x);

% Reference mass per unit surface
% Take mu_ref at maximum amplitude, so at top H
rho_H = 153; % kg/m^3
M = m_e*h;
mu_ref = rho_H * b;

% Characteristic peak acceleration
T=600;
nu=n_1x*sqrt(R2/(B2+R2)); %estimate of frequency during a wind gust
k_p=sqrt(2*log(nu*T))+0.6/sqrt(2*log(nu*T)); % peak value

if k_p < 3
    k_p=3;
else
```

```matlab
end

% Standard deviation of the acceleration
sigma_ax = c_f * rho * I_vzs * v_mzs^2 * R * ...
    ((K_y * K_z * Phi_1x)/(mu_ref * Phi_max))

% Peak accelerations
acc=k_p*sigma_ax;
a_max = max(acc)

figure
plot(acc,z,'b');
title('Characteristic peak accelerations');
xlabel('peak accelerations, a_{max} [m/s^2]');
ylabel('Height [m]');
grid on
plottools
print -deps peak_accelerations
%export: W=13; H=16

table_acc=[z' acc'];
input.data = table_acc;
input.dataFormat = {'%.2f'};
latext = latexTable(input);

save('peak_factor_EC','k_p')
```

Spectral analysis

Listing E.5: Spectral analysis calculation

```matlab
clear all
close all
clc
%%%%%%%%%%%%%%%%%%%%%%%%%%%%%%%%%%%%%%%%%%%%%%%%%%%%%%%%%%%%%%%%%%%%%
%            Spectral Analysis (Davenport method)            %
%%%%%%%%%%%%%%%%%%%%%%%%%%%%%%%%%%%%%%%%%%%%%%%%%%%%%%%%%%%%%%%%%%%%%

% Along-wind response spectrum

% Input parameters
H=300; % [m]
B=31.5; % [m]
D=31.5; % [m]
m_z=245164; % equivalent mass per unit length [kg/m]
rho=1.25; % [kg/m^3]
n_1x=0.13; % fundamental frequency [Hz]

% Spectral Analysis (Davenport method)

S = load('EC_variables.mat');
v_m = S.v_m; % mean wind velocity [m/s]
v_mzs = v_m(180); % mean wind velocity at ref. height
v_H = v_m(300); % mean wind velocity at top
I_v=S.I_v; % turbulence intensity
I_vzs=I_v(180); % turbulence intensity at ref. height
```

```matlab
L_z=S.L_z; % turbulence length scale
L_zs=216.9; % turbulence length scale at ref. height
f = logspace(-4,1,1000); % frequency [Hz]
C_D = S.c_f; % dynamic factor

sigma_v = I_vzs*v_mzs; % Standard deviation of wind velocity
variance_v = sigma_v^2; % Variance of wind velocity

L = 217; % characteristic turbulence length scale [m]
f_star = f*L/v_m(200); % non-dimensional frequency

% Reduced spectrum of wind velocity
S_v_star = (2/3)*(f_star.^2)./((1+f_star.^2).^(4/3));
% Spectrum of the variance of the fluctuating wind velocity
S_v = (S_v_star*variance_v)./f;

variance_S_v_star = trapz(f_star,S_v_star);
variance_S_v = trapz(f,S_v);

% Power density spectrum for small surfaces
S_F_small = (C_D*rho*v_mzs*B*H)^2 * S_v;
S_F_small_star = (C_D*rho*v_mzs*B*H)^2 * S_v_star;

% Aerodynamic admittance function
chi_squared = (1 ./ ( 1 + ( (2*f*sqrt(B*H))./v_mzs).^(4/3) )).^2;

% Power density spectrum (including aerodynamic admittance)
S_F = (C_D*rho*v_mzs*B*H)^2 * S_v .* chi_squared;
variance_F = trapz(f,S_F);
S_F_point = S_F/(B*H)^2;
sigma_F = sqrt(variance_F);

S_F_star = S_v_star .* chi_squared;
max_S_F_star = max(S_F_star);
S_F_max = max(S_F);
indexOfFirstMax_S_F = find(S_F == S_F_max, 1, 'first');
f_of_S_F_max = f(indexOfFirstMax_S_F);

% Curve fitting
S_F_fit = fit(f',S_F','cubicinterp');

% Mechanical admittance function, |H(f)|^2
Z = load('SDOF_output','omega_1damping','xi_tot');
omega = 2*pi*f; % angular frequency [rad/s]
f_n=0.13;
omega_n = (2 * pi) * f_n;
xi = Z.xi_tot; % damping ratio

H_squared = ( 1 ./ ((1- (omega/omega_n).^2).^2 +...
    (2*xi*omega/omega_n).^2).^(1/2) ).^2;

% Response spectrum for displacements
k = 3.15*10^7; % stiffness of structure [N/m]
S_x = 1/k^2* S_F .* abs(H_squared);
max_S_x = max(S_x)
```

```matlab
% Response spectrum for accelerations
S_a = S_x.*(2*pi*f).^4;
max_S_a = max(S_a)

f4 = 2*pi*f.^4;

figure
plot(f,f4,'b');
title('Relationship between the displacement and acceleration spectra');
xlabel('frequency, f [Hz]');
ylabel('$2\pif^4$','Interpreter','Latex');
axis([0 1 0 7]);
grid on
plottools

% Variance of the displacements and accelerations
% Numerical integration - trapezoid rule
variance_x = trapz(f,S_x);
variance_a = trapz(f,S_a);

% Standard deviation of the displacements and accelerations
sigma_x = sqrt(variance_x); % [m/s]
sigma_a = sqrt(variance_a); % [m/s2]

% Estimate of the peak response for accelerations
a_max = g_p*sigma_a

%%%%%%%%%%%%%%%%%%%%%%%%%%%%%%%%%%%%%%%%%%%%%%%%%%%%%%%%%%%%%%%%%%%%%%
%                       Vary global damping                        %
%%%%%%%%%%%%%%%%%%%%%%%%%%%%%%%%%%%%%%%%%%%%%%%%%%%%%%%%%%%%%%%%%%%%%%

xi_1 = 0.0;
xi_2 = 0.010;
xi_3 = 0.0215;
xi_4 = 0.05;
xi_5 = 0.10;
xi_6 = 0.50;

H_squared_1 = ( 1 ./ ((1- (omega/omega_n).^2).^2 +...
    (2*xi_1*omega/omega_n).^2).^(1/2) ).^2;

H_squared_2 = ( 1 ./ ((1- (omega/omega_n).^2).^2 +...
    (2*xi_2*omega/omega_n).^2).^(1/2) ).^2;

H_squared_3 = ( 1 ./ ((1- (omega/omega_n).^2).^2 +...
    (2*xi_3*omega/omega_n).^2).^(1/2) ).^2;

H_squared_4 = ( 1 ./ ((1- (omega/omega_n).^2).^2 +...
    (2*xi_4*omega/omega_n).^2).^(1/2) ).^2;

H_squared_5 = ( 1 ./ ((1- (omega/omega_n).^2).^2 +...
    (2*xi_5*omega/omega_n).^2).^(1/2) ).^2;

H_squared_6 = ( 1 ./ ((1- (omega/omega_n).^2).^2 +...
    (2*xi_6*omega/omega_n).^2).^(1/2) ).^2;
```

```matlab
figure
plot(f,H_squared_1,'b');
hold on
plot(f,H_squared_2,'r');
hold on
plot(f,H_squared_3,'g');
hold on
plot(f,H_squared_4,'m');
hold on
plot(f,H_squared_5,'c');
hold on
%plot(f,H_squared_6,'y');
%hold on
title('Mechanical admittance function, H^2(f)');
xlabel('frequency, f [Hz]');
ylabel('H(f)');
set(gca, 'XScale', 'log', 'YScale', 'log');
axis([10^-1 2*10^-1 10^-0 10^5])
grid on
plottools
```

Tuned Mass Damper

> *restart*

Undamped TMD

Particular solutions

>

> $x\_1 := C1 \cdot \sin(\text{Omega} \cdot t)$:

> $x\_1\_diff := diff(x\_1, t)$:

> $x\_1\_diff\_2 := diff(x\_1, t\$2)$:

> $x\_2 := C2 \cdot \sin(\text{Omega} \cdot t)$:

> $x\_2\_diff := diff(x\_2, t)$:

> $x\_2\_diff\_2 := diff(x\_2, t\$2)$:

Equation of motions

> $EOM\_1 := m\_1 \cdot x\_1\_diff\_2 + k\_1 \cdot x\_1 + k\_2 \cdot x\_1 - k\_2 \cdot x\_2 = F\_0 \cdot \sin(\text{Omega} \cdot t);$

$$EOM\_1 := k\_1\,C1\,\sin(\Omega\,t) + k\_2\,C1\,\sin(\Omega\,t) - k\_2\,C2\,\sin(\Omega\,t) - m\_1\,C1\,\Omega^2\,\sin(\Omega\,t) \tag{1}$$
$$= F\_0\,\sin(\Omega\,t)$$

> $EOM\_2 := m\_2 \cdot x\_2\_diff\_2 + k\_2 \cdot x\_2 - k\_2 \cdot x\_1 = 0;$

$$EOM\_2 := -k\_2\,C1\,\sin(\Omega\,t) + k\_2\,C2\,\sin(\Omega\,t) - m\_2\,C2\,\Omega^2\,\sin(\Omega\,t) = 0 \tag{2}$$

> $C1 := solve(EOM\_2, C1);$

$$C1 := -\frac{C2\left(\Omega^2\,m\_2 - k\_2\right)}{k\_2} \tag{3}$$

> $EOM\_1 := -\Omega^2 \cdot m\_1 \cdot C1 + k\_2 \cdot (C1 - C2) + k\_1 \cdot C1 - F\_0;$

$$EOM\_1 := \frac{\Omega^2\,m\_1\,C2\left(\Omega^2\,m\_2 - k\_2\right)}{k\_2} + k\_2\left(-\frac{C2\left(\Omega^2\,m\_2 - k\_2\right)}{k\_2} - C2\right) \tag{4}$$
$$-\frac{k\_1\,C2\left(\Omega^2\,m\_2 - k\_2\right)}{k\_2} - F\_0$$

> $C2 := solve(EOM\_1, C2);$

$$C2 := \frac{F\_0\,k\_2}{\Omega^4\,m\_1\,m\_2 - \Omega^2\,k\_1\,m\_2 - \Omega^2\,k\_2\,m\_1 - k\_2\,\Omega^2\,m\_2 + k\_1\,k\_2} \tag{5}$$

> $C1;$

$$-\frac{F\_0\left(\Omega^2\,m\_2 - k\_2\right)}{\Omega^4\,m\_1\,m\_2 - \Omega^2\,k\_1\,m\_2 - \Omega^2\,k\_2\,m\_1 - k\_2\,\Omega^2\,m\_2 + k\_1\,k\_2} \tag{6}$$

Static response

> $x\_stat := \dfrac{F\_0}{k\_1};$

$$x\_stat := \frac{F\_0}{k\_1} \tag{7}$$

> $H\_dyn\_1 := \dfrac{C1}{x\_stat};$

$$H\_dyn\_1 := -\frac{\left(\Omega^2\,m\_2 - k\_2\right)k\_1}{\Omega^4\,m\_1\,m\_2 - \Omega^2\,k\_1\,m\_2 - \Omega^2\,k\_2\,m\_1 - k\_2\,\Omega^2\,m\_2 + k\_1\,k\_2} \tag{8}$$

> $H\_dyn\_2 := \dfrac{C2}{x\_stat};$

$$H\_dyn\_2 := \frac{k\_2\,k\_1}{\Omega^4\,m\_1\,m\_2 - \Omega^2\,k\_1\,m\_2 - \Omega^2\,k\_2\,m\_1 - k\_2\,\Omega^2\,m\_2 + k\_1\,k\_2} \tag{9}$$

Tuned Mass Damper

Frequency ratio, beta

> Omega := beta·ω_1;

$$\Omega := \beta\,\omega_1 \qquad (10)$$

Natural frequencies

> #ω_1 := sqrt$\left(\dfrac{k\_1}{m\_1}\right)$: #ω_2 := sqrt$\left(\dfrac{k\_2}{m\_2}\right)$:

> #$m\_1 := \dfrac{k\_1}{\omega_1^2}$; #$m\_2 := \dfrac{k\_2}{\omega_2^2}$;

> $k\_1 := m\_1 \cdot \omega_1^2$; $k\_2 := m\_2 \cdot \omega_2^2$;

$$k\_1 := m\_1\,\omega_1^2$$

$$k\_2 := m\_2\,\omega_2^2 \qquad (11)$$

> H_dyn_1;

$$-\frac{\left(\beta^2\,\omega_1^2\,m\_2 - m\_2\,\omega_2^2\right) m\_1\,\omega_1^2}{\beta^4\,\omega_1^4\,m\_1\,m\_2 - \beta^2\,\omega_1^4\,m\_1\,m\_2 - \beta^2\,\omega_1^2\,m\_2\,\omega_2^2\,m\_1 - \beta^2\,\omega_1^2\,m\_2^2\,\omega_2^2 + m\_1\,\omega_1^2\,m\_2\,\omega_2^2} \qquad (12)$$

Mass ratio

> m_2 := mu·m_1;

$$m\_2 := \mu\,m\_1 \qquad (13)$$

> #algsubs$\left(\dfrac{\Omega}{\omega_1} = \beta, H\_dyn\_1\right)$;

Assume

> $\omega_2 := \omega_1$; $\omega_1 := 1$; mu := 0.02; $m\_1 := 1$;

$$\omega_2 := \omega_1$$
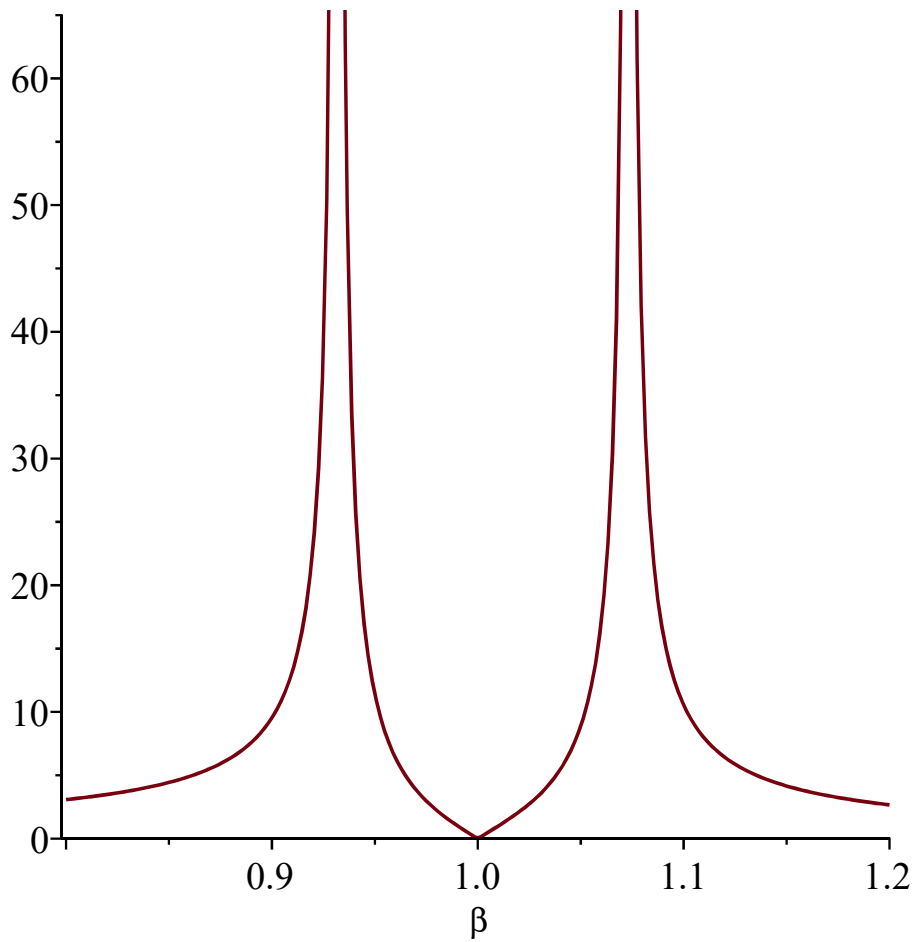
$$\omega_1 := 1$$

$$\mu := 0.02$$

$$m\_1 := 1 \qquad (14)$$

> H_dyn_1;

$$-\frac{0.02\,\beta^2 - 0.02}{0.02\,\beta^4 - 0.0404\,\beta^2 + 0.02} \qquad (15)$$

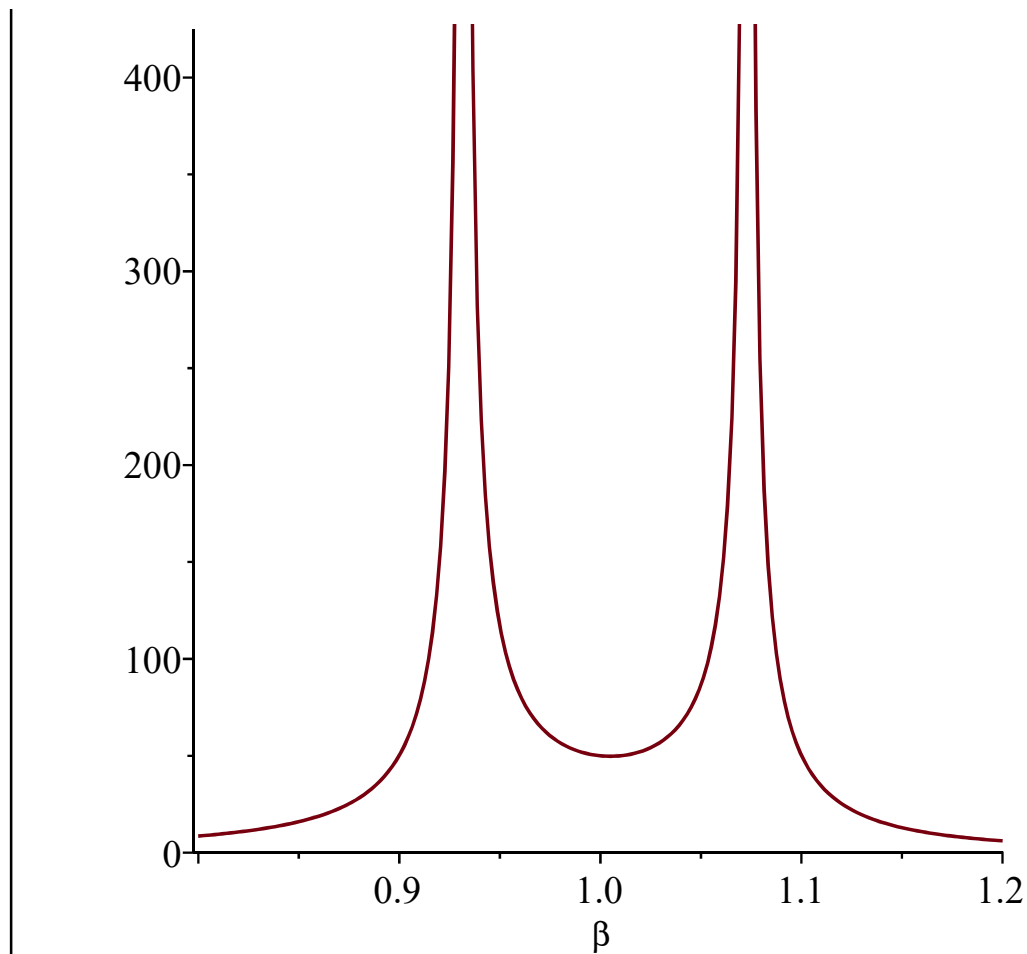> plot(abs(H_dyn_1), beta = 0.8 .. 1.2);

Tuned Mass Damper

> *H_dyn_2*;

$$\frac{0.02}{0.02\,\beta^4 - 0.0404\,\beta^2 + 0.02}$$

(16)

> $plot(\text{abs}(H\_dyn\_2), \text{beta} = 0.8..1.2)$;

Tuned Mass Damper

> *restart*;

Dynamic amplification factor H

> $H\_dyn\_1 := \dfrac{\left(1 - \left(\dfrac{Omega^2}{\omega_2^2}\right)\right)}{\left(\left(1 - \dfrac{Omega^2}{\omega_2^2}\right) \cdot \left(1 + \dfrac{m\_2}{m\_1} - \dfrac{Omega^2}{\omega_1^2}\right) - \dfrac{m\_2}{m\_1}\right)}$;

$$H\_dyn\_1 := \frac{1 - \dfrac{\Omega^2}{\omega_2^2}}{\left(1 - \dfrac{\Omega^2}{\omega_2^2}\right)\left(1 + \dfrac{m\_2}{m\_1} - \dfrac{\Omega^2}{\omega_1^2}\right) - \dfrac{m\_2}{m\_1}} \tag{17}$$

> $H\_dyn\_2 := \dfrac{1}{\left(\left(1 - \dfrac{Omega^2}{\omega_2^2}\right) \cdot \left(1 + \dfrac{m\_2}{m\_1} - \dfrac{Omega^2}{\omega_1^2}\right) - \dfrac{m\_2}{m\_1}\right)}$;

$$H\_dyn\_2 := \frac{1}{\left(1 - \dfrac{\Omega^2}{\omega_2^2}\right)\left(1 + \dfrac{m\_2}{m\_1} - \dfrac{\Omega^2}{\omega_1^2}\right) - \dfrac{m\_2}{m\_1}} \tag{18}$$
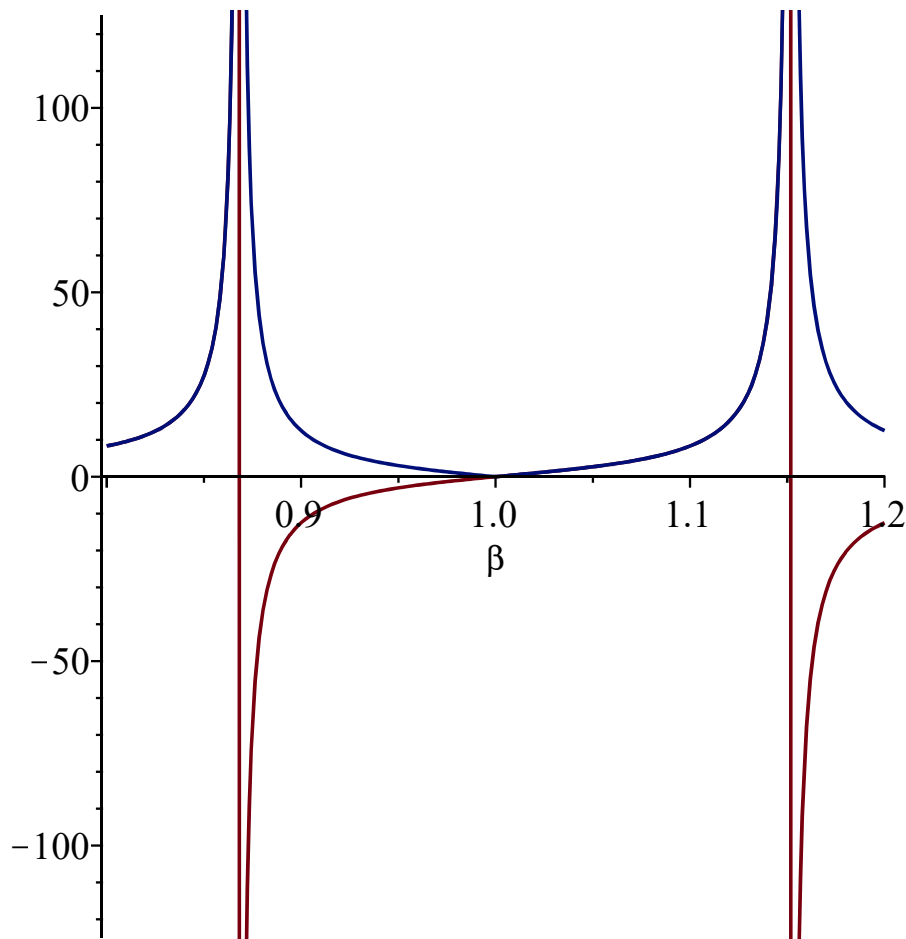
Tuned Mass Damper

Tuning mass damper (omega_2=omega_1)

> $\omega_1 := \omega_2:$

> $subs\left(\dfrac{Omega^2}{\omega_2^2} = beta, \dfrac{m\_2}{m\_1} = \dfrac{1}{50}, H\_dyn\_1\right);$

$$\frac{1 - \beta}{(1 - \beta)\left(\dfrac{51}{50} - \beta\right) - \dfrac{1}{50}} \qquad \textbf{(19)}$$

> $plot\left(\left\{\left\{subs\left(\dfrac{Omega^2}{\omega_2^2} = beta, \dfrac{m\_2}{m\_1} = \dfrac{1}{50}, H\_dyn\_1\right), abs\left(subs\left(\dfrac{Omega^2}{\omega_2^2} = beta, \dfrac{m\_2}{m\_1}\right.\right.\right.\right.\right.$
> $\left.\left.\left.\left.\left. = \dfrac{1}{50}, H\_dyn\_1\right)\right)\right\}, beta = 0.8..1.2\right);$

> $plot\left(\left\{\left\{subs\left(\dfrac{Omega^2}{\omega_2^2} = beta, \dfrac{m\_2}{m\_1} = \dfrac{1}{50}, H\_dyn\_2\right), abs\left(subs\left(\dfrac{Omega^2}{\omega_2^2} = beta, \dfrac{m\_2}{m\_1}\right.\right.\right.\right.\right.$
> $\left.\left.\left.\left.\left. = \dfrac{1}{50}, H\_dyn\_2\right)\right)\right\}, beta = 0.8..1.2\right);$

Tuned Mass Damper